Upgrading Biogas to Biomethane Using Absorption

Faculty of Mechanical Science and Engineering

Technische Universität Dresden

Submitted in partial fulfilment of the requirements for the academic degree of

Doktoringenieur (Dr.-Ing.)

Approved Dissertation

By

Dipl.-Ing. Onkar Dixit

Born on 7th of June, 1988, in Pune, India

Date of submission: 15.04.2015
Date of defence: 17.11.2015

First advisor: Prof. Dr.-Ing. Norbert Mollekopf
Second advisor: Prof. Dr. rer. pol. habil. Dominik Möst

Doctoral-committee chair: Prof. Dr.-Ing. Michael Beckmann

ACKNOWLEDGEMENTS

I am grateful to Prof. Dr.-Ing. Norbert Mollekopf for giving me the opportunity to complete my dissertation at his research department. His support has been vital in the completion of this work.

I am thankful to Prof. Dr. phil. habil. Wolfgang Donsbach and Thomas Meyer, M.A. for managing the public survey, and Prof. Dr. rer. pol. habil. Edeltraud Günther and Dipl.-Kfm. (FH) Stefan Münch for managing the life cycle assessment. I thank Dipl.-Ing. Jens Hennig and Ms. Anja Seifert for their assistance at the test rig and in the laboratory. I also thank all members of the Boysen-TU Dresden-Graduiertenkolleg for their critical discussions.

I am grateful to the Friedrich and Elisabeth Boysen Trust and TU Dresden for their financial support, and I am obliged to Mother Nature for being a source of ideas and inspiration.

TABLE OF CONTENTS

LIST OF FIGURES

LIST OF TABLES

LIST OF SYMBOLS

LATIN SYMBOLS

A	area	m^2
a	attraction parameter	$kPa \cdot (m^3 \cdot mol^{-1})^2$
Ab	absorption factor	-
b	van der Waal covolume	$m^3 \cdot mol^{-1}$
C	capacity factor	$m \cdot s^{-1}$
c	molar concentration	$mol \cdot m^{-3}$
CP	capacity parameter	-
d	diameter	m
D	diffusion coefficient	$m^2 \cdot s^{-1}$
E	void fraction	-
F	F-factor	$m \cdot s^{-1} \cdot (kg \cdot m^{-3})^{0,5}$
f	fugacity	kPa
FP	flow parameter	-
Fr	Froude number	-
G	gas flow rate	no generic unit
h	height	m
HETP	height equivalent to a theoretical plate	m
ho	holdup	-
HP	hazard points	-
HTU	height of a (one) transfer unit	m
I	ionic strength	-

J	molar flux	$mol \cdot (m^2 \cdot s)^{-1}$
k	constant	no generic unit
l	length	m
L	solvent flow rate	no generic unit
m	molality	$mol \cdot kg^{-1}$
M	molecular mass	$g \cdot mol^{-1}$
N	number	-
NTU	number of transfer units	-
p	partial pressure	kPa, bar
P	pressure	kPa, bar
PF	packing factor	ft^{-1}
Q	charge	J
r	radius	m
R	universal gas constant	$bar \cdot m^3 \cdot (K \cdot mol)^{-1}$
Re	Reynolds number	-
sl	slope of the equilibrium curve	-
T	temperature	°C, K
v	velocity	$m \cdot s^{-1}$
V	volume	m^3
w	mass fraction	$kg \cdot kg^{-1}$
WF	wall factor	-
x	mole fraction in the liquid phase	$mol \cdot mol^{-1}$
X	mole ratio in the liquid phase	$mol \cdot mol^{-1}$
y	mole fraction in the gas phase	$mol \cdot mol^{-1}$

Y	mole ratio in the gas phase	$mol \cdot mol^{-1}$
z	charge number	-
Z	compressibility factor	-

GREEK SYMBOLS

α	loading	$mol \cdot mol^{-1}$
β	nonrandomness factor	-
γ	activity coefficient	-
δ	interaction coefficient	-
Δ	difference	no generic unit
ε	dielectric constant (relative permittivity)	-
λ	volumetric flow ratio	-
μ	dynamic viscosity	mPa·s
ν	kinematic viscosity	cSt
ρ	density	$kg \cdot m^{-3}$
σ	surface tension	$mN \cdot m^{-1}$
τ	binary interaction parameter	-
$\varnothing$	fugacity coefficient	-
Ψ	resistance coefficient	-
ω	acentric factor	-

INDICES

Both subscript and superscript indices are presented here. Numbers as indices are not further subscripted or superscripted.

0	reference state
*	at equilibrium

A	Avogadro
abs	absorbed
av	average
B	Boltzmann
Born	Born model
bot	column bottom
bu	bulk
c	critical
ca	carrier
CH4	methane
CO2	carbon dioxide
col	column
DGA	diglycolamine
DH	Debye-Hückel model
di	dielectric
diff	diffusion
e	electron
E	excess
el	electric
eq	equilibrium
exp	determined by experiments
fl	at the flooding point
fo	form
fr	flow ratio

G	gas phase
gas	gas
H	Henry
h	hydraulic
H2O	water
in	inlet
int	interface
ip	interaction parameter
irr	irrigated
L	liquid phase
liq	liquid
lm	log mean
m	mass
min	minimum
mix	mixture
mo	molar
N2	nitrogen
NRTL	non-random two liquid model
OG	overall gas phase
OL	overall liquid phase
op	at the operating point
out	outlet
p	packing
PDH	Pitzer-Debye-Hückel model

pl	theoretical plate
r	reduced
re	reaction
reb	reboiler
saf	safety
sim	determined by simulations
solv	solvent
St	Sauter
th	thermal
theo	determined by theoretical calculations
top	column top (head)
tot	total
v	volumetric
vap	vapour
w	water

LIST OF ABBREVIATIONS

ADEG	amino-diethylene glycol
ADP	abiotic resource depletion potential
AMP	aminomethylpropanol
AP	acidification potential
AV	actual value
BDL	below detectable limit
BTX	benzene, toluene, xylene
CAS	Chemical Abstracts Service
CFC	chlorofluorocarbon
CML	Centrum voor Milieukunde
DCB	dichlorobenzene
DEA	diethanolamine
DGA	diglycolamine
DIPA	diisopropanolamine
DQI	data quality indicator
DVGW	Deutscher Verein des Gas- und Wasserfaches
EDTA	ethylenediaminetetraacetic acid
eNRTL	electrolyte non-random two liquid
EP	eutrophication potential
eq.	equivalent
EU	European Union
exp	determined by experiments

FAETP	freshwater aquatic ecotoxicity potential
GESTIS	Gefahrstoffinformationssystem
GPDC	generalized pressure drop correlation
GWP	global warming potential
H	high
HDPE	high-density polyethylene
HP	high pressure
HTP	human toxicity potential
ISO	International Organization for Standardization
L	low
LCA	life cycle assessment
LO-CAT	liquid oxidation catalyst
LP	low pressure
MAETP	marine aquatic ecotoxicity potential
MDEA	N-methyldiethanolamine
MEA	monoethanolamine
MP	medium pressure
MSDS	material safety datasheet
NMVOC	non-methane volatile organic compound
No.	number
NRTL	non-random two liquid
ODP	ozone depletion potential
OECD	Organization for Economic Co-operation and Development
PP	polypropylene

PSA	pressure swing adsorption
PTFE	polytetrafluoroethylene
PVC	polyvinylchloride
PZ	piperazine
sim	determined by simulations
SP	set point
Sr.	serial
TETP	terrestrial ecotoxicity potential
TIC	total inorganic carbon
tpd	ton per day
VOC	volatile organic compound
vol.	volume
wt.	mass

1 MOTIVATION AND AIM

The fervour of mitigating climate change is gripping the world, and measures are being undertaken to reduce greenhouse-gas emissions, which have been adjudged culprits of climate change. Fossil fuel consumption leads to greenhouse-gas emissions, and the transition from a fossil-fuel energy system to a renewable-fuel energy system is a consequent measure to reduce greenhouse-gas emissions. In Germany, the *Energiewende* represents this energy transition. Examples of renewable energy are solar energy (e.g. electricity produced by photovoltaic cells), wind energy (e.g. electricity produced by windmills) and bioenergy (e.g. combustible gas produced by the fermentation of biomass). Bioenergy is obtained from biomass, which is the largest source of renewable energy in the world: bioenergy caters to 10 % of the global primary-energy demand as of 2010 (IRENA, 2013).

1.1 WHY BIOMETHANE?

Biomethane (a form of bioenergy) is a renewable energy carrier that can substitute natural gas (a fossil fuel). Biomethane has the same chemical composition as natural gas and can be transported through natural-gas pipelines, which is existing infrastructure in most regions. Biomethane is a versatile energy carrier. It can be used to produce heat and electricity in a cogeneration plant; it can be used as a vehicular fuel, or it can be used as a chemical feedstock in manufacturing processes (DENA, 2014).

Biomethane has several advantages over other renewable energy carriers. When compared with other biofuels (e.g. bioethanol), biomethane is more efficient in terms of land use. For bioethanol production, only the oil and sugar content of the crop is used, whereas for biomethane or biogas production, the whole crop is used. Electricity produced by photovoltaic cells or windmills has temporal fluctuations, but in a cogeneration plant fired by biomethane, electricity is produced at a constant rate throughout the year. Thus, biomethane is a base-load provider (DENA, 2014).

Biomethane also offers a politically strategic advantage. In Germany, as per 2014, 85 % of the total natural-gas demand was met by imports. Biomethane production in Germany reduces natural-gas imports, and this is a step towards making Germany self-sufficient in energy (DENA, 2014).

The number of biomethane plants in Germany is increasing (Figure 1.1). It is expected that biomethane will meet around 2 % of the total primary-energy demand of Germany by the year 2020, which will be a 100 fold increase since the year 2010. The European Union (EU) and the Federal German Government have set a target of injecting 6 billion Nm^3 of biomethane in natural-gas pipelines until 2020. An investment of approximately 12 billion € is expected for the necessary machinery (DENA, 2011).

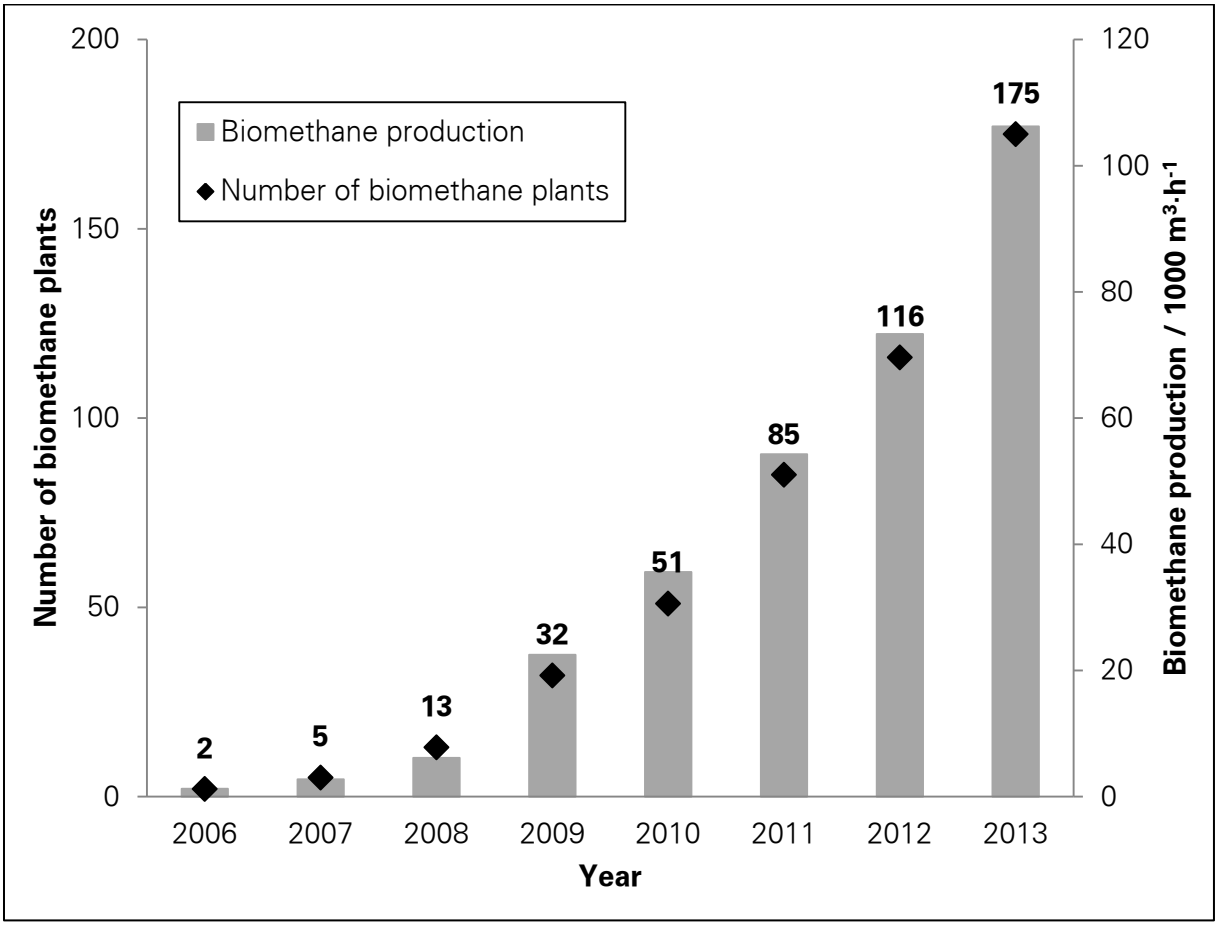

Figure 1.1 Number of biomethane plants and biomethane production in Germany (based on data from Biogaspartner, 2014)

1.2 BIOMETHANE PRODUCTION

Biomethane is obtained by purifying biogas, which in turn is produced by the bacterial, anaerobic digestion of biomass. The major components of biogas are methane (CH_4), carbon dioxide (CO_2), hydrogen sulphide (H_2S) and water (H_2O). If biogas is used to generate electricity, biogas undergoes a primary treatment only (dotted box in Figure 1.2) which includes filtering, drying and rough desulphurisation. Reasons for this primary treatment are as follows: biogas components should not damage the generator in the power plant, and

combustion products (gases) should fulfil emission standards as stipulated by law. Well-developed technologies for this primary treatment are currently available in the market.

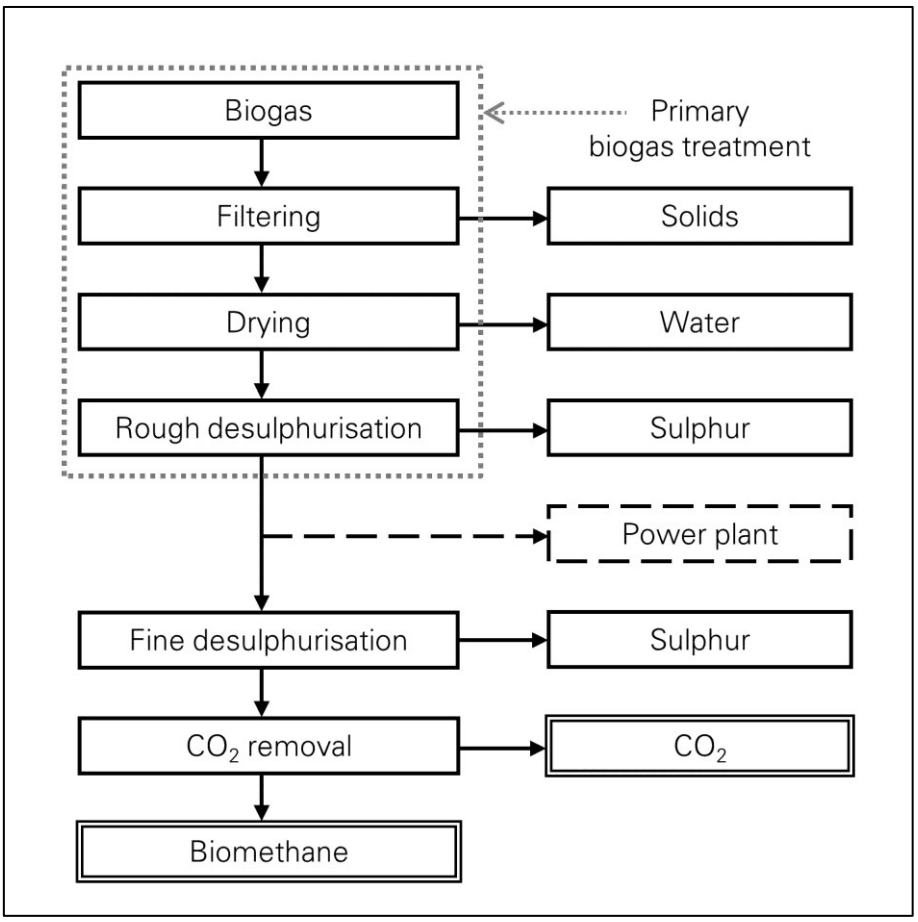

Figure 1.2 Schematic diagram of biogas treatment
(adapted from Dixit and Mollekopf, 2014c)

In addition to the primary biogas treatment, if biogas undergoes fine desulphurisation (H_2S < 5 ppm) and CO_2 separation (CO_2 < 4 volume (vol.) %), biomethane or pipeline-quality natural gas is produced (Figure 1.2). However, only limited knowledge and experience are available about these processes.

The crucial part of the final gas-treatment operation is CO_2 separation, and four processes are mainly used for it: adsorption, absorption, permeation (membrane separation) and cryogenic separation. The absorption process, which employs an absorption solvent (a liquid) to absorb unwanted gases, has several advantages over other processes: CH_4 with high purity (above 99 vol. %) can be produced; H_2S can be simultaneously separated; operational flexibility with respect to feed gas is high, and energy (heat and electricity) consumption is low.

The absorption process has been an integral part of natural gas and synthesis gas (or syngas) treatment plants. Therefore, it is tempting to choose well-known absorption solvents of the industry such as monoethanolamine (MEA) and diethanolamine (DEA) to treat biogas. However, there are differences in gas composition and in conditions under which gases such as natural gas, syngas, flue gas and biogas are available (Table 1.1). The amount of acid gas (e.g. CO_2) in biogas is extremely high (typically around 40 vol. %): biogas is very acidic. Flue gas contains only 8 to 14 vol. % CO_2. Biogas is available at atmospheric pressure in contrast to natural gas, which is typically available at over 50 bar pressure. Syngas has a temperature of around 90 °C at the desulphurisation-unit inlet, whereas biogas has around 20 °C temperature. Consequently, the same absorption solvents and the same process design as used in natural gas or syngas treatment cannot be used to treat biogas. So which absorption solvents are suitable for biogas treatment?

Table 1.1 Characteristic parameters of natural gas, syngas, flue gas and biogas (based on data from KOMETEC Karl Oelkers e.K., 2003; Klinski, 2006; Arbeitsgemeinschaft für sparsamen und umweltfreundlichen Energieverbrauch e.V., 2011; Dixit et al., 2012; US Department of Energy, 2012)

Parameter	Natural gas	Syngas	Flue gas	Biogas
CO_2 / vol. %	0 to 3	40 to 70	8 to 14	25 to 55
H_2S or SO_2 / vol. %	0,01 to 10	0,2 to 1	0,02	0,01 to 3
Major component	methane	hydrogen	nitrogen	methane
Temperature / °C	35 to 50	90 to 110	90 to 110	20 to 50
Pressure / bar	> 50	40 to 100	> 1	1,2

The main aim of this study is to design an absorption process that is capable of separating CO_2 or CO_2-and-H_2S from biogas and is more energy-efficient and safer than the currently used absorption processes. This will make the new process more economical, and it will enjoy a greater public acceptance.

1.3 RESEARCH TASKS

In order to achieve the aim of this study, several tasks were defined, and to fulfil each task, a specific course of action was selected (Table 1.2). Solutions to these tasks are presented in subsequent chapters in the same sequence as shown in Table 1.2.

Table 1.2 Tasks and methods used to fulfil the tasks

What?	How?
Select a process to desulphurize biogas knowing that the absorption process will be used to separate CO_2	from literature
Define criteria to shortlist absorption solvents, capable of absorbing CO_2 from biogas, and select the best absorption solvent	from literature and experiments
Collate properties of the selected solvent (aqueous diglycolamine)	from literature
Determine unknown solvent properties (equilibrium CO_2 solubility, density, viscosity and surface tension)	from experiments
Select optimal diglycolamine content in the solvent and optimal desorption temperature	from experiments
Setup a thermodynamic model to simulate equilibrium CO_2 solubility in aqueous diglycolamine solvents	from literature and experiments
Revamp the test rig: change the solvent and increase the gas-treating capacity	from own concept and experiments
Determine the optimal liquid to gas ratio and heat demand of the absorption process	from experiments
Design a model absorption plant to separate CO_2 from biogas: a scale up	from own concept and experiments
Devise a method to quantitatively compare hazards of absorption solvents and determine the disposition of the German population towards hazards from biogas plants	from own concept and experiments
Determine the environmental impacts of biomethane and compare them with those of natural gas	from literature and experiments

2 INTRODUCTION AND STATE OF THE ART

Background information on biogas treatment and the absorption process is presented in this chapter. Inferences drawn from this information that have guided the research towards its aim of developing an improved biogas-treatment process are highlighted at the end of each subchapter.

2.1 BOUNDARY CONDITIONS

When developing a process to upgrade biogas to biomethane, at the outset, input parameters (biogas composition) and output parameters (prerequisites for injecting biomethane in a natural-gas pipeline) must be identified.

2.1.1 BIOGAS COMPOSITION

The fermentation process in the biogas reactor (fermenter) mainly converts biomass into CH_4, CO_2, H_2O, H_2S and ammonia (NH_3). The proportion of these components depends on the substrate used (biomass used in the fermenter). In some cases, aromatic hydrocarbons (benzene, toluene, ethylbenzene, xylene and cumene), and mercaptans (organosulphur compounds) such as methanethiol (CH_3-SH) and ethanethiol (CH_3CH_2-SH) are produced. Occasionally, biogas also contains chlorine, fluorine and siloxanes. Depending upon reactor construction and operation, oxygen (O_2) and other air components can be found in biogas. The typical components of biogas are enlisted in Table 2.1. For a model biogas-treatment process, the biogas composition shown under "Design value" in Table 2.1 was selected based upon data available in literature and plant-specific analyses (Klinski, 2006). "BDL" in Table 2.1 is the acronym for below detectable limit, and "BTX" stands for benzene, toluene and xylene.

2.1.2 PREREQUISITES FOR INJECTING BIOMETHANE IN A NATURAL-GAS PIPELINE

In Germany, paragraph 36 of *Gasnetzzugangsverordnung* (2010), describes the prerequisites for injecting biomethane in the natural-gas pipeline. Paragraph 36 specifies that the gas quality requirements stipulated by the manual G 260 DVGW (Deutsche Vereinigung des Gas- und Wasserfachs e.V.) should be fulfilled by biomethane. The pipeline specifications for High (H) and Low (L) calorific natural gas are shown in Table 2.2. Biomethane can be injected in high pressure (HP) pipelines (2 to 120 bar), medium pressure (MP) pipelines (1,1 to

2,0 bar) or low pressure (LP) pipelines (1,0 to 1,1 bar) (Klinski, 2006). As biogas is produced at atmospheric pressure and gas pressurization costs energy, biomethane injection should be preferred at near-atmospheric pressure, i.e. in MP and LP pipelines.

Table 2.1 Biogas composition

Component	Range	Average	Design value
CH_4 / vol. %	45 to 70	60	57
CO_2 / vol. %	25 to 55	35	39,7
N_2 / vol. %	0,01 to 5	1	0,01
O_2 / vol. %	0,01 to 2	0,3	0,01
H_2S / vol. %	0,01 to 3	0,05	0,31
Mercaptans / ppm	0,1 to 30	0,1	BDL
NH_3 / ppm	0,01 to 2,5	0,7	BDL
BTX / ppm	0,1 to 5	0,1	BDL
Siloxanes / ppm	0,1 to 5	0,1	BDL
H_2O / vol. %	2 to 4	3,1	3,1

Table 2.2 Pipeline specifications of High (H) and Low (L) calorific natural gas

Parameter	Prerequisite	
	H-Gas	L-Gas
O_2 / vol. %	< 3	
Temperature	> dew point in pipeline	
H_2S / ppm	< 5	
Wobbe index / $MJ \cdot m^{-3}$	46,1 to 56,5	37,8 to 46,8
Heating value / $MJ \cdot m^{-3}$	30,2 to 47,2	
Relative density / -	0,55 to 0,75	
CH_4 / vol. %	> 96	> 90
CO_2 / vol. %	< 4	< 10

Inferences

The process of upgrading biogas to biomethane includes the removal of solids, liquids (e.g. H_2O) and certain gases (e.g. CO_2, H_2S) from biogas. The target biomethane composition is 96 vol. % CH_4 and 4 vol. % CO_2. Biogas is available at atmospheric pressure, and biomethane should be preferably injected in the natural-gas distribution grid at near-atmospheric pressure (< 2 bar).

2.2 DESULPHURISATION

Sulphur (S) mainly occurs as H_2S in biogas in concentrations from 100 to 30000 ppm or from 0,01 to 3 vol. %. The exact concentration depends on the substrate used during fermentation and on the process conditions prevalent in the fermenter.

H_2S is an extremely poisonous, corrosive and flammable gas. The Federal Ministry of Environment, Nature Conservation and Nuclear Safety in Germany states in its technical instructions on air quality control (*TA Luft*) that H_2S emissions into the atmosphere may not exceed 3 ppm or 15 $g \cdot h^{-1}$. Apart from that, the maximum permissible H_2S concentration in biomethane is 5 ppm (Table 2.2). Therefore, H_2S must be separated from biogas at the earliest and converted into an innocuous form (e.g. elemental sulphur).

A quintessential H_2S-removal process not only fulfils the obligatory standards, but also possesses two further attributes:

- The process converts H_2S into a useful product that saves resources, necessary for subsequent disposal of the sulphur-containing product.
- The process does not adversely affect the performance of subsequent biogas-treatment processes such as CO_2 absorption.

Typically, biogas desulphurisation is divided into rough and fine desulphurisation where H_2S concentration is reduced to about 100 ppm in the first step and to less than 5 ppm in the second step. A desulphurisation process includes H_2S separation and conversion. This occurs either simultaneously or individually; some conversion processes include an inherent separation function. Two processes are predominantly used for H_2S separation: adsorption and absorption.

Adsorption: Adsorption is the adhesion of atoms or molecules to a solid surface. When a mixture of gases is passed over a solid adsorbent, certain gases tend to be more adsorbed than others. This selective adsorption can be based upon the size of the molecule relative to the structure of the adsorbent, the kinetics of the adsorption process, or the charge and polarity of the gas molecules and the adsorbent material. Typical industrial adsorbents are activated carbon, silica gel, alumina and zeolite. High pressure facilitates adsorption of gases on solid surfaces, whereas pressure reduction regenerates the adsorbent (the solid is freed of the gas). In pressure swing adsorption (PSA), two adsorbent vessels are utilized where one is pressurized and the other is depressurized; subsequently, pressure is switched. This cyclic switching of pressure allows for continuous separation (Kohl and Nielsen, 1997).

Absorption: In absorption, a gas (solute) is transferred from the gas phase into a liquid (solvent) wherein the gas reacts chemically with the solvent and/or physically dissolves in the solvent. Absorption is different from adsorption in that gas molecules undergoing absorption are taken up by the entire volume of the liquid and not just by the surface, which is the case in adsorption (Kohl and Nielsen, 1997). The process of removing the solute from the solvent is called as desorption. Stripping is the process wherein a gas stream carries away the solute (dissolved gas) with it, thereby freeing the solvent of the solute. The stripping gas can be endogenous (vapours of the solvent, e.g. steam) or exogenous (a strip gas, e.g. air).

The output gas stream of a separation process is concentrated with H_2S, and a conversion process should be used to convert H_2S into a less malign product.

H_2S-removal processes can be classified according to their mode of operation into four categories (Kohl and Nielsen, 1997):

Gas-phase oxidation: H_2S is oxidized in the gas phase itself to elemental sulphur in the presence of a catalyst.

Liquid-phase oxidation: The H_2S-containing gas stream is brought in contact with a liquid in which H_2S gets absorbed. Subsequently, H_2S is oxidized to elemental sulphur either chemically or biologically.

Liquid scavenging: The process employs a sacrificial liquid (scrubbing liquid) that comes in contact with the H_2S-containing gas stream in a bubble column or a spray tower.

Solid scavenging: A solid (adsorbent) is used to bind H_2S on its surface where it chemically reacts with the adsorbent, thereby converting H_2S into an innocuous product.

Characteristics of major H_2S-removal processes are shown in Table 2.3, and they are briefly described in Appendix A. Table 2.3 can be used to select a process that is suitable to desulphurize a given gas mixture.

Inferences

To upgrade biogas to biomethane, total desulphurisation of biogas is necessary which can be achieved by combining rough and fine desulphurisation. The choice of the desulphurisation process depends on biogas characteristics such as gas load (volume), H_2S and O_2 concentration, as well as on the desired H_2S separation (H_2S concentration in the treated gas).

Table 2.3 Characteristics of H_2S-removal processes

Process / technology	Treatment range	End purity	End form of sulphur	Oxygen demand	Regeneration
Modified Claus process	> 15 tpd sulphur	< 20000 ppm	sulphur	yes	no
LO-CAT process	0,2 to 20 tpd sulphur	< 10 ppm	sulphur	yes	no
Biological desulphurisation	> 500 ppm	< 100 ppm	sulphates	yes	yes
Liquid scavenging (with aqueous triazine or aqueous glyoxal)	< 25 kg sulphur· day^{-1}	< 100 ppm	organic, cyclic sulphur compounds	no	no
THIOPAQ process	10 kg to 50 tpd sulphur	< 50 ppm	sulphur	no	yes
SulfaCheck process	< 2000 ppm	< 50 ppm	sulphur	no	no
Solid scavenging with zinc oxide	< 30 ppm	< 1 ppm	zinc sulphate	no	no
Solid scavenging with iron sponge or SulfaTreat process	25 to 200 kg sulphur· day^{-1}	< 100 ppm	ferric sulphide	no	no
Solid scavenging with activated carbon	< 150 ppm	< 5 ppm	sulphur or sulphuric acid	yes	no
Solid scavenging with impregnated activated carbon	< 150 ppm	< 5 ppm	sulphur	no	no

If chemical absorption is planned for CO_2 separation, desulphurisation processes that do not require O_2 for operation must be selected because the unconsumed O_2 will react with the absorption solvent and degrade it. For biogas units handling more than 200 kg sulphur per day, the LO-CAT process combined with selective H_2S separation or the THIOPAQ process is recommended for rough desulphurisation. In biogas units that deal with less than 200 kg sulphur per day, the THIOPAQ process should be used for rough desulphurisation.

If adsorption or physical absorption is planned for CO_2 separation, desulphurisation processes can be selected from a larger palette. In addition to the LO-CAT and the THIOPAQ processes, biological desulphurisation is also suitable for rough desulphurisation.

Activated carbon (solid scavenging) is recommended for fine desulphurisation. Activated carbon can be impregnated with an oxidizer (e.g. potassium permanganate ($KMnO_4$)) if the presence of O_2 in biogas is undesired. If the desired H_2S concentration is less than 1 ppm, zinc oxide (ZnO) should be used as a solid scavenger (Dixit and Mollekopf, 2014c).

2.3 CO_2 SEPARATION USING ABSORPTION

For the production of H-Gas in Germany, CO_2 content in biogas should be reduced from around 40 vol. % to less than 4 vol. %. Although the presence of CO_2 in biogas is undesired, pure CO_2 is a valuable product. CO_2 can be used in several manufacturing processes (e.g. in the production of carbonated beverages) (Lutsch, 2013).

Four major processes are being used to separate CO_2 from biogas: adsorption, absorption, permeation (membrane separation) and cryogenic separation. Absorption is the most suitable process to separate CO_2 from biogas as justified in Section 1.2.

2.3.1 STATE-OF-THE-ART ABSORPTION SOLVENTS

The key component of the absorption process is the absorption solvent. Absorption solvents can be classified according to their method of CO_2 capture: chemical, physical and hybrid solvents.

Chemical solvent: The solvent reacts chemically with CO_2, and a chemical bond is formed between the solvent and CO_2.

Physical solvent: CO_2 is dissolved in the solvent; van der Waal forces (physical bonds) hold the solvent and CO_2 together.

Hybrid solvent: Chemical and physical bonds are formed between the solvent and CO_2.

Chemical and physical solvents have been used till date to separate CO_2 from biogas (Dixit et al., 2012). The performance of these solvents as presented in the report of Fachagentur für Nachwachsende Rohstoffe e.V. (2012) is shown in Table 2.4.

When a physical absorption solvent such as water is used, methane slip is large (above 1 vol. %) (Table 2.4), and the off gas must be additionally treated (e.g. using a regenerative thermal oxidizer). This is a twofold problem: firstly, CH_4, a valuable commodity, is lost, and secondly, off-gas treatment exacts extra costs. Moreover, CH_4 is a greenhouse gas, which is around 20 times more harmful than CO_2. Therefore, CH_4 emissions must be avoided.

When physical absorption solvents are used, the operating pressure in the absorber is typically above 4 bar (Table 2.4): physical solvents are recommended for CO_2 separation when CO_2 partial pressure is above 1 bar. As biogas is produced at atmospheric pressure, it must be compressed before it enters the absorber, and this costs energy. A substantial

amount of the compression energy is lost when the separated CO_2 is let off into the atmosphere as CO_2 makes up around 40 vol. % of biogas. Furthermore, if biomethane is injected in the gas-distribution grid at near-atmospheric pressure, the compression energy stored in biomethane is also lost. Thus, physical absorption is an electricity-intensive operation, which can turn out to be energy inefficient.

Table 2.4 Process characteristics of chemical and physical absorption solvents

Parameter	Chemical solvent (e.g. monoethanolamine)	Physical solvent (e.g. water)
Pretreatment	yes	no
Operating pressure / bar	1 to 2	4 to 7
Methane slip / vol. %	< 0,1	1 to 2
Product purity / vol. %	> 99	~ 97
Electrical duty / kWh·(Nm^3 biogas)$^{-1}$	0,06 to 0,15	0,23 to 0,33
Heat duty / kWh·(Nm^3 biogas)$^{-1}$	0,5 to 0,8	~ 0,3

Chemical absorption solvents are, however, not veritably impeccable. They have two notable downsides: chemical solvents need a lot of heat during desorption (Table 2.4), and they react with O_2. If waste heat from a cogeneration plant is used for desorption, the first drawback can be overcome, and by using desulphurisation processes that do not require O_2 for operation, the second drawback can also be overcome.

Thus, chemical absorption is the most attractive option for separating CO_2 from biogas at atmospheric pressure. However, not all chemical absorption solvents available in the market are recommended for separating CO_2 from biogas. The blanket hint presented in Klinski (2006) and Urban et al. (2009) that absorption solvents that have been used to treat natural gas, syngas and flue gas can be used to treat biogas is misleading.

2.3.2 SEARCH FOR THE SUITABLE ABSORPTION SOLVENT

Information was compiled about 31 popular absorption solvents that have been used on a commercial scale for separating CO_2 and/or H_2S. Solvents were deemed suitable if they function at atmospheric pressure and absorb CO_2 or CO_2-and-H_2S. Solvents that have a small differential CO_2 loading at atmospheric pressure and ambient temperature or are designed to primarily separate other impurities (e.g. mercaptans, carbonyl sulphide) were considered to have low suitability (Dixit et al., 2012). The segregation of solvents is shown in Figure 2.1.
A quintessential absorption solvent has not only a large CO_2 loading, but also low volatility, high reaction rate, unrestricted access in the market and low hazard potential. As shown in Figure 2.1, diglycolamine (DGA) or amino-diethylene glycol (ADEG) or

2-(2-aminoethoxy)ethanol was selected as the most appropriate absorption solvent. Specific reasons for excluding other solvents are presented in Appendix B.

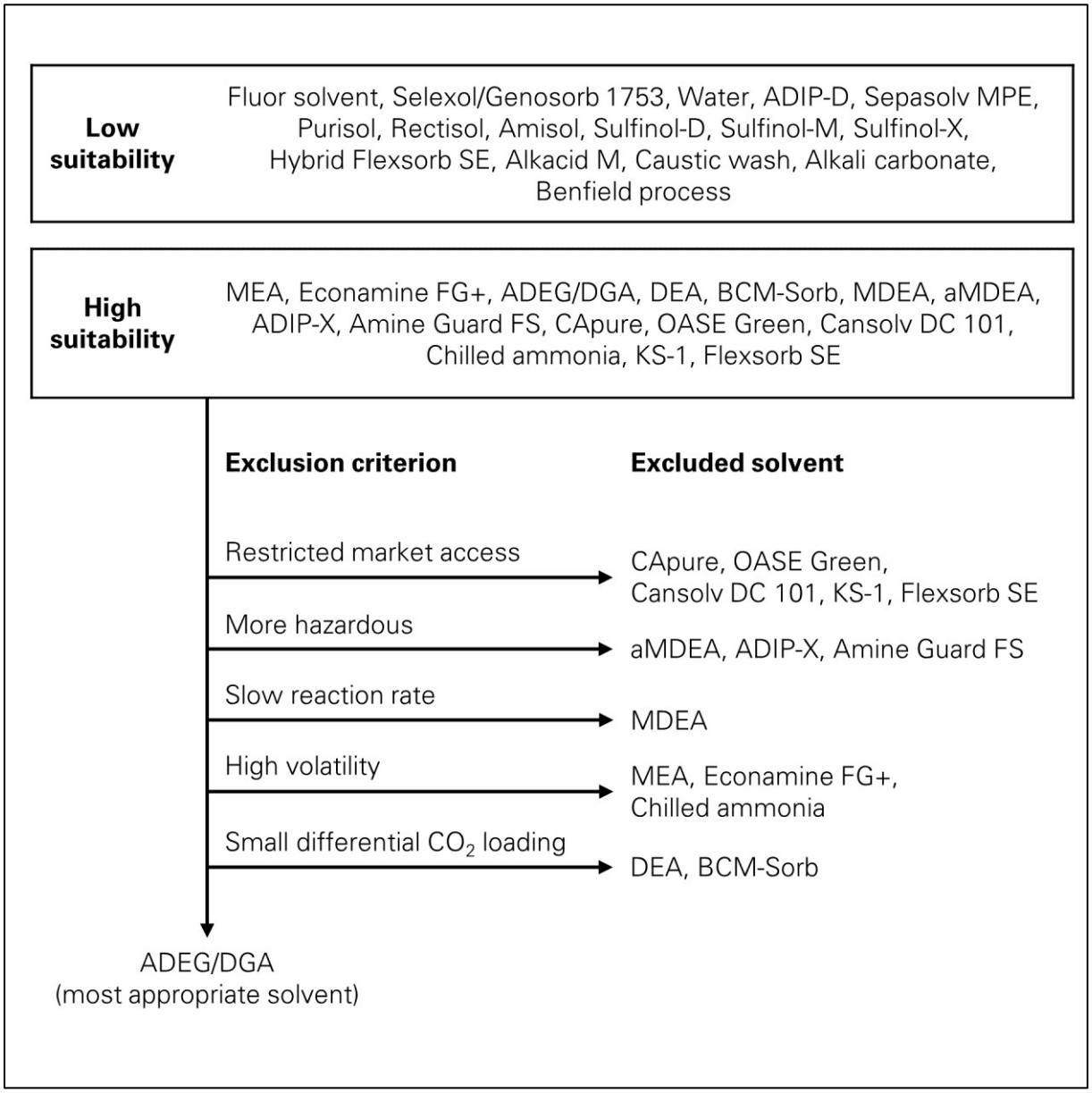

Figure 2.1 Segregation of absorption solvents

Inferences

When biomethane injection is intended at near-atmospheric pressure (< 2 bar), chemical absorption should be used to separate CO_2 from biogas. The feed gas to the absorption process must be free of H_2S and O_2. The absorber and desorber should be operated at atmospheric pressure, and the absorber temperature should be near ambient temperature.

Factors that influence the choice of the absorption solvent include differential CO_2 loading, volatility, reaction rate and safety. Diglycolamine (DGA) or amino-diethylene glycol (ADEG) is the most appropriate solvent to separate CO_2 from biogas at atmospheric pressure.

2.4 AQUEOUS DIGLYCOLAMINE AS AN ABSORPTION SOLVENT

In 1955, the patent proposing the use of DGA for acid-gas treatment was issued to Fluor Corporation (Blohm and Riesenfeld, 1955). The company has changed hands since then and is currently owned by the Huntsman Corporation. The first commercial-scale natural-gas-treating plant that used DGA was started in El Paso, USA in 1965 (Holder, 1966). Since then, aqueous DGA solvents with DGA content varying from 40 to 70 mass (wt.) % have been used to treat gases with 0,5 to 25 mol % CO_2 at pressures from 1 to 80 bar at temperatures from 25 to 55 °C (Moore et al., 1984).

The research question posed now is, "what is the optimal proportion of DGA and water in the solvent?" In order to answer this question and subsequently design an absorption plant, thermodynamic and transport properties of aqueous DGA must be determined. In the DGA datasheet provided by Huntsman Corporation (2005), properties such as pH, surface tension, vapour pressure, viscosity, density and thermal conductivity of pure and aqueous DGA can be found. In addition, information on the effects of CO_2 loading on viscosity and density is presented. Other data available in literature are as follows: reaction enthalpies of CO_2 with aqueous DGA (Hikita et al., 1977; Christensen et al., 1986), heat capacity of aqueous DGA (Chiu and Li, 1999), reaction kinetics of CO_2 with aqueous DGA (Hikita et al., 1977; Alper, 1990; Al-Juaied and Rochelle, 2006a), density and viscosity of aqueous DGA (Hikita et al., 1981; Henni et al., 2001), and CH_4 solubility in aqueous DGA (Jou et al., 1998). The property of aqueous DGA that crucially influences the absorption plant design is the equilibrium CO_2 solubility α_{CO2}.

2.4.1 EXPERIMENTAL DATA ON EQUILIBRIUM CO_2 SOLUBILITY

In literature, an array of data on α_{CO2} in aqueous DGA solvents is available. The conditions under which α_{CO2} was determined are shown in Table 2.5. In the past, aqueous solvents with DGA content varying from 20 to 65 wt. % have been experimentally investigated. The investigated range of CO_2 partial pressure p_{CO2} is large which can be ascribed to the variety of gases treated by DGA, i.e. associated gas at low pressures (approximately 1 bar) and natural gas at high pressures (up to 65 bar). The predominantly investigated temperatures are from 25 to 60 °C (absorption conditions). There is a dearth of α_{CO2} data determined under desorption conditions (temperatures above 90 °C).

As seen in Table 2.5, different apparatuses have been used to determine α_{CO2}: bubble column, stirred or shaken-cell reactor, and wetted-wall column. This variety can be ascribed to the aims of the experiments (e.g. using the wetted-wall column, reaction kinetics can be investigated in addition to determining α_{CO2}), and to the available resources.

Table 2.5 Experimental conditions (apparatus used, DGA mass fraction w_{DGA}, temperature T, and CO_2 partial pressure p_{CO2}) under which equilibrium CO_2 solubility was determined in the past

Source	**Apparatus**	$\mathbf{w_{DGA}}$ **kg DGA· (kg DGA+H_2O)$^{-1}$**	**T °C**	$\mathbf{p_{CO2}}$ **kPa**
Martin et al., 1978	bubble column	0,60	50	1,6 to 300
		0,60	100	2,5 to 302
Dingman et al., 1983	shaken-cell filled with DGA into which gas was injected	0,65	38	7, 12, 188
		0,65	82	6, 11, 196
Maddox et al., 1987	shaken-cell filled with gas into which DGA was injected	0,20	25	10 to 5700
		0,40	40	10 to 4000
		0,40	60	10 to 4000
		0,60	50	7 to 6500
Pacheco et al., 2000	wetted-wall column	0,25	35	0,47
		0,25	60	4,85
		0,50	40	0,001 to 0,055
Al-Juaied and Rochelle, 2006b	wetted-wall column	0,65	25	0,02 to 0,74
		0,65	40	0,01 to 2,12
		0,65	60	0,14 to 14,8
Chen et al., 2011	wetted-wall column	0,50	40	0,02 to 5,8
		0,50	60	0,1 to 26,9
		0,50	80	1 to 50
		0,50	100	6 to 18
Xu and Rochelle, 2011	stirred-cell reactor	0,50	100	57 to 356

After comparing α_{CO2} data, it can be concluded that data sets are not in harmony with each other. At low pressures (15 to 150 kPa), data from Dingman et al. (1983) deviates from the data presented by Maddox et al. (1987).

In addition to experiments, α_{CO2} can also be determined by simulations.

2.4.2 SIMULATED DATA ON EQUILIBRIUM CO_2 SOLUBILITY

α_{CO2} in aqueous DGA can be calculated using the Henry's law when mole fraction x of the gas in the solvent is approaching 0: Henry's law can be practically used when x is between 0 and 0,5. Equation 2.1 depicts the Henry's law for CO_2 where k_H is the Henry's constant. $\emptyset$ is the fugacity coefficient, and γ is the activity coefficient, and they represent the degree of non-ideality of the gas and the liquid phase, respectively (Prausnitz et al., 1999). The derivation of Equation 2.1 is shown in Appendix C.

$$p_{CO2}\emptyset_{CO2} = x_{CO2}\gamma_{CO2}k_H \qquad 2.1$$

When calculating equilibrium CO_2 solubility, p_{CO2} is given, and the task is to calculate x_{CO2} or vice-versa. The usual solution is as follows: k_H is retrieved from a databank, and thermodynamic models are used to estimate $\emptyset$ and γ.

Table 2.6 Models used in literature to simulate equilibrium CO_2 solubility in DGA solvents

Source	Fugacity coefficient model	Activity coefficient model
Dingman et al., 1983	Redlich-Kwong	Bromley
Hu and Chakma, 1990	Kent-Eisenberg	
Weiland et al., 1993	Peng-Robinson	Deshmukh-Mather
Al-Juaied and Rochelle, 2006b	Soave-Redlich-Kwong	electrolyte NRTL
Chen et al., 2011	semi-empirical correlation	
Xu and Rochelle, 2011	empirical correlation	

An equation of state is a mathematical relation in between the state variables and can be used to calculate $\emptyset$. The well-known Ideal Gas law is an equation of state that is valid under ideal conditions only; therefore, it cannot be applied to the CO_2-aqueous DGA system. Under real (non-ideal) conditions, two equations of state are predominantly used to calculate $\emptyset$: Virial equation and cubic equation of state (Prausnitz et al., 1999). The Virial equation consists of several substance-specific coefficients, but since these coefficients for DGA are not available, the Virial equation cannot be used. Cubic equations of state are modified versions of the van der Waal equation and are bestowed with the adjective "cubic" because pressure can be written as a cubic function of the molar volume. Three cubic equations of state have been used in the past to calculate $\emptyset$ of components in the CO_2-aqueous DGA system (Table 2.6): Redlich-Kwong (Redlich and Kwong, 1949), Soave-Redlich-Kwong (Soave, 1972), and Peng-Robinson (Peng and Robinson, 1976) equations. These equations differ in their method of calculating the attractive pressure due to intermolecular forces. A detailed description of the equations of state can be found in Poling et al. (2001). All three

equations are suitable to calculate $\emptyset$, but in order to select the most suitable equation, further investigations are necessary.

The ability of a cubic equation of state to estimate the fugacity of liquids (high-density fluids) or the activity coefficient γ is limited (Prausnitz et al., 1999). Therefore, other models are used to estimate γ of components in the liquid phase.

The liquid phase of the CO_2-aqueous DGA system is an electrolytic solution in which ions (charged species) are present. Coulombic forces act on ions, and these forces have a longer range than the van der Waal forces. Coulombic forces were first reckoned with in the Debye-Hückel theory, which was proposed to calculate γ of electrolytic solutions (Prausnitz et al., 1999). Therefore, a model based on this theory is suitable to calculate γ of components in the CO_2-aqueous DGA system. The models of Bromley (1973), Deshmukh and Mather (1981) and the electrolyte non-random two liquid (eNRTL) model (Chen et al., 1982; Chen and Evans, 1986) have been used in the past to calculate γ (Table 2.6) and consider the long-range forces in their calculations. However, each model incorporates other forces too, and therein lies the difference between the models. Readers can refer to Zemaitis et al. (1986) for a discourse on electrolytic solutions including the development of the various models. Therefore, the most suitable model to calculate γ can be selected only after further investigations.

The study by Hu und Chakma (1990) confirms that it is crucial to estimate $\emptyset$ and γ correctly. They used the empirical Kent-Eisenberg model (Kent and Eisenberg, 1976) to estimate equilibrium CO_2 solubility α_{CO2} wherein $\emptyset$ and γ were assumed to be unity. Predicted and experimental data deviated substantially at high temperatures (> 100 °C) and low CO_2 partial pressures (< 100 kPa). Therefore, the non-idealities of the vapour-liquid system must be reckoned with.

Inferences

DGA has never been used in concentrations above 70 wt. % in solvent, although there is a motivation to increase DGA content in the solvent because an increase in primary amine (e.g. DGA) content increases CO_2 loading. Therefore, aqueous DGA solvents with DGA content varying from 50 to 100 wt. % must be systematically investigated.

No equilibrium CO_2 solubility data for aqueous DGA solvents with DGA content varying from 65 to 100 wt. % has been published. Furthermore, discrepancies can be found amongst experimental data itself and also amongst experimental and modelled data. Therefore, it is

necessary to experimentally determine equilibrium CO_2 solubility at absorption conditions (temperature $T \sim 30$ °C) and at desorption conditions ($T > 90$ °C).

Density, viscosity and surface tension of the raw solvent (aqueous DGA without CO_2) are available in literature, but raw solvent is transiently present in an absorption plant. Properties of solvent loaded with CO_2 are decisive, and these properties must be determined. Huntsman Corporation (2005) is the lone source that presents the effects of CO_2 loading on solvent density and viscosity; this data is noteworthy, but not comprehensive. In case of surface tension of CO_2-loaded solvents, no data at all is available. Therefore, it is imperative to experimentally determine density, viscosity and surface tension of the solvents before absorption (raw form), after absorption (spent form) and after desorption (lean form).

Equilibrium CO_2 solubility in aqueous DGA solvents can be determined by simulations. Several models have been used in simulations, but a best model or a combination thereof cannot be easily selected. To determine the fugacity coefficient, a cubic equation of state should be used, but the choice of the cubic equation is a research question. To determine the activity coefficient, a thermodynamic model that is suitable for electrolytic solutions should be used, but the specific model choice is again a research question. Once the model is setup, simulations can also be used to design an absorption plant.

2.5 ABSORPTION-PROCESS DESIGN

A simplified absorption-process scheme is shown in Figure 2.2. In the absorber, the feed gas or biogas enters at the bottom and flows to the top, whereas the absorption solvent flows in the opposite direction (a countercurrent operation). Inside the absorber, CO_2 is transferred from the gas into the solvent, and the solvent loaded with CO_2 (spent solvent) flows into the stripper. Inside the absorber, the gas stream with little or no CO_2 exits the absorber at the top as treated gas or biomethane. In the stripper, the spent solvent is heated by the reboiler, thereby releasing CO_2, which exits as off gas at the stripper top. The solvent then, almost free of CO_2 (lean solvent), flows back into the absorber (Sattler, 1995; Kohl and Nielsen, 1997). As CO_2 absorption is facilitated by lower temperatures and CO_2 desorption by higher temperatures, a heat exchanger is employed to transfer heat from the lean solvent to the spent solvent.

The foremost task in designing an absorption process is to determine the solvent flow rate necessary to treat the given gas.

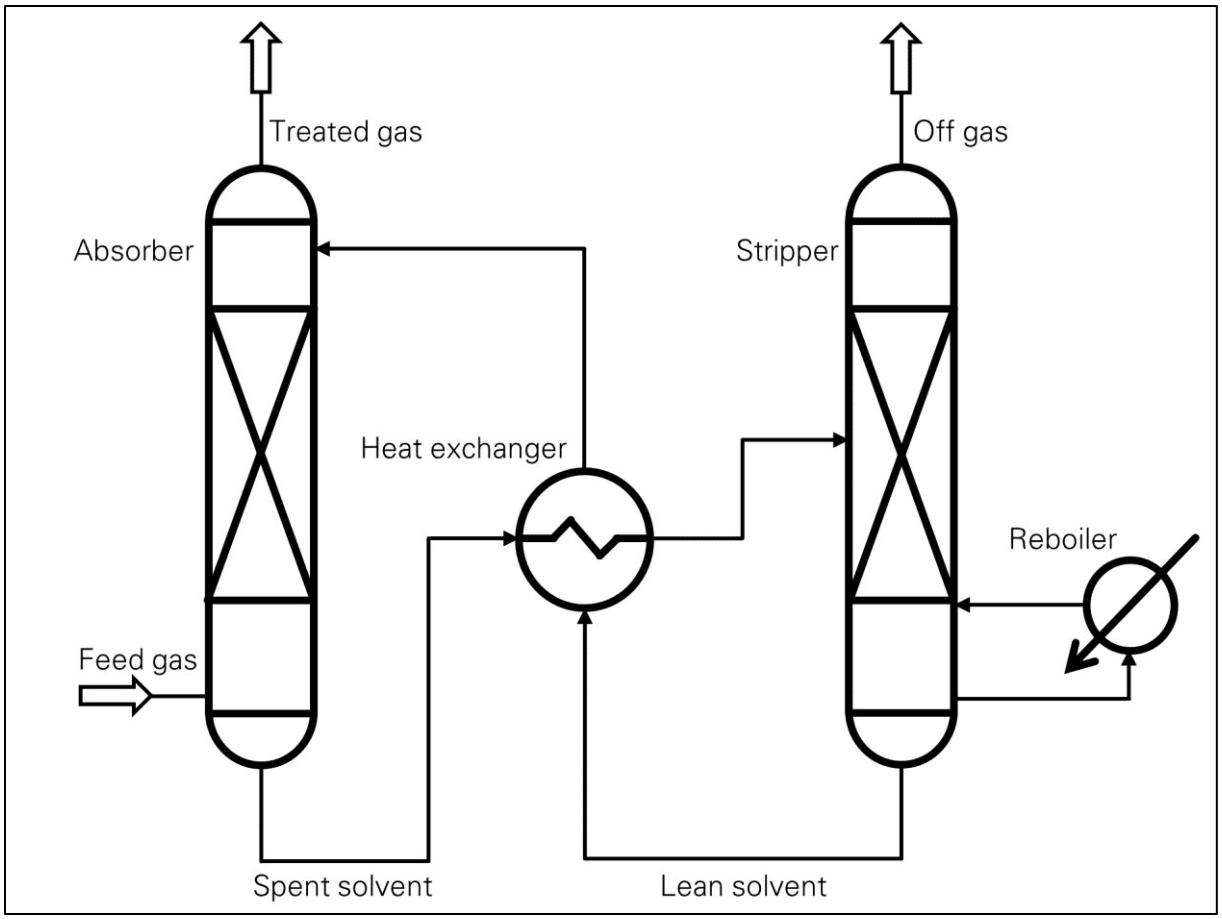

Figure 2.2 Simplified absorption-process scheme

2.5.1 SOLVENT FLOW RATE

Assuming that the solvent has been shortlisted, this section describes how the solvent flow rate is determined. At first, using a mass balance, the minimum solvent flow rate that is necessary is estimated, and then, by applying heuristics and conducting calculations, the ultimate solvent flow rate is determined.

Parameters necessary to conduct a mass and component balance across a column (an absorber or a stripper) are shown in Figure 2.3. These parameters are unambiguously defined in Table 2.7 and are also included in the list of symbols.

The mass balance across the column is given by Equation 2.2, and the component balance by Equation 2.3a.

$$L_{m,in} + G_{m,in} = L_{m,out} + G_{m,out} \qquad 2.2$$

$$x_{in}L_{mo,in} + y_{in}G_{mo,in} = x_{out}L_{mo,out} + y_{out}G_{mo,out} \qquad 2.3a$$

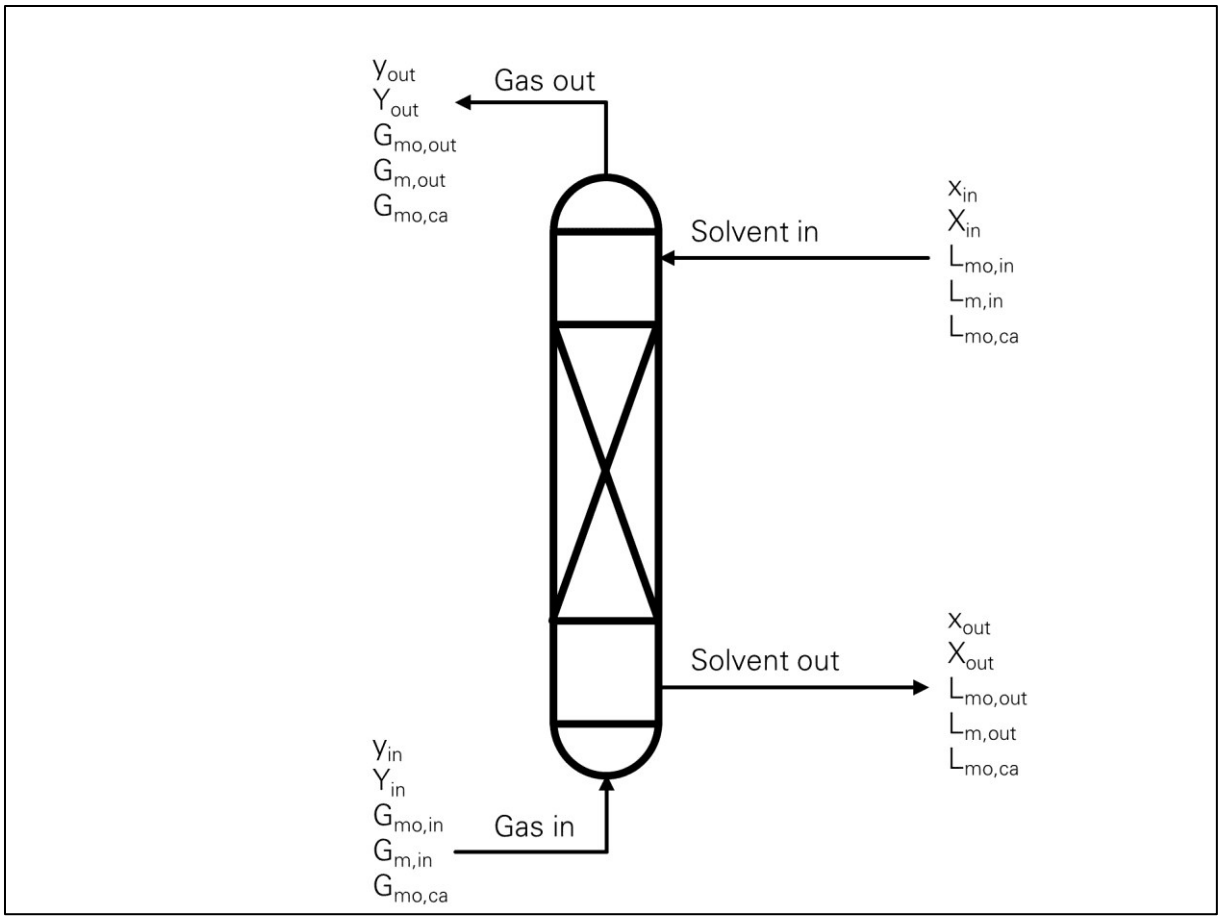

Figure 2.3 Column parameters

In a column, as CO_2 is transferred from one phase into another, the concentration of CO_2 in a phase and the total solvent and gas flow rates change continuously. However, the carrier solvent and carrier gas flow rates do not change. Thus, the component balance can be rewritten as Equation 2.3b, which is mathematically simpler than Equation 2.3a.

$$G_{mo,ca}(Y_{in} - Y_{out}) = L_{mo,ca}(X_{out} - X_{in}) \qquad 2.3b$$

Presenting CO_2 content as moles of CO_2 per mole carrier fluid (X or Y) offers a mathematical advantage: as the solvent and gas flow through the column, only the numerator in X or Y changes; the denominator remains constant. The relation between capital X and small x and capital Y and small y is shown in Equation 2.4.

$$X = \frac{x}{1-x} \qquad 2.4a$$

$$Y = \frac{y}{1-y} \qquad 2.4b$$

Table 2.7 Column parameters for a gas stream of CO_2 and CH_4 and a solvent stream of aqueous DGA

Symbol	Definition	Unambiguous unit
y	mole fraction of the component in the gas phase	mol CO_2·(mol CO_2+CH_4)$^{-1}$
Y	moles of the component in gas per mole carrier gas (mole ratio)	mol CO_2·(mol CH_4)$^{-1}$
G_{mo}	total molar flow of gas	(mol CO_2+CH_4)·h^{-1}
G_m	total mass flow of gas	(kg CO_2+CH_4)·h^{-1}
G_v	total volumetric flow of gas	(Nm^3 CO_2+CH_4)·h^{-1}
$G_{mo,ca}$	molar flow of carrier gas	mol CH_4·h^{-1}
$G_{m,ca}$	mass flow of carrier gas	kg CH_4·h^{-1}
$G_{v,ca}$	volumetric flow of carrier gas	Nm^3 CH_4·h^{-1}
x	mole fraction of the component in the liquid phase	mol CO_2·(mol CO_2+DGA+H_2O)$^{-1}$
X	moles of the component in liquid per mole carrier solvent (mole ratio)	mol CO_2·(mol DGA+H_2O)$^{-1}$
L_{mo}	total molar flow of solvent	(mol CO_2+DGA+H_2O)·h^{-1}
L_m	total mass flow of solvent	(kg CO_2+DGA+H_2O)·h^{-1}
L_v	total volumetric flow of solvent	(Nm^3 CO_2+DGA+H_2O)·h^{-1}
$L_{mo,ca}$	molar flow of carrier solvent	(mol DGA+H_2O)·h^{-1}
$L_{m,ca}$	mass flow of carrier solvent	(kg DGA+H_2O)·h^{-1}
$L_{v,ca}$	volumetric flow of carrier solvent	(Nm^3 DGA+H_2O)·h^{-1}

The component balance across any cross section in the column will have the same form as Equation 2.3b; thus, X and Y at any particular point inside the column are related as shown in Equation 2.5. Y is a linear function of X, and the segment between the coordinates (X_{in}, Y_{out}) and (X_{out}, Y_{in}) is called the operating line.

$$Y = \left(\frac{Y_{in}-Y_{out}}{X_{out}-X_{in}}\right)X + \left(\frac{Y_{out}X_{out}-Y_{in}X_{in}}{X_{out}-X_{in}}\right) \qquad 2.5a$$

$$Y = \left(\frac{L_{mo,ca}}{G_{mo,ca}}\right)X + \left(\frac{Y_{out}G_{mo,ca}-X_{in}L_{mo,ca}}{G_{mo,ca}}\right) \qquad 2.5b$$

The operating line (Equation 2.5) can also be formulated in terms of x and y, but then, $y = f(x)$ will not be a linear function (Treybal, 1981), but a concave downward curve. If the concentration of the component that is to be separated is small ($y \leq 0{,}1$), the gas is termed as "dilute", and $y \approx Y$ and $x \approx X$ (McCabe et al., 1993). Moreover, solvent and gas flow rates can be assumed to remain constant throughout the column: $G_{m,in} = G_{m,out}$ and $L_{m,in} = L_{m,out}$. Thus for dilute gases, the operating-line equation is reduced to Equation 2.5c, which is often found in university textbooks (Henley et al., 2011). The opposite of a dilute gas is a

concentrated gas wherein the concentration of the component that is to be separated is large. For concentrated gases, the previously mentioned assumptions do not apply, and the use of Equation 2.5c for concentrated gases is erroneous.

$$y = \left(\frac{L_{mo}}{G_{mo}}\right) x + y_{out} - \left(\frac{L_{mo}}{G_{mo}}\right) x_{in} \qquad 2.5c$$

CO_2 content at equilibrium in the gas and liquid phase are mathematically related by an equilibrium curve $Y^* = f(X)$ or $y^* = f(x)$ where the slope of the equilibrium curve is denoted as *sl*. The equilibrium CO_2 solubility values are denoted by adding the superscript "*" to the symbols y, Y, x and X. The function $y^* = f(x)$ is a line in the region where x approaches 0: here *sl* is constant and is equal to the Henry's constant. The form of the function $y^* = f(x)$ cannot be generically stated for the entire range of x, i.e. between 0 and 1. Nevertheless, $y^* = f(x)$ can be approximated by a line or an exponential function for a smaller range of x. Similarly, $Y^* = f(X)$ can also be approximated.

While designing an absorption plant, the absorber is designed at first, followed by the stripper. The quantity and composition of the feed gas are given, and the composition of the treated gas is specified. Thus the parameters $G_{mo,ca}$, Y_{in} and Y_{out} for the absorber are given. Subsequently, the solvent is selected, and the vapour-liquid equilibrium data for the solute-solvent system at the absorption and desorption temperatures is ascertained. Thus $Y^* = f(X)$ is determined for the absorber and the stripper. In the case that no exogenous strip gas is used, the minimum possible solute concentration in the solvent at absorber inlet X_{in} is the equilibrium solute concentration at the reboiler temperature in the stripper.

The graphical method for determining the minimum molar solvent flow rate $L_{mo,ca,min}$ is illustrated with the help of Figure 2.4. With X and Y as axes, the equilibrium curve $Y^* = f(X)$ at the column temperature is plotted (Step 1). Then, the point (X_{in}, Y_{out}) is plotted (Step 2), and it constitutes one end of the operating line. Y_{in} is located on the Y-axis and a horizontal marking line is drawn till the equilibrium curve (Step 3). A line is drawn starting from the point (X_{in}, Y_{out}) till the intersection point of the marking line and the equilibrium curve (Step 4). The coordinates of this intersection point are (X^*_{out}, Y_{in}). The slope of this line is $L_{mo,ca,min}/G_{mo,ca}$ where $L_{mo,ca,min}$ is the minimum solvent flow rate necessary to treat the feed gas (Equation 2.6).

$$L_{mo,ca,min} = G_{mo,ca}\left(\frac{Y_{in} - Y_{out}}{X^*_{out} - X_{in}}\right) \qquad 2.6$$

The ultimate solvent flow rate $L_{mo,ca}$ is typically 1,1 to 1,5 times the minimum solvent flow rate $L_{mo,ca,min}$, and the absorption factor *Ab* typically lies between 1,2 and 2,0 (Treybal, 1981).

Ab is defined in Equation 2.7 where sl_{av} is the average slope of the equilibrium curve in the germane *x* range. As a first guess, ultimate solvent flow rate $L_{mo,ca}$ can be considered to be 1,3 times $L_{mo,ca,min}$, but the ratio $L_{mo,ca}$:$L_{mo,ca,min}$ needs to be fine-tuned, and this procedure is later described in Section 3.5.2.

$$Ab = \frac{L_{mo,ca}}{sl_{av}G_{mo,ca}} \qquad 2.7$$

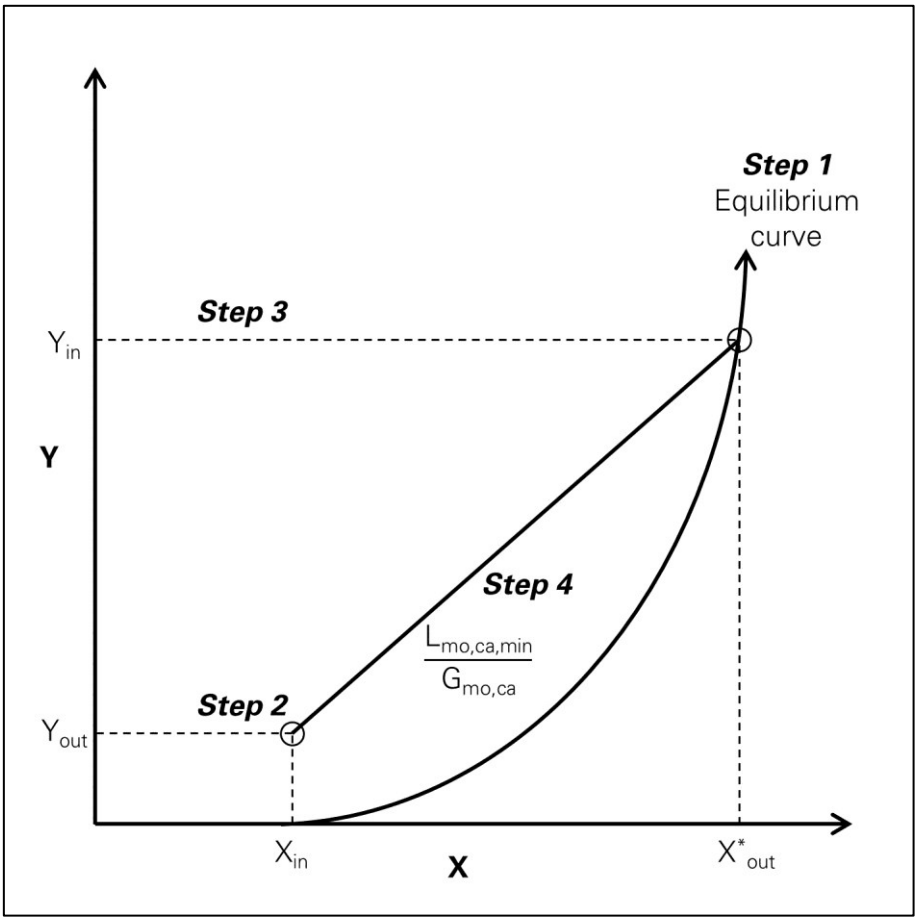

Figure 2.4 Graphical determination of minimum solvent flow rate

The graphical method as illustrated in Figure 2.4 can also be used for the stripper. However for a stripper, the operating line is below the equilibrium curve.

Now, the design of the gas-liquid contact equipment, which is the absorber and the stripper, is a topic that is delved into.

2.5.2 TRAYS AND PACKINGS

The absorber and the stripper are vertical cylinders (called columns or towers) in which the solvent and gas enter through vapour and liquid distributors, respectively. These individual streams emanating from the distributor orifices must come in contact with one another so

that the solute (e.g. CO_2) can be transferred from the gas into the liquid phase or vice versa. Trays or packings function as contact surfaces for the solvent and gas, and therefore, the column is filled with trays or packings (Figure 2.5). There are several types of trays and packings available in the market. Interested readers can refer to Coker (2007) to see photographs of an assortment of trays and packings. In a tray column, mass transfer occurs only at definite intervals (at trays), whereas in a packed column, mass transfer occurs throughout the column.

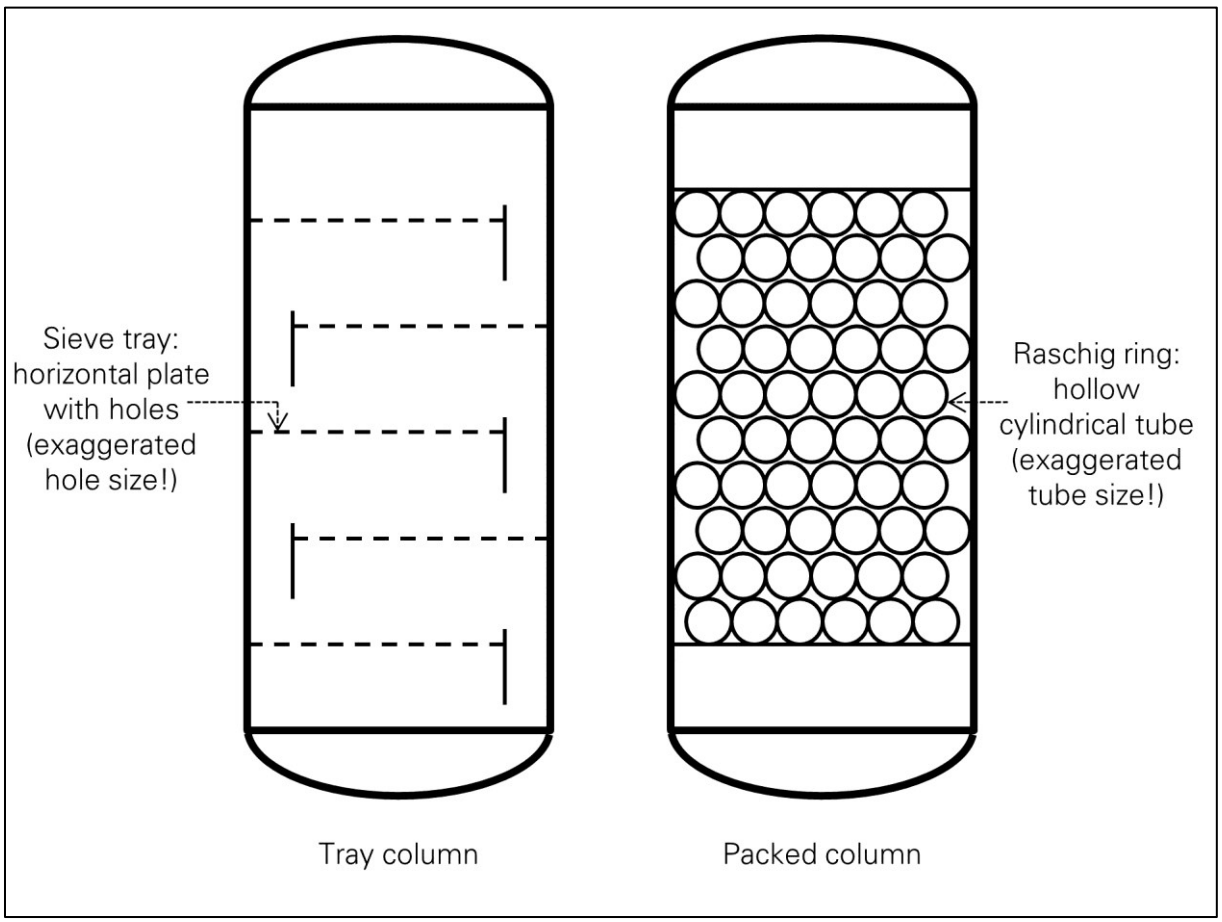

Figure 2.5 A tray column with sieve trays and a packed column with Raschig rings

A packed column has several advantages over a tray column. Inside any column, the gas flows through openings in trays or in packings. The area of openings in trays is between 8 and 15 % of the cross-sectional column area, whereas packings have an opening area of over 50 %. Therefore, the liquid holdup in a tray column is greater than the liquid holdup in the packed column. Consequently, a packed column has a lower pressure drop compared to a tray column. The lower the pressure drop, the lesser the pumping energy, and smaller the operating costs (Coker, 2007). Compared to trays, packings are faster replaced, and the turnaround time for packed columns is shorter than for tray columns. As liquid holdup in a packed column is smaller than in a tray column, solvent entrainment is also small in a packed

column (Thakore and Bhatt, 2007). Therefore, for corrosive as well as chemically and thermally sensitive gas-solvent systems, packed columns are preferred (Coker, 2007).

Under certain process conditions, however, it is pragmatic to use trays instead of packings. For columns with large diameters, trays are preferred because packed columns may suffer from non-uniform solvent distribution (channelling). When the solvent flow rate is too small, packings may remain dry as they need a minimum solvent flow rate to wet them; therefore, trays are preferred in such columns. In case, side streams are drawn from a column, trays are preferred over packings.

In absorptions plants that are designed to separate CO_2 from biogas, feed gas flow rate is between 400 and 15000 $Nm^3 \cdot h^{-1}$, and packings are more suitable than trays.

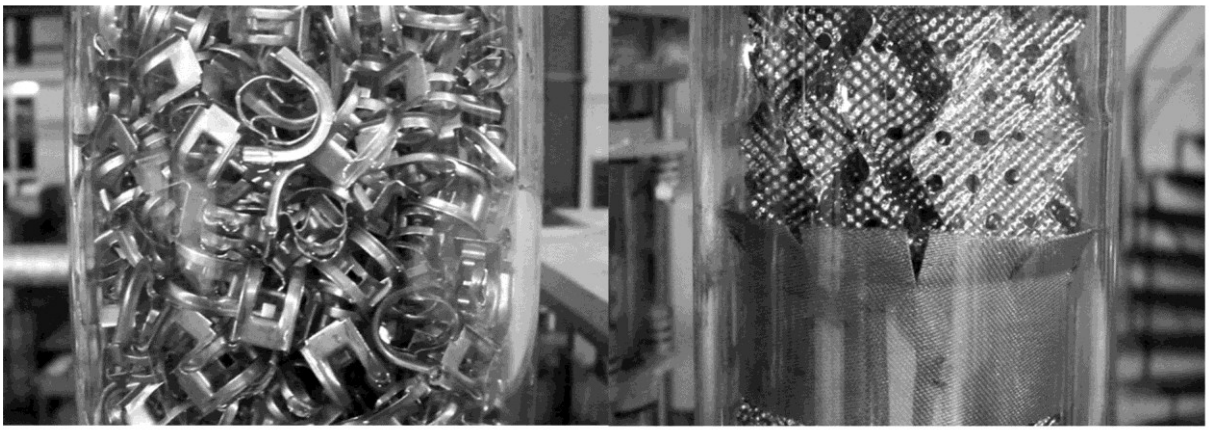

Figure 2.6 Glass column filled with random packing (left) and structured packing (right)

Packings are classified as random and structured (Figure 2.6). The choice of the packing type depends on the flow parameter *FP* of the column (Table 2.8) which is the ratio of the square root of kinetic energy of the solvent and the gas (Equation 2.8).

$$FP = \frac{L_m}{G_m}\sqrt{\frac{\rho_{gas}}{\rho_{solv}}} \qquad 2.8$$

L_m and G_m are the mass flow rates of the solvent and the gas, respectively, and ρ_{solv} and ρ_{gas} are the densities of the solvent and gas, respectively. A large *FP* is usually found in high-pressure columns, whereas a small *FP* is typical of low pressure or vacuum columns (Kister et al., 2007). In columns with small *FP*s, structured packings should be preferred, whereas in columns with large *FP*s, random packings should be preferred (Table 2.8).

Table 2.8 Correlation between flow parameter and suitable packing type (Coker, 2007)

Flow parameter	Suitable packing type
< 0,1	structured packing
0,1 to 0,5	structured or random packing
> 0,5	random packing

The specific surface area of structured packings is generally larger than that of random packings. Consequently, if the packings were entirely covered with a solvent film, the structured packings would offer a larger surface area for mass transfer. At low solvent flow rates, the solvent is present primarily as a film in random and structured packings, and the structured packings outperform random packings. As solvent flow rate increases, film thickness on structured packings increases, keeping the mass transfer area almost constant. However in random packings, as solvent flow rate increases, the solvent film is broken down into droplets, thus creating extra area for mass transfer. Therefore at higher solvent flow rates, random packings offer a larger effective mass-transfer area than structured packings.

In addition to form, packings differ in construction material, and random packings differ in size too. The size of random packings is quantified by their effective diameter known as the packing diameter. The size ratio (the ratio of column diameter to packing diameter) should be between 8:1 and 20:1. If the ratio is smaller, solvent will flow out of the packing and down the column walls (McCabe et al., 1993). If the ratio is larger, pressure drop and liquid holdup will be larger. The liquid holdup is the liquid (solvent) present in the void spaces of the packing. Liquid holdup is necessary for mass transfer, but high holdup increases column pressure drop and the load on column support structures (Strigle, 1994). Therefore liquid holdup should not be extremely high or low.

The packing material can be broadly classified into three categories: plastic, metal and ceramic. The choice of the material depends upon the required mechanical and chemical strength, operating temperature and solvent flow rate. The packing should be sturdy, but supple; it should sustain pressure from the solvent and gas, but also its own weight. Columns operating at atmospheric pressure can be filled with plastic, metal or ceramic packings. The packing must be inert to the solvent, the gas, the reaction products and by-products (Kunesh, 1987); therefore for systems that involve extremely corrosive substances, ceramic packings are recommended. Operating temperature is a constraint with plastic packings; the operating temperature must be at least 30 °C below the long-term heat

deflection temperature (Coker, 2007). Therefore plastic packings are not suitable for a stripper. Furthermore, the solvent must form a uniform film over the packing surface. As a rule of thumb, the ratio of minimum solvent rate to achieve complete wetting for ceramic, metal and plastic packings is 0,5:1:3 (Coker, 2007). Reckoning with the aforementioned factors, the absorber for CO_2-aqueous DGA system can be filled with plastic or metal packings, whereas the stripper should be filled with metal packings; the use of ceramic packings is not necessary.

With all the discussed hints, packings can be shortlisted, but the ultimate choice of the packing depends upon its performance, i.e. capacity and efficiency. In the design context, for a given solvent and gas flow rate, column diameter indicates packing capacity, and column height indicates packing efficiency. The smaller the column diameter, the higher the packing capacity, and the lesser the column height, the higher the packing efficiency. Packings influence column diameter and height, and the best packing leads to a column with the smallest diameter and the least height.

2.5.3 COLUMN DIAMETER AND HEIGHT

The absorber and the stripper are two packed columns, whose diameter and height need to be determined.

Column diameter

Column diameter d_{col} depends upon the packing, and the solvent and gas flow rates. d_{col} is calculated such that the solvent and gas come in sufficient contact with each other in the presence of the packing. The specific pressure drop $\Delta P/l$ in the packed column is an indicator of the degree of contact between the solvent and gas.

Figure 2.7 shows the $\Delta P/l$ at various gas flow rates and two solvent flow rates for a packing. The gas flow rate is represented by the F-factor F_{gas} that indicates the force exerted by the gas in the direction of the gas flow, i.e. upwards (Equation 2.9 where v_{gas} is the superficial gas velocity, and ρ_{gas} is the gas density).

$$F_{gas} = v_{gas}\sqrt{\rho_{gas}} \qquad 2.9$$

Starting with a gas flow rate of 0, as gas flow rate increases, $\Delta P/l$ or resistance to the gas flow increases because more gas squeezes through a fixed cross section of the column. Initially or at small gas flow rates, the downward flow of the solvent is not impeded. However, when the gas flow rate increases beyond a definite point called the loading point,

solvent flow is impeded, and the upward gas flow experiences additional resistance. The loading point is the first kink in the specific-pressure-drop curve in Figure 2.7, and the slope of the specific-pressure-drop curve increases after the loading point. As gas flow rate further increases, more solvent is impeded, and at a certain point called the flooding point, the downward flow of the solvent is completely blocked. Concomitantly, the upward gas flow is severely hindered, and $\Delta P/l$ increases rapidly. The flooding point is represented by the second kink in the specific-pressure-drop curve in Figure 2.7. The region between the loading and the flooding point is called the loading region. A column should be operated in the loading region where the solvent and gas come in sufficient contact with each other which ensures mass transfer. Nevertheless, the operating point must not be too close to the flooding point, or else the column may flood when the gas or solvent flow rate surges.

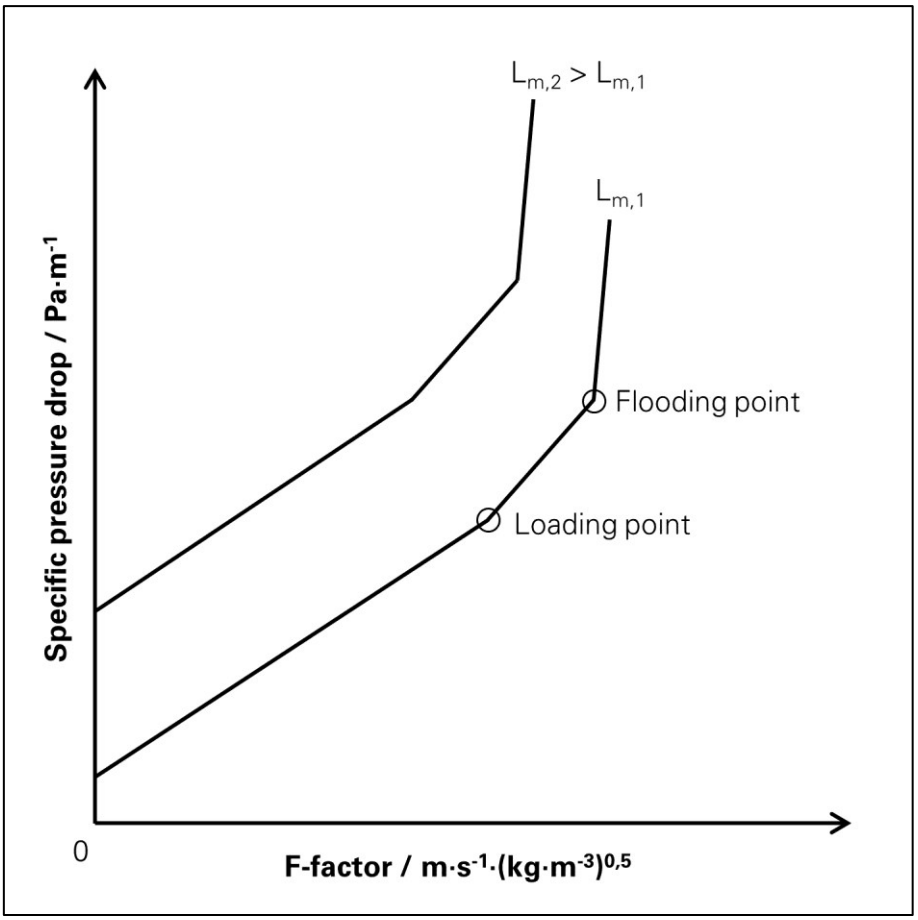

Figure 2.7 Specific pressure drop at two solvent flow rates against F-factor

For a given gas flow rate, liquid holdup and pressure drop increase (not necessarily linearly) with increasing solvent flow rate. For a given solvent flow rate, as gas flow rate increases, liquid holdup remains constant till the loading point. After the loading point, liquid holdup begins to rise, and after the flooding point, liquid holdup increases exponentially (Coker, 2007).

Thus the solvent is acted upon by upward forces exerted by the gas and by downward forces exerted by gravity. The capacity factor *C* represents the balance between the upward and the downward forces acting upon a solvent drop (Equation 2.10 where v_{gas} is the superficial gas velocity; ρ_{gas} is the gas density, and ρ_{solv} is the solvent density).

$$C = v_{gas}\sqrt{\frac{\rho_{gas}}{\rho_{solv}-\rho_{gas}}} \qquad 2.10$$

Another factor that influences the $\Delta P/l$ is the packing geometry, which is characterised by the packing factor *PF*. The specific pressure drop at flooding $\Delta P_{fl}/l$ can be calculating using *PF* as per Equation 2.11, which is an empirical correlation (Kister et al., 2007). While using Equation 2.11, *PF* must have a unit of ft^{-1}, and $\Delta P_{fl}/l$ will have a unit of inch H_2O per feet packing.

$$\frac{\Delta P_{fl}}{l} = 0{,}12PF^{0{,}7} \qquad 2.11$$

C and *PF* are consolidated using the term capacity parameter *CP* as shown in Equation 2.12 where μ_{solv} is the dynamic viscosity of the solvent, and ρ_{solv} is the solvent density.

$$CP = C\ PF^{0{,}5}\left(\frac{\mu_{solv}}{\rho_{solv}}\right)^{0{,}05} \qquad 2.12$$

For a given solvent and gas flow rate, a higher *CP* indicates a higher $\Delta P_{fl}/l$. *CP* and the flow parameter *FP* are correlated using constant $\Delta P/l$ curves in a graph called the generalized pressure drop correlation (GPDC) chart. When *FP* is kept constant, specific pressure drop increases with increasing *CP*.

The column diameter d_{col} should be such that it ensures intensive contact between the solvent and gas, but avoids column flooding. Therefore at the design point or the operating point of the column, the superficial gas velocity $v_{gas,op}$ is selected to be 80 % of the superficial gas velocity at the flooding point $v_{gas,fl}$ (Coker, 2007). The procedure to calculate d_{col} is as follows:

1. Flow parameter *FP* of the column is calculated as per Equation 2.8 where L_m and G_m are the solvent and gas mass flow rates, respectively, and ρ_{solv} and ρ_{gas} are the solvent and gas densities, respectively.
2. The packing factor *PF* of the packing is determined from literature.
3. Pressure drop at flooding $\Delta P_{fl}/l$ is calculated using Equation 2.11. While using Equation 2.11, *PF* must have a unit of ft^{-1}, and $\Delta P_{fl}/l$ will have a unit of inch H_2O per feet packing.

4. In the generalized pressure drop correlation (GPDC) chart, a unique point is located with $\Delta P_{fl}/l$ and FP (abscissa) known. Subsequently, the capacity parameter CP (ordinate) at this point is ascertained.
5. Using CP, capacity factor C is determined using Equation 2.12 where the PF value has a unit of ft^{-1}, and the dynamic viscosity of the solvent μ_{solv} has a unit of centipoise, and ρ_{solv} has a unit of $kg \cdot m^{-3}$ (and not $lb \cdot ft^{-3}$).
6. Using the C value, the superficial gas velocity at the flooding point $v_{gas,fl}$ is determined using Equation 2.10. Solvent and gas density must have a unit of $lb \cdot ft^{-3}$, and the unit of v_{gas} will be $ft \cdot s^{-1}$.
7. The superficial gas velocity at the operating point $v_{gas,op}$ is fixed at 80 % of $v_{gas,fl}$. The unit of $v_{gas,op}$ must be at last converted to the SI unit of $m \cdot s^{-1}$.
8. Column diameter d_{col} is then calculated using Equation 2.13. If v_{gas} and volumetric flow rate of feed gas G_v have SI units ($m \cdot s^{-1}$ and $m^3 \cdot h^{-1}$, respectively), d_{col} will also have a SI unit, i.e. m.

$$\frac{G_v}{3600}\frac{1}{v_{gas}} = \frac{\pi d_{col}^2}{4} \qquad 2.13$$

The procedure can be repeated for different packings, and the resultant d_{col} values can be used to compare packing capacity. A smaller d_{col} value means a larger packing capacity. For a fixed column height, the column with the smallest diameter will have the lowest column surface area (investment costs), and therefore, the packing with the highest capacity must be preferred.

Packings also influence the operating costs: the energy consumption of the gas blower depends on the total pressure drop in the column ΔP_{tot}. For a fixed packing height, the smallest specific pressure drop at the operating point $\Delta P_{op}/l$ will lead to the smallest ΔP_{tot} and the smallest energy consumption by the blower. Therefore the packing with the smallest $\Delta P_{op}/l$ should be preferred.

Column height

Active column height or packing height h depends upon the solvent and gas flow rates in the column, the desired degree of separation (solute content in feed gas, in treated gas, and in the solvent at column inlet), and the packing itself.

An empirical method, known as the equilibrium approach, was developed in times when columns were predominantly fitted with trays to calculate h wherein h was a product of the number of theoretical plates N_{pl} and the height equivalent to a theoretical plate $HETP$

(Equation 2.14). The concept of theoretical plates is based upon the working principle of a tray. A tray is a structurally modified plate over which solvent accumulates due to damming by weirs. The gas bubbles through the accumulated solvent and both phases begin to equilibrate. In an ideal or a theoretical situation, at each tray, the solvent and the gas come into complete equilibrium, and the tray (the plate) represents an ideal or a theoretical equilibrium stage. Thus the column can be represented by a series of theoretical equilibrium stages or theoretical plates.

$$h = N_{pl}\, HETP \qquad 2.14$$

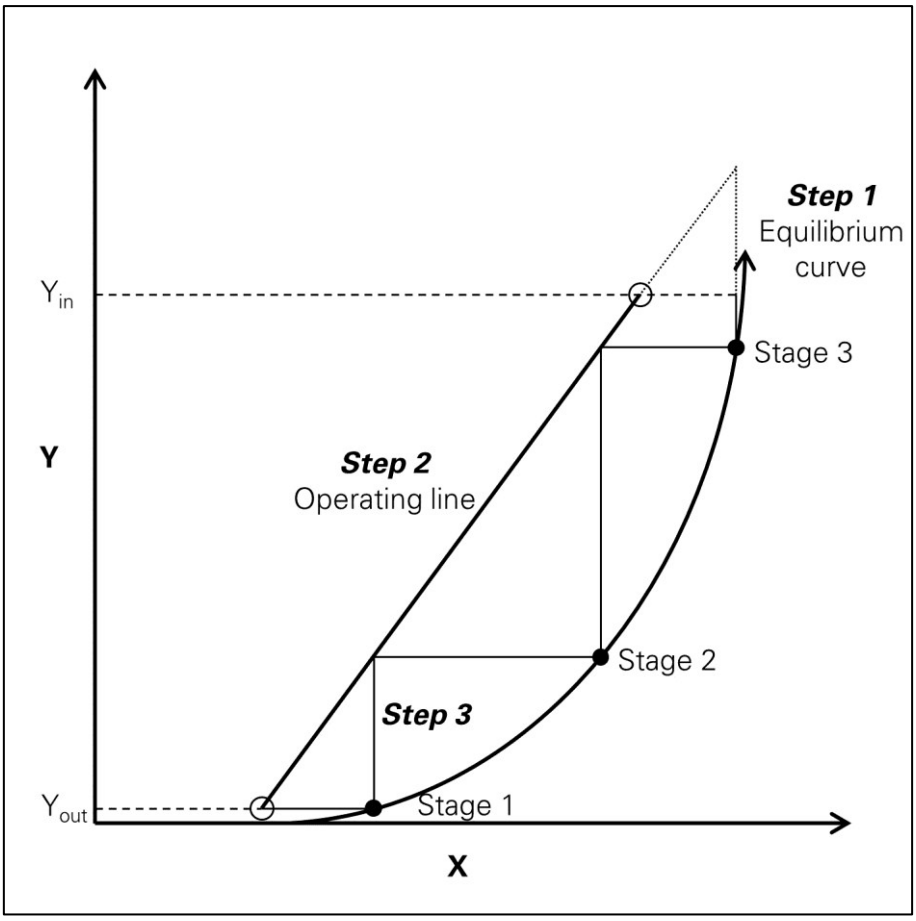

Figure 2.8 Graphical determination of theoretical stages or plates in an absorber

For a given gas-solvent system, N_{pl} necessary to achieve the desired solute transfer can be determined algebraically or graphically (Treybal, 1981). The graphical method is illustrated using Figure 2.8. With X and Y as axes, the equilibrium curve $Y^* = f(X)$ is plotted (Step 1). The operating line is plotted between the coordinates (X_{in}, Y_{out}) and (X_{out}, Y_{in}) (Step 2). In an absorber, the operating line lies above the equilibrium curve, and the bottom end of the operating line represents the column top. For a stripper, the operating line lies below the equilibrium curve, and the top end of the operating line represents the column top. Starting

from the point on the operating line that represents the column top, a horizontal line is drawn till the equilibrium curve. From this intersection point, a vertical line is drawn till it intersects the operating line. This process is repeated till the other end of the operating line (Step 3). Every intersection point on the equilibrium curve represents a theoretical stage. Even when a vertical line does not entirely fit between the operating line and the equilibrium curve, the intersection point is counted as a theoretical stage. For the case illustrated in Figure 2.8, three theoretical stages are necessary to achieve the desired solute transfer in the absorber.

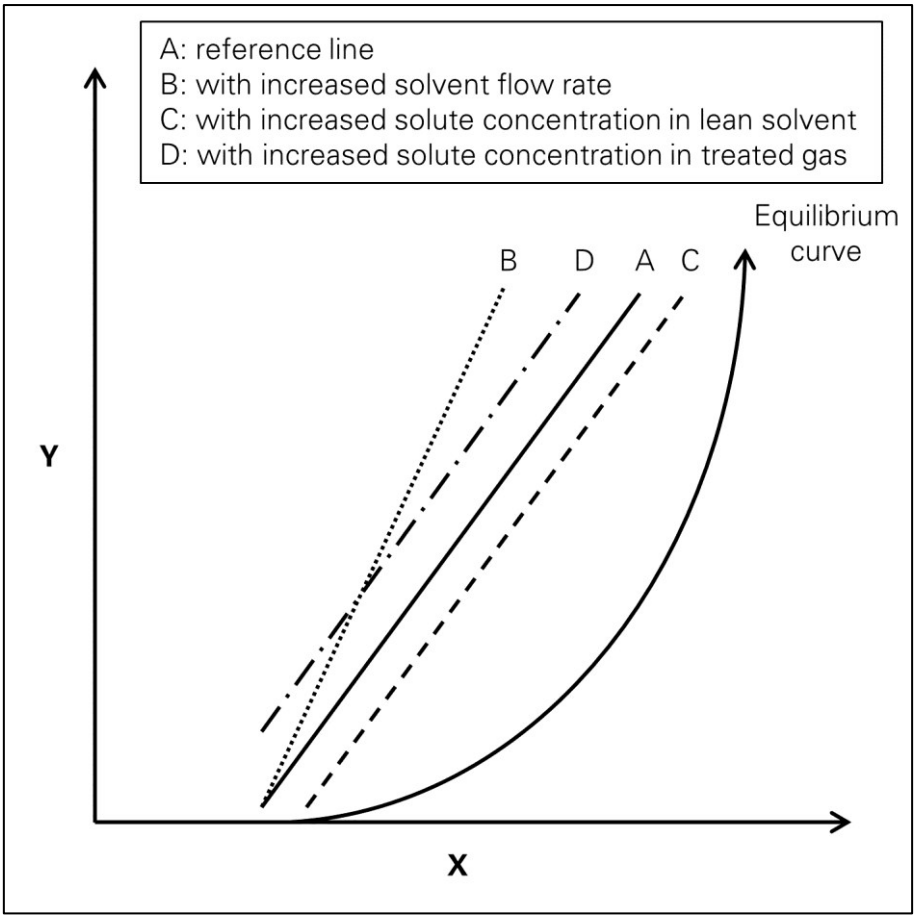

Figure 2.9 Dependence of operating line on solvent and gas parameters

HETP can be only experimentally determined. It varies with the properties of the solute and solvent, their flow rates, and the packing itself. Therefore this method (equilibrium approach) of calculating *h* can be used only if a large amount of experimental data for the solute-solvent system is available (Treybal, 1981). Nevertheless, the graphical method of determining N_{pl} helps to visualize the influence of changes in solute-solvent system on column height and diameter (Figure 2.9 and Table 2.9).

Table 2.9 Influence of increase in solvent flow rate, solute concentration in lean solvent and solute concentration in treated gas on column diameter and height

Change	Slope of operating line	Column diameter	Number of theoretical stages	Column height
Increase in solvent flow rate	increases	increases	decreases	decreases
Increase in solute concentration in lean solvent	unchanged	unchanged	increases	increases
Increase in solute concentration in treated gas	unchanged	unchanged	decreases	decreases

Packing height *h* can also be determined using a theoretical method, which is known as the non-equilibrium or the rate-based approach.

CO_2 in the gas phase diffuses through the gas mixture (here biogas) and is absorbed in the solvent (aqueous DGA). As the solubility of the other gas-phase components (carrier gas, e.g. CH_4) in the solvent is negligible, it can be assumed that the carrier gas does not diffuse through the gas mixture. Furthermore as the vapour pressure of diglycolamine (DGA) is low, the evaporation of liquid DGA into the gas phase can be considered negligible. The evaporation of liquid water from the solvent and the reaction of water vapour with liquid DGA can also be assumed to be negligible. Thus CO_2 absorption in aqueous DGA contains gaseous CO_2 diffusing through a non-diffusing gas mixture.

The CO_2 flux through the gas phase $J_{CO2,G}$ between two points, points 1 and 2, is given by Equation 2.15a where k_G is the gas-phase mass transfer coefficient (Equation 2.15b); p_{CO2} is the partial pressure of CO_2; $D_{CO2\text{-}gas}$ is the diffusion coefficient of CO_2 through the carrier gas; P_{tot} is the total pressure; R is the universal gas constant; T is the gas temperature; l is the distance between points 1 and 2; $p_{ca,lm}$ is the log mean difference in the partial pressure of the carrier gas (Equation 2.15c).

$$J_{CO2,G} = k_G\left(p_{CO2,1} - p_{CO2,2}\right) \quad 2.15a$$

$$k_G = \frac{D_{CO2-gas}P_{tot}}{RTlp_{ca,lm}} \quad 2.15b$$

$$p_{ca,lm} = \frac{p_{ca,2}-p_{ca,1}}{ln\left(\frac{p_{ca,2}}{p_{ca,1}}\right)} \quad 2.15c$$

Similarly, CO_2 flux through the liquid phase $J_{CO2,L}$ is given by Equation 2.16a where k_L is the liquid-phase mass transfer coefficient (Equation 2.16b); c_{CO2} is the molar concentration of

CO_2; $D_{CO2\text{-}solv}$ is the diffusion coefficient of CO_2 through the carrier solvent; ρ is the liquid density; M is the molecular mass of the liquid; $c_{solv,lm}$ is the log mean difference in molar concentration of the carrier solvent (Equation 2.16c).

$$J_{CO2,L} = k_L\left(c_{CO2,1} - c_{CO2,2}\right) \quad 2.16a$$

$$k_L = \frac{D_{CO2-solv}}{lc_{solv,lm}}\frac{\rho}{M} \quad 2.16b$$

$$c_{solv,lm} = \frac{c_{solv,2} - c_{solv,1}}{ln\left(\frac{c_{solv,2}}{c_{solv,1}}\right)} \quad 2.16c$$

During the absorption of CO_2 in the solvent, CO_2 flux in the gas phase is equal to the CO_2 flux in the liquid phase. CO_2 from the bulk gas phase diffuses to the interface between the gas and the liquid phase and then to the bulk of the liquid phase (Equation 2.17a). $p_{CO2,bu}$ is the CO_2 partial pressure in the bulk gas phase; $p_{CO2,int}$ is the CO_2 partial pressure at the gas-liquid interface; $c_{CO2,int}$ is the CO_2 molar concentration at the gas-liquid interface; and $c_{CO2,bu}$ is the CO_2 molar concentration in the bulk liquid phase.

$$J_{CO2} = k_G\left(p_{CO2,bu} - p_{CO2,int}\right) = k_L\left(c_{CO2,int} - c_{CO2,bu}\right) \quad 2.17a$$

As it is not possible to take measurements at the gas-liquid interface, the overall gas K_G and liquid K_L phase coefficients are usually used (Equation 2.17b) where p^*_{CO2} is the CO_2 partial pressure at equilibrium with the bulk liquid phase, and c^*_{CO2} is the CO_2 molar concentration at equilibrium with the bulk gas phase.

$$J_{CO2} = K_G\left(p_{CO2,bu} - p^*_{CO2}\right) = K_L\left(c^*_{CO2} - c_{CO2,bu}\right) \quad 2.17b$$

The resistance to mass transfer in the liquid phase is given by $1/k_L$, and resistance in the gas phase is $1/k_G$. For the absorption of sparingly soluble gases in a liquid (e.g. O_2 in H_2O), the resistance to mass transfer lies principally in the liquid phase. For the absorption of highly soluble or reactive gases in a liquid (e.g. NH_3 in H_2O), the resistance to mass transfer lies principally in the gas phase. For CO_2 absorption in aqueous DGA, the resistance to mass transfer lies in the gas and the liquid phase.

The overall gas-phase mass transfer coefficient K_G is related to the individual mass transfer coefficients as shown in Equation 2.18 where *sl* is the slope of the segment joining the interface point on the equilibrium curve and the point on the equilibrium curve that corresponds to the bulk liquid-phase concentration. As it is difficult to determine the interface point, *sl* is assumed to be equal to the slope of the equilibrium curve.

$$\frac{1}{K_G} = \frac{1}{k_G} + \frac{sl}{k_L} \quad \text{2.18a}$$

$$\left(p_{CO2,bu} - p^*_{CO2}\right) = \left(p_{CO2,bu} - p_{CO2,int}\right) + \left(p_{CO2,int} - p^*_{CO2}\right) \quad \text{2.18b}$$

$$\left(p_{CO2,int} - p^*_{CO2}\right) = sl\left(c_{CO2,int} - c_{CO2,bu}\right) \quad \text{2.18c}$$

In a packed column, it is not possible to determine CO_2 flux J_{CO2} because the interfacial area actually available to the solvent and gas is not known. Nonetheless, it is possible to measure the CO_2 transfer in a unit packing volume. Therefore, the volumetric mass transfer coefficients are usually used where *a* denotes the used interfacial area per unit packing volume (Equation 2.18d).

$$\frac{1}{K_G a} = \frac{1}{k_G a} + \frac{sl}{k_L a} \quad \text{2.18d}$$

Now by integrating the mass balance equation for a column cross section with infinitesimal height, packing height *h* is calculated (Equation 2.19). The derivation of the Equation 2.19a is given in Treybal (1981).

$$h = \int_{y_{bot}}^{y_{top}} \left[\frac{G_{mo}}{K_G a P_{tot} (1-y)_{*,lm}}\right] \left[\frac{(1-y)_{*,lm}}{(1-y)(y-y^*)}\right] dy \quad \text{2.19a}$$

$$(1-y)_{*,lm} = \frac{(1-y)-(1-y^*)}{ln\left[\frac{(1-y)}{(1-y^*)}\right]} \quad \text{2.19b}$$

The term in the first square bracket in Equation 2.19a is called the overall gas-phase height of a (one) transfer unit HTU_{OG}, and the term in the second square bracket is called the overall gas-phase number of transfer units NTU_{OG} (Equation 2.19c). *NTU* symbolizes the difficulty in separation or the inverse of the driving force of CO_2 mass transfer. G_{mo} is the molar gas flow rate; $K_G a$ is the overall volumetric gas-phase mass transfer coefficient; *A* is the cross-sectional area of the column; P_{tot} is the total pressure in the column. For dilute gases, Equation 2.19a is simplified as Equation 2.19d; however, the use of Equation 2.19d for CO_2 separation from biogas is not recommended as CO_2 content in biogas is approximately 40 vol. % which makes biogas a concentrated gas.

$$h = HTU_{OG}\, NTU_{OG} \quad \text{2.19c}$$

$$h = \left[\frac{G_{mo}}{K_G a P_{tot}}\right] \int_{y_{bot}}^{y_{top}} \left[\frac{1}{(1-y)}\right] dy \quad \text{2.19d}$$

Inferences

With biogas as the feed gas with a composition of 60 vol. % CH_4 and 40 vol. % CO_2, biogas cannot be considered a dilute gas. For biogas, $y \neq Y$ and $G_{m,in} \neq G_{m,out}$; biogas is a concentrated gas. While designing the absorber of a real plant to separate CO_2 from biogas, the operating line of the absorber and the stripper are described using Equations 2.5b and 2.5d, respectively.

$$Y = \left(\frac{L_{mo,c}}{G_{mo,c}}\right) X + \left(\frac{Y_{out} G_{mo,c} - X_{in} L_{mo,c}}{G_{mo,c}}\right) \quad 2.5b$$

$$Y = \left(\frac{L_{mo,c}}{G_{mo,c}}\right) X + \left(\frac{Y_{in} G_{mo,c} - X_{out} L_{mo,c}}{G_{mo,c}}\right) \quad 2.5d$$

The equilibrium curve [$Y^* = f(X)$] of CO_2 in aqueous DGA cannot be assumed to be a straight line between X_{in} and X_{out}. The slope of the equilibrium curve *sl* changes with X. Denoting *sl* generically as the Henry's constant k_H is a misnomer. *sl* is equal to k_H only when X is approaching zero. Consequently, with X, *sl* changes, k_H does not.

In the absorption plant designed to separate CO_2 from biogas at atmospheric pressure, the absorber and the stripper must be filled with packings. Tray columns are not recommended. In a column with a small solvent to gas ratio (flow parameter $FP < 0{,}1$) structured packings perform better than random packings, whereas in a column with a large solvent to gas ratio ($FP > 0{,}5$), random packings perform better. Packings play a key role in calculating the column diameter and height as well as the column pressure drop; thus, the choice of the packing has an impact on the investment and operating costs.

Active column height or packing height h and column diameter d_{col} are determined independently of each other. h should be calculated using the non-equilibrium approach (the one with the transfer units) using Equation 2.19a. Furthermore, as biogas is a concentrated gas, the height of a transfer unit HTU will change substantially with y.

$$h = \int_{y_{bot}}^{y_{top}} \left[\frac{G_{mo}}{K_G a P_{tot} (1-y)_{*,lm}}\right] \left[\frac{(1-y)_{*,lm}}{(1-y)(y-y^*)}\right] dy \quad 2.19a$$

In this way, the absorption process can be designed to separate CO_2 from biogas. The process that is developed can be successfully implemented only if it enjoys public acceptance (Grubb et al., 2008). A component of public acceptance is community acceptance, which refers to the support by the local stakeholders such as residents and local authorities (Wüstenhagen et al., 2007).

2.6 HAZARDS OF ABSORPTION SOLVENTS

Community acceptance of biogas plants is essential because they are often located near residential areas (Soland, 2013). As biogas-treatment plants, which include the absorption plants, are built next to biogas plants, community acceptance of absorption plants is indispensable.

The key component of the absorption process is the absorption solvent. However, the local community where the absorption plant is (to be) built is occasionally sceptical towards absorption solvents (Knudsen et al., 2009). Thus the community acceptance, which constitutes public acceptance, of the absorption solvents is low. Designing an absorption process with less hazardous solvents can be a step towards increasing community acceptance of the absorption solvents.

Majority of humans rely on intuitive judgement to perceive hazards. Not everybody is familiar with and comprehends the underlying mechanisms of technologies (Slovic, 1987). Therefore, technology experts and laymen have different perceptions of how dangerous a technology is (Flynn et al., 2006). In order to win public acceptance, the public must be actively engaged in discussion, in dialogue (Slovic, 1987), and their concerns must be addressed. The public should be provided with information; else, they will fill the knowledge gap using ideology (Flynn et al., 2006).

Solvent hazards are perfunctorily provided by manufacturers. Although the format of the material safety datasheet (MSDS) is comprehensive, data provided therein is not. Often, statements such as "data not available" can be read in the MSDS (Dixit and Mollekopf, 2013). Therefore since the last decade, governmental and non-governmental organizations have started carrying out independent studies on the hazards of absorption solvents (Brooks, 2008; Lag et al., 2009; Shao and Stangeland, 2009). Their reports present raw data on the effects of solvents on subjects such as terrestrial animals, aquatic flora and fauna, the atmosphere, and so on. A variety of hazards originate from solvents, and hazards vary from solvent to solvent; for example: solvent X is flammable and explosive, whereas solvent Y is poisonous to aquatic life. Directly comparing either the raw data or the hazards is not possible due to differences in experimental methods used to collect raw data and differences in guidelines used to evaluate the severity of a hazard using raw data. Therefore, a method needs to be developed that can assess hazard severity (intra-hazard analysis) and compare different hazards (inter-hazard analysis).

While designing the absorption process, rather than selecting the cheapest solvent, the least hazardous solvent can be selected, or at least, solvent hazards can be incorporated in the solvent-shortlisting procedure.

Inferences

In order to select less hazardous absorption solvents, a method must be developed that can be used to quantitatively compare absorption solvents based upon their hazard potential. The public should be informed about the facts on the safety of the absorption plant which can facilitate in improving its public acceptance.

2.7 SUSTAINABLE PROCESS DEVELOPMENT

Absorption is a part of the process that converts biomass into biomethane. In order to make biomethane a sustainable energy carrier, it is necessary that the conversion process itself is developed in a sustainable manner, i.e. in a way that ensures economical, ecological and social sustainability. The sustainability of a process can be assessed using sustainability indicators such as global warming potential and human toxicity (Azapagic and Perdan, 2000). In this study, the sustainability of the absorption process is discussed using its life cycle assessment (LCA).

LCA is the compilation and evaluation of the inputs, outputs and the potential environmental impacts of a product system throughout its life cycle from cradle to grave, i.e. from raw material acquisition, or generation from natural resources, to final disposal. The product system under consideration can be a tangible product such as an absorption solvent or a service such as the transport of the absorption solvent (ISO 14040, 2006).

LCA is a tool that can be used to identify opportunities to improve the environmental performance of a product at various points in its life cycle, or to assist decision-makers in the industry and the government in strategic planning, or for marketing (e.g. making an environmental claim or producing an environmental product declaration) (ISO 14040, 2006).

Inferences

The LCA of the absorption process can be used to identify hot spots of resource consumption in the absorption process, thereby identifying areas where improvements in process technology are necessary. The LCA also provides an environmental evaluation of biomethane (the product of the absorption process), which can be used by the government and the industry to design policies.

3 EXPERIMENTAL AND THEORETICAL METHODS

This section will help the reader to visualize and thus easily comprehend research procedures that were used during this study. The procedures are written in a way that will enable readers to repeat experiments and calculations. Furthermore, potential sources of safety hazards and pitfalls in the procedures have been mentioned.

3.1 MATERIALS

The supplier and the purity of substances that were used during experiments are mentioned here. Additional substance properties can be obtained either from the substance datasheet or from the supplier.

3.1.1 GASES

Carbon dioxide (CO_2): Technical grade CO_2 (99,7 vol. % purity) was supplied by Air Liquide. This CO_2 was used for experiments conducted in the laboratory (Section 3.2.1). Information about CO_2 that was used in the test rig can be found in Section 3.4.1.

Nitrogen (N_2): Technical grade N_2 (99,8 vol. % purity) was supplied by Air Liquide. This N_2 was used for experiments conducted in the laboratory (Section 3.2.1). Information about N_2 that was used in the test rig can be found in Section 3.4.1.

3.1.2 LIQUIDS

Diglycolamine (DGA): DGA or 2-(2-aminoethoxy)ethanol (CAS No.: 929-06-6) was supplied by BASF SE. The product had a purity of 98,7 wt. %, and the impurities were diethylene glycol and water.

N-methyldiethanolamine (MDEA): MDEA (CAS No.: 105-59-9) with a purity of above 98 wt. % was supplied by Applichem GmbH. The impurities consisted of water (0,5 wt. %) and other unknown substances.

Water: Water was supplied by the Coschütz Wasserwerke Dresden, and the water had a pH value of approximately 8.

3.1.3 POTENTIAL HAZARDS AND NECESSARY PRECAUTIONS

Potential hazards of the aforementioned substances and the necessary precautions are described here.

Cylinders filled with compressed CO_2 and N_2 can explode when heated. Therefore, gas cylinders should not be exposed to direct sunlight for long duration and must be placed in the shade outdoors. CO_2 is an asphyxiant gas, and CO_2 concentration in the workplace should not exceed 5000 ppm. The workplace must be kept ventilated at all times.

The absorption solvents, DGA and MDEA, are irritants and should not come in contact with the skin. Chemical-resistant workwear, gloves and safety goggles must be worn while handling these solvents. If a solvent spills, it must be cleaned using an oil-and-chemical adsorbent, which must be disposed of as special waste. The solvents should not be discharged in sewers, but must be disposed of as special waste. DGA and MDEA are corrosive, and they must be stored in polypropylene (PP), high-density polyethylene (HDPE) or stainless steel containers.

3.2 EXPERIMENTAL DETERMINATION OF SOLVENT PROPERTIES

In the CO_2-absorption process, a mixture of DGA and water is to be used as the absorption solvent. The concentration of DGA in the solvent is not predefined, and it must be specifically determined for the given task. The apt DGA concentration depends on solvent properties (e.g. equilibrium CO_2 solubility and viscosity) as well as on process parameters (e.g. partial pressure of CO_2 in feed gas and feed-gas temperature).

Industrially used DGA solvents typically contain 40 to 70 wt. % DGA in solvent (kg DGA·(kg DGA+H_2O)$^{-1}$). Furthermore, it is known that for primary amines such as DGA, equilibrium CO_2 solubility in the solvent increases with increasing solvent concentration. On this premise, five aqueous DGA solvents, namely 50, 60, 70, 80 and 90 wt. % DGA in solvent, were selected for further evaluation.

This section describes how four crucial solvent properties, namely equilibrium CO_2 solubility, density, viscosity and surface tension, were experimentally determined. These properties were subsequently used to determine an apt DGA concentration in the solvent as well as to design the absorption plant.

3.2.1 EQUILIBRIUM CO_2 SOLUBILITY (CO_2 LOADING)

Equilibrium CO_2 solubility or CO_2 loading α_{CO2} in five DGA solvents was determined at 30, 90 and 105 °C. 30 °C was selected for the absorption experiments because it was estimated to be the average temperature in the absorber. It should be noted that the absorber feed gas has a temperature of 10 to 20 °C; the solvent at the absorber inlet has a temperature of 20 to 30 °C, and the solvent at the absorber outlet has a temperature of around 30 to 40 °C. For desorption experiments, 105 °C was selected because 105 °C is near the solvent boiling point, whereas 90 °C was selected because 90 °C is below the boiling point of the solvents and pure water.

In order to validate the experimental setups, equilibrium CO_2 solubility in aqueous MDEA with 50 wt. % MDEA in solvent was determined and compared with values from literature.

Absorption setup

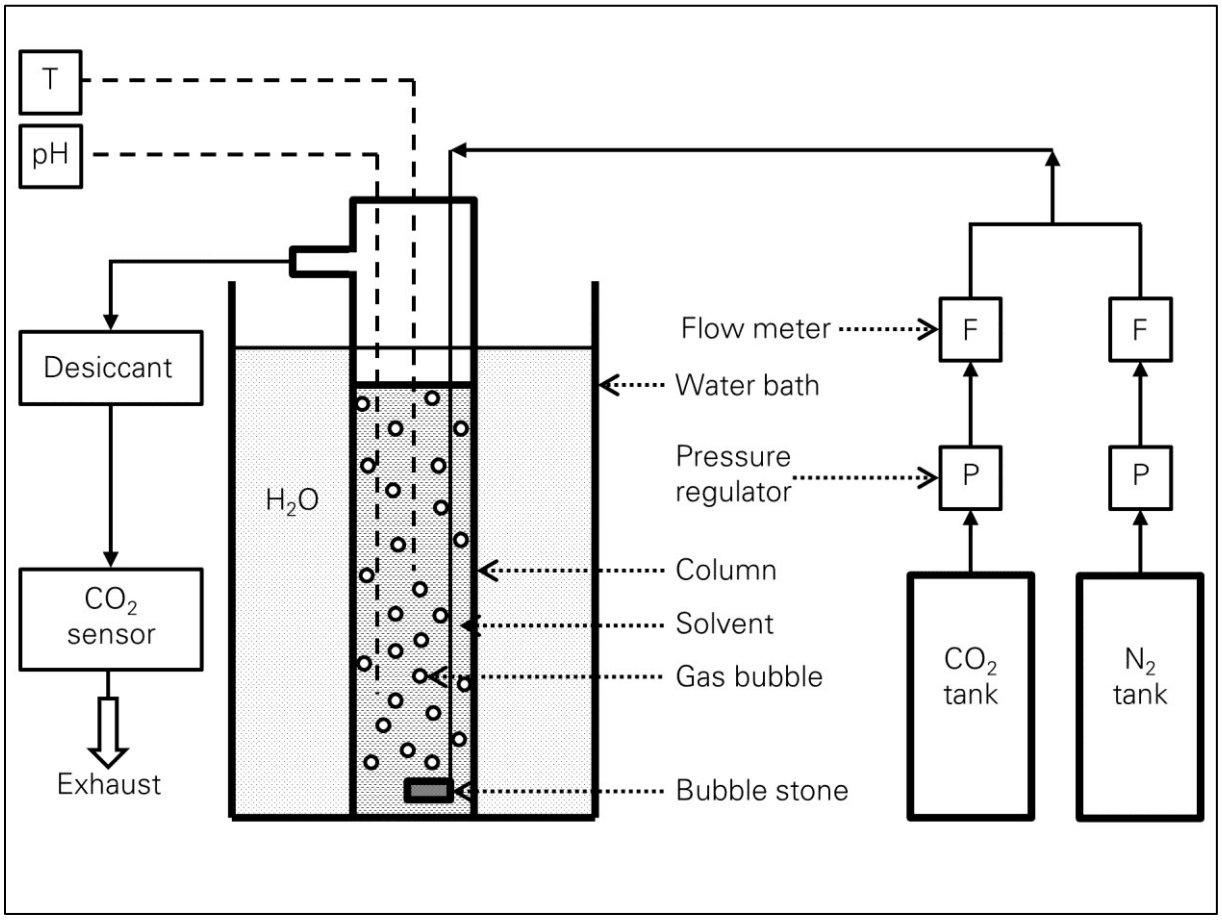

Figure 3.1 Setup used to determine equilibrium CO_2 solubility under absorption conditions (adapted from Dixit and Mollekopf, 2014a)

Equilibrium CO_2 solubility in aqueous DGA solvents under absorption conditions was determined using a bubble column (Figure 3.1). The solvents were prepared by mixing DGA with tap water. 1600 g of solvent was poured into the bubble column, a glass cylinder (9 cm in diameter and 48 cm in height), and the column was sealed with a polytetrafluoroethylene (PTFE) lid. The bubble column was placed in a water bath where the water temperature was maintained at 30 °C. Solvent temperature and pH value were recorded every two minutes using a Ni-Cr thermometer and a pH electrode (Mettler Toledo, InLab Reach), respectively. The gauge pressure inside the bubble column on top of the solvent was determined using an inclined manometer. The volumetric content of CO_2 in the outlet-gas stream was measured using an Infralyt (a calibrated instrument that uses the infrared signal from CO_2 to determine CO_2 content). The different parts of the setup were connected using polyvinylchloride (PVC) pipes of 10 mm diameter.

A gas mixture of CO_2 and N_2 (vol. ratio of 2:3) was bubbled at a flow rate of 240 $l \cdot h^{-1}$ through the solvent using an airstone. The CO_2 was partially absorbed by the solvent, and the remaining gas flowed out of the column into the desiccator and then through the Infralyt into the exhaust. When the solvent temperature increased due to the exothermic reaction between CO_2 and DGA, freezer packs (with phase change material) were inserted in the water bath to cool the solvent. The experiment was concluded when the pH value remained constant (± 0,05) for more than 30 minutes. A typical experiment lasted for at least 150 minutes. The mass of the solvent before and after the experiment was measured. The solvent before CO_2 loading was termed as "raw" and the solvent after CO_2 loading as "spent". Each experiment was conducted twice (Meier, 2013).

A long-duration experiment with 70 wt. % DGA was conducted for 12 hours. The objective was to confirm the equilibrium CO_2 solubility in the solvent. For this experiment only, the water vapour carried by the gas was condensed (at 15 °C) and returned back into the bubble column.

Desorption setup

A stirred-cell reactor (Figure 3.2) was used to determine the equilibrium CO_2 solubility of all spent DGA solvents at 90 and 105 °C. 1000 g of the spent solvent was poured into the glass reactor, and the reactor was sealed with a PTFE lid. The reactor was placed in an oil bath, and the oil was heated to the desired temperature. Silicone oil (M100) was used as a heating medium, and the temperature was regulated using a contact thermometer. The solvent was continuously stirred using a PTFE stirrer at 50 rpm. The different parts of the experimental

setup were connected using 10 mm diameter pipes made out of silicone because the desorption apparatus had to sustain high temperatures.

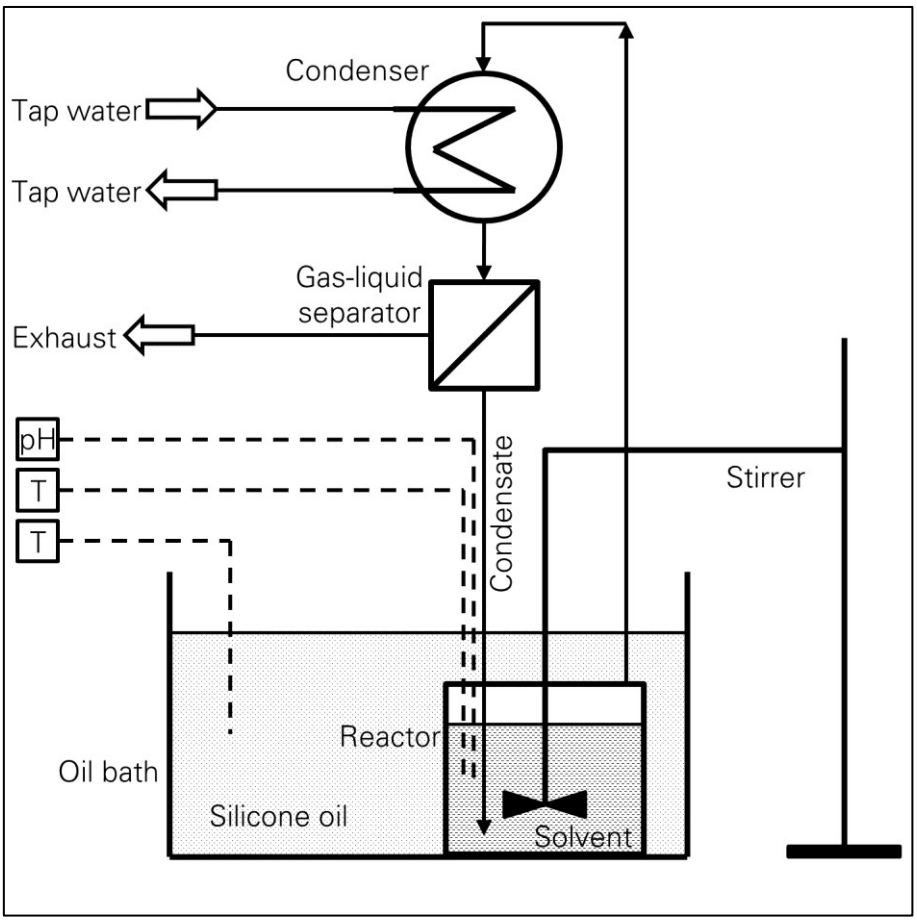

Figure 3.2 Setup used to determine equilibrium CO_2 solubility under desorption conditions (adapted from Dixit and Mollekopf, 2014a)

The solvent was heated to 90 °C, and the temperature was maintained until equilibrium was reached (no bubbles observed for more than 30 minutes). Subsequently, 100 ml of the solvent was pipetted and analysed to determine the CO_2 content. The remaining solvent was further heated to 105 °C, and the pipetting-and-analysing process was repeated. The mass of all the solvent portions was measured, and these solvent samples were termed as "lean". Each experiment was carried out twice. Heat-resistant hand gloves were worn while handling the desorption setup (Kraut, 2014).

CO_2 content in the solvent

The total inorganic carbon (TIC) content in the solvent was determined using a photometric method (cuvette test LCK 380 from HACH Lange). The reagents were provided by HACH Lange, and the photometer was also from HACH Lange (model ISiS 6000). It was assumed that all the inorganic carbon in the solvent originated from CO_2.

3.2.2 DENSITY

The density of raw, spent and lean solvents was determined using an oscillating U-tube density meter (Mettler Toledo, model DE40). The instrument was calibrated using deionised water. Solvent temperature was held constant at 30 °C by an inbuilt thermostat. Each measurement was carried out thrice, and the average of resultant values was further used.

3.2.3 VISCOSITY

The viscosity of raw, spent and lean solvents was determined using a falling-sphere viscometer (MLW Intermed). The spheres were calibrated using calibration oils of varying viscosities. Each measurement was carried out five times, and the resultant values were averaged. Solvent temperature was maintained constant by water from a thermostat.

3.2.4 SURFACE TENSION

The surface tension of raw, spent and lean solvents was determined using a Du-Nüoy ring tensiometer (Krüss GmbH, model K12). The instrument was calibrated as per the Organization for Economic Co-operation and Development (OECD) guideline 115. Each solvent sample was heated to a temperature of approximately 30 °C and then used for measurements. Each measurement was carried out thrice, and the average of the resultant values was used.

3.2.5 ABILITIES AND LIMITATIONS OF USED APPARTUSES

Key characteristics of apparatuses used to determine solvent properties are shown in Table 3.1.

Table 3.1 Apparatus characteristics

Determined property	Apparatus used	Operating temperature / °C	Minimum sample size / ml
Equilibrium CO_2 solubility	bubble column	10 to 90	1600
Equilibrium CO_2 solubility	stirred-cell reactor	90 to 150	1000
Density	oscillating U-tube density meter	4 to 90	40
Viscosity	falling-sphere viscometer	10 to 90	150
Surface tension	Du-Nüoy ring tensiometer	25 to 90	50

A bubble column was used to determine equilibrium CO_2 solubility under absorption conditions due to two reasons. Firstly, the gas is forced to come in contact with the entire volume of the solvent, thereby avoiding dead zones and inhomogeneous solvent samples. Secondly, gas bubbles cause the solvent to mix, thereby obviating the use of an additional mixing apparatus such as the stirrer. The bubble column is not suitable for desorption experiments due to the absence of a vigorous gas flow. During desorption, gaseous CO_2 and water vapour emanate out of the solvent (liquid phase) and enter the gas phase. The gas is endogenous, and the gas is slow-flowing. Therefore, a stirred-cell reactor was used to determine equilibrium CO_2 solubility under desorption conditions. The large sample (solvent) size in the bubble column and the stirred-cell reactor ensures precise determination of equilibrium CO_2 solubility under conditions of fluctuating gas flow rates and temperature.

The bubble column and the stirred-cell reactor are made out of glass and can be used to determine equilibrium CO_2 solubility at atmospheric pressure only. Similarly, the instruments used to determine density, viscosity and surface tension can be operated at atmospheric pressure only.

Density, viscosity and surface tension of the solvent can be determined in a temperature range that is limited by the properties of the thermal fluid, viz. water. The freezing and boiling point of water restrict the minimum and maximum attainable temperature, respectively. Density meter DE40 from Mettler Toledo and tensiometer K12 from Krüss GmbH have an inbuilt thermostat that regulates the solvent sample temperature. Other models of density meter and tensiometer can be used to determine properties in a larger temperature range. In the falling-sphere viscometer, if silicon oil M100 is used instead of water as the thermal fluid, the temperature range in which viscosity is determined can be extended. However, as temperature increases, solvent vapour pressure increases, and the solvent sample that is placed in a confined space poses an explosion hazard. Therefore, precautions must be taken when operating at high temperatures.

3.3 MODELLING AND SIMULATION

Equilibrium CO_2 solubility α_{CO2} can also be determined by modelling the vapour-liquid equilibrium of the CO_2-aqueous DGA system. Different thermodynamic models have been used in the past to determine α_{CO2} in aqueous DGA solvents. Consequently, at the outset, a study was conducted to identify suitable models and model parameters that could estimate the fugacity and the activity coefficients. The study is described in Section 3.3.1. After

setting up the thermodynamic model, α_{CO2} was computationally determined using a procedure (the simulation) that is described in Section 3.3.2.

3.3.1 MODELLING VAPOUR-LIQUID EQUILIBRIUM

This section describes the study conducted to setup a thermodynamic model that can be used to determine equilibrium CO_2 solubility in aqueous DGA solvents.

Calculation of the fugacity coefficient

The literature survey (Section 2.4.2) confirmed that a cubic equation of state is suitable to calculate the fugacity coefficient $\emptyset$. For the CO_2-aqueous DGA system, three cubic equations of state have been used in the past: Redlich-Kwong, Soave-Redlich-Kwong and Peng-Robinson equation. The Soave-Redlich-Kwong equation is more accurate than the Redlich-Kwong equation in estimating $\emptyset$ at temperatures near and above critical (Soave, 1972). As the temperature in the absorber and desorber is near or above the critical temperature of CO_2 (approximately 31 °C), the Soave-Redlich-Kwong equation should be preferred over the Redlich-Kwong equation.

To select between the Soave-Redlich-Kwong and the Peng-Robinson equation, an analysis was conducted where both equations were used to calculate $\emptyset_{CO2}$ at atmospheric pressure and at temperatures of 30, 90 and 105 °C. Results showed that at all tested temperatures, $\emptyset$ values obtained from both equations were plausible and differed by less than 1 % (Table 3.2). Therefore at atmospheric pressure, both equations are suitable to calculate $\emptyset_{CO2}$. However as the Peng-Robinson equation is expected to perform better than the Soave-Redlich-Kwong equation at above-atmospheric pressures (Wei and Sadus, 2000), the Peng-Robinson equation was selected to calculate $\emptyset$. Appendix C.1 describes the calculation procedure and the necessary parameters.

Table 3.2 Fugacity coefficient of CO_2 $\emptyset_{CO2}$ at atmospheric pressure

Equation	$\emptyset_{CO2}$		
	30 °C	**90 °C**	**105 °C**
Peng-Robinson	1,0031	1,0285	1,0381
Soave-Redlich-Kwong	0,9958	1,0231	1,0330

Calculation of the activity coefficient

A thermodynamic model that is suitable for electrolytes should be used to calculate the activity coefficient γ of components in the CO_2-aqueous DGA system. The Bromley model is suitable for dilute electrolytes (ionic strength below 6) where long-range forces dominate

(Bromley, 1973; Prausnitz et al., 1999). Therefore, the Bromley model is not recommended for the CO_2-aqueous DGA system (Dingman et al., 1973). The Deshmukh-Mather model (Deshmukh and Mather, 1981) is suitable to estimate γ, although it neglects the short-range interactions of ions present in small concentrations. Nevertheless, the system-specific interaction parameters that the model requires are not accurately known (Weiland et al., 1993), and therefore, the model cannot be used. The electrolyte non-random two liquid (eNRTL) model is valid for strong and weak electrolytes as well as for concentrated and diluted ionic solutions (Chen et al., 1982; Chen and Evans, 1986). The model has a sound theoretical basis because it reckons with the long-range and short-range forces (Chen and Evans, 1986), and it involves less mathematical complexity compared to other models (Chen, 2006). Therefore, the eNRTL model was selected to calculate γ. The calculation procedure is shown in Appendix C.2.

The eNRTL model uses several system properties (parameters) to estimate γ. Not all of these parameters are uniquely available in literature: different values exist for the same parameter. For the dielectric constant of DGA ε_{DGA} and the NRTL interaction parameters τ, more than one data set is available. The following section describes the study conducted to identify the most accurate and suitable values.

Dielectric constant of DGA: Dielectric constant ε is substance and temperature dependent as shown in Equation 3.1. A_{di}, B_{di} and C_{di} are substance-specific coefficients of the dielectric-constant equation, and T is the temperature. For DGA, three different sets of coefficients are available in literature (Table 3.3). In order to select the most accurate set, equilibrium CO_2 solubility α_{CO2} was estimated using each data set and compared with experimental α_{CO2} values available in literature (Martin et al., 1978) and in this study (Section 3.2.1). α_{CO2} values obtained by using each data set turned out to be identical, thus showing that α_{CO2} is not sensitive to ε_{DGA}, and any set of coefficients can be used. It was decided to use coefficients as presented in the ASPEN Plus 20 databank because they were determined using rigorous theoretical calculations.

$$\varepsilon = A_{di} + B_{di}\left(\frac{1}{T} - \frac{1}{C_{di}}\right) \qquad 3.1$$

Table 3.3 Multiple data sets of coefficients of the dielectric-constant equation of DGA

Source	A_{di}	B_{di}	C_{di}
Dingman et al., 1983	25,97	31989,38	298,15
Weiland et al., 1993	78,54	31989,38	298,15
Aspen Plus 20	28,01	9277,00	273,15

NRTL interaction parameters: NRTL interaction parameter τ is dependent on temperature T as shown in Equation 3.2. A_{ip} and B_{ip} are system-specific coefficients of the NRTL-interaction-parameter equation.

$$\tau = A_{ip} + \frac{B_{ip}}{T} \qquad 3.2$$

Various sets of interaction parameters τ are available in literature for the interaction between CO_2, H_2O and DGA. To ascertain the suitability of these parameters, α_{CO2} was calculated using each data set and α_{CO2} values were compared with experimental data available in literature (Martin et al., 1978) and in this study (Section 3.2.1). The calculation results deviated from the experimental data, and therefore, it was decided to modify the parameters as follows:

Step 1 (defining):
$A_{ip,CO2\text{-}DGA} = A_{ip,DGA\text{-}CO2}$ and $A_{ip,DGA\text{-}H2O} = A_{ip,H2O\text{-}DGA}$ and
$B_{ip,CO2\text{-}DGA} = B_{ip,DGA\text{-}CO2}$ and $B_{ip,DGA\text{-}H2O} = B_{ip,H2O\text{-}DGA}$

Step 2 (regressing):
Varying $B_{ip,CO2\text{-}DGA}$ such that calculated and experimentally measured α_{CO2} values are in congruence

The selected coefficients are shown in Table 3.4.

Table 3.4 Selected coefficients of the NRTL-interaction-parameter equation

System	A_{ip}	B_{ip}	Source
CO_2-DGA	-1,980	-1000,000	This study
DGA-CO_2	-1,980	-1000,000	This study
DGA-H_2O	1,992	-770,410	This study
H_2O-DGA	1,992	-770,410	This study
H_2O-CO_2	10,064	-3268,135	Austgen, 1989
CO_2-H_2O	10,064	-3268,135	Austgen, 1989

Equilibrium constant

Solutes such as CO_2 react with aqueous DGA (solvent) to form a solution, i.e. reaction products, and additional molecular species exist in the solvent. The reactions are shown as Equations 3.3a to 3.3f.

$$2H_2O \leftrightarrow H_3O^+ + OH^- \qquad 3.3a$$

$$CO_2 + 2H_2O \leftrightarrow HCO_3^- + H_3O^+ \qquad 3.3b$$

$$HCO_3^- + H_2O \leftrightarrow H_3O^+ + CO_3^{2-}$$ 3.3c

$$RNH_2 + H_3O^+ \leftrightarrow RNH_3^+ + H_2O$$ 3.3d

$$RNH_2 + HCO_3^- \leftrightarrow RNHCO_2^- + H_2O$$ 3.3e

$$RNHCO_2^- + H_2O \leftrightarrow RNH_3^+ + CO_3^{2-}$$ 3.3f

The equilibrium constant k_{eq} of the reactions can be used to determine the quantity of different species (ions and molecules) in the liquid phase. k_{eq} is dependent upon temperature T as shown in Equation 3.4 where A_{re}, B_{re} and C_{re} are reaction-specific coefficients. For example: the reaction stoichiometry and k_{eq} will change if the hydronium ion (H_3O^+) is replaced by the proton (H^+).

$$k_{eq} = A_{re} + \frac{B_{re}}{T} + C_{re} \ln T$$ 3.4

For the reactions Equations 3.3a, 3.3b, 3.3c and 3.3f, coefficients of Equation 3.4 are precisely available in literature (Table 3.5), but for reactions Equations 3.3d and 3.3e, more than one data set is available and the coefficients therein are not precise (Table 3.6). Three sets of coefficients are available for the protolysis of DGA (Equation 3.3d) and two sets for the carbamate-formation reaction of DGA (Equation 3.3e).

Table 3.5 Uniquely available coefficients of the equilibrium-constant equation

Reaction	A_{re}	B_{re}	C_{re}	Source
3.3a	132,90	-13445,90	-22,48	Austgen, 1989
3.3b	231,47	-12092,10	-36,78	Austgen, 1989
3.3c	216,05	-12431,70	-35,48	Austgen, 1989
3.3f	-22,12	4875,00	0,00	Dingman et al., 1983

Table 3.6 Multiple data sets of coefficients of the equilibrium-constant equation

Reaction	A_{re}	B_{re}	C_{re}	Source
3.3d	-13,34	-4218,71	0,00	Aspen Plus 25
	1,70	-8431,65	0,00	Austgen, 1989
	-5,36	-6079,60	0,00	Dingman et al., 1983
3.3e	3,37	-3696,17	0,00	Aspen Plus 25
	8,83	-5274,40	0,00	Austgen, 1989

In order to identify the most suitable values, equilibrium CO_2 solubility α_{CO2} was calculated using the different sets of coefficients and compared against the experimental values from

Martin et al. (1978) and this study (Section 3.2.1). The coefficients provided by Austgen (1989) gave the best fit and were selected (Table 3.7).

Table 3.7 Selected coefficients of the equilibrium-constant equation

Reaction	A_{re}	B_{re}	C_{re}	Source
3.3d	1,70	-8431,65	0,00	Austgen, 1989
3.3e	8,83	-5274,40	0,00	Austgen, 1989

Henry's constant

Henry's constant k_H is specific to the solute-solvent system and the temperature T (Equation 3.5). A_H, B_H, C_H and D_H are coefficients of the Henry's-constant equation. For the CO_2-H_2O and N_2-H_2O system, the coefficients are available in the Dortmund databank and the Aspen Plus 25 databank (Table 3.8).

$$k_H = A_H + \frac{B_H}{T} + C_H lnT + D_H T \qquad 3.5$$

Table 3.8 Coefficients of Henry's-constant equation

System	A_H	B_H	C_H	D_H
CO_2-H_2O	159,8651	-8741,5500	-21,6690	0,0011
N_2-H_2O	164,9941	-8432,7700	-21,5580	-0,0084

k_H for the CO_2 (solute) and 70 wt. % DGA in solvent system is, however, not known. Therefore, it was decided to use k_H for the CO_2-H_2O system. It should be kept in mind that k_H symbolizes the fugacity of a reference state, and any arbitrary value can be used (Appendix C). Nevertheless, the justification of the choice of k_H is as follows. Every gas (solute) dissolves in and reacts with every liquid (solvent). The extent of dissolution and reaction depend on the solute-solvent system. For gaseous CO_2 and pure liquid H_2O, dissolution is substantially larger than reaction, whereas for gaseous CO_2 and liquid DGA, reaction is substantially larger than dissolution. Thus, it can be considered that CO_2 in equilibrium with pure liquid water exists only as liquid molecular CO_2 in the liquid phase, whereas CO_2 in equilibrium with liquid DGA exists only in the form of ions (non-molecular CO_2) in the liquid phase. Consequently, CO_2 in aqueous DGA exists as molecules and as ions. To estimate liquid fugacity of CO_2 in aqueous DGA, k_H for the CO_2-H_2O system is used which reckons with the molecules, whereas the activity coefficient γ reckons with the presence of ions.

Turnkey model setup

The equilibrium CO_2 solubility α_{CO2} in aqueous DGA at atmospheric pressure was determined using Henry's law. Fugacity coefficient $\varnothing$ was calculated using the Peng-Robinson equation combined with the Twu generalized α-function and the generalized mixing rule. Activity coefficient γ was calculated using the eNRTL model. Henry's constant k_H for the CO_2-H_2O system was used, and the Poynting correction factor was assumed to be one.

3.3.2 SIMULATIONS

A commercial software was used to calculate α_{CO2} in aqueous DGA using the following procedure. A single absorption solvent stream flowed through a cascade of columns: solvent output from column one formed the solvent input to column two and so on. Every column had a new, but identical gas input. Inside the column, solvent and gas flowed in a countercurrent direction. To neutralise the rise in solvent temperature due to the exothermic CO_2-solvent reaction, solvent temperature was corrected using a cooler. Thus, solvent input to every column had the same temperature (Figure 3.3). After flowing through five to ten columns, the solvent came to equilibrium with the gas (Roscher, 2014).

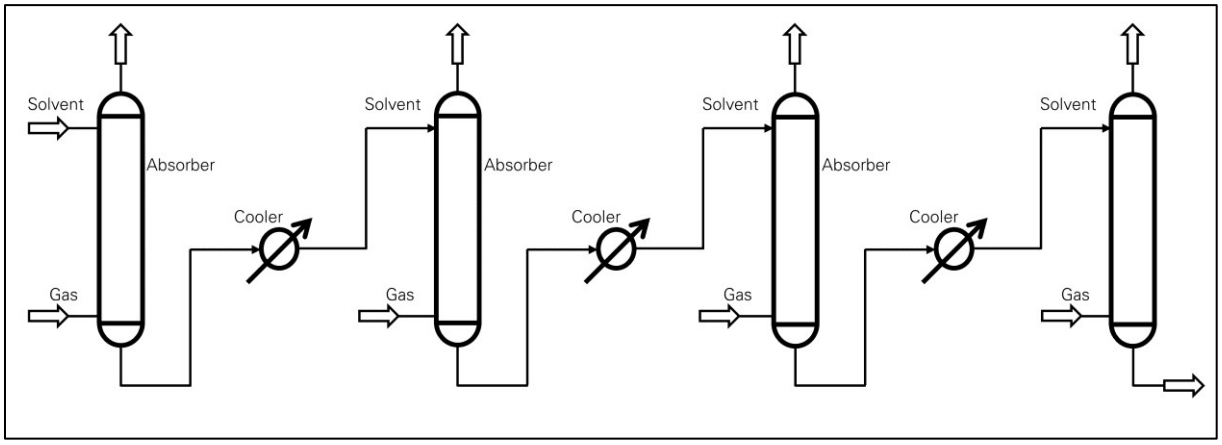

Figure 3.3 Column cascade used to computationally determine equilibrium CO_2 solubility

Using the above procedure, α_{CO2} in aqueous DGA solvents (50, 60, 70, 80 and 90 wt. % DGA in solvent) was calculated at temperatures of 30, 90 and 105 °C and at a particular CO_2 partial pressure between 30 and 90 kPa. In addition, α_{CO2} in the selected DGA solvent (70 wt. % DGA in solvent) was determined for the selected absorption and desorption temperatures (30 and 105 °C) for CO_2 partial pressure varying from 1 to 50 kPa; this data is essential for designing the absorption plant.

3.4 ABSORPTION TEST RIG

This section describes the absorption test rig, the major modifications made to the test rig to revamp it, and the new operational range of the test rig.

3.4.1 TEST-RIG DESCRIPTION

The absorption test rig is made up of six components (Figure 3.4):

I. N_2-PSA (pressure swing adsorption) unit
II. CO_2-cylinder battery
III. Gas-regulator unit
IV. Process unit
V. Switchboard
VI. Computer

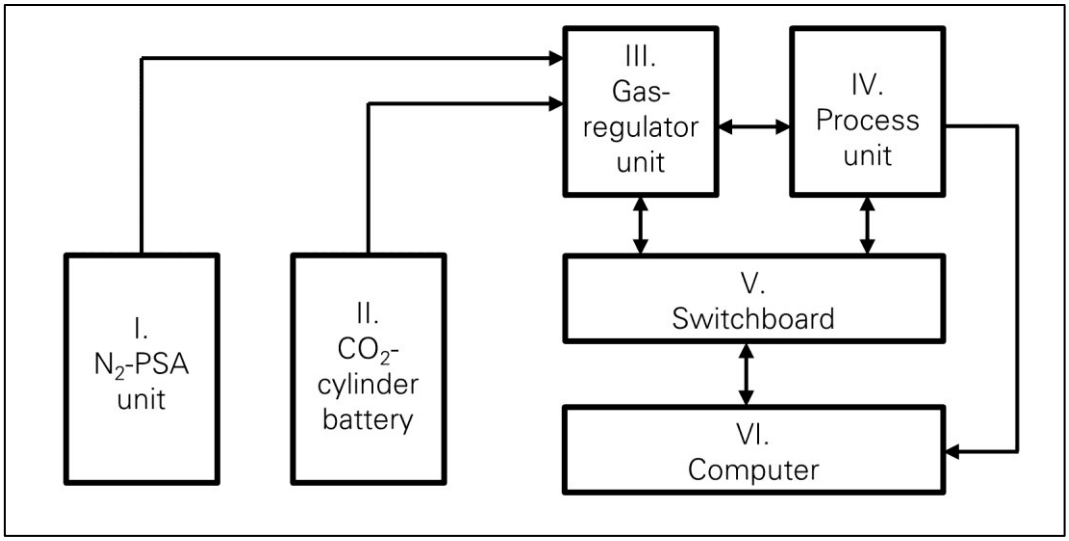

Figure 3.4 Block diagram of the absorption test rig

I. N_2-PSA unit

The unit consists of a pressure swing adsorber that produces N_2 with a concentration of 99,0 ± 0,2 vol. %. O_2 and H_2O are separated from pressurized air (at 7 bar) to obtain N_2, which is stored in a vessel (with a volume of 500 l) at a pressure of up to 6,4 bar. The PSA unit was given as a gift by Linde AG.

II. CO_2-cylinder battery

The battery consists of twelve cylinders, and each cylinder is filled with 30 kg of liquid CO_2. 360 kg of CO_2 corresponds to approximately 194 m^3 CO_2 at 15 °C and 1 bar. This technical

grade CO_2 has a purity of 99,7 vol. % and is supplied by Air Liquide AG. The gas from the cylinders flows to a decompressor station where the pressure is reduced to approximately 11 bar and then to a second decompressor station where the pressure is reduced to 6 bar.

III. Gas-regulator unit

N_2 and CO_2 from the N_2-PSA unit and the CO_2-cylinder battery, respectively, enter the gas-regulator unit through N_2 and CO_2 headers. Each header is connected to a flow regulator, which regulates the volumetric flow rate of the gas. The outlet of each regulator is connected to a single feed-gas copper pipe (inner diameter of DN8) in which N_2 and CO_2 mix on their own accord.

IV. Process unit

A simplified process flow diagram of the process unit is shown as Figure 3.5.

Humidifier: The feed-gas copper pipe containing the gas mixture (CO_2 and N_2) is connected to a plastic pipe that directs the feed gas to a humidifier in which the gas is bubbled through a glass vessel K4 that is half filled with tap water. The total volume of the glass vessel is 50 l. The feed gas is saturated with water vapour so that the feed gas does not carry water (from the absorber) in the form of vapour with it. If the water loss is not prevented, DGA concentration in the solvent will increase.

Absorption column (absorber): The absorber K1 is a glass column with an inner diameter of DN100 and is filled with a single packing layer of height 3000 mm. The packing is Novalox-M 15 mm, a random packing, made of stainless steel and manufactured by Vereinigte Füllkörper Fabriken GmbH & co. KG. The lean solvent is distributed in the absorber using a pipe-orifice header made up of a ring with multiple-drip points. The gas enters the absorber through a horizontal pipe with a single opening. The spent solvent flows vertically downwards into a buffer vessel B1 with 20 l volume and then is pumped to the heat exchanger W5.

Heat exchanger, preheater and cooler: A plate-and-frame heat exchanger W5 is used to transfer heat from the lean solvent coming from the stripper K3 to the spent solvent coming from the absorber K1. The spent solvent from heat exchanger W5 flows through the preheater W6 into the stripper K3. The preheater W6 is an electric, horizontal heater with an electric power of 20 kW. The lean solvent from the heat exchanger W5 flows through a cooler W1 into the absorber K1. The cooler W1 is a plate-and-frame heat exchanger where the second fluid is water (cooling water).

Desorption column (stripper): The stripper K3 is a glass column with an inner diameter of DN100 and is filled with two packing layers that have a height of 1500 mm each. The packing is Mellapak 250.Y, a structured packing, made of stainless steel and manufactured by Sulzer AG. Stripper K3 is insulated with glass wool (20 mm thickness) and an aluminium foil. The spent solvent is introduced into the stripper K3 at half height and is distributed in the column using a pipe-orifice header made up of a ring with multiple-drip points. A coiled condenser W3 is installed at the top of the stripper in a horizontal, but inclined configuration. The cooling medium in the spiral tube of the condenser is water. The gas escapes at the higher end of the condenser, while the condensate (liquid) flows at the lower end of the condenser into the stripper. The solvent at the stripper bottom flows into a reboiler W4.

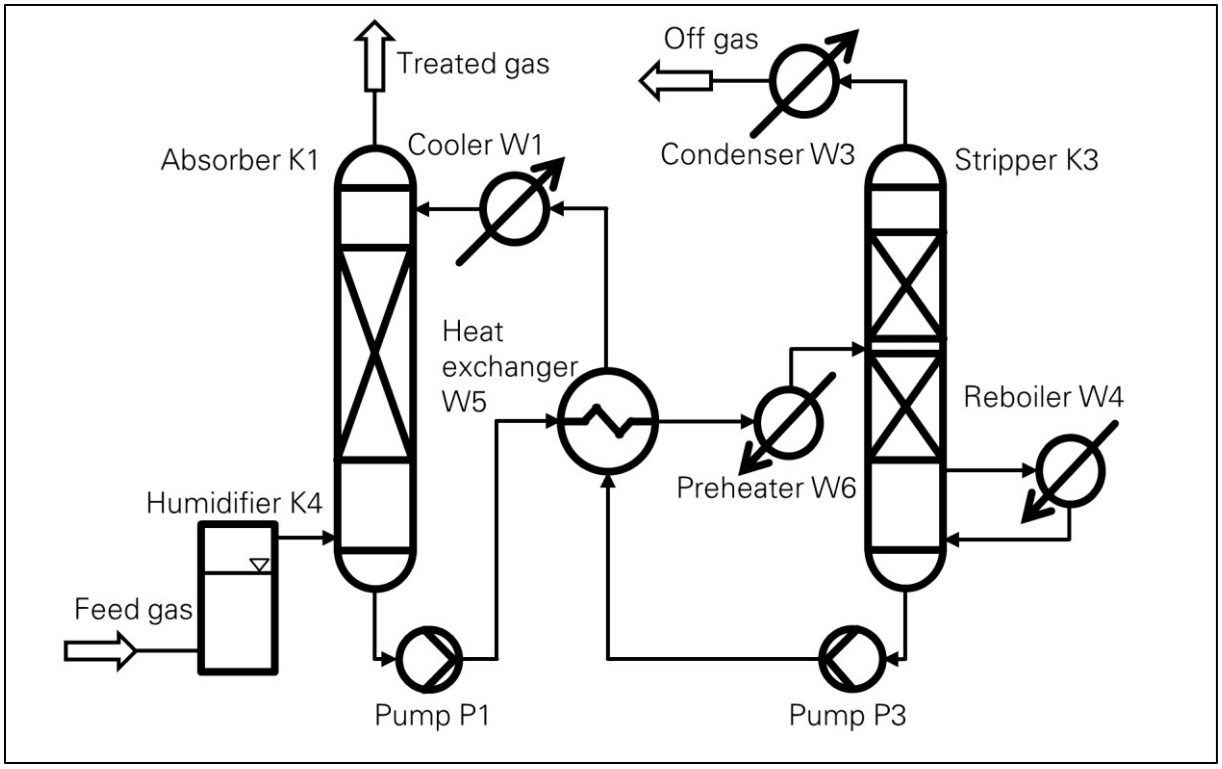

Figure 3.5 Simplified process flow diagram of the process unit
(adapted from Dixit and Mollekopf, 2014b)

Exhaust: Gases exiting the absorber K1 and the condenser W3 tops are directed through a polypropylene (PP) pipe (inner diameter of DN50) into the open atmosphere.

Reboiler: An electric, vertical, thermo-siphon reboiler W4 with an electric power of 9 kW is used to heat the solvent at the bottom of the stripper K3. The vapour generated flows from the top of the reboiler W4 into the stripper K3, while the remaining solvent flows into the buffer vessel B3 which has a volume of 20 l. The reboiler temperature cannot be regulated, but the reboiler power W4.y can be regulated.

Pumps: One centrifugal pump (1,1 kW) is placed at the bottom of the absorber and desorber, each, P1 and P3, respectively, to pump the solvent to the heat exchanger W5. The buffer vessels B1 and B3 are located physically above the pumps P1 and P3 so that the solvent can automatically prime the pumps under gravity.

Gas sampling: The copper feed-gas pipe coming from the gas-regulator unit is connected to a sampling point (Y-joint) where the first end is connected to the plastic feed-gas pipe and the second end is connected to a gas dryer. Similarly, the gas exiting the absorber K1 top has a sampling point where the first end is connected to the exhaust pipe and the second end is connected to the gas dryer. The gas dryer is then connected to the Infralyt, an instrument that measures CO_2 concentration.

V. Switchboard

The switchboard houses the electrical systems of the test rig. Three knobs are present on the switchboard that must be manually regulated. One knob controls the electric supply to the process unit, gas-regulator unit and the computer. Two knobs control the electric supply to the pumps P1 and P3. In addition, the power consumed by the reboiler W4 and the preheater W6 is displayed on two digital panels. The emergency shutdown button is also present on the switchboard.

VI. Computer

Table 3.9 Process variables that must be regulated using the process-control software

Process variable	Code	Unit
N_2 flow rate	F9	$Nm^3 \cdot h^{-1}$
CO_2 flow rate	F10	$Nm^3 \cdot h^{-1}$
Solvent flow rate from pump P1	F2	$kg \cdot h^{-1}$
Level in buffer vessel B3	L3	%
Reboiler W4 power	W4.y	%
Solvent temperature at preheater W6 outlet	T5	°C

Table 3.10 Process variables that must be manually regulated

Process variable	Code	Unit
Cooling-water flow rate through cooler W1	F6	$l \cdot min^{-1}$
Cooling-water flow rate through condenser W3	F8	$l \cdot min^{-1}$

On a computer, the process-control software WinersRT developed by SCOOP Software GmbH is installed that is used to control the gas-regulator and the process unit. Process variables that must be regulated using the software are shown in Table 3.9, and variables that must be manually regulated are shown in Table 3.10. In addition, the process-control software also records various process parameters at a rate of at least one data point per minute.

3.4.2 TEST-RIG REVAMP

When the currently discussed biomethane project started, the absorption test rig had a gas-treating capacity of 4 $Nm^3 \cdot h^{-1}$ and was operated using a hybrid absorption solvent. The biomethane project demanded that a chemical absorption solvent, namely aqueous diglycolamine (DGA), be used as the absorption solvent (Section 2.3.2). The procedure used to change the absorption solvent is described in Appendix D.1. Furthermore, as part of a strategic concept to improve the test rig, it was decided to increase the gas-treating capacity of the test rig to at least 10 $Nm^3 \cdot h^{-1}$ and preferably to 25 $Nm^3 \cdot h^{-1}$, which would improve the scalability of the data obtained using the test rig.

The N_2-PSA unit with a N_2 capacity of 25 $Nm^3 \cdot h^{-1}$ was installed and connected to the test rig through a flow regulator. This flow regulator has an operating range from 0 to 16 $Nm^3 \cdot h^{-1}$. The CO_2-cylinder battery and the decompressing stations were installed and connected to the test rig through a flow regulator. This flow regulator has an operating range from 0 to 9,1 $Nm^3 \cdot h^{-1}$.

Absorber K1 was equipped with the random packing Pall rings 15 mm and 30 mm. The absorber was not designed to handle a gas flow rate of 25 $Nm^3 \cdot h^{-1}$, and therefore, the packing had to be changed. It was decided to use the random packing Novalox-M 15 mm, which could handle the increased gas flow. This decision can be attributed to the packing capacity as well as its size and material.

Two sizes of commercially available packings were considered: 15 and 30 mm. For a column with an inner diameter of DN100, the ratio of column to packing diameter is 7:1 and 3:1, respectively. As a ratio between 8:1 and 20:1 is recommended, a random packing with 15 mm diameter was deemed to be suitable.

The packing material was chosen to be stainless steel, which would allow the absorber to operate under various process conditions such as high temperatures and low solvent flow rates. Stainless steel can be used at high temperatures (at least up to 150 °C) unlike

polyethylene (plastic). Furthermore, the minimum solvent flow rate for wetting plastic is higher than that of wetting stainless steel; hence, plastic was deemed unsuitable. Ceramic was also rejected because ceramic is brittle, and ceramic packings cost more than stainless steel packings.

Not many types of commercially available random packings have a size of 15 mm and are made of stainless steel. Novalox-M manufactured by Vereinigte Füllkörper Fabriken GmbH & co. KG, IMTP manufactured by Koch-Glitsch LP and I-ring manufactured by Sulzer Chemtech AG fit the above criteria. Novalox-M was selected due to lower costs, easy logistics and better support by the manufacturers.

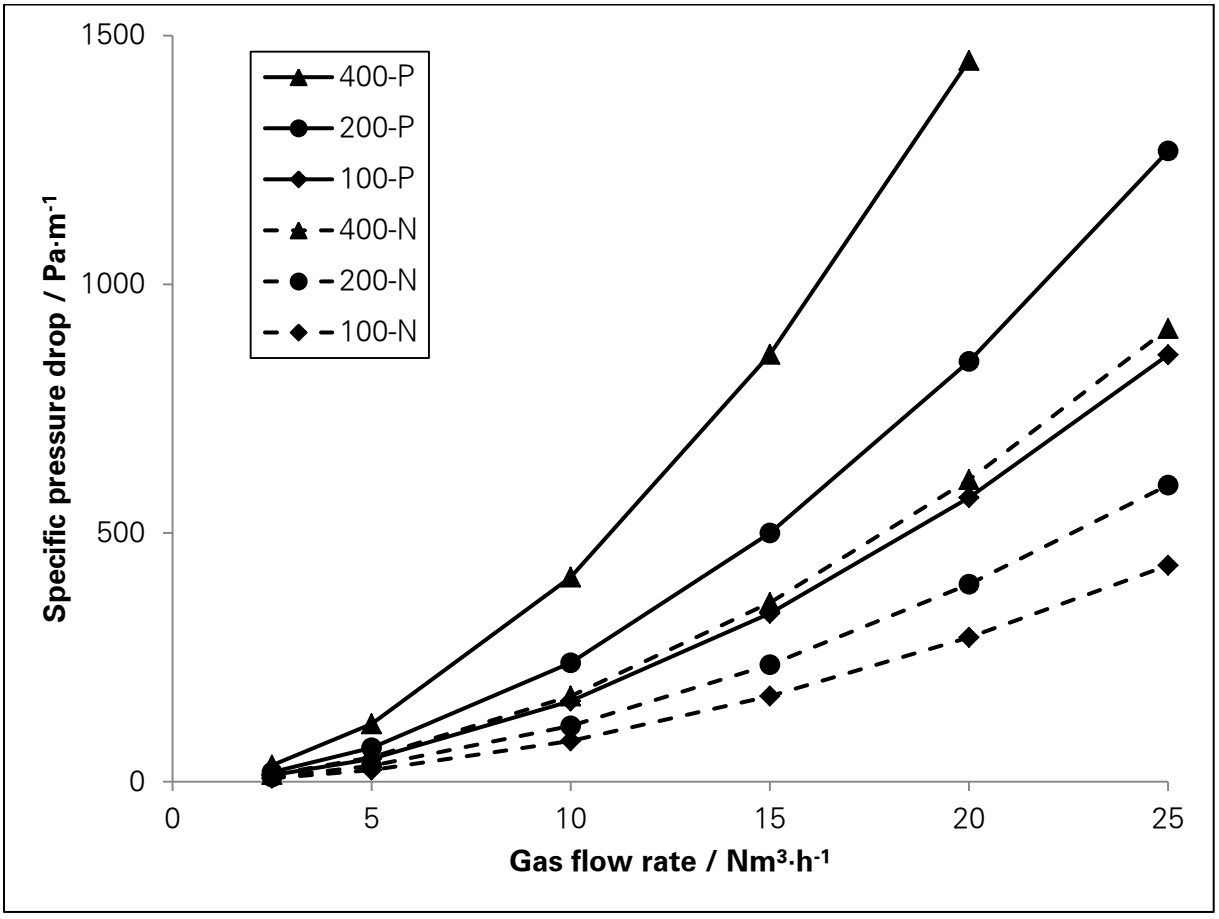

Figure 3.6 Specific pressure drop against gas flow rate for Pall rings (P) 15 mm and Novalox-M (N) 15 mm for three solvent flow rates 100, 200 and 400 kg·h^{-1}

The specific pressure drop in the absorber (a column with an inner diameter of DN100) was calculated for the two random packings, namely Pall rings 15 mm and Novalox-M 15 mm, using the VFF-Software version 3.34. In these calculations, 70 wt. % DGA in solvent was the solvent, and the feed gas was a mixture of 60 vol. % N_2 and 40 vol. % CO_2 (Figure 3.6).

For a given solvent and gas flow rate, the specific pressure drop offered by the Pall rings is more than double the specific pressure drop offered by Novalox-M (Figure 3.6). Consequently, the total pressure drop in the absorber (a column with fixed height) is smaller in case of Novalox-M. At higher gas flow rates (above 15 $Nm^3 \cdot h^{-1}$), the increase in the slope of the specific-pressure-drop curves for Pall rings is higher than that of Novalox-M (Figure 3.6). This implies that the Novalox-M has a higher capacity than Pall rings. The absorber filled with Pall rings floods at a gas flow rate between 20 and 25 $Nm^3 \cdot h^{-1}$ when the solvent rate is 400 $kg \cdot h^{-1}$. Under these conditions, an absorber filled with Novalox-M does not flood. Thus, Novalox-M offers a larger capacity and a smaller pressure drop compared to Pall rings. Therefore, absorber K1 was retrofitted with the random packing Novalox-M 15 mm.

3.4.3 OPERATIONAL RANGE OF THE TEST RIG

Table 3.11 Operational range of process variables

Process variable	Code	Unit	Operational range	Reason for the restriction
N_2 flow rate	F9	$Nm^3 \cdot h^{-1}$	0 to 12	large pressure drop
CO_2 flow rate	F10	$Nm^3 \cdot h^{-1}$	0 to 8	large pressure drop
Solvent flow rate from pump P1	F2	$kg \cdot h^{-1}$	100 to 400	difficult flow regulation and overload
Level in buffer vessel B3	L3	%	20 to 60	dry running of pump
Cooling-water flow rate through cooler W1	F6	$l \cdot min^{-1}$	0 to 25	small pipe diameter
Cooling-water flow rate through condenser W3	F8	$l \cdot min^{-1}$	0 to 14	small pipe diameter
Reboiler W4 power	W4.y	%	0 to 80	solvent degradation temperature
Solvent temperature at preheater W6 outlet	T5	°C	80 to 95	solvent inlet temperature and boiling point

The process variables or process parameters that can be regulated (set) in the test rig are shown in Table 3.11. The operational range of the process variables was determined through preliminary tests conducted on the test rig. The reasons for restricting the range, i.e. setting the lower limit (if nonzero) and the upper limit, are presented in Table 3.11. The operational range of the test rig depends upon safety regulations, capacity of its inbuilt components, process controller, and properties of the solvent and gas.

The availability of N_2 and CO_2 was increased to 16 and 9,1 $Nm^3 \cdot h^{-1}$, respectively, by the newly installed N_2-PSA unit, CO_2-cylinder battery and the flow regulators (Section 3.4.2). The

ratio of actual value (AV) to set point (SP) provided by the flow regulators is 0,98, which remains constant till a SP of 15 $Nm^3 \cdot h^{-1}$ and then decreases as the SP approaches its upper limit (Figure 3.7). The error (difference between SP and AV) increases with increasing SP, and AV is always less than the SP. The ratio of AV to SP should be used to choose a SP for a desired AV.

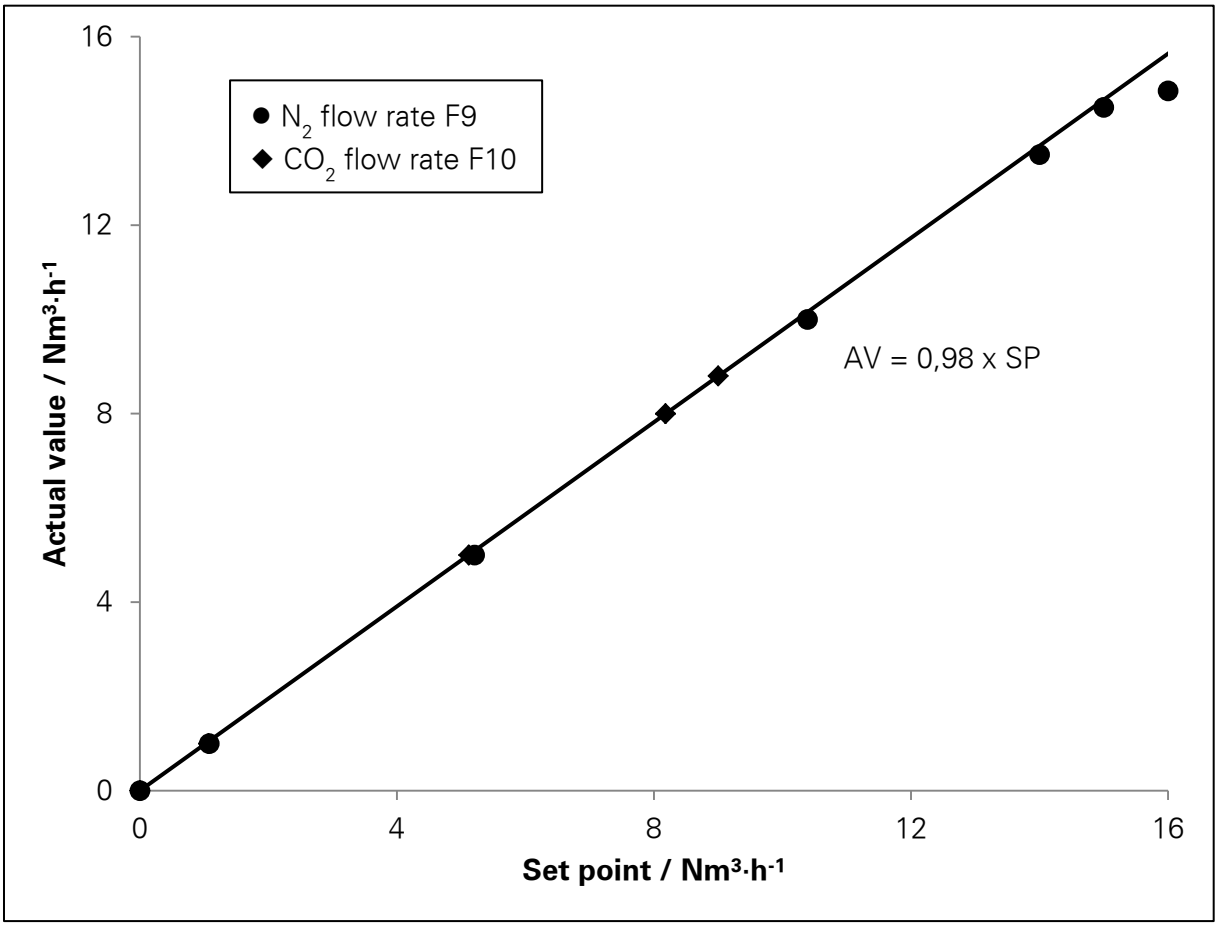

Figure 3.7 Actual value (AV) and set point (SP) for N_2 flow rate F9 and CO_2 flow rate F10

The upper limit of the N_2 flow rate F9 was set at 12 $Nm^3 \cdot h^{-1}$ in spite of the operating range of its flow controller being up to 25 $Nm^3 \cdot h^{-1}$. As gas flow rate increases, pressure drop ΔP increases and reaches its safety threshold ΔP_{saf} of 0,76 bar for a N_2 flow rate of slightly above 12 $Nm^3 \cdot h^{-1}$. The test rig is designed to principally operate at near-atmospheric pressure, and ΔP between the flow regulator and the absorber top (gas outlet) may not exceed ΔP_{saf} (0,76 bar). If $\Delta P \geq \Delta P_{saf}$, the test rig automatically shuts down. The flow rate at which a certain ΔP is created depends on gas density; consequently, the upper limit of the gas flow rate depends upon the gas itself. CO_2 flow rate F10 is regulated using a flow controller whose range is from 0 to 9,1 $Nm^3 \cdot h^{-1}$; however, the upper limit of F10 is 8 $Nm^3 \cdot h^{-1}$ due to aforementioned safety restrictions ($\Delta P < \Delta P_{saf}$).

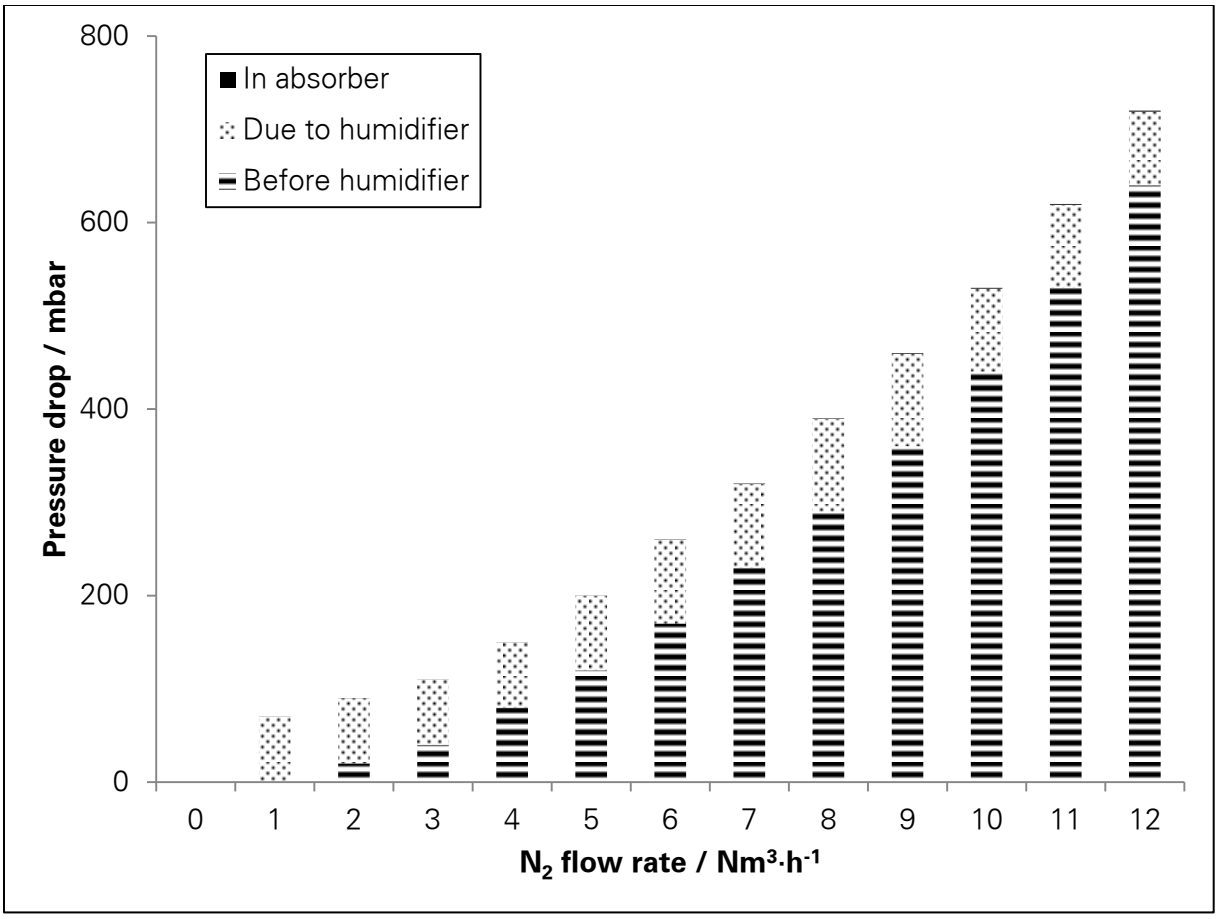

Figure 3.8 Pressure drop in the test rig at various N_2 flow rates

For a gas mixture of 60 vol. % N_2 and 40 % CO_2, the maximum permissible gas flow rate is 10 $Nm^3 \cdot h^{-1}$, which is the gas-treating capacity of the revamped test rig. The capacity can be further increased if ΔP is decreased. The majority of the pressure drop is observed between the flow regulator and the humidifier (Figure 3.8), and ΔP can be decreased by increasing the diameter of the feed-gas pipe which will reduce friction losses. If the inner pipe diameter is doubled from its current value of DN8, ΔP can be reduced by ten times.

Solvent flow rate F2 is a process variable that is regulated using the process-control software with an inbuilt controller (a regulation mechanism). For a SP of 50 $kg \cdot h^{-1}$, the AV was 49 ± 7 $kg \cdot h^{-1}$, but the minimum value was 21 $kg \cdot h^{-1}$, which is 42 % of SP and close to 0 $kg \cdot h^{-1}$. Although such dips in F2 were transient, they were frequent, and operation at the SP of 50 $kg \cdot h^{-1}$ was considered to be unsteady and hence unsuitable. The fluctuations can be attributed to the quick response of the controller, and it is conjectured that the problem can be solved by increasing the time constant of the controller. For a set point of 100 $kg \cdot h^{-1}$, the AV varied from 100 ± 12 to 100 ± 2 $kg \cdot h^{-1}$ depending upon the solvent temperature; the former value was for a temperature of ~ 30 °C, whereas the latter value was for a slightly

higher temperature (~ 40 °C). Therefore the lower limit of the operational range was set at 100 $kg \cdot h^{-1}$. The upper limit is dependent upon the pump load. The pump can, but should not be continuously operated at a load of more than 80 % of its maximum load. For 70 wt. % DGA in solvent as the solvent, the pump load F.P1 was 79,5 ± 0,3 % for F2 of 400 $kg \cdot h^{-1}$. Therefore the upper limit of solvent flow rate F2 was set at 400 $kg \cdot h^{-1}$. The upper limit must be determined anew for a different solvent because the pump load changes with solvent viscosity and density.

Pump P3 is level controlled in contrast to pump P1, which is flow controlled. Solvent level L3 in buffer vessel B3 of pump P3 is a process variable (Table 3.11). On one hand, L3 should not be set to a value below 20 % as a transient drop in the solvent flow rate may cause the pump to run dry which will damage the pump. On the other hand, L3 should not be set to a value greater than 60 %, or else vessel level L1 of pump P1 will become too low, and the pump P1 might run dry. These limits are valid irrespective of the solvent used.

The cooling-water flow rates F6 and F8 are restricted by the diameter of the water pipes and the corresponding valves. Another key property of the cooling water is its temperature, which cannot be regulated here because ground water is used as cooling water. Ground-water temperature fluctuates with the season between 7 and 14 °C where the test rig is located.

The reboiler W4 is an electrical heater, whose operating power can be regulated; the maximum (100 %) power of the reboiler W4 is 9 kW. Solvent temperature at reboiler outlet depends upon set reboiler power W4.y, solvent flow rate F2, solvent temperature at reboiler inlet and solvent heat capacity. The maximum temperature of the solvent at the reboiler outlet is the solvent's boiling point, which is approximately 107 °C for 70 wt. % DGA in solvent. However, solvent temperature on the surface of the heating coils (heat sources) is higher than the average solvent temperature. Because the solvent degrades at high temperatures (120 °C for DGA), reboiler power output W4.y should not be excessively high. Inconveniently, no temperature sensors are located on the surface of heating coils or at the reboiler outlet; therefore, the upper limit of the reboiler power W4.y was determined by an educated guess. Measuring the temperature of the surface of the reboiler vessel and observing the size of solvent-vapour slugs on the heating coils, it was determined that W4.y should not be more than 20 % of the power necessary to boil the solvent. The direction of the solvent and vapour flow in the reboiler W4 is not typical of a thermo-siphon reboiler (Figure 3.5). The upper end of the heating coils in the reboiler W4 is above the upper end of the buffer vessel B3. If the reboiler W4 is operated in the classical thermo-siphon mode, the

solvent will flow from the reboiler W4 into the buffer vessel B3, and the upper part of the heating coils in the reboiler W4 will be exposed which will damage the reboiler W4.

The preheater W6 is an electrical heater with a power rating of 20 kW. It is regulated using the solvent temperature T5 measured at its outlet. The preheater W6 heats the spent solvent after it has exited the heat exchanger W5; the solvent at the preheater inlet has a temperature that is 2 to 10 K below the temperature T15 of the lean solvent coming from the stripper K3. T15 is between 90 and 105 °C depending upon the reboiler power W4.y and the solvent flow rate F2. As the preheater W6 is not a thermostat, which can cool the solvent, the lowest value of T5 (temperature of the solvent at the preheater W6 outlet) is 80 °C. The upper limit of the T5 is a value that is below the boiling point and the degradation temperature of the solvent. The preheater W6 should heat the solvent to just below its boiling point, which is approximately 107 °C for the solvent (70 wt. % DGA in solvent). As typical for an electrical heater, the solvent temperature on the surface of the heating coils (heat sources) is higher than the average solvent temperature. The electrical heater has a heating volume of 6 l and a power rating of 20 kW, making it a disproportionately large heat source even assuming uniform heating, i.e. within 1 s the solvent temperature rises by approximately 1 K for a solvent density of 1100 $kg \cdot m^{-3}$ and a heat capacity 3 $kJ \cdot (kg \cdot K)^{-1}$. In reality, the heat is supplied at first to the solvent surrounding the coils which causes a local temperature rise of 10 to 30 K. Thus locally, the solvent boils, which is indicated by the intermittent bursts of solvent-vapour at the preheater outlet. In order to reduce the severity of these bursts, the upper limit of T5 (solvent temperature at the preheater W6 outlet) was set at 95 °C, which is more than 10 K below the solvent's boiling point.

With this well-equipped test rig, experiments were conducted to determine the optimal process conditions for separating CO_2 from a concentrated gas (e.g. biogas).

3.5 DETERMINING OPTIMAL PROCESS PARAMETERS

The goal is to use the test rig to collect data that can be used to design the absorption process that uses 70 wt. % DGA in solvent as the absorption solvent to separate CO_2 from biogas, thereby upgrading it to biomethane. Section 3.5.1 describes how a model was selected to predict the specific pressure drop in the columns of the test rig. Section 3.5.2 describes how the influence of process parameters such as regeneration energy and liquid to gas ratio on CO_2 separation was determined. Section 3.5.3 describes how CO_2 purity in the off gas was measured to determine if the absorption process can be used as a source of

CO_2, and Section 3.5.4 describes how a model absorption plant was designed using the optimal process parameters.

3.5.1 SPECIFIC PRESSURE DROP

Specific pressure drop $\Delta P/l$ indicates the degree of contact between the solvent and gas, and $\Delta P/l$ data can be used to select the region (below or above the loading point) in which the column is operated (Section 2.5.3). In addition, $\Delta P/l$ is used to calculate the total pressure drop in the column which is indispensable information when selecting the feed-gas compressor (blower).

Packing manufacturers provide softwares that can be used to predict $\Delta P/l$. However, these softwares may provide incorrect results for thin columns (column diameter $d_{col} < 1$ m), and smaller the d_{col}, bigger is the deviation between actual and predicted $\Delta P/l$ values. The test-rig columns have a diameter of DN100 and such columns generally suffer from solvent maldistribution as an appreciable amount of solvent flows down the column walls (Kister, 1992). The solvent flowing down the column walls does not impede the upward gas flow as the gas chooses a path of least resistance and flows through the central region of the column cross section. Consequently, the total resistance experienced by the gas and $\Delta P/l$ are lower in the case where solvent flows down the column walls. Therefore, it is necessary to find a method that can be used to predict $\Delta P/l$ in the test-rig columns.

Two generic methods that can be used to predict $\Delta P/l$ are discussed here. One method uses the generalized pressure drop correlation (GPDC) chart and the packing-specific constant packing factor *PF* to determine $\Delta P/l$ (Section 2.5.3). The other method uses a modified version of the model (Equation 3.6) developed by Darcy and Weißbach to predict $\Delta P/l$ in a bundle of tubes (Reichelt, 1972). Ψ is the resistance coefficient, which is calculated using packing-specific constants; ρ is the density; v is the velocity, and d is the tube diameter. Two popular examples of the modified model are the Billet-and-Schultes model (1999) and the Mackowiak model (2010), which are later described in this section.

$$\frac{\Delta P}{l} = \Psi \frac{\rho_{gas} v_{gas}^2}{2} \frac{1}{d} \qquad 3.6$$

Section 2.5.3 describes the method that uses the GPDC chart and packing factor *PF* to determine $\Delta P/l$. However, GPDC charts can be used when $\Delta P/l$ is at least 80 $Pa \cdot m^{-1}$ and capacity parameter *CP* is at least 0,2, which corresponds to approximately 6 $Nm^3 \cdot h^{-1}$ N_2 flowing through a test-rig column. Therefore, this method cannot be used to predict $\Delta P/l$ in the entire operational range of the test-rig columns. In addition, reading the chart is an

analogue step, and $\Delta P/l$ values obtained using this method have a large uncertainty (at least 120 Pa·m^{-1}).

A mathematical model developed by Billet and Schultes (1999) uses column dimensions, packing characteristics, properties of the solvent and gas, and their flow rates to predict $\Delta P/l$. $\Delta P/l$ in a packed column is given by Equation 3.7. $A_{p,v}$ is the volume-specific area of the packing; E is the void fraction of the packing, and $k_{p,0}$ is the reference constant of the packing. Ψ is the resistance coefficient (Equation 3.8), and Ψ_0 is the dry (unirrigated) resistance coefficient (Equation 3.9) Re is the Reynolds number (Equations 3.10 and 3.11), and Fr is the Froude number (Equation 3.12). WF is the wall factor (Equation 3.13), which takes into account the increased void fraction at the column walls. ho_{solv} is the liquid (solvent) holdup below the loading region (Equation 3.14). Equation 3.14a is applicable for laminar solvent flow ($Re_{solv} < 5$), and Equation 3.14b is valid for turbulent flow ($Re_{solv} \geq 5$). In the laminar flow regime, the viscous force dominates, and in the turbulent regime, the resistance force dominates; therefore, different equations are used to calculate the liquid holdup. k_h is the hydraulic constant of the packing. d_{col} is the column diameter. g is the acceleration due to gravity. ρ is the density, and μ is the dynamic viscosity. F_{gas} is the F-factor for the gas (Equation 2.9), and v is the velocity. This set of equations can be numerically solved, and the procedure does not involve any analogue step.

$$\frac{\Delta P}{l} = \Psi \frac{A_{p,v}}{(E - ho_{solv})^3} \frac{F_{gas}^2}{2} \frac{1}{WF} \qquad 3.7$$

$$\Psi = k_{p,0}\left(\frac{64}{Re_{gas}} + \frac{1{,}8}{Re_{gas}^{0,08}}\right)\left(\frac{E - ho_{solv}}{E}\right)^{1,5} exp\left(\frac{13300}{A_{p,v}^{1,5}}\sqrt{Fr_{solv}}\right) \qquad 3.8$$

$$\Psi_0 = k_{p,0}\left(\frac{64}{Re_{gas}} + \frac{1{,}8}{Re_{gas}^{0,08}}\right) \qquad 3.9$$

$$Re_{gas} = \frac{\rho_{gas} v_{gas}}{\mu_{gas} A_{p,v}} 6WF \qquad 3.10$$

$$Re_{solv} = \frac{\rho_{solv} v_{solv}}{\mu_{solv} A_{p,v}} \qquad 3.11$$

$$Fr_{solv} = \frac{v_{solv} A_{p,v}}{g} \qquad 3.12$$

$$\frac{1}{WF} = 1 + \frac{4}{A_{p,v} d_{col}} \qquad 3.13$$

$$ho_{solv} = \left(\frac{12}{g}\frac{\mu_{solv}}{\rho_{solv}} v_{solv} A_{p,v}^2\right)^{1/3} \left(k_h (Re_{solv})^{0,15} (Fr_{solv})^{0,1}\right)^{2/3} \qquad 3.14a$$

$$ho_{solv} = \left(\frac{12}{g}\frac{\mu_{solv}}{\rho_{solv}} v_{solv} A_{p,v}^2\right)^{1/3} (0{,}85 k_h (Re_{solv})^{0{,}25} (Fr_{solv})^{0{,}1})^{2/3} \quad 3.14b$$

$$F_{gas} = v_{gas}\sqrt{\rho_{gas}} \quad 2.9$$

To solve the above set of equations, solvent and gas properties were obtained either from a database or were experimentally determined (Section 3.2). Packing characteristics were obtained from the packing manufacturer and the literature, and column diameter and height were obtained from the column manufacturer (Table 3.12). Constants $k_{p,0}$ and k_h were known for the structured packing Mellapak 250.Y, but $k_{p,0}$ and k_h for Novalox-M 15 mm were not known.

Table 3.12 Packing and column characteristics

Parameter	Unit	Novalox-M 15 mm	Mellapak 250.Y	Source
Packing factor	ft^{-1}	51	20	Strigle, 1994
Void fraction	-	0,96	0,97	Billet and Schultes, 1999;
Volume-specific area	$m^2 \cdot m^{-3}$	290	250	VFF, 2012
Column diameter	m	0,1010 ± 0,0034		Ohle, 2009; De Dietrich Process
Packing height	m	3,0 ± 0,1		Systems GmbH, 2014

The reference constant of the packing $k_{p,0}$ was determined by regressing the measured $\Delta P/l$ values against calculated values; calculations were made according to Equation 3.7, and measurements were conducted as follows.

N_2 flow rate through the absorber (a column filled with Novalox-M 15 mm) was varied from 1 to 12 $Nm^3 \cdot h^{-1}$ in steps of 1 $Nm^3 \cdot h^{-1}$. No solvent was pumped through the column. Total pressure drop ΔP inside the column was recorded, and the specific pressure drop $\Delta P/l$ was calculated. After changing the gas flow rate, a stabilisation time of 60 s was given before recording ΔP. This procedure was repeated for another column filled with Mellapak 250.Y (stripper), and the results were compared with the values obtained from literature to validate this method of determining the constant $k_{p,0}$.

The hydraulic constant of the packing k_h was also determined by regressing the measured $\Delta P/l$ values against the calculated values. The solvent flow in the test rig was always laminar and had a $Re_{solv} < 1$. The calculations were made according to Equations 3.7 and 3.14a, and the measurements were conducted as follows.

The absorption solvent was pumped through the absorber (a column filled with Novalox-M 15 mm) at the mass flow rate of 300 $kg \cdot h^{-1}$. N_2 flow rate through the absorber was varied

from 1 to 12 $Nm^3 \cdot h^{-1}$ in steps of 1 $Nm^3 \cdot h^{-1}$. Total pressure drop ΔP inside the column was recorded, and the specific pressure drop $\Delta P/l$ was calculated. After changing the gas flow rate, a stabilisation time of 60 s was given before recording ΔP. This procedure was repeated for the column filled with Mellapak 250.Y (stripper), and the results were compared to the values obtained from literature to validate this method of determining the constant k_h.

The packing-specific constants thus determined can be used to predict $\Delta P/l$ below the loading region in the test-rig columns. To predict $\Delta P/l$ in the loading region, Billet and Schultes (1999) provide another set of equations (not shown here), which employ two additional packing-specific constants. As operation in the loading region of the test-rig columns was not possible on account of the operational limitations on the solvent and gas flow rates (Section 3.4.3), the two additional packing-specific constants could not be experimentally determined. Moreover, if the constants were to be obtained from literature, it would not be possible to check their validity for the test rig.

The model developed by Mackowiak (2010) uses just one set of equations, which are valid below and above the loading point. The Mackowiak model uses a different method than the Billet-and-Schultes model to calculate the resistance coefficient and the liquid holdup in the column. Equation 3.15 is used to predict $\Delta P/l$ in the dry column, and the dry resistance coefficient Ψ_0 is given by Equation 3.16. To predict $\Delta P/l$ in the irrigated column, the model uses three packing-specific constants: the irrigated constant k_{irr}, k_1 and k_2. Equation 3.17a is valid for laminar solvent flow ($Re_{solv} < 2$), and Equation 3.17b is valid for turbulent solvent flow ($Re_{solv} \geq 2$). k_1 and k_2 take on different values below and above Re_{gas} of 2100, but do not change with Re_{solv}.

$$\frac{\Delta P}{l} = \Psi_0 \frac{A_{p,v}}{E} \frac{F_{gas}}{6WF} \tag{3.15}$$

$$\Psi_0 = \left(\frac{725{,}6}{Re_{gas}} + 3{,}203\right)\left(1 - k_{fo}\right) \tag{3.16}$$

$$\frac{\Delta P}{l} = \left(k_1 Re_{gas}^{k_2}\right) \frac{A_{p,v}}{E} \frac{F_{gas}}{6WF} \left[1 - \frac{0{,}674}{E} A_{p,v}^{2/3} \left(v_{solv} \frac{\mu_{solv}}{\rho_{solv}}\right)^{1/3}\right]^{-5} \tag{3.17a}$$

$$\frac{\Delta P}{l} = \left(k_1 Re_{gas}^{k_2}\right) \frac{A_{p,v}}{E} \frac{F_{gas}}{6WF} \left[1 - \frac{k_{irr}}{E} (Fr_{solv})^{1/3}\right]^{-5} \tag{3.17b}$$

The solvent flow in the test rig is always laminar and has a $Re_{solv} < 1$. Therefore it is not possible to determine k_{irr} by conducting experiments on the test rig. Form constant k_{fo} and k_1 were determined by regressing the measured $\Delta P/l$ values against the calculated values.

Experimental data used to determine $k_{p,0}$ and k_h was used here too, but the calculations were conducted using Equations 3.15 and 3.17a.

As the packing-specific constants are not dependent on the gas-solvent system, the validity of k_{fo}, k_1 and k_2 to a different gas system was checked as follows. The Mackowiak model was used to predict $\Delta P/l$ at feed gas (60 vol. % N_2 and 40 vol. % CO_2) flow rates of 1,25, 2,5, 5, 7,5 and 10 $Nm^3 \cdot h^{-1}$. The resultant values were compared with experimentally determined values.

3.5.2 INFLUENCE OF PROCESS PARAMETERS ON CO_2 SEPARATION

The influence of process parameters, namely the liquid to gas ratio and regeneration energy on CO_2 separation was determined using experiments.

Definition of an experiment

Every experiment consisted of at least two runs, and every run lasted for at least fifteen minutes, preferably sixty minutes. Runs were carried out on operation days. An operation day lasted for three to eight hours and consisted of three phases: start-up, measurement and shutdown. The start-up and shutdown procedures are described in Appendix D. The measurement phase included the time period necessary to achieve steady state operation and to conduct the run itself. For each run, process parameters (data) were recorded by the computer (Table E.1) at a rate of at least one data point per minute. In addition, some parameters were recorded by hand (Table E.2) at a rate of one data point per run. The data generated from the two runs was averaged and used for further analysis. Parameter range shown in Table E.1 and Table E.2 is the characteristic of the sensor, and not the operational characteristic of the process variable. In addition, CO_2 loading in the spent solvent was determined using the procedure described in Section 3.2.1.

Influence of regeneration energy on CO_2 separation

Regeneration energy is the energy added to the solvent to desorb CO_2 and make the solvent reusable in the absorber. The regeneration energy is the sum of the energy input of the preheater and the reboiler as it is assumed that all of the energy consumed by the electrical preheater and reboiler is dissipated as heat into the solvent.

Changing the regeneration energy changes the CO_2 loading in the lean solvent, which affects the degree of separation and the concentration of CO_2 in the treated gas. Therefore,

the desired CO_2 concentration in the treated gas (biomethane) can be achieved by appropriately selecting the regeneration energy.

Experiments were conducted at constant solvent and gas flow rates, but the operating power of the reboiler was varied. The power of the preheater cannot be directly regulated, and its energy consumption depends upon the set solvent temperature at its outlet which was kept constant at 95 °C. The experimental matrix is shown in Table 3.13.

Table 3.13 Experimental matrix used to determine the influence of regeneration energy

Solvent flow rate	**Gas flow rate**	**Liquid to gas ratio**	**Reboiler power**
F2 / $kg \cdot h^{-1}$	**F9 + F10 / $Nm^3 \cdot h^{-1}$**	**mol DGA· $(mol\ CO_2)^{-1}$**	**W4.y / % of 9 kW**
100	2,5	15,0	0
100	2,5	15,0	20
100	2,5	15,0	30
100	2,5	15,0	40
100	10,0	3,8	20
100	10,0	3,8	40
100	10,0	3,8	80

Influence of liquid to gas ratio on regeneration energy

Liquid to gas ratio is the ratio of the molar flow rate of DGA (in the solvent without CO_2) to the molar flow rate of CO_2 (in the feed gas). As the mole fraction of CO_2 in the feed gas and the mole fraction of DGA in the solvent are predefined, the liquid to gas ratio changes with the solvent and gas flow rates.

Table 3.14 Experimental matrix used to determine the influence of liquid to gas ratio in which the gas flow rate was varied

Solvent flow rate	**Gas flow rate**	**Liquid to gas ratio**	**Reboiler power**
F2 / $kg \cdot h^{-1}$	**F9 + F10 / $Nm^3 \cdot h^{-1}$**	**mol DGA· $(mol\ CO_2)^{-1}$**	**W4.y / % of 9 kW**
100	2,5	15,0	30
100	4,0	9,5	50
100	5,0	7,5	60
100	6,0	6,3	80
100	7,5	5,0	80
100	10,0	3,8	80

The liquid to gas ratio was changed by changing the gas flow rate for a constant solvent flow rate. The regeneration power was selected such that a constant degree of separation of approximately 0,98 mol CO_2·(mol CO_2)$^{-1}$ was obtained. The experimental matrix is shown in Table 3.14.

Experiments were also conducted for various liquid to gas ratios in which the gas flow rate was kept constant and the solvent flow rate was varied. The regeneration power was selected such that a constant degree of separation of approximately 0,35 mol CO_2·(mol CO_2)$^{-1}$ was obtained. Due to the limitations on the operational range of the test rig, experiments could not be conducted to obtain the constant degree of separation of 0,98 mol CO_2·(mol CO_2)$^{-1}$ for the case of varying solvent flow rates. The experimental matrix is shown in Table 3.15.

Table 3.15 Experimental matrix used to determine the influence of liquid to gas ratio in which the solvent flow rate was varied

Solvent flow rate	**Gas flow rate**	**Liquid to gas ratio**	**Reboiler power**
F2 / kg·h^{-1}	**F9 + F10 / Nm^3·h^{-1}**	**mol DGA· (mol CO_2)$^{-1}$**	**W4.y / % of 9 kW**
100	10,0	3,8	40
200	10,0	7,5	40
400	10,0	15,0	40

This data was used to determine the optimal liquid to gas ratio, and to calculate the heating and cooling energy demands in a model absorption plant.

Determination of the mass transfer coefficient

The overall volumetric mass transfer coefficients K_Ga in the absorber were determined during the experiments of Table 3.14 using Equations 3.18 and 3.19 where $G_{mo,CO2,abs}$ is the molar flow rate of absorbed CO_2; V_p is the packing volume, and $\Delta(\Delta p_{CO2})_{lm}$ is the log mean difference of the difference in CO_2 partial pressure and vapour pressure at the column top and bottom.

$$K_G a = \frac{G_{mo,CO2,abs}}{\Delta(\Delta p_{CO2})_{lm} V_p} \qquad 3.18$$

$$\Delta(\Delta p_{CO2})_{lm} = \frac{\Delta p_{CO2,top} - \Delta p_{CO2,bot}}{ln\left(\frac{\Delta p_{CO2,top}}{\Delta p_{CO2,bot}}\right)} \qquad 3.19$$

3.5.3 CO_2 CONTENT IN OFF GAS

CO_2 that is desorbed from the solvent in the stripper is an entity that can be sold as a product if it is available in high purity. Therefore, the CO_2 content in the off gas was measured to determine the purity of CO_2 obtained from the absorption process with 70 wt. % DGA as the solvent.

A Y-joint was connected to the off gas (the gas stream at the stripper top after the condenser) pipe where one end was open, and the other end was connected to the Infralyt (a CO_2-measuring instrument) through an adsorption dryer (silica-gel bottle). This ensured that gas under pressure did not flow into the Infralyt and that no water vapour entered the Infralyt. The experimental matrix is shown in Table 3.16

Table 3.16 Experimental matrix used to determine CO_2 content in off gas

Solvent flow rate	**Gas flow rate**	**Liquid to gas ratio**	**Reboiler power**
F2 / $kg \cdot h^{-1}$	**F9 + F10 / $Nm^3 \cdot h^{-1}$**	**mol DGA· $(mol\ CO_2)^{-1}$**	**W4.y / % of 9 kW**
200	5	15	40

3.5.4 PROCESS SCALE UP

The average size of biomethane plants in Germany is 600 $Nm^3 \cdot h^{-1}$ biomethane (Biogaspartner, 2014). Therefore for process scale up, the feed gas of the absorption plant was considered to be 1000 $Nm^3 \cdot h^{-1}$ biogas. The absorption solvent was 70 wt. % DGA in solvent, which upgraded biogas to biomethane.

Diameter and height of the absorber and stripper were calculated for the process conditions shown in Table 3.17. Ultimate solvent flow rate was calculated based upon the given feed-gas flow rate and the experimentally determined optimal liquid to gas ratio. Absorber operation was considered isothermal at 30 °C, which is the average temperature of the solvent at absorber inlet and outlet. It was assumed that CH_4 was not absorbed in the solvent, and solvent was not lost (entrained, evaporated, vaporized or degraded) in the absorber. In the stripper, the reboiler heated the solvent and generated steam only. In other words, the CO_2 content in the solvent at the stripper bottom was already below the equilibrium CO_2 content at the reboiler temperature of 105 °C, and consequently, CO_2 partial pressure in the gas phase at the stripper bottom was 0 kPa. Steam from the reboiler flowed upwards in the stripper and stripped off CO_2 from the solvent. Solvent entering the stripper was at equilibrium: CO_2 partial pressure and CO_2 content in the solvent at the stripper inlet

(solvent inlet) were the respective equilibrium values at 95 °C. This is explained by the phenomenon of "acid-gas breakout" (Addington and Ness, 2014), which means that as solvent is heated in the solvent-solvent heat exchanger and preheater, CO_2 begins to desorb and the solvent almost reaches equilibrium at the stripper inlet. This implied that CO_2 content in the solvent at the stripper inlet was smaller than the CO_2 content at the absorber outlet. It was assumed that no solvent was lost in the stripper.

Table 3.17 Mole fraction of CO_2 in the gas y, molar flow rate of the gas G_{mo} at absorber bottom and stripper top

Symbol	Unit	Design value
Absorber		
y_{in}	mol CO_2·(mol CO_2+CH_4)$^{-1}$	0,40
y_{out}	mol CO_2·(mol CO_2+CH_4)$^{-1}$	0,02
$G_{mo,bot}$	(mol CO_2+CH_4)·h^{-1}	44768
Stripper		
y_{in}	mol CO_2·(mol CO_2+H_2O)$^{-1}$	0,00
y_{out}	mol CO_2·(mol CO_2+H_2O)$^{-1}$	0,44
$G_{mo,top}$	(mol CO_2+H_2O)·h^{-1}	21979

Column diameter

For a given column packing, depending upon which packing-specific constants are known, a method can be selected to calculate the superficial gas velocity at the flooding point $v_{gas,fl}$. One method, which uses the packing-specific constant packing factor PF is described in Section 2.5.3, and this method was used to calculate d_{col}.

Another method based on the model of Billet and Schultes (1999) uses two packing-specific constants to calculate $v_{gas,fl}$, but the calculation procedure is iterative and complex, and this method was not used in this study to calculate d_{col}.

A third method is based on the model developed by Mackowiak (2010), which uses one packing-specific constant to calculate $v_{gas,fl}$ (Equation 3.20). Ψ_{fl} is the resistance coefficient at the flooding point which is a packing-specific constant. g is the acceleration due to gravity. E is the void fraction of the packing; $A_{p,v}$ is the void fraction of the packing, and d_h is the hydraulic diameter of the packing (Equation 3.21). ρ is the density, and σ is the surface tension. d_{St} is the Sauter diameter of the solvent droplets (Equation 3.22). $ho_{solv,fl}$ is the liquid holdup at flooding (Equation 3.23). λ_{fl} is the volumetric flow ratio at the flooding point (Equation 3.24). L_v and G_v are the volumetric flow rates of the solvent and the gas,

respectively. k_{fr} is the flow ratio constant (Equation 3.25); Equation 3.25a is valid for laminar solvent flow ($Re_{solv} < 2$), and Equation 3.25b is valid for turbulent flow $Re_{solv} \geq 2$.

$$v_{gas,fl} = 0{,}8\, E^{6/5} \Psi_{fl}^{-1/6} \sqrt{\frac{d_{St} g (\rho_{solv} - \rho_{gas})}{\rho_{gas}}} \left(\frac{d_h}{d_{St}}\right)^{1/4} \left(1 - h_{solv,fl}\right)^{7/2} \left(\frac{\rho_{gas}}{1{,}165}\right)^{0{,}18} \quad 3.20$$

$$d_h = \frac{4E}{A_{p,v}} \quad 3.21$$

$$d_{St} = \sqrt{\frac{\sigma_{solv}}{(\rho_{solv} - \rho_{gas}) g}} \quad 3.22$$

$$ho_{solv,fl} = \frac{\sqrt{\lambda_{fl}^2 (k_{fr}+2)^2 + 4\lambda_{fl}(k_{fr}+1)(1-\lambda_{fl})} - (k_{fr}+2)\lambda_{fl}}{2(k_{fr}+1)(1-\lambda_{fl})} \quad 3.23$$

$$\lambda_{fl} = \frac{L_v}{G_v} \quad 3.24$$

$$k_{fr} = -0{,}90 + \frac{\lambda_{fl}}{\lambda_{fl}+0{,}5} \quad 3.25a$$

$$k_{fr} = -0{,}82 + \frac{\lambda_{fl}}{\lambda_{fl}+0{,}5} \quad 3.25b$$

Packing manufacturers such as Koch-Glitsch LP recommend self-developed models to estimate $v_{gas,fl}$ for their packings (Koch-Glitsch LP, 2010). As these models are not generally applicable (e.g. for packings from other manufacturers), they are not discussed here.

Column height

Column height or packing height h was determined using the non-equilibrium or the rate-based approach (Equation 2.19c). NTU_{OG} was calculated using Equation 3.26, and HTU_{OG} was calculated using Equation 3.27.

$$h = HTU_{OG}\, NTU_{OG} \quad 2.19c$$

$$NTU_{OG} = \int_{y_{bot}}^{y_{top}} \left[\frac{(1-y)_{*,lm}}{(1-y)(y-y^*)}\right] dy \quad 3.26$$

$$HTU_{OG} = \frac{G_{mo}}{K_G a A P_{tot} (1-y)_{*,lm,av}} \quad 3.27$$

3.6 QUANTITATIVE HAZARD ANALYSIS

The method used to quantitatively compare the real hazards of absorption solvents is presented in Section 3.6.1, and the method used to determine the disposition of the German population towards hazards from biogas plants is described in Section 3.6.2.

3.6.1 DETERMINING REAL HAZARDS

Six principal reactants that can be used in absorption solvents, which are suitable to upgrade biogas to biomethane at atmospheric pressure, were selected for analysis: monoethanolamine (MEA), diglycolamine (DGA), diethanolamine (DEA), N-methyldiethanolamine (MDEA), piperazine (PZ) and aminomethylpropanol (AMP) (Dixit et al., 2012). These substances are mixed with water in different proportions and used as absorption solvents. PZ is always used with another principal reactant such as MDEA. AMP may be used solitarily or in combination with MEA (Kohl and Nielsen, 1997). The solvents react with CO_2 and O_2 present in biogas to produce reaction products, which were also considered in the analysis. Fifty-six reaction by-products were identified on the basis of a literature survey (Gahlert, 2013). The main reaction product that is produced during CO_2 absorption and is destroyed during desorption was not considered in the analysis.

The European Union (EU) regulation EC 1272 (2008) enlists possible physical, health and environmental hazards of substances and mixtures (Table 3.18). It provides guidelines on classifying substances or mixtures as hazardous and on further categorizing them based upon the severity of the hazard. The number of hazard categories varies with the hazard, and each hazard category has a unique hazard (H)-statement and an H-number.

After sifting through publicly available information such as the MSDSs and the GESTIS (*Gefahrstoffinformationssystem*) database, the classification of the investigated substances as hazardous or non-hazardous as per EC 1272 (2008) was determined. If the substance was hazardous, the hazard category was noted.

Data compiled on the classification and categorization of substances was used in a quantitative assessment method developed in this study to compare hazards of absorption solvents. For every hazard that a substance had, it was allocated hazard points *HP* on a linear scale from zero to one. E.g. for the hazard of acute oral toxicity, there are four categories one to four and no sub-categories; therefore, the number of divisions on the linear scale were four (Table 3.18). A hazard of category one (most hazardous) was allocated 1 *HP*, of category two was allocated 0,75 *HP*, of category three was allocated 0,5 *HP*, of category four (least hazardous) was allocated 0,25 *HP*, and non-hazardous substances were allocated 0 *HP*. If no information on the hazards of a substance was available, the substance was allocated 0,5 *HP*.

Table 3.18 Hazards and number of hazard categories as per EC 1272 (2008)

Hazard	Categories	Divisions on linear scale	Sr. No.
Flammable gas	1 to 2	2	1
Flammable liquid	1 to 3	3	2
Flammable solid	1 to 2	2	3
Oxidizing gas	1 to 3	3	4
Acute toxicity, oral	1 to 4	4	5
Acute toxicity, dermal	1 to 4	4	6
Acute toxicity, inhalant	1 to 4	4	7
Harmful to skin	1 to 2	4	8
Harmful to eyes	1 to 2	2	9
Respiratory sensitizer	1	1	10
Skin sensitizer	1	1	11
Carcinogenicity	1 to 2	3	12
Reproductive toxicity	1 to 3	4	13
Specific target organ toxicity, single exposure	1 to 3	3	14
Specific target organ toxicity, repeated exposure	1 to 2	2	15
Aquatic toxicity, acute	1	1	16
Aquatic toxicity, chronic	1 to 4	4	17

Table 3.19 Analysed absorption solvents

Sr. No.	Solvent name
1	30 wt. % MEA
2	60 wt. % DGA
3	30 wt. % DEA
4	50 wt. % MDEA
5	50 wt. % MDEA with 10 wt. % PZ
6	60 wt. % AMP
7	30 wt. % MEA with 30 wt. % AMP

Water, MEA, DGA, DEA, MDEA, PZ, AMP and their corresponding reaction by-products were combined to form seven absorption solvents, which are shown in Table 3.19. The typical mass proportions of water and the principal reactant as obtained from Kohl and Nielsen (1997) are also presented in Table 3.19. As the proportion of the reaction by-products varies with process conditions, the total amount of reaction by-products was assumed to be 10 % of the total solvent mass wherein all the by-products had equal mass. The hazards of absorption solvents, which are mixtures of substances, were determined using the procedure described in EC 1272 (2008). For hazards of the mixtures, *HP* were allocated in the same way as *HP* were allocated to substances.

Using this method, the hazards of absorption solvents were quantitatively compared, and the results of this study were used to rank absorption solvents based upon their hazard potential.

3.6.2 DETERMINING PERCEIVED HAZARDS

In February and March of 2014, a representative survey of the German population was conducted to determine if they think that biogas plants are hazardous; if yes, which hazards originate from biogas plants; how serious physical, health and environmental hazards are considered compared to each other, and how close they reside to a biogas plant.

Surveying method

The telephone was the medium through which questions were asked in the survey. Landline, household (not business) telephone numbers were randomly picked and dialled. If the telephone call was not answered, the telephone number was dialled six more times on four different dates (not more than two call attempts per day). If no contact was established in the seven attempts, another telephone number was randomly picked and dialled. If the telephone call was answered, a so-called contact was made. The individual whose birthday was nearest to and before the survey date, and was an adult (above 18 years of age) was the target individual, who was asked questions. If the target individual did not want to answer the questions, the individual was not surveyed. If the target individual could not answer the questions due to not being home, not having time and so on, the target individual was contacted later. Not more than seven attempts were made to contact a target individual. If the target individual was ready to answer the questions, a so-called cooperation was made. When an individual responded to all the questions, a so-called complete response was obtained.

Questionnaire

In the survey, thirty-three questions were asked out of which four questions were about biogas plants. These questions are translated into English and presented here with their serial numbers. Questions in German can be read verbatim in Appendix F.2.

Question 15: "Now a question about biogas plants. They are used to generate electricity and heat. Do you actually think that hazards originate from biogas plants or you don't think so?" Answer options were 'yes', 'no', and 'do not know / cannot assess'.

Question 16 for those who answered 'yes' to question 15: "And which hazards from biogas plants do you know of?" Multiple answers were possible, and no answer options were provided.

Question 17: "I will now read a list of hazards. Please tell me on a scale from 1 to 10 how serious you consider each hazard to be. '1' means not serious, and '10' means very serious. With the values in between, you can rate your opinion.

- Fire and explosion hazard
- Threat to human beings due to polluted air and water
- Environmental threat to animals and plants"

Answer options were whole numbers from 1 to 10, and 'do not know / cannot assess'.

Question 18: "Do you reside in the immediate neighbourhood of a biogas plant or within 3 km?" Answer options were 'in immediate neighbourhood', 'within 3 km', 'none of these', and 'do not know / cannot assess'.

When all the questions were answered, information on the gender, age and education of the respondent was collected.

The data collected in the survey will help to understand the disposition of the German population towards hazards from biogas plants. This information can then be used to develop strategies to gain public acceptance.

3.7 LIFE CYCLE ASSESSMENT

The life cycle assessment (LCA) study consists of four phases (ISO 14040, 2006):

- Goal and scope definition phase
- Inventory analysis phase
- Impact assessment phase
- Interpretation phase

A brief description of the LCA study conducted is presented here; details are available in Muench et al. (2015).

3.7.1 GOAL AND SCOPE

The goal was to determine the environmental impacts of the biomethane-production process that constitutes upgrading biogas to biomethane using 70 wt. % DGA in solvent as the

absorption solvent. The LCA study was used to identify the main sources of adverse environmental effects in the biomethane-production process. Furthermore, the environmental impacts of biomethane production were compared with those of natural-gas production (the reference system) to determine conditions under which natural gas should be substituted by biomethane. The LCA results should be of interest to the engineering industry, process researchers in the academia as well as in the industry, and policy-making institutions.

The primary function of the investigated product system is biomethane production. The functional unit was defined as 1 MJ of natural-gas equivalent in the H-Gas pipeline (Table 2.2) at near-atmospheric pressure (< 2 bar) at the consumer.

The system boundary included four key processes: biogas production, solvent production, biogas upgrading, and biomethane transport (Figure 3.9), which are described in Section 3.7.2. Ancillary processes within the system boundary were transport of process elements, and plant construction and decommissioning.

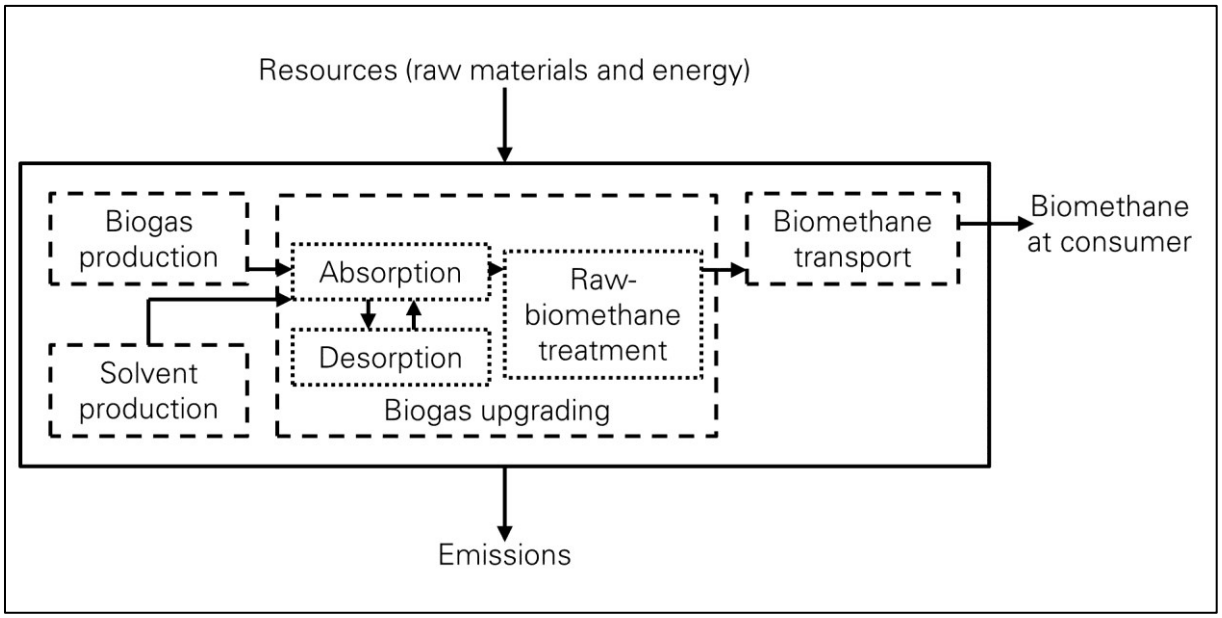

Figure 3.9 Product system and system boundary
(adapted from Muench et al., 2015)

The input parameters to the LCA were either experimentally determined or were obtained from the ecoinvent database (Ecoinvent association, 2014).

The environmental impacts of the product system were assessed using the baseline impact categories of Centrum voor Milieukunde (CML) which are described in Section 3.7.3. They constitute the so-called mid-point approach because the impact categories are at the middle

of the cause-effect chain (Guinee, 2004). This approach has been predominantly used to assess the environmental impacts of bioenergy systems (Muench and Guenther, 2013).

3.7.2 LIFE CYCLE INVENTORY ANALYSIS

This section describes the unit processes that constitute the product system in the LCA, the procedures of allocating environmental impacts in multi-output processes, and the quality assessment of the input data.

Biogas production

Biogas was produced by the fermentation of liquid manure and biowaste (feedstock). Liquid manure was available on site, but biowaste had to be transported to the biogas plant. The composition of biogas was as follows: 67,0 vol. % CH_4, 32,1 vol. % CO_2, 0,7 vol. % N_2, 0,3 vol. % O_2, and 0,0005 vol. % H_2S. This biogas plant had a production capacity of 500 $Nm^3 \cdot h^{-1}$ biogas. The hourly energy demand of the plant was 170 MJ_{el} and 2833 MJ_{th} (Jungbluth et al., 2007). The lifetime of the plant was presumed to be 20 years with 8000 operating hours per year.

Solvent production

DGA ($C_4H_{11}NO_2$) was produced by a catalytic reaction between diethylene glycol ($C_4H_{10}O_3$) and NH_3 in the presence of H_2 (Katdare et al., 2012) as shown in Equation 3.28. Morpholine (C_4H_9NO) was also produced during the reaction.

$$0{,}69C_4H_{10}O_3 + 22{,}47NH_3 \rightarrow 0{,}58C_4H_{11}NO_2 + 0{,}11C_4H_9NO + 0{,}69H_2O + 21{,}85NH_3 \qquad 3.28$$

Production of 1 kg DGA required an energy of 1 MJ_{el} and 0,46 MJ_{th}. The distance between the DGA-production and the biomethane-production plant was considered to be 450 km. The solvent had a life time of 3 years. Data on material transport, electricity demand, construction and decommissioning of the solvent-production plant was considered equivalent to the ethanolamine-production facility described in Althaus et al. (2007).

Biogas upgrading

Biogas was transported with the help of a compressor from the biogas plant to the biogas-upgrading plant, which had a life of 10 years.

Absorption: The biogas then flowed into the absorber where the solvent reacted with CO_2 and O_2 in the biogas. The methane slip was not more than 0,1 vol. %. The process yielded

raw biomethane with a composition of 95,7 vol. % CH_4, 2,3 vol. % H_2O, 1,0 vol. % N_2 and 1,0 vol. % CO_2. The hourly energy demand of the process was 67 MJ_{el}.

Raw-biomethane treatment: Water was separated from raw biomethane using an adsorption dryer, thereby producing biomethane with a purity of 98 vol. % CH_4. Biomethane was odourised, compressed and fed into the H-Gas pipeline at near-atmospheric pressure (< 2 bar). The hourly energy demand of the process was 148 MJ_{el}. Odourization of biomethane was not considered in the LCA because its environmental impacts are negligible (Jury et al., 2010).

Desorption: CO_2-loaded solvent (spent solvent) from the absorber was pumped into a stripper in which it was heated to 105 °C, thereby freeing the CO_2 and CH_4 which were emitted into the air. O_2 remained in the solvent in the form of degradation products. The lean solvent was then pumped through a heat exchanger and a cooler into the absorber. The heat exchanger transferred heat from the lean solvent to the spent solvent which reduced the energy demand of the stripper by 67 %. The hourly energy demand of this process was 41 MJ_{el} and 2237 MJ_{th}.

Biomethane transport

Biomethane is transported to the consumer via the H-Gas pipeline at near-atmospheric pressure. The environmental impacts of the process were derived from the ecoinvent database (Ecoinvent association, 2014).

Allocation of environmental impacts

The environmental impacts of a multi-output process were allocated between its products: the environmental impacts of waste products were allocated to the valuable product, and if a process yielded multiple valuable products, the allocation was based on molar mass.

Data-quality assessment

The quality of input parameters was quantitatively assessed using a pedigree matrix, which employs data quality indicators (DQIs) such as reliability, completeness, temporal correlation, geographical correlation, and further technological correlation to build data quality indices that are converted into standard deviation, termed as the additional standard deviation (Weidema and Wesnaes, 1996; Weidema et al., 2013). The additional standard deviation together with the basic standard deviation, which exists due to uncertainty in parameter determination, constitutes the total standard deviation. The DQIs and the additional standard

deviation of the input parameters are shown in Table G.1 where the DQI value of one stands for the best and five for the worst.

Approximately 76 % of the input data parameters have good quality (additional standard deviation $\leq$ 0,1), and in fact 32 % have the best quality (additional standard deviation of 0). Approximately 24 % of the parameters have poor data quality (additional standard deviation > 0,1), and the reason for their poor quality is explained below.

Parameters describing the DGA-production process have poor data quality because they are derived from a patent and not from a real production process. Similarly, parameters describing the construction, operation and decommissioning of the DGA-production plant are of poor quality because they are based upon an ethanolamine plant and not upon a DGA-production plant. The parameter that describes CH_4 content in biogas has poor quality because the characteristics of the biomass feedstock vary. Parameters describing the construction, operation and decommissioning of the biogas-treatment plant also have poor quality because the data is based on a biogas-treatment plant that uses MEA as the absorption solvent (Muench et al., 2015).

Uncertainty importance analysis

The input parameters were varied one at a time by one total standard deviation, and the change in the so-called ReCiPe 2008 score (hierarchist perspective) was recorded. The ReCiPe score incorporates the environmental impacts into one single value (Goedkoop et al., 2013). The percentage change in the ReCiPe 2008 score is termed sensitivity, and the sum of the sensitivity of each parameter is called the cumulative sensitivity.

Monte Carlo simulation

The LCA model was run 10000 times, and during each run, input parameters were randomly varied (Ragas et al., 1999). Only those input parameters were varied, which contributed to more than 90 % of the cumulative sensitivity of the uncertainty importance analysis. These input parameters were presumed to have normal distribution, and a range of LCA results was obtained. This data was used to comprehend the influence of the uncertainty in input parameters on LCA results.

3.7.3 LIFE CYCLE IMPACT CATEGORIES

The various impact categories used in this LCA are as follows (Guinee, 2004).

Abiotic resource depletion potential (ADP) describes the consumption of non-living, natural resources such as iron ore and crude oil. ADP is expressed using the unit kilogram antimony equivalent (kg Sb eq.).

Acidification potential (AP) describes the adverse impact of acidifying pollutants such as SO_2, NO_x and NH_x on soil, ground and surface water, ecosystems, biological organisms, and material. AP is expressed using the unit kilogram sulphur dioxide equivalent (kg SO_2 eq.).

Ecotoxicity potential describes the adverse effects of toxic substances on different ecosystems, namely fresh water, marine and terrestrial ecosystems. The ecotoxicity potential of each ecosystem is uniquely designated: freshwater aquatic ecotoxicity potential (FAETP), marine aquatic ecotoxicity potential (MAETP), and terrestrial ecotoxicity potential (TETP), respectively. These potentials are expressed using the unit kilogram 1,4-dichlorobenzene equivalent (kg 1,4-DCB eq.).

Eutrophication potential (EP) describes the environmental enrichment of macronutrients such as nitrogen and phosphorous. Eutrophication may lead to a change in composition of species, increase in biomass production in aquatic and terrestrial ecosystems, and decrease in potability of surface water. EP is expressed using the unit kilogram phosphate equivalent (kg PO_4^{3-} eq.).

Global warming potential (GWP) describes the impact of greenhouse-gas emissions on the heat-radiation absorption, which causes an increase in the earth's surface temperature. GWP is expressed using the unit kilogram carbon dioxide equivalent (kg CO_2 eq.).

Human toxicity potential (HTP) describes the adverse effects of toxic substances on human health. HTP is expressed using the unit kilogram 1,4-dichlorobenzene equivalent (kg 1,4-DCB eq.).

Ozone depletion potential (ODP) describes the thinning of the stratospheric ozone layer due to anthropogenic emissions, which results in more ultraviolet B radiation reaching the earth's surface. ODP is expressed using the unit kilogram trichlorofluoromethane equivalent (kg CFC-11 eq.).

Photo oxidant creation potential (POCP) describes the formation of reactive chemical compounds such as ozone formed by the interaction between sunlight and air pollutants. POCP is expressed using the unit kilogram ethene equivalent (kg C_2H_4 eq.).

Using these impact categories, the environmental impacts of biomethane production process were determined and compared with those of the natural-gas production.

4 RESULTS AND DISCUSSION

Solvent properties determined by experiments and by simulations, process characteristics determined by experiments and calculations, and the assessment of solvent hazards and biomethane lifecycle are presented in this chapter. At the end of each subchapter, the conclusions drawn are presented.

4.1 SOLVENT PROPERTIES

Experimentally determined solvent properties such as the equilibrium CO_2 solubility, density, viscosity and surface tension are presented in this section (Meier, 2013; Kraut, 2014; Dixit and Mollekopf, 2014a).

4.1.1 EQUILIBRIUM CO_2 SOLUBILITY

A bubble column was selected to determine equilibrium CO_2 solubility α_{CO2} under absorption conditions. The bubbling gas carried water with it, but the water loss was not more than 2 wt. % of the total solvent. Gauge pressure in the bubble column above the solvent was never more than 7 Pa, and no pressure was built up above the solvent. Therefore, the pressure above the solvent can be assumed to be equal to the atmospheric pressure. The temperature variation in the solvent was not more than ± 0,7 K, and the variation in the pH value was not more than ± 0,01. The solvent remained homogeneous throughout an experiment. Foaming, phase change or precipitation in the solvent was not observed during the experiments.

A stirred-cell reactor was used to determine α_{CO2} under desorption conditions. The temperature variation in the solvent was not more than ± 0,2 K, and the pH variation was not more than ± 0,1. The solvent remained homogeneous throughout an experiment.

The experimental setups that were used to determine α_{CO2} were validated by comparing α_{CO2} values of 50 wt. % N-methyldiethanolamine (MDEA) in solvent (kg MDEA·(kg MDEA+H_2O)$^{-1}$) obtained using the setups with those from literature (Table 4.1). α_{CO2} values obtained in this study followed the trend shown by α_{CO2} data available in literature. At a given temperature T, as CO_2 partial pressure p_{CO2} increased, α_{CO2} increased, and at a given p_{CO2}, as T increased, α_{CO2} decreased.

Table 4.1 Equilibrium CO_2 solubility α_{CO2} of 50 wt. % MDEA in solvent determined at temperature T and CO_2 partial pressure p_{CO2}

Source	T K	p_{CO2} kPa	α_{CO2} mol CO_2·(mol MDEA)$^{-1}$
Huttenhuis et al., 2008	298	37	0,42
Huttenhuis et al., 2008	298	70	0,55
This study	303	44	0,44
Rho et al., 1997	373	45	0,05
Rho et al., 1997	373	11	0,02
This study	363	39*	0,15
This study	381	1*	0,02

** calculated values*

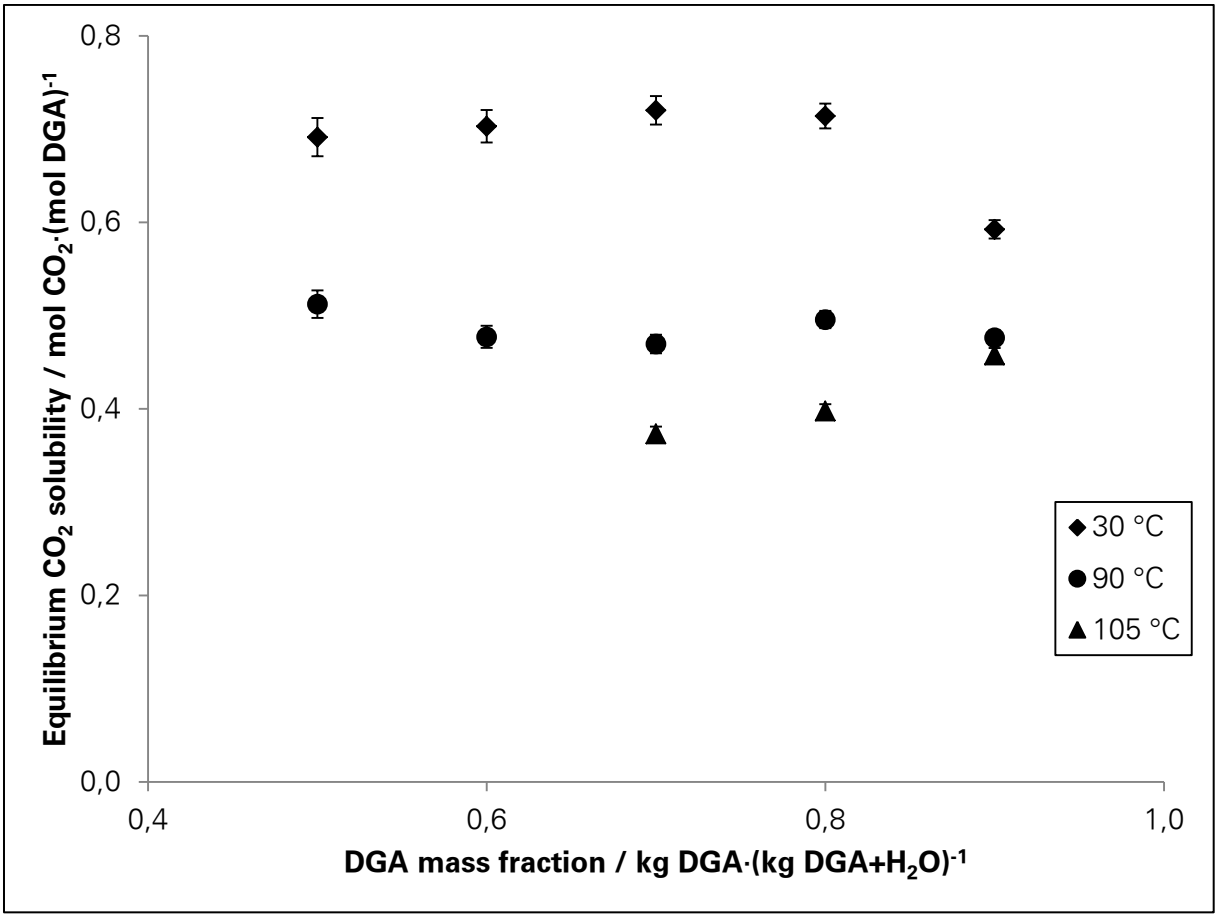

Figure 4.1 Equilibrium CO_2 solubility against DGA mass fraction after absorption at 30 °C and after desorption at 90 and 105 °C

α_{CO2} of spent DGA solvents (α_{CO2} at 30 °C) and of lean solvents (α_{CO2} at 90 and 105 °C) are shown in Figure 4.1 and Table H.2. α_{CO2} of spent solvents remained almost constant in the DGA mass fraction w_{DGA} range from 0,5 to 0,8 kg DGA·(kg DGA+H_2O)$^{-1}$ or from 50 to

80 wt. % DGA; then, α_{CO2} at 90 wt. % DGA decreased (Figure 4.1). When the number of moles of DGA exceeds the number of moles of H_2O in the solvent, not all of DGA can react with CO_2; therefore, α_{CO2} decreases. CO_2 molality m_{CO2} increased with increasing w_{DGA}; it reached a maximum and then decreased. The m_{CO2} maxima was between a w_{DGA} of 0,8 and 0,9 kg DGA·(kg DGA+H_2O)$^{-1}$ (Figure 4.2 and Table H.2), which corresponds to the DGA mole-fraction range from 0,41 to 0,61 mol DGA·(mol DGA+H_2O)$^{-1}$. It should be noted that the solvent with 70 wt. % DGA absorbs a larger mass of CO_2 than the solvent with 60 wt. % DGA, even though α_{CO2} of both solvents is equal.

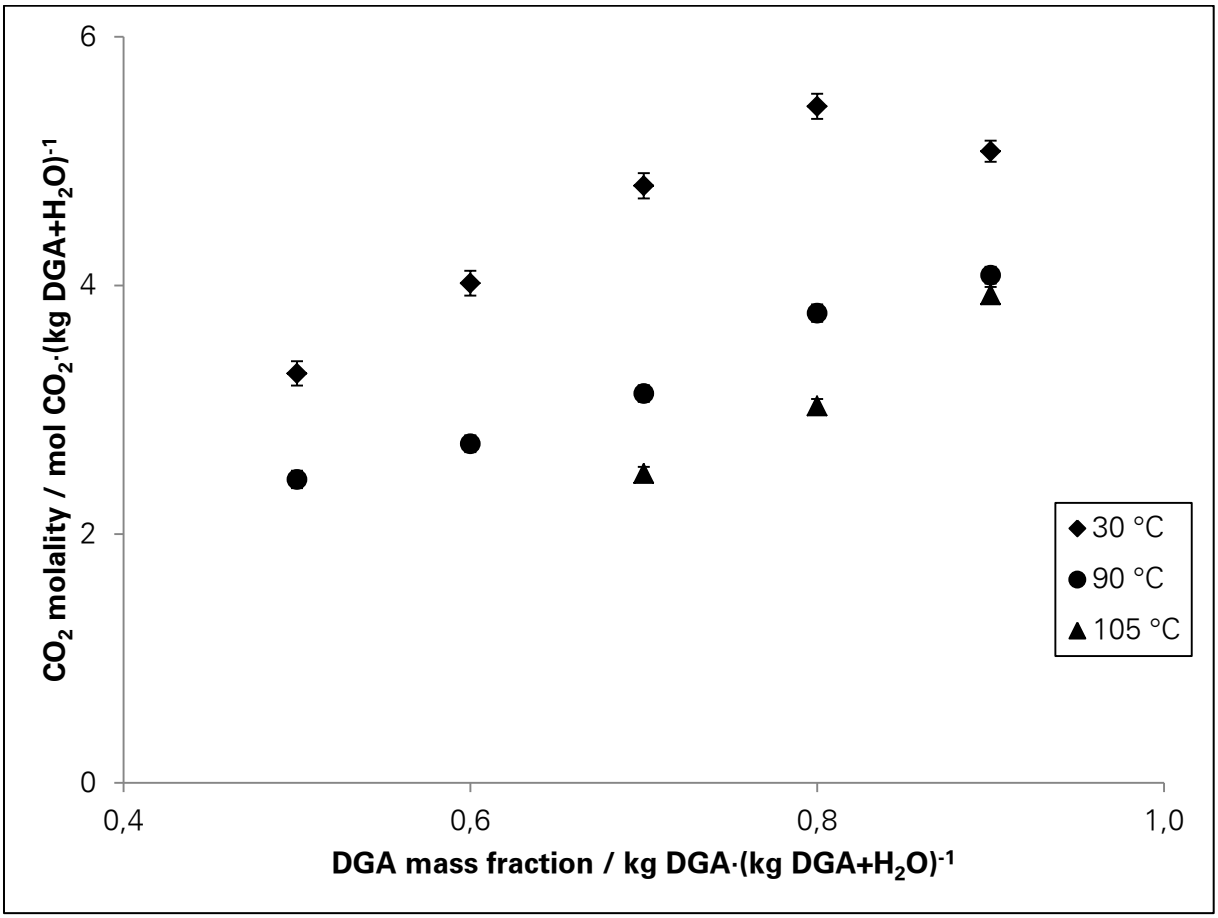

Figure 4.2 CO_2 molality against DGA mass fraction after absorption at 30 °C and after desorption at 90 and 105 °C

The long-duration experiment with 70 wt. % DGA showed that the difference in α_{CO2} after 3 and 12 hours was negligible, and the pH value decreased by mere 0,06.

For a given w_{DGA}, α_{CO2} decreases after the solvent is heated (desorption). Higher the desorption temperature, lower is the α_{CO2}. However, the maximum desorption temperature is the boiling point of the solvent. For solvents with 50 and 60 wt. % DGA, the boiling point

at 101 kPa (atmospheric pressure) is 104,2 and 106,6 °C (Huntsman, 2005), respectively. Therefore, it was practically not possible to determine α_{CO2} of these solvents at 105 °C.

After desorption at 90 °C, α_{CO2} of lean solvents remained constant for w_{DGA} from 0,5 to 0,8 kg DGA·(kg DGA+H_2O)$^{-1}$. However after desorption at 105 °C, α_{CO2} increased with increasing w_{DGA} which is ascribed to the increase in p_{CO2} with increasing w_{DGA} at the same temperature. With increasing w_{DGA}, the quantity of water in the liquid phase decreases; therefore, at equilibrium, the partial pressure of water in the vapour phase decreases in turn causing p_{CO2} to increase.

α_{CO2} data for aqueous DGA solvents obtained in this study followed the trend shown by data available in literature (Figure 4.3 and Table H.3). As p_{CO2} increased, α_{CO2} increased, whereas as temperature increased, α_{CO2} decreased.

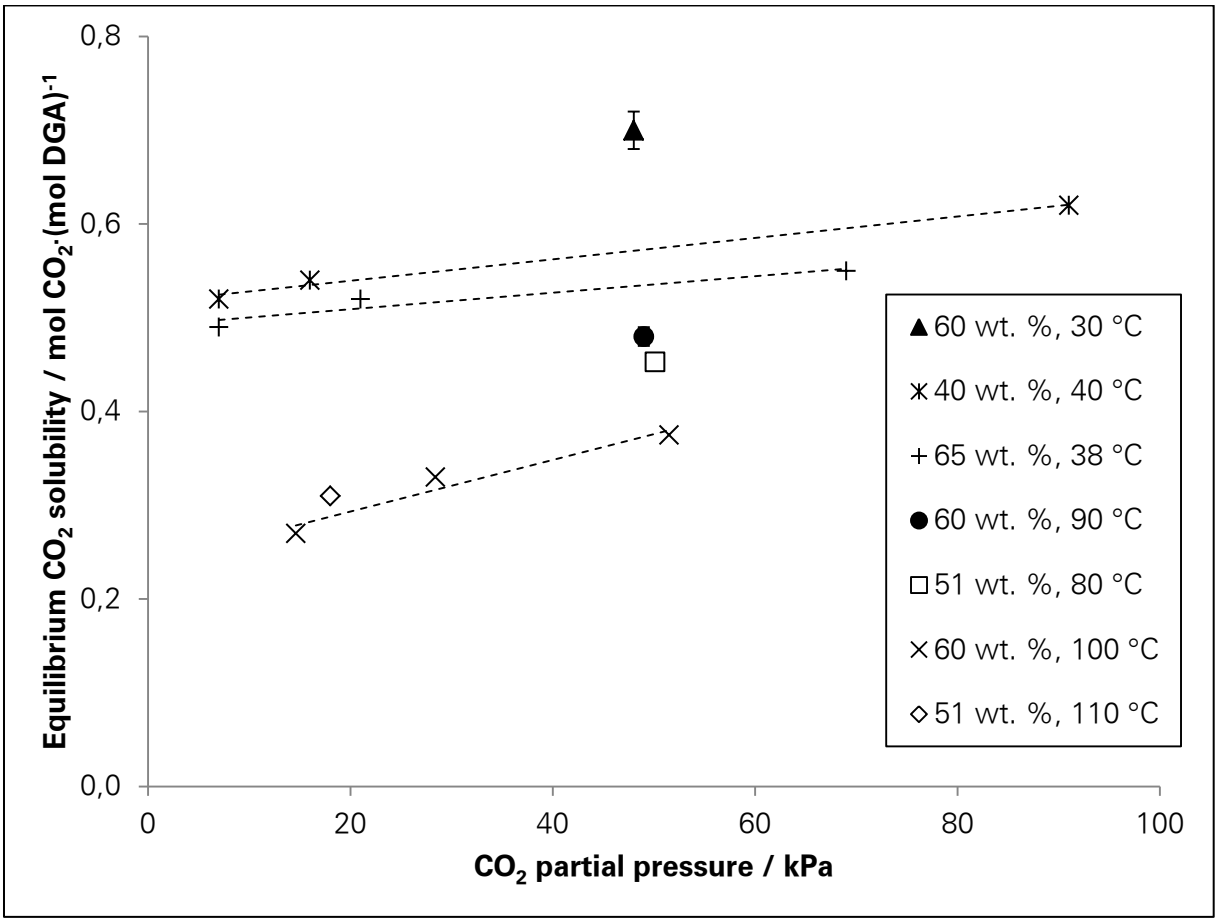

Figure 4.3 Equilibrium CO_2 solubility in aqueous DGA solvents at various temperatures and CO_2 partial pressures

(Solid points are values from this study, and other points are from literature.)

From a process perspective, the difference in equilibrium CO_2 solubility at absorption and desorption conditions is decisive and not the individual CO_2 solubility. A high differential

solubility is preferred because it reduces the solvent circulation rate, which reduces the energy consumption by the solvent pumps and by the preheater and the reboiler during desorption. Considering absorption at 30 °C and desorption at 90 °C, and absorption at 30 °C and desorption at 105 °C, the difference in CO_2 molality Δm_{CO2} is presented in Figure 4.4 and Table H.4. The maximum Δm_{CO2} was seen for 80 wt. % DGA, but the maximum value was only slightly more than the Δm_{CO2} for 70 wt. % DGA.

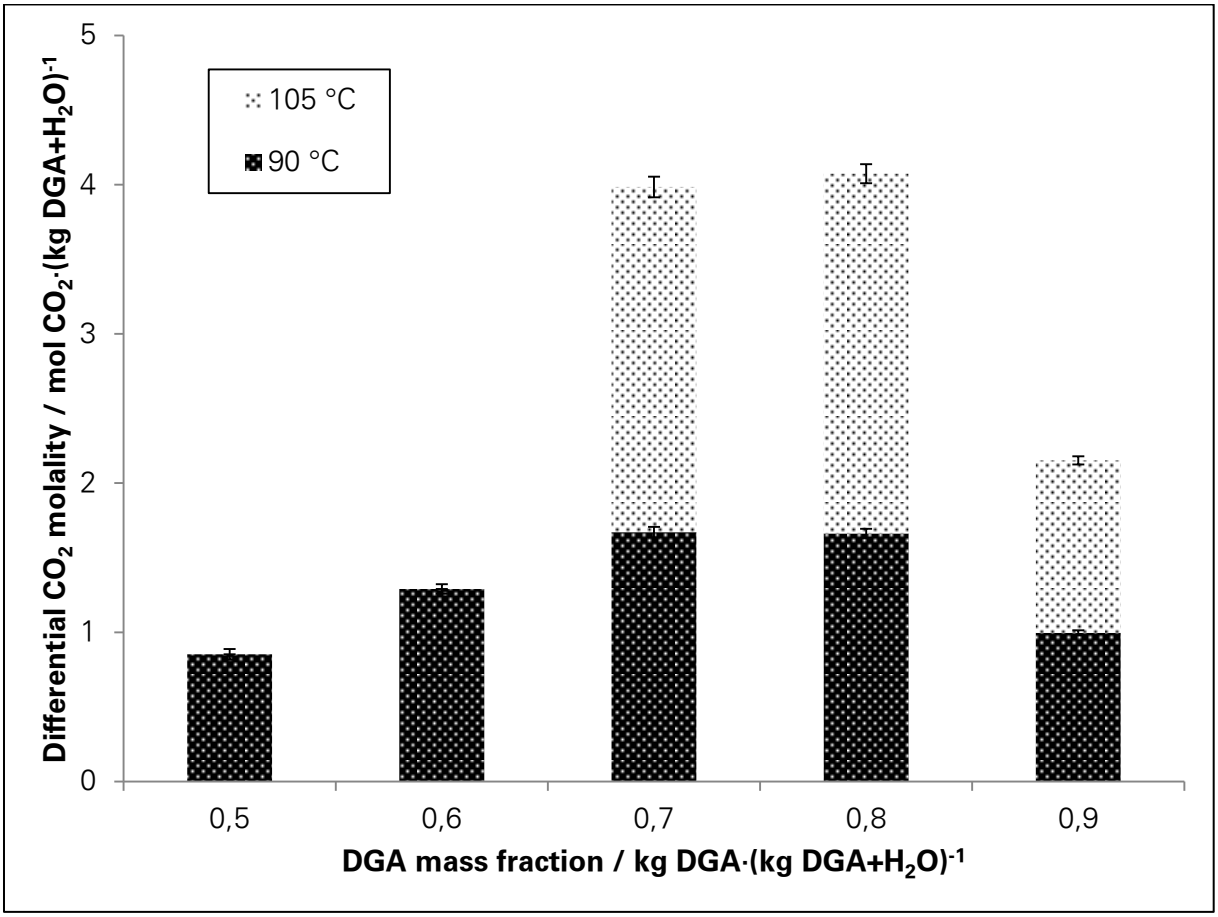

Figure 4.4 Differential CO_2 molality after absorption at 30 °C and desorption at 90 °C, and after absorption at 30 °C and desorption at 105 °C against DGA mass fraction

While designing a column, it must be kept in mind that CO_2 loading in the spent solvent at the absorber outlet will be equal to or less than the equilibrium CO_2 solubility α_{CO2} at the existing T and p_{CO2}. However, CO_2 loading in the lean solvent at the stripper outlet will be equal to, greater than or less than α_{CO2} at a particular T obtained by the desorption experiment in this study. CO_2 loading in the lean solvent at the stripper outlet depends upon the T and p_{CO2} profiles in the stripper, a vertical column, which are influenced by the solvent temperature at column inlet, the reboiler temperature and the use of an external strip gas such as N_2. In this way, α_{CO2} data should be used as an input to the basic-engineering calculations.

4.1.2 DENSITY, VISCOSITY AND SURFACE TENSION

Density ρ, viscosity μ and surface tension σ are key solvent properties that influence hydraulics and mass transfer in the absorption and desorption (stripping) columns. Thus, ρ, μ and σ play an important role in column design. In an operational plant, the absorption solvent almost always contains dissolved CO_2; therefore, determining properties of the spent and lean solvents is paramount. In this section, at first, ρ, μ and σ of the raw solvent are discussed; then, ρ, μ and σ of spent solvents (after CO_2 absorption) and of lean solvents (after CO_2 desorption) are discussed.

For raw DGA solvents, with increasing DGA mole fraction x_{DGA}, ρ increases, reaches a maximum and then decreases. The ρ profile is a non-monotonic function. In fact, ρ was even larger than the density of pure DGA for x_{DGA} between 0,2 and 0,6 (Table H.5 and Figure H.1). A similar trend is shown by literature data at other temperatures (Table H.6). For data obtained in this study, with increasing x_{DGA}, μ always increases, whereas σ always decreases (Figure H.2 and Figure H.3, and Table H.7 and Table H.9). Although, μ values obtained at 25 °C by Henni et al. (2001) show that the μ profile is a non-monotonic function (Table H.8), values obtained in this study neither support nor contradict this observation. Not enough data on σ of raw DGA solvents is available, even in literature, to draw conclusions about the monotonicity of the σ profile (Table H.10). Change in ρ, μ and σ is large at small x_{DGA} values, and the change decreases with increasing x_{DGA}. This trend is comparable to the one seen at other temperatures as shown in Figure H.1, Figure H.2 and Figure H.3. The influence of temperature is also visible in the figures: with increasing temperature, ρ, μ and σ decrease.

DGA is a primary alkanolamine like MEA; both are single-chain molecules with an alcohol group at one end and an amine group at the other end. However, the DGA molecule ($C_4H_{11}NO_2$) has more atoms than the MEA molecule (C_2H_7NO). Therefore, the van der Waal forces between DGA molecules are greater than those between MEA molecules. Furthermore, compared to MEA, DGA has an extra electronegative atom of oxygen (in the form of ether) that can participate in H-bonding. Therefore, pure DGA has a higher ρ, μ and boiling point than pure MEA. However, σ of pure DGA is lower than the surface tension of pure MEA due to steric effects caused by the long DGA molecules which decrease the surface area per molecule. A similar trend for octaethyleneglycol-n-alkyl ethers was reported by Ueno et al. (1981).

ρ, μ and σ of the raw DGA solvent (mixture) can be related to the corresponding properties of its constituent components using Equation 4.1.

$$\rho^E = \rho_{mix} - (\rho_{DGA}x_{DGA} + \rho_{H2O}x_{H2O}) \quad 4.1a$$

$$\mu^E = \mu_{mix} - (\mu_{DGA}x_{DGA} + \mu_{H2O}x_{H2O}) \quad 4.1b$$

$$\sigma^E = \sigma_{mix} - (\sigma_{DGA}x_{DGA} + \sigma_{H2O}x_{H2O}) \quad 4.1c$$

ρ^E, μ^E and σ^E are the excess properties, and x is the mole fraction. Excess density ρ^E, excess viscosity μ^E and excess surface tension σ^E can be described by a third-order Redlich-Kister equation (Redlich and Kister, 1948) shown as Equation 4.2:

$$\rho^E = A(x_{DGA})^3 + B(x_{DGA})^2 + C(x_{DGA})^1 \quad 4.2a$$

$$\mu^E = A(x_{DGA})^3 + B(x_{DGA})^2 + C(x_{DGA})^1 \quad 4.2b$$

$$\sigma^E = A(x_{DGA})^3 + B(x_{DGA})^2 + C(x_{DGA})^1 \quad 4.2c$$

Equations 4.1 and 4.2 can be combined to obtain Equation 4.3 where the coefficients *A*, *B* and *C* are related as shown in Equation 4.4.

$$\rho_{mix} = A(x_{DGA})^3 + B(x_{DGA})^2 + (\rho_{DGA} - \rho_{H2O} + C)(x_{DGA})^1 + \rho_{H2O} \quad 4.3a$$

$$\mu_{mix} = A(x_{DGA})^3 + B(x_{DGA})^2 + (\mu_{DGA} - \mu_{H2O} + C)(x_{DGA})^1 + \mu_{H2O} \quad 4.3b$$

$$\sigma_{mix} = A(x_{DGA})^3 + B(x_{DGA})^2 + (\sigma_{DGA} - \sigma_{H2O} + C)(x_{DGA})^1 + \sigma_{H2O} \quad 4.3c$$

$$B = -(A + C) \quad 4.4$$

Table 4.2 Coefficients of the Redlich-Kister equation for aqueous DGA solvents at 30 °C

	A	**B**	**C**
For ρ^E	0,3989	-0,7742	0,3453
For μ^E	-23,5	9,0	14,5
For σ^E	-88,5	177,0	-88,5

ρ^E profile is non-monotonic and is positive for the major portion of x_{DGA} (Figure H.4 and Table H.11). For all x_{DGA}, μ^E is positive, whereas σ^E is negative (Figure H.5 and Table H.11). Equation 4.2 was fitted to the experimental data, and the polynomial coefficients of Equation 4.2 were determined which are shown in Table 4.2. Profiles of ρ^E, μ^E and σ^E against x_{DGA} are non-linear and asymmetric. The coefficient of determination of the fit for ρ^E, μ^E and σ^E is 98, 98 and 96 %, respectively: the data is thermodynamically consistent at a confidence level of above 95 %. Henni et al. (2001) also used the Redlich-Kister equation to correlate ρ^E

and μ^E to x_{DGA}, but they used a fifth-order polynomial equation in contrast to a third-order polynomial used in this study. No σ^E data for DGA is available in literature, but σ^E profile similar to that obtained in this study was presented by Vazquez et al. (1997) for aqueous MEA.

The extremities of ρ^E, μ^E, and σ^E profiles of DGA are greater than the extremities of MEA profiles (Vazquez et al., 1997; Kapadi et al., 2002), or an aqueous DGA solvent is more non-ideal than an aqueous MEA solvent. This implies that the intermolecular forces between the DGA and water are greater than the forces between MEA and water.

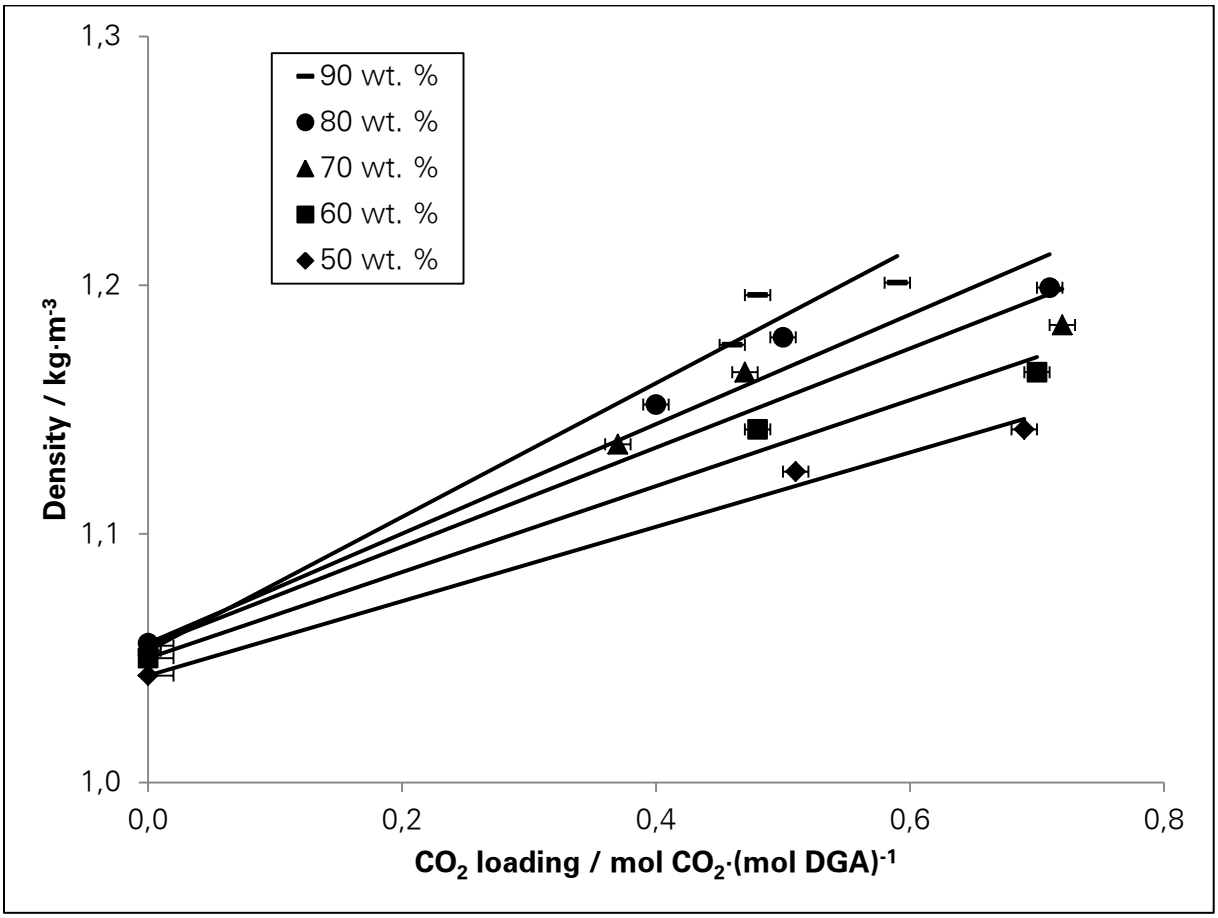

Figure 4.5 Density at 30 °C for various CO_2 loadings in solvents with various DGA mass fractions

Spent DGA solvents have a higher ρ than the raw DGA solvents, and the difference between the two increases linearly with increasing x_{DGA}. After desorption, ρ decreases. For a given x_{DGA} and w_{DGA}, ρ linearly increases with CO_2 loading α_{CO2}. In addition, for higher w_{DGA}, increase in ρ is steeper (Table H.5 and Figure 4.5). These results are in accordance with the observations of Weiland et al. (1998). MEA shows an identical trend (Table H.12 and

Figure H.6): for a given MEA mass fraction w_{MEA}, ρ increases with increase in α_{CO2}. Furthermore, the slope of the MEA profiles (ρ against α_{CO2}) increases with increase in w_{MEA}.

When CO_2 reacts with aqueous DGA (solvent), CO_2 in the form of bicarbonate (HCO_3^-) and carbonate (CO_3^{2-}) ions takes up the intermolecular space in the solvent; therefore, in a given solvent volume, more atoms and more mass are introduced which cause the density to increase. MEA profiles (ρ against α_{CO2}) are steeper than those of DGA which can be explained by the hypothesis that intermolecular forces in CO_2-loaded MEA solvents are greater than those in CO_2-loaded DGA solvents.

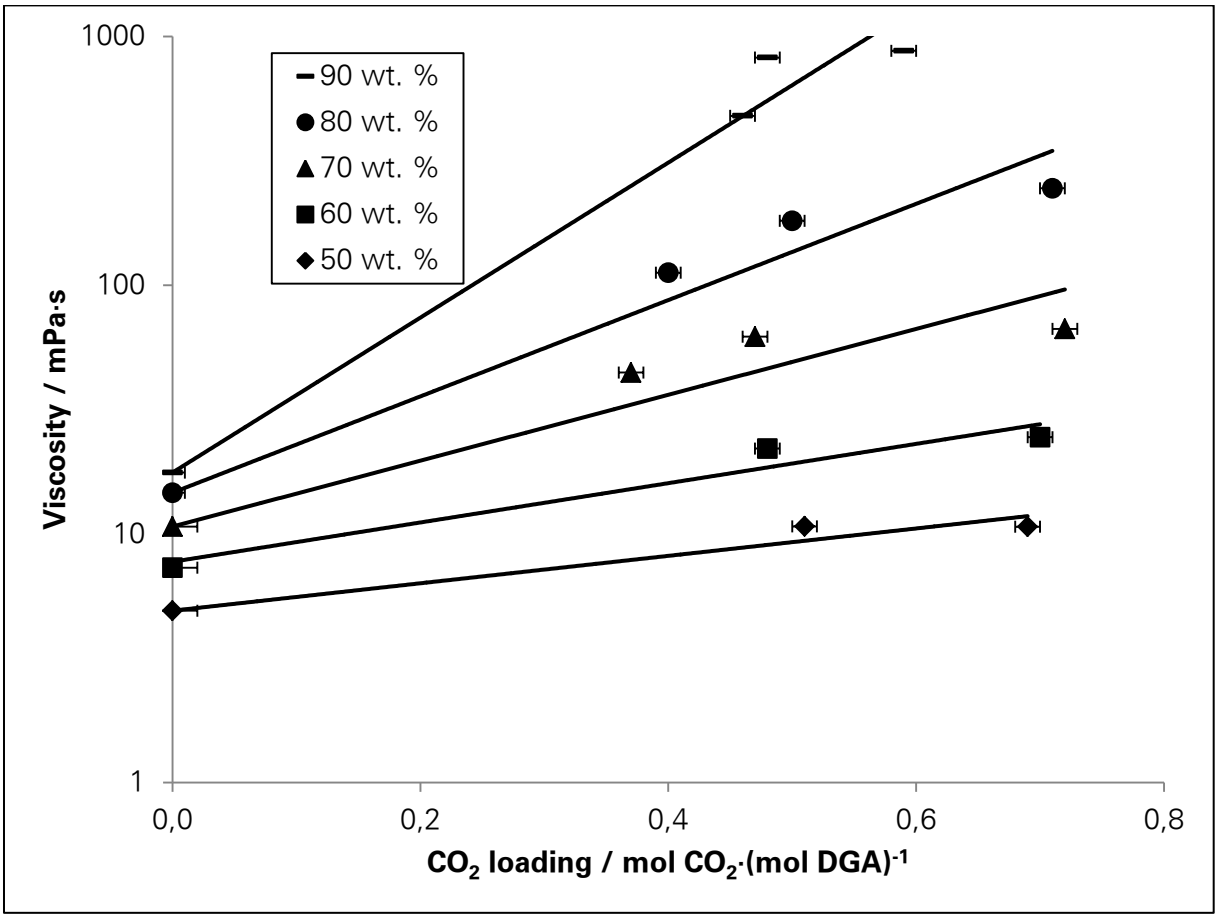

Figure 4.6 Viscosity at 30 °C for various CO_2 loadings in solvents with various DGA mass fractions

Spent DGA solvents have a higher μ than the raw DGA solvents, and the difference between the two increases exponentially with increasing x_{DGA}. After desorption, μ decreases. For a given x_{DGA} and w_{DGA}, μ exponentially increases with CO_2 loading α_{CO2}. In addition, for higher w_{DGA}, increase in μ is steeper (Table H.7 and Figure 4.6). This is a disadvantage because with increasing solvent viscosity, the energy consumed by a pump to circulate the solvent increases. These results are in accordance with the hypothesis proposed by

Weiland et al. (1998) that μ is exponentially related to α_{CO2}. MEA too shows an identical trend (Table H.13 and Figure H.7): for a given MEA mass fraction w_{MEA}, μ increases exponentially with increase in α_{CO2}. Furthermore, the exponent of the MEA profiles (μ against α_{CO2}) increases with increase in w_{MEA}.

On comparing the μ profile of 40 wt. % MEA (MEA molality of 10,91 mol MEA·(kg H_2O)$^{-1}$) with 50 wt. % DGA (DGA molality of 9,52 mol DGA·(kg H_2O)$^{-1}$) profile, it is observed that the degree of increase of μ is greater for MEA than for DGA. This observation supports the hypothesis that intermolecular forces in CO_2-loaded MEA solvents are greater than those in CO_2-loaded DGA solvents.

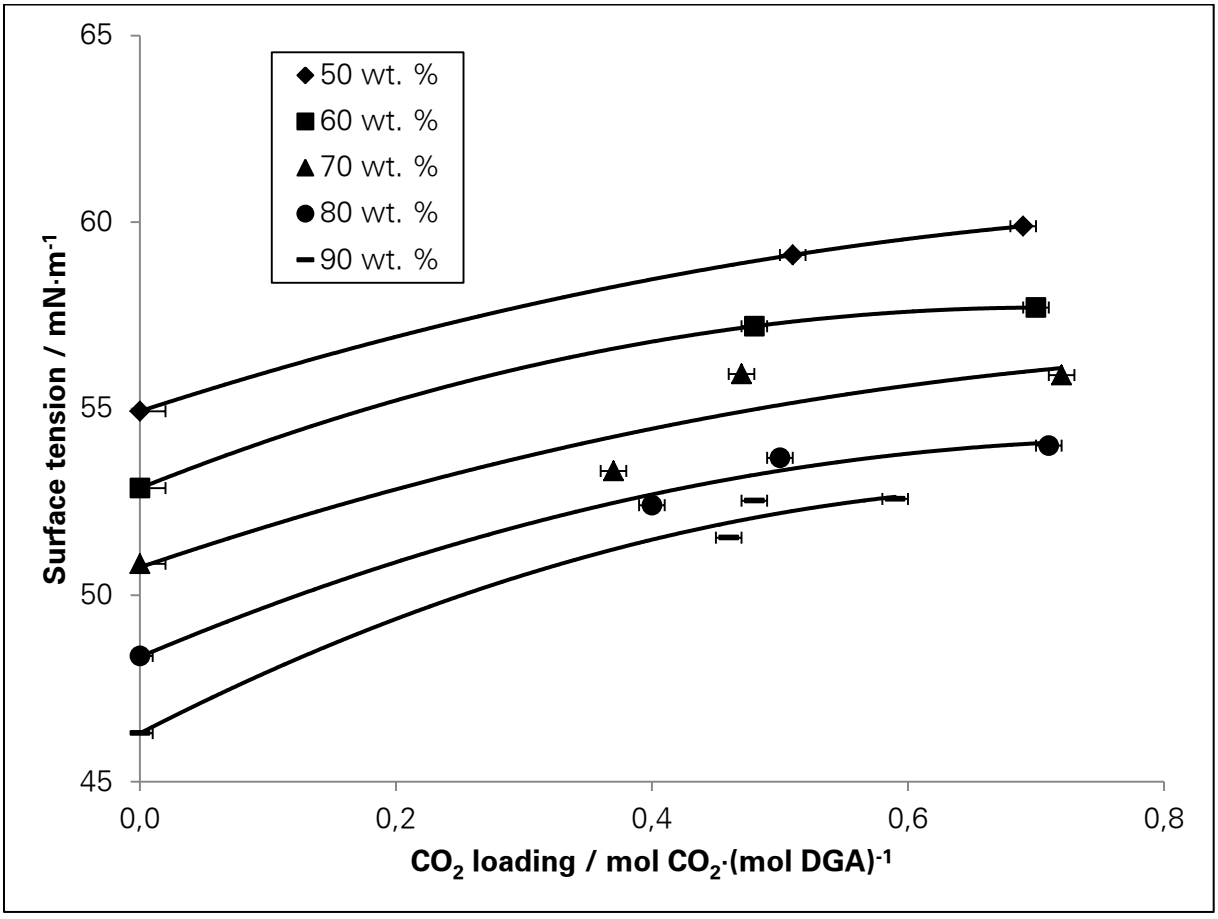

Figure 4.7 Surface tension at 30 °C for various CO_2 loadings in solvents with various DGA mass fractions

σ of spent DGA solvents is higher than that of raw DGA solvents, and the difference between the two increases linearly with increasing x_{DGA}. Looking at the spent solvents alone, with increasing x_{DGA} and w_{DGA}, σ decreases (Table H.9 and Figure 4.7). In an absorption column, σ increases as the solvent flows down the column, and the Marangoni effect can be neglected during mass-transfer calculations (Billet and Schultes, 1999). When

CO_2 is desorbed from the solvent, σ decreases. In other words, for a given w_{DGA}, σ increases with increasing α_{CO2}. Results show that after desorption at 90 °C, decrease in σ is negligible; however, after desorption at 105 °C, decrease in σ is noteworthy. This implies that increase in σ at lower CO_2 loading is more distinct than the increase in σ at higher loading. Therefore, cross plotting of σ against α_{CO2} reveals a quadratic curve and not a line (Figure 4.7).

The change in σ of DGA solvents due to the presence of water and CO_2 can be explained by the following thesis. DGA is a linear molecule with the primary amine group ($-NH_2$) at one end and an alcohol group (–OH) at the other end. When DGA is added to water, the amine group acquires a proton (H^+) and forms an ammonium group ($-NH_3^+$); the ammonium group is hydrophilic and causes σ to decrease (Asprion, 2005). During absorption, CO_2 reacts with the ammonium group to form a carbamate group ($-NH_2COO^-$), a hydrophobic entity, which causes σ to re-increase. During desorption, the carbamate group is transformed back into the ammonium group that decreases σ.

On comparing σ of MEA solvents with DGA solvents, a couple of similarities are seen (Table H.14 and Figure H.8): for a given w_{MEA}, σ increases with increase in α_{CO2}, and with increasing w_{MEA}, σ decreases. MEA profiles (σ against α_{CO2}) are steeper than those of DGA which can be explained by the thesis that intermolecular forces in CO_2-loaded MEA solvents are greater than those in CO_2-loaded DGA solvents.

Conclusions

Equilibrium CO_2 solubility values determined using the absorption and desorption setups are plausible and thermodynamically consistent.

Publicly available literature contains limited data on the density, viscosity and surface tension of CO_2-loaded solvents. As these properties are crucial in designing absorption plants, which are existing since several decades, substantial data on solvent properties must be available in private libraries. Therefore, further experimental data on properties of CO_2-loaded amines must be collected and published in libraries with public access. Once data is available, efforts can be made to rigorously model properties of CO_2-loaded solvents.

Properties such as density, viscosity and surface tension of single-chain primary alkanolamines are affected by the total number of atoms in the molecule and by the presence of other functional groups (such as the ether group) in the molecular chain. In addition, trends followed by the properties of raw aqueous alkanolamines (solvents without CO_2) are not necessarily valid for spent aqueous alkanolamines (CO_2-loaded solvents).

Properties of DGA and MEA are different, although both are single-chain primary alkanolamines. The degree of self-association between DGA molecules is greater than the degree of self-association between MEA molecules. In addition, intermolecular forces between DGA and water molecules are stronger than intermolecular forces between MEA and water molecules. However, the intermolecular forces prevalent within a CO_2-loaded DGA solvent are weaker than those within a CO_2-loaded MEA solvent.

If one were to increase the concentration of a primary amine (e.g. DGA) in the solvent, CO_2 loading would increase which would decrease the solvent circulation rate and thus reduce energy consumption. However, this tactic has limitations. With increasing DGA content in the solvent, CO_2 loading increases until a break-even point; subsequently, CO_2 loading decreases. Moreover, the CO_2 loading at absorption conditions is not the crucial factor, but the difference in CO_2 loading at absorption and desorption conditions is. With increasing desorption temperature, CO_2 loading decreases, but the maximum desorption temperature is limited by the boiling point and the degeneration temperature of the solvent. In addition, the increase in DGA mass content has an adverse effect on the energy demand of the solvent pump as viscosity increases exponentially with CO_2 loading and DGA mole fraction. Surface tension of the solvent does not play a decisive role while selecting DGA content in the solvent.

To treat biogas (40 vol. % CO_2 at atmospheric pressure), a DGA solvent of 70 wt. % DGA in solvent is recommended because of its large differential CO_2 loading and moderate viscosity. For a biogas-treatment plant with an absorption temperature of 30 °C, a desorption temperature of 105 °C is suitable.

4.2 SIMULATING EQUILIBRIUM CO_2 SOLUBILITY

Simulated equilibrium CO_2 solubility α_{CO2} values showed trends similar to those shown by the experimental data in Martin et al. (1978) (Figure 4.8 and Table I.1). α_{CO2} increased with increasing CO_2 partial pressure p_{CO2}. For a given p_{CO2}, α_{CO2} decreased with increase in temperature. At 50 °C, simulations underestimated α_{CO2} by less than 10 % throughout the p_{CO2} range from 1 to 70 kPa. At 100 °C, simulations overestimated α_{CO2} values by less than 10 % in the p_{CO2} range from 30 to 50 kPa. As p_{CO2} decreased below 30 kPa, deviation between simulated and experimental values increased (Roscher, 2014). Since no information is available about the uncertainty in the experimentally determined values in Martin et al. (1978), the discrepancies between experimental and simulated are worst-case values.

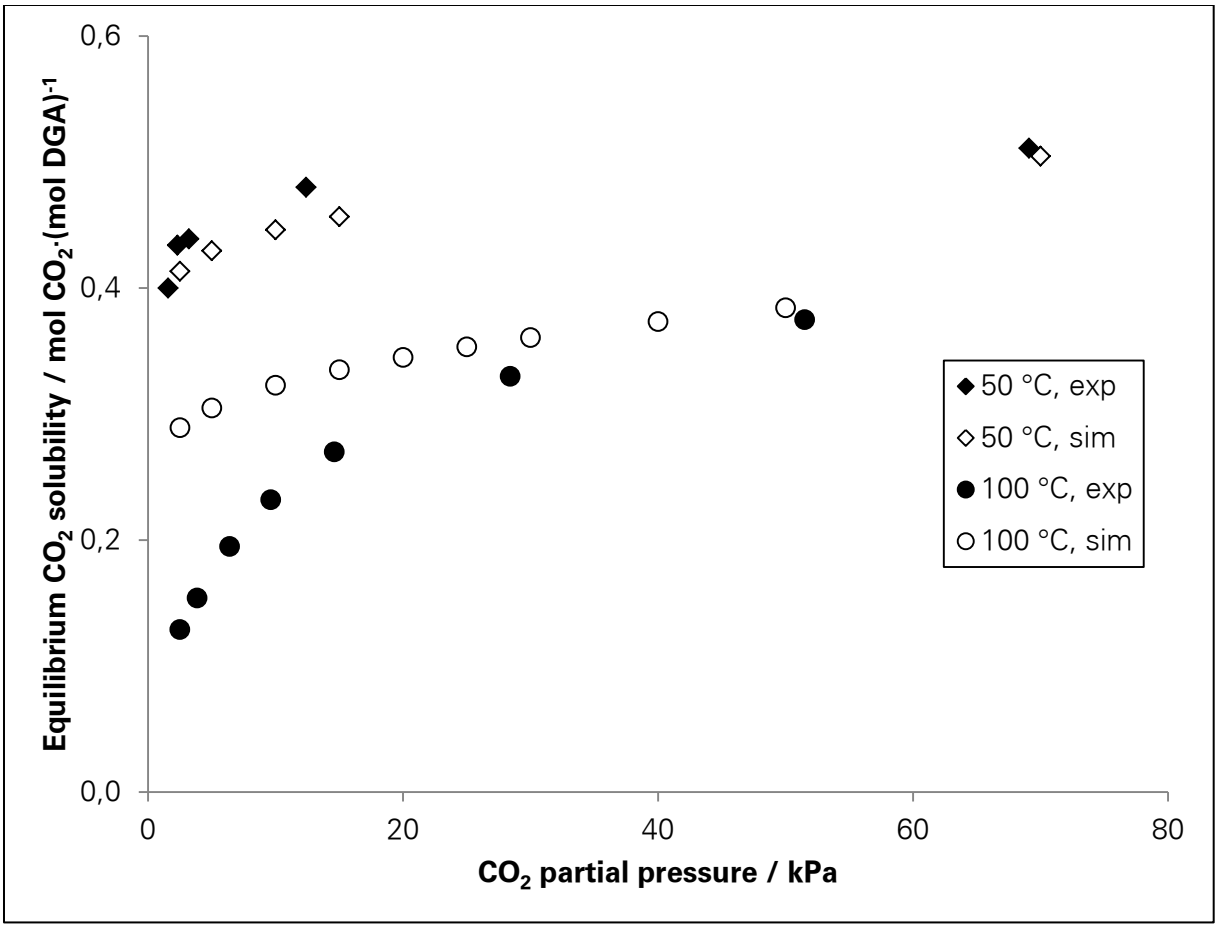

Figure 4.8 Equilibrium CO_2 solubility of 60 wt. % DGA in solvent determined by experiments (exp) in Martin et al. (1978) and by simulations (sim) in this study for various CO_2 partial pressures

Figure 4.9 and Table I.2 show simulated α_{CO2} values for the experimentally determined α_{CO2} values from this study. The simulated data did not replicate the trend shown by the experimental data at 30 °C. Simulated α_{CO2} values decreased with increasing DGA mass fraction from 0,5 kg DGA·(kg DGA+H_2O)$^{-1}$ onwards which is not plausible. The trend shown by the experimental data at 90 °C was not similar to the trend shown by the simulated data, but identical trends were shown by data at 105 °C (Roscher, 2014). The discrepancy between simulated and experimental data varied from -30 % to +10 % for different DGA mass fractions and temperatures. Simulated and experimental α_{CO2} values for 60, 70 and 90 wt. % DGA differed by less than 20 %, whereas for 80 wt. % DGA at 30 °C and 50 wt. % DGA at 90 °C, the values differed by more than 20 %. This implies that the model parameters, namely the NRTL interaction parameters, are not valid for a large range of DGA concentrations.

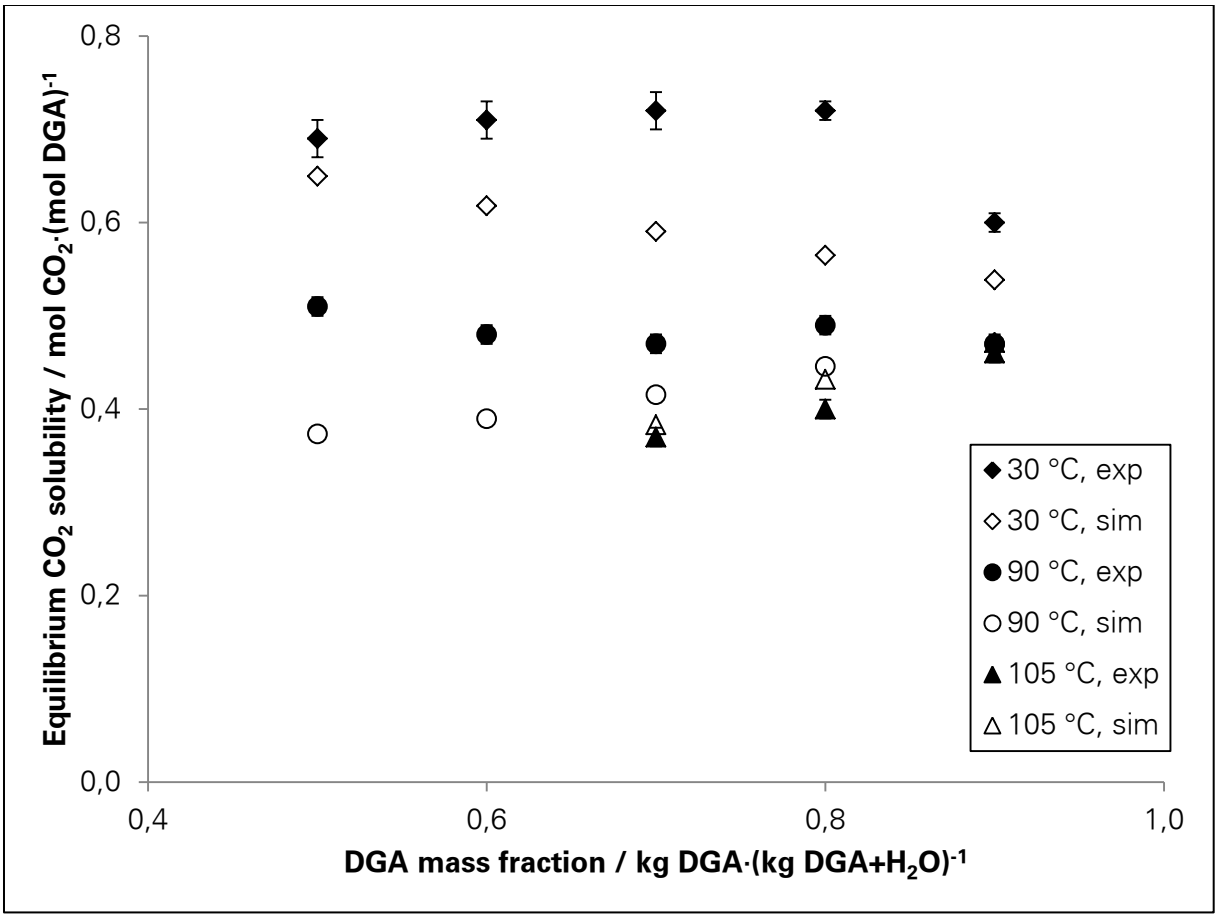

Figure 4.9 Equilibrium CO_2 solubility determined by experiments (exp) and by simulations (sim) in this study for solvents with various DGA mass fractions

Equilibrium CO_2 solubility of 70 wt. % DGA in solvent at 30 and 105 °C for various CO_2 partial pressures was simulated as shown in Figure 4.10 and Table I.3. This data is necessary to design an absorption plant that can separate CO_2 from biogas. Simulated α_{CO2} values at 30 °C are expected to be smaller than measured values by less than 20 % for p_{CO2} ranging from 1 to 60 kPa (the relevant range for designing the absorption column). Simulations are expected to estimate α_{CO2} values at 105 °C with an uncertainty of ± 10 % for p_{CO2} ranging from 30 to 50 kPa. For p_{CO2} values lower than 30 kPa at 105 °C, the uncertainty of the simulated data will be larger than ± 10 %.

Conclusions

The thermodynamic model and the model parameters presented in a study should be considered as one entity or package. If equilibrium constants of reactions are newly determined, the NRTL interaction parameters must be freshly determined.

The basis for the regression of the NRTL model parameters is experimental data, and as experimental data in literature itself has a discrepancy of at least ± 10 % (Figure 4.3), simulations involving DGA will have an uncertainty of over ± 10 %.

The thermodynamic framework of the model and the model parameters used in this study are apt to simulate equilibrium CO_2 solubility in aqueous DGA (60 to 70 wt. %) solvents at absorption temperatures from 30 to 50 °C in the germane p_{CO2} range with an uncertainty of less than ± 20 %. The same or even lower uncertainty will be possessed by α_{CO2} values simulated at desorption temperatures (90 to 105 °C) for p_{CO2} above 30 kPa, but the uncertainty will increase at lower p_{CO2} values.

The model and its parameters can be used in a research study to simulate an absorption plant for separating CO_2 from biogas at atmospheric pressure. An uncertainty of ± 20 % in results should be expected while designing the plant.

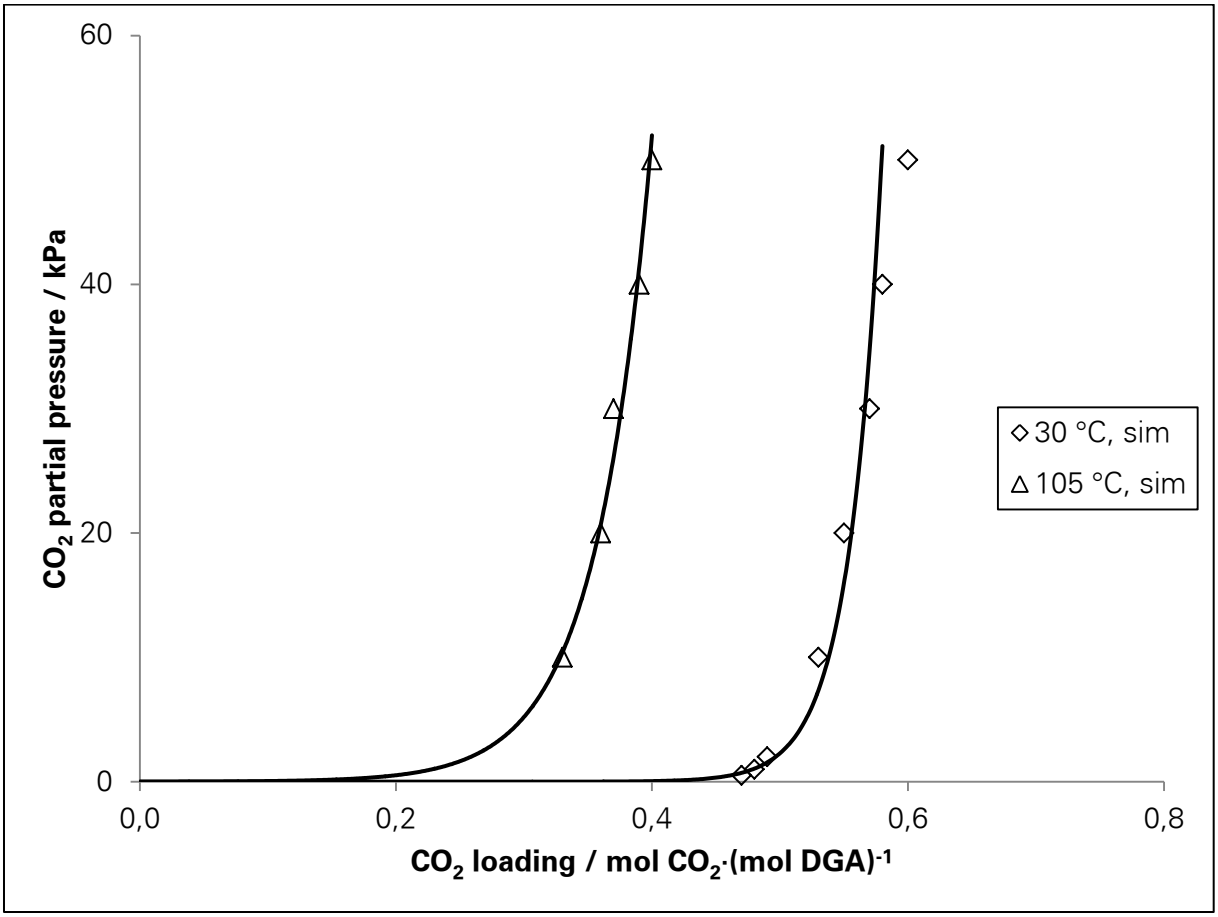

Figure 4.10 Simulated (sim) equilibrium CO_2 solubility of 70 wt. % DGA in solvent at 30 and 105 °C for various CO_2 partial pressures

4.3 COLUMN PRESSURE DROP

4.3.1 OPERATING REGION

For a given solvent flow rate, specific pressure drop $\Delta P/l$ increases with increasing gas flow rate (Figure 4.11). As gas flow rate increases, gas velocity through the column and frictional loss increase which cause $\Delta P/l$ to increase (Equation 3.6). For a given gas flow rate, with increasing solvent flow rate, $\Delta P/l$ increases. As more solvent flows through the column, the cross-sectional area of the column available to the gas decreases which causes $\Delta P/l$ to increase.

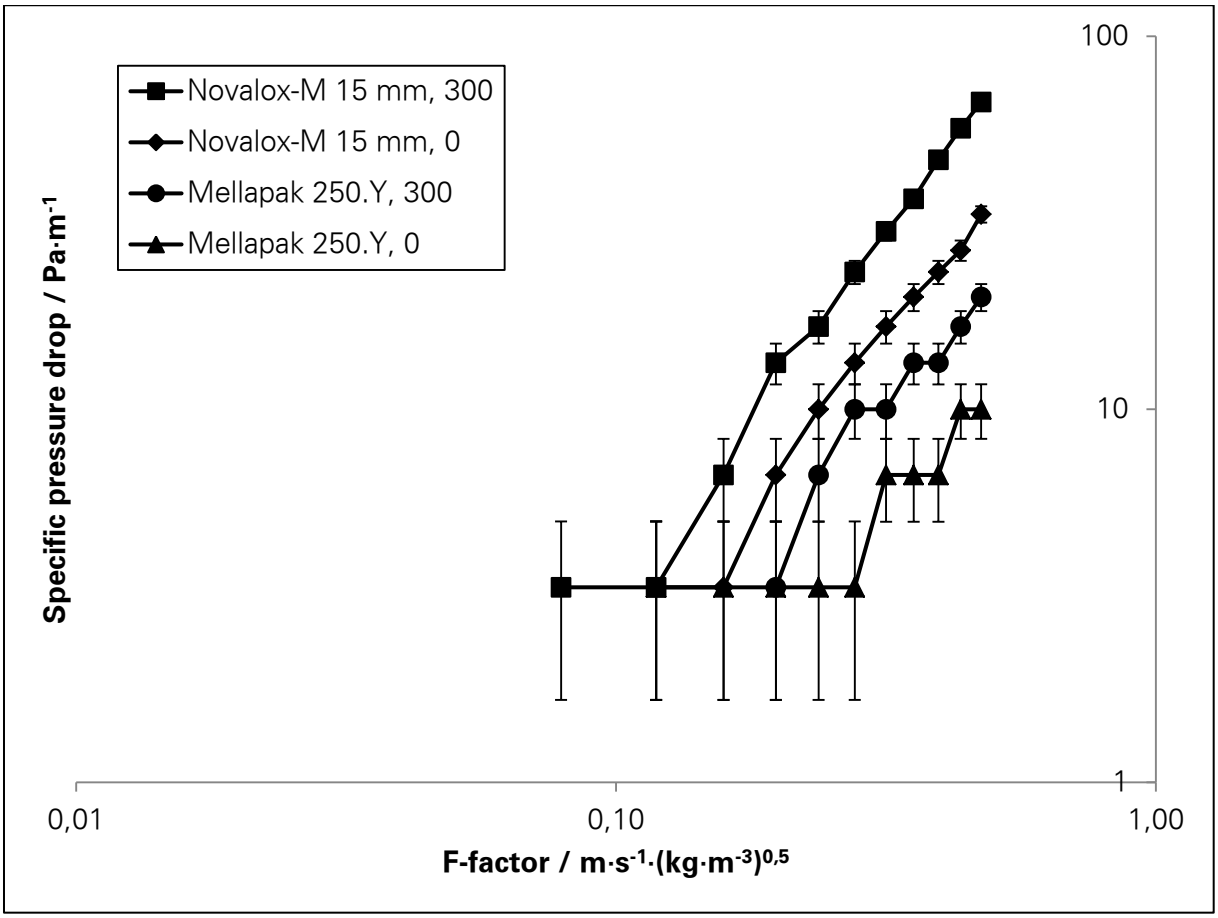

Figure 4.11 Experimentally determined $\Delta P/l$ values for Novalox-M 15 mm and Mellapak 250.Y at solvent flow rates of 0 and 300 kg·h^{-1}

In the log-log diagram (Figure 4.11), $\Delta P/l$ in the dry column (solvent flow rate of 0 kg·h^{-1}) increases linearly with the F-factor and with the superficial gas velocity (Equation 2.9). The profile of $\Delta P/l$ at the solvent flow rate of 300 kg·h^{-1} is a line, which is parallel to the $\Delta P/l$ profile of the dry column. This implies that the column is operated below the loading region

even at a gas flow rate of 12 $Nm^3 \cdot h^{-1}$ and a solvent flow rate of 300 $kg \cdot h^{-1}$, which is the upper region of the column's operational range.

For a given solvent and gas flow rate, $\Delta P/l$ in the column filled with Mellapak 250.Y is smaller than the $\Delta P/l$ in the column filled with Novalox-M 15 mm. Therefore to pump the same amount of gas through both columns, the gas blower for the column filled with Novalox-M 15 mm will consume more energy than the gas blower for the Mellapak 250.Y column. However, this does not imply that the gas-handling capacity $G_{v,op}$ of Mellapak 250.Y is larger than that of Novalox-M 15 mm. In order to estimate $G_{v,op}$ and the superficial gas velocity at flooding $v_{gas,fl}$, the procedure as described in Section 2.5.3 should be used. For the case that test-rig columns are operated with 70 wt. % DGA in solvent as the absorption solvent and 60 vol. % N_2 and 40 vol. % CO_2 as feed gas, $v_{gas,fl}$ and $G_{v,op}$ are shown in Table 4.3. Mellapak 250.Y indeed has a larger gas-handling capacity than Novalox-M 15 mm, and the absorber in the test rig can handle feed-gas flow rates of up to 27 $Nm^3 \cdot h^{-1}$.

Table 4.3 Superficial gas velocity at flooding and gas-handling capacity of Novalox-M 15 mm and Mellapak 250.Y at the flow parameter *FP* of 0,5

Parameter	Unit	Novalox-M 15 mm	Mellapak 250.Y
Specific pressure drop at flooding	$Pa \cdot m^{-1}$	1538	802
Superficial gas velocity at flooding	$m \cdot s^{-1}$	1,27	1,75
Gas-handling capacity	$Nm^3 \cdot h^{-1}$	27	38

4.3.2 PREDICTION OF SPECIFIC PRESSURE DROP

To predict $\Delta P/l$ in the test-rig columns, the GPDC chart cannot be used at feed-gas flow rates below 5 $Nm^3 \cdot h^{-1}$, which corresponds to the capacity parameter of 0,2, the lower limit of the GPDC chart. Therefore, this method cannot be used in the entire operating region of the columns.

Table 4.4 Packing-specific constants necessary to calculate specific pressure drop

Name of constant	Symbol	Novalox-M 15 mm		Mellapak 250.Y	
		From regression	From literature	From regression	From literature
Reference constant	$k_{p,0}$	0,668 ± 0,124	-	0,271 ± 0,089	0,292
Hydraulic constant	k_h	1,393 ± 0,268	-	0,898 ± 0,346	0,554
Form constant	k_{fo}	0,487 ± 0,108	-	0,754 ± 0,090	0,716
-	k_1	4,560 ± 1,177	-	3,722 ± 1,539	8,190
-	k_2	-	-0,206	-	-0,321

The models developed by Billet and Schultes (1999) and Mackowiak (2010) can be used to predict $\Delta P/l$ if certain packing-specific constants are known. These packing-specific constants were determined by regressing measured $\Delta P/l$ values against calculated $\Delta P/l$ values and are shown in Table 4.4. The uncertainty in constants arises due to the uncertainty in column diameter and packing height (Table 3.12) as well as due to the sensitivity of the pressure sensors (Table E.1). The regressed constants are compared with constants known from literature in Table 4.4.

The reference constant $k_{p,0}$ and the form constant k_{fo} of Mellapak 250.Y determined by regression are similar to the values obtained from literature (Billet and Schultes, 1999; Mackowiak, 2010). k_{fo} of Novalox-M 15 mm is greater than 0,280, which is the k_{fo} of Pall rings 15 mm (Mackowiak, 2010). This is plausible as Pall rings have a larger $\Delta P/l$ than Novalox-M (Section 3.4.2), and a larger k_{fo} implies a smaller $\Delta P/l$.

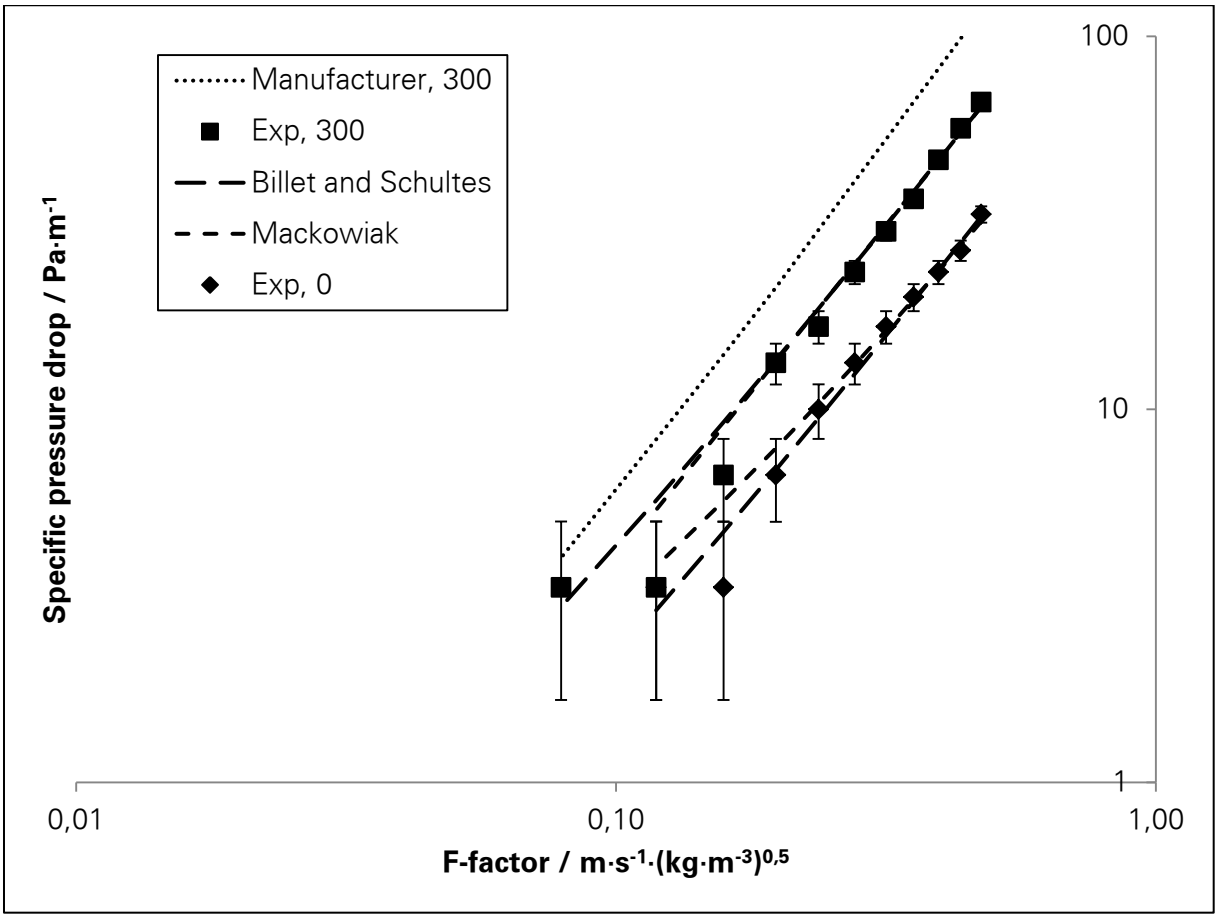

Figure 4.12 Experimentally determined and predicted $\Delta P/l$ values for the random packing Novalox-M 15 mm at solvent flow rates of 0 and 300 kg·h^{-1}

The constant k_1 of Mellapak 250.Y is smaller than the value obtained from literature; k_2 is a constant obtained from literature (Mackowiak, 2010). This implies that the solvent flowing in

the columns of the test rig does not impede the gas flow as it should. This explanation is corroborated by the fact that the software provided by the manufacturer of the packing Novalox-M 15 mm overestimates $\Delta P/l$ in the absorber of the test rig (Figure 4.12). Therefore, test-rig columns are thin columns, which suffer from solvent maldistribution. In a column where solvent flows down the column walls, the resistance experienced by the upward-flowing gas is smaller than in a column where the solvent flows down uniformly through the column cross section. Consequently, k_h and k_1 determined using a non-thin column are not valid for thin columns and vice versa.

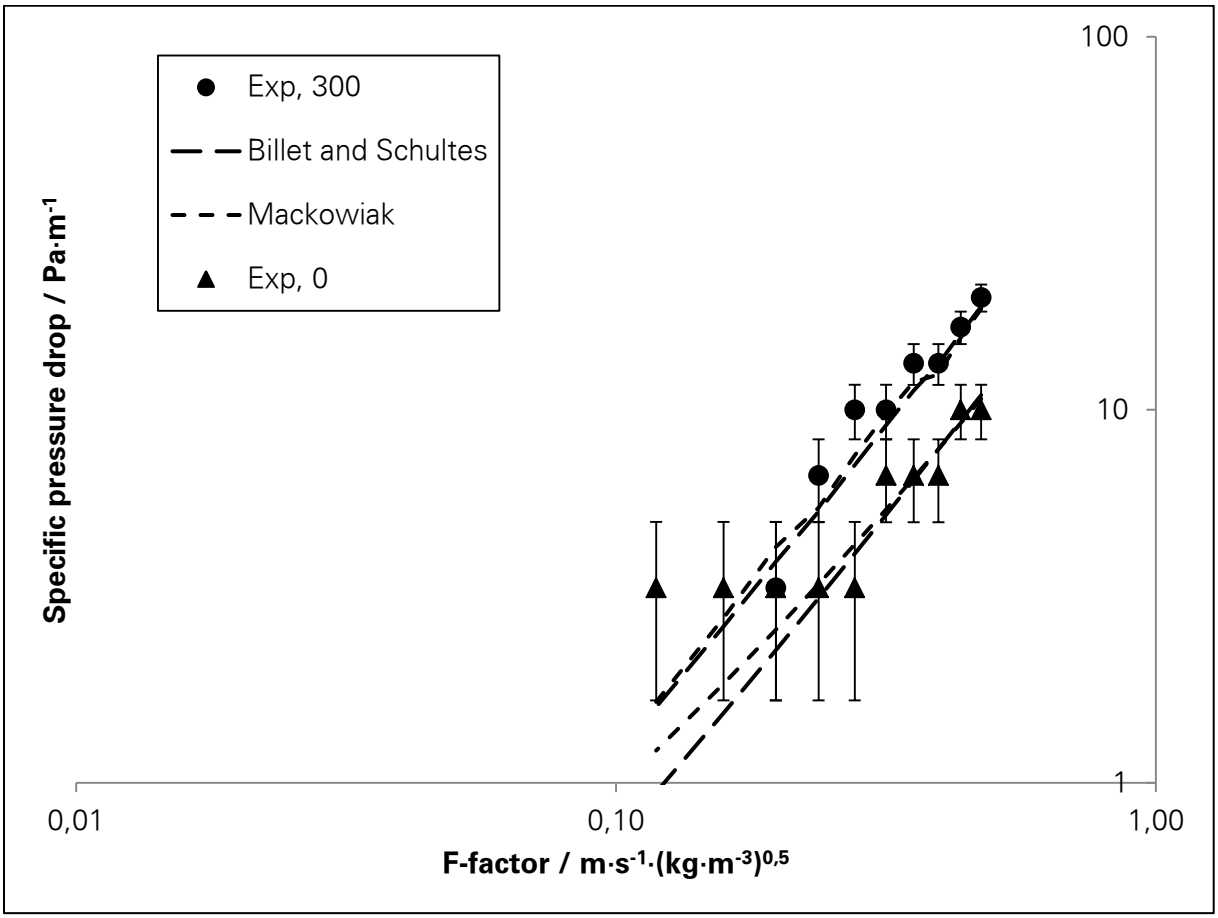

Figure 4.13 Experimentally determined and predicted $\Delta P/l$ values for the structured packing Mellapak 250.Y at solvent flow rates of 0 and 300 kg·h^{-1}

Packing constants $k_{p,0}$ and k_{fo} of Novalox-M 15 mm and Mellapak 250.Y are valid irrespective of the column diameter because the constants are determined by conducting experiments on a dry column where solvent maldistribution cannot occur as no solvent flows through the column. In addition, $k_{p,0}$ and k_{fo} of Novalox-M 15 mm should be applicable to similar random packings such as I-ring, IMTP and Rauschert metal saddle ring.

The model from Billet and Schultes and the model from Mackowiak are suitable to predict $\Delta P/l$ in the test-rig columns below the loading point (Figure 4.12 and Figure 4.13). However, the Billet-and-Schultes model cannot be used to predict $\Delta P/l$ above the loading point as the two additional packing-specific constants the models needs are not known. The Mackowiak model uses the same three packing-specific constants k_{fo}, k_1 and k_2 to predict $\Delta P/l$ below and above the loading point, and these constants have already been determined (Table 4.4). Nevertheless, k_1 and k_2 are valid as long as the Reynolds number of the gas flow Re_{gas} remains below 2100, which corresponds to 36 $Nm^3 \cdot h^{-1}$ feed gas (60 vol. % N_2 and 40 vol. % CO_2), which is more than the gas-handling capacity of the absorber (Table 4.3). Therefore, the Mackowiak model can be used to predict $\Delta P/l$ in the test-rig columns in their current and future operational range.

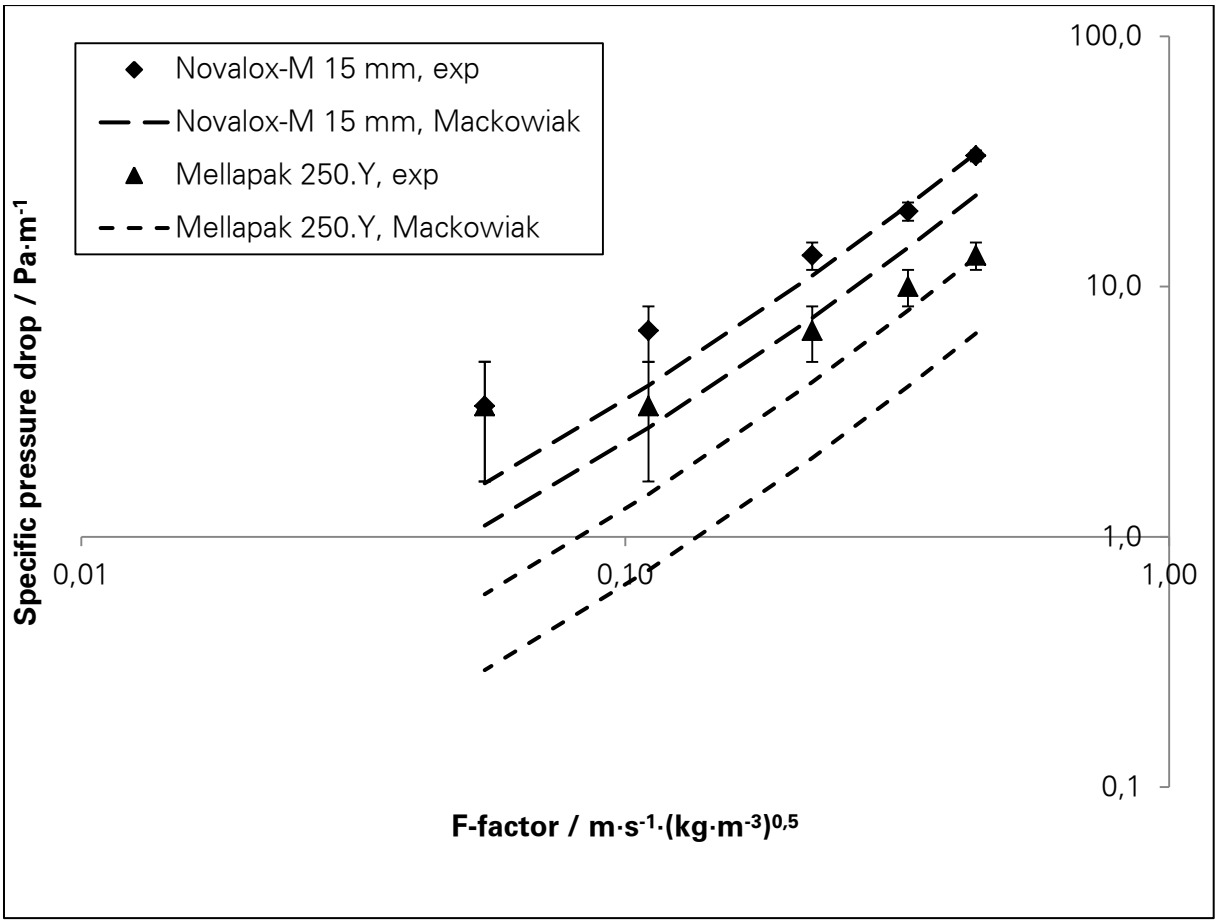

Figure 4.14 Experimentally determined (exp) and predicted (area between dashed lines) $\Delta P/l$ values at various feed-gas flow rates in dry columns

$\Delta P/l$ values determined in the test rig at different flow rates of the feed gas (60 vol. % N_2 and 40 vol. % CO_2) and the range of $\Delta P/l$ predicted by the Mackowiak model are shown in Figure 4.14. The range arises on account of the uncertainty in the packing-specific constants. Thus, constants k_{fo}, k_1 and k_2 can be used in the Mackowiak model to predict $\Delta P/l$.

Conclusions

The columns in the test rig are thin columns that suffer from solvent maldistribution as a noteworthy amount of solvent flows down the column walls. This solvent portion cannot interact with the gas as much as the solvent flowing through the central part of the column cross section. Packing and mass-transfer coefficients obtained using the test-rig columns must be modified based upon the column diameter before using these coefficients to design or rate a column with a different diameter. Furthermore, the accuracy of softwares provided by packing manufacturers to predict hydraulic behaviour as well as heat and mass transfer in thin columns should not be taken for granted.

The Billet-and-Schultes model (1999) and the Mackowiak model (2010) are suitable to predict $\Delta P/l$ in packed columns. Packing-specific constants necessary for these models can be determined by regressing experimentally determined $\Delta P/l$ values against calculated $\Delta P/l$ values. Constants such as the reference constant $k_{p,0}$ and the form constant k_{fo}, which are determined using a dry column, are valid for packed columns irrespective of column diameter. Constants such as the hydraulic constant k_h, k_1 and k_2, which are determined using an irrigated column, are not valid for thin columns if they are determined using a non-thin column and vice versa.

Packing-specific constants can be used to compare the performance of different packings. A bigger $k_{p,0}$ means a larger $\Delta P/l$; a bigger k_h means a larger liquid holdup; a bigger k_{fo} means a smaller $\Delta P/l$, and a bigger k_1 means a larger $\Delta P/l$.

When the task is to predict $\Delta P/l$ in a packed column with laminar solvent flow, and the packing-specific constants are not known, the easiest solution is to use the Mackowiak model. The model needs three packing-specific constants k_{fo}, k_1 and k_2, which are valid below and above the loading point, and the constants can be determined with limited experimental and mathematical effort. The Mackowiak model can be used to predict $\Delta P/l$ in the test-rig columns under current operational conditions and is expected to function when the test-rig capacity is further increased.

4.4 OPTIMAL PROCESS PARAMETERS

This section describes how the optimal liquid to gas ratio was determined and also how process parameters such as regeneration energy and liquid to gas ratio influence CO_2 separation.

4.4.1 MINIMUM SOLVENT FLOW RATE

The minimum solvent flow rate was determined as per the procedure described in Section 2.5.3. The equilibrium curves for the CO_2-aqueous DGA system at the absorption and desorption temperatures, i.e. at 30 and 105 °C, were obtained from simulations (Section 4.2). CO_2 content in the feed gas and treated gas was 40 and 2 vol. %, respectively. CO_2 loading in the lean solvent was the equilibrium CO_2 concentration at desorption temperature of 105 °C which is approximately 0,10 mol CO_2·(mol DGA+H_2O)$^{-1}$. CO_2 loading in the spent solvent was calculated by conducting a mass balance. The minimum liquid to gas ratio was determined to be 5 mol DGA·(mol CO_2)$^{-1}$, and the $L_{mo,ca,min}/G_{mo,ca}$ was 11 (mol DGA+H_2O)·(mol N_2)$^{-1}$. Therefore to treat a feed gas of 10 $Nm^3 \cdot h^{-1}$, a minimum solvent flow rate of 130 $kg \cdot h^{-1}$ is necessary, or for a solvent flow rate of 100 $kg \cdot h^{-1}$, the maximum feed gas that can be treated is 6,5 $Nm^3 \cdot h^{-1}$.

4.4.2 INFLUENCE OF REGENERATION ENERGY ON CO_2 SEPARATION

At a given solvent and gas flow rate (constant liquid to gas ratio), with increasing regeneration power (hourly regeneration-energy input), CO_2 absorption (kilograms of CO_2 absorbed per hour) increased (Figure 4.15). As the power of the electric reboiler was increased, solvent temperature in the reboiler increased, and the lean CO_2 loading in the solvent decreased; consequently, CO_2 absorption and the degree of separation increased with increasing regeneration power.

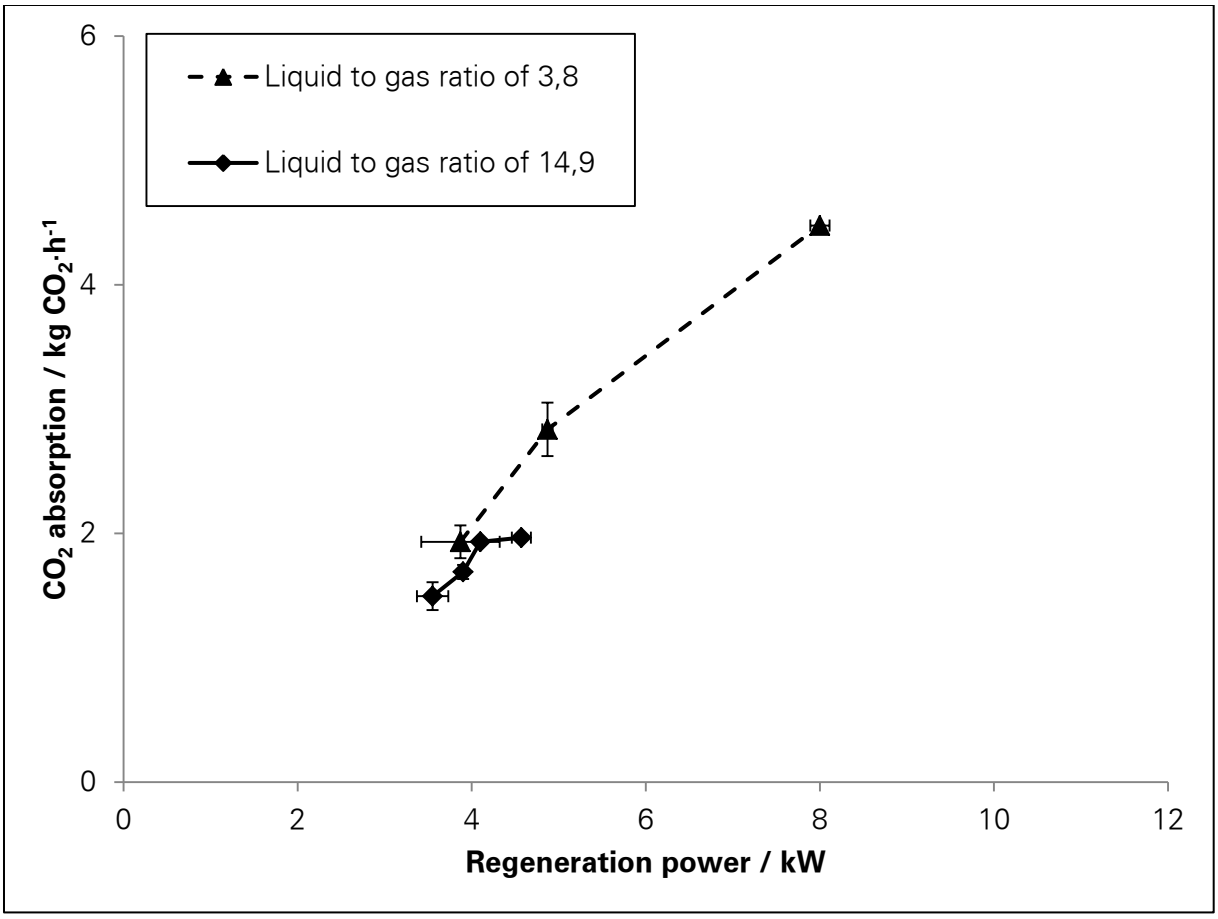

Figure 4.15 CO_2 absorption against regeneration power at the solvent flow rate of 100 $kg \cdot h^{-1}$ and gas flow rates of 2,5 and 10 $Nm^3 \cdot h^{-1}$

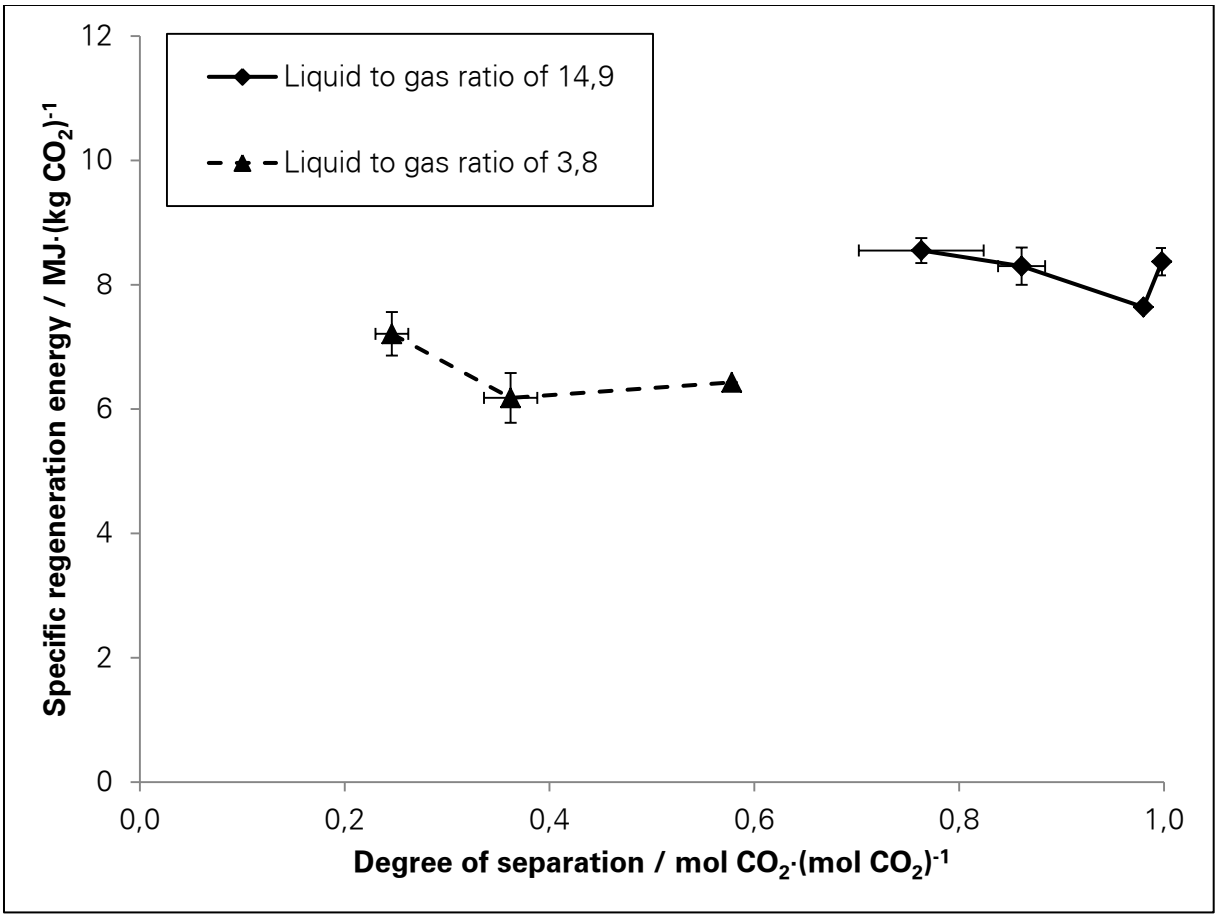

Figure 4.16 Specific regeneration-energy demand against degree of separation at the solvent flow rate of 100 kg·h^{-1} and gas flow rates of 2,5 and 10 Nm^3·h^{-1}

With increasing degree of separation, the specific regeneration-energy consumption decreased; it reached a minimum and then increased (Figure 4.16). The decrease in specific regeneration energy is attributed to the increase in driving force of CO_2 mass transfer caused by the decrease in lean CO_2 loading. This relationship is valid only in a particular CO_2 loading range and is not generic; the range can change with temperature, pressure and the solute-solvent system (Smith and Harvey, 2007). The specific regeneration-energy consumption increased after the minima because lean CO_2 loading became so low (approached its equilibrium value) that disproportionately high amount of energy was spent in achieving the lean CO_2 loading.

The way in which the low lean CO_2 loading enabled the increase in degree of separation after the minima of the specific regeneration energy is different for the two cases shown in Figure 4.16. For the case of the liquid to gas ratio of 3,8 mol DGA·(mol CO_2)$^{-1}$, the driving force for CO_2 mass transfer in the absorber approached zero towards the bottom of the absorber, and the difficulty level of mass transfer increased (Figure E.1). Thus, the number of transfer units *NTU* in the absorber approached infinity, and decreasing the lean CO_2 loading

decreased the *NTU*. For the case of the liquid to gas ratio of 14,9 mol DGA·(mol CO_2)$^{-1}$, the driving force for the mass transfer approached zero at the absorber top (Figure E.1). Thus, *NTU* approached infinity, and decreasing the lean CO_2 loading decreased the *NTU*.

4.4.3 INFLUENCE OF LIQUID TO GAS RATIO ON REGENERATION ENERGY

Figure 4.17 shows regeneration power and specific regeneration-energy demand against liquid to gas ratio for a constant degree of separation. As the solvent flow rate increased, the liquid to gas ratio increased, and at a given degree of separation, regeneration power and specific regeneration-energy demand increased as more solvent was heated.

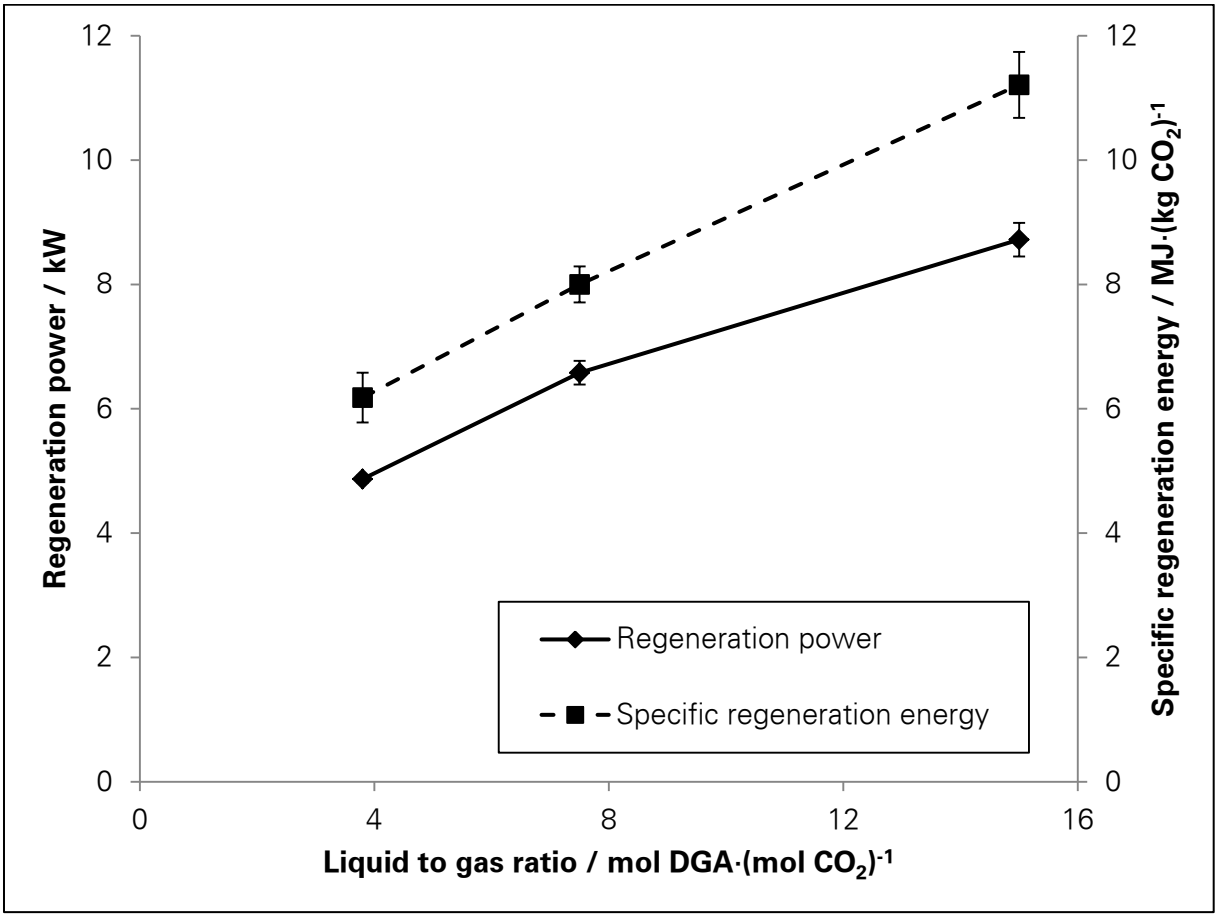

Figure 4.17 Regeneration power and specific regeneration energy for the degree of separation of 0,35 mol CO_2·(mol CO_2)$^{-1}$ at various liquid to gas ratios

4.4.4 OPTIMAL LIQUID TO GAS RATIO

Minimum specific regeneration-energy demand was the criterion that was used to determine the optimal liquid to gas ratio. From the perspective of energy costs, which constitute operating costs, the specific regeneration-energy demand is minimum at the optimal solvent flow rate.

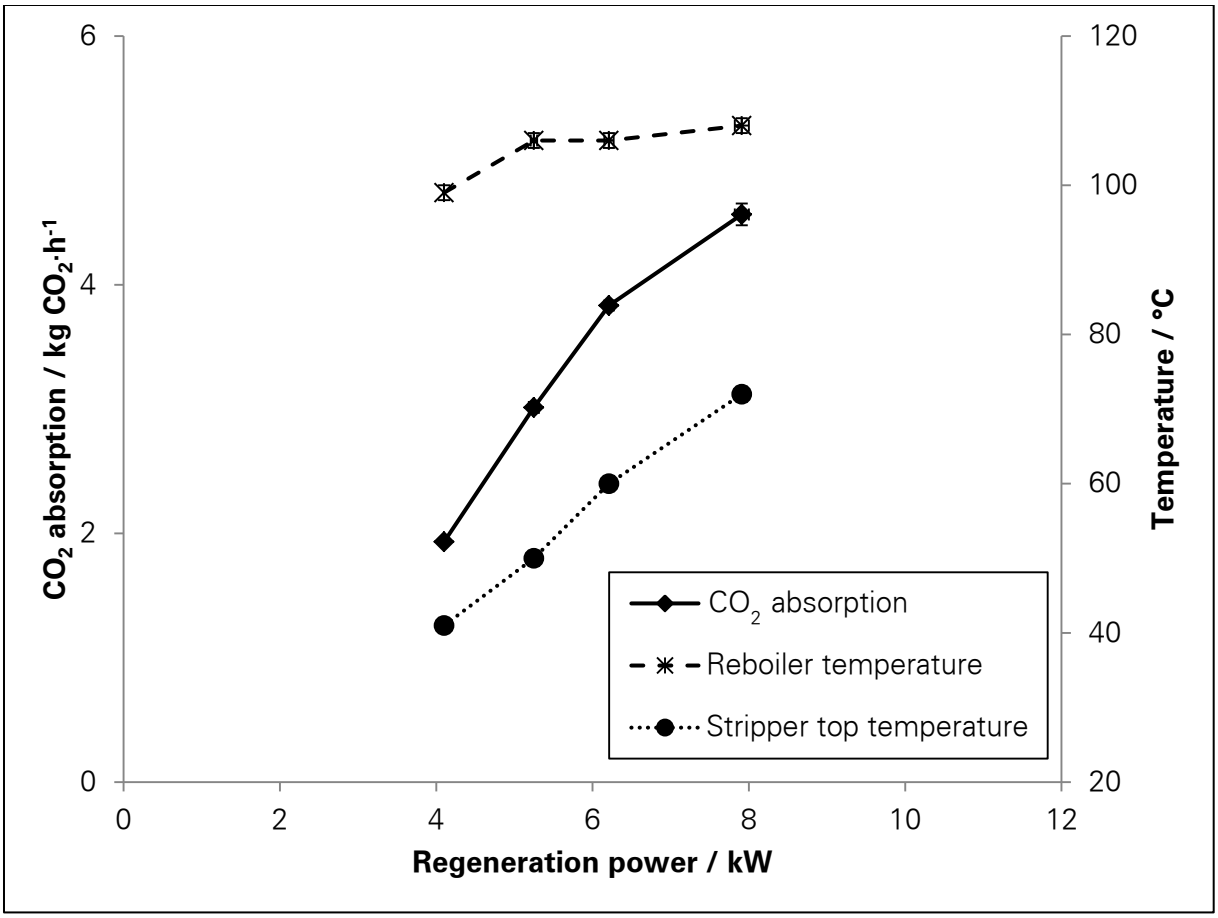

Figure 4.18 CO_2 absorption against regeneration power at the solvent flow rate of 100 $kg \cdot h^{-1}$ and gas flow rates of 2,5, 4, 5, and 6 $Nm^3 \cdot h^{-1}$

Figure 4.18 shows CO_2 absorption (kilograms of CO_2 absorbed per hour) against regeneration power. As the regeneration power increased, CO_2 absorption increased. Figure 4.19 shows the influence of liquid to gas ratio on specific regeneration-energy demand at a degree of separation of 0,98 mol $CO_2 \cdot (mol\ CO_2)^{-1}$ as necessary in a biogas-treatment plant. During the experiments, liquid to gas ratio was changed by changing the gas flow rate for a constant solvent flow rate. As the liquid to gas ratio decreased, specific regeneration-energy demand decreased; it reached a minimum and then increased.

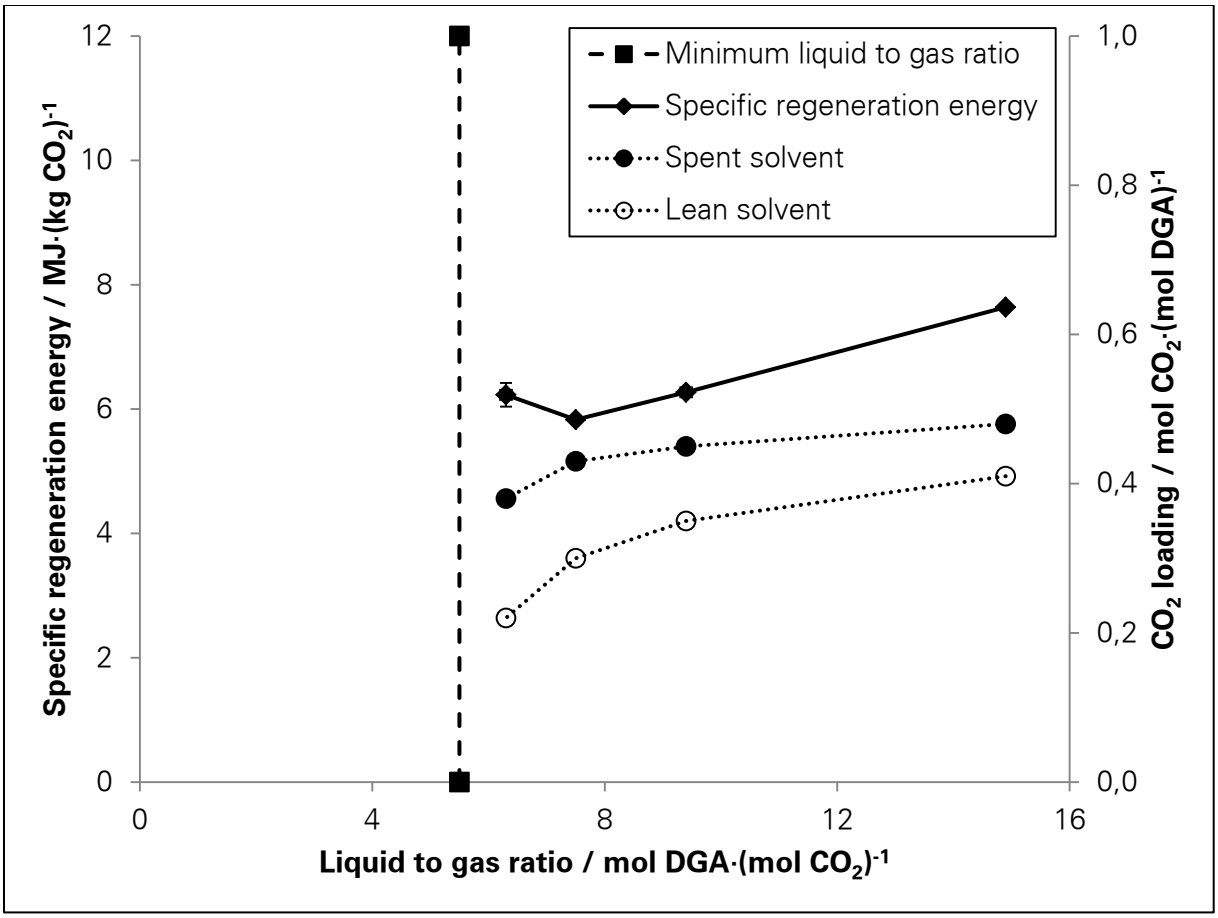

Figure 4.19 Specific regeneration-energy demand against degree of separation at the solvent flow rate of 100 kg·h^{-1} and gas flow rates of 2,5, 4, 5, and 6 Nm^3·h^{-1}

The lean CO_2 loading decreased with decreasing liquid to gas ratio (Figure 4.19) because the increase in regeneration energy led to a larger CO_2 desorption. The difference between the lean and spent CO_2 loading increased with decreasing liquid to gas ratio. As the gas flow rate was changed and the solvent flow rate was kept constant, more CO_2 had to be absorbed for a lower liquid to gas ratio in order to achieve the same degree of separation. The spent CO_2 loading decreased with decreasing liquid to gas ratio which is typical of an absorber with constant, inadequate height (Notz et al., 2012); the solvent did not get enough time in the absorber to use its full potential.

Regeneration energy is utilized for four key purposes: heating the solvent, desorbing CO_2 from the solvent, generating boil-up, i.e. steam, gaseous CO_2 and DGA vapours, and heating internal reflux, i.e. condensed steam and liquid DGA (Mangalapally et al., 2009). CO_2-desorption enthalpy decreases with increasing temperature but increases with decreasing CO_2 loading (Christensen and Christensen, 1986); therefore, specific energy spent for desorbing CO_2, viz. MJ·(kg CO_2)$^{-1}$, can be assumed to remain constant with decreasing liquid to gas ratio. Energy spent in heating the solvent increases with decreasing

liquid to gas ratio as the same amount of solvent is heated to a higher temperature (from left to right in Figure 4.18 or with increasing gas flow rate), and moreover, the specific heat capacity of the solvent increases with increasing temperature (Chiu and Li, 1999). Energy spent in generating the boil-up increases with decreasing liquid to gas ratio, and the temperature at the stripper top (before condenser) increases with decreasing liquid to gas ratio (from left to right in Figure 4.18 or with increasing gas flow rate). The generated boil-up increases with decreasing lean CO_2 loading (Mangalapally et al., 2009) as the CO_2 vapour pressure over the solvent decreases and the H_2O vapour pressure increases. In addition, as the solvent temperature in the reboiler increases and reaches the boiling point, vapour pressure of solvent increases (Huntsman, 2005), and the generated boil-up further increases. Consequently, energy spent in heating the internal reflux also increases with decreasing liquid to gas ratio as more internal reflux must be reheated.

Extreme care must be taken while operating the column under conditions of heavy boil-up generation:

- The large amount of steam generated in the stripper may overload the condenser, and all the DGA vapours and steam will not be condensed and returned, but will be carried off by the off gas (CO_2) resulting in a solvent loss.
- The large amount of gases generated in the reboiler will lead to an increase in the absolute pressure at the stripper bottom which will increase the stresses on the stripper walls, and the column may explode.
- If the large amount of steam and CO_2 that is produced in the reboiler cannot escape through the stripper, the gases will be carried by the solvent into the solvent pump which will damage the pump. The pump may cavitate as the solvent temperature is so close to the boiling point that the solvent will boil if the pressure slightly decreases or water content in the solvent slightly increases.

For a liquid to gas ratio that was lower than or equal to the minimum liquid to gas ratio (5 mol DGA·(mol CO_2)$^{-1}$), the desired degree of separation (0,98 mol CO_2·(mol CO_2)$^{-1}$) was not obtained. The optimal liquid to gas ratio was determined to be 7 mol DGA·(mol CO_2)$^{-1}$. This value is valid for gas-treatment processes that have columns with a height of at least 3 m, which is typical of biogas-treatment and natural-gas-treatment plants. The ultimate carrier solvent flow rate $L_{mo,ca}$ is approximately 1,4 times the minimum carrier solvent flow rate $L_{mo,ca,min}$.

4.4.5 MASS TRANSFER COEFFICIENTS

The overall volumetric mass transfer coefficients K_Ga in the absorber were determined using Equations 3.18 and 3.19 for the experiments discussed in Section 4.4.4 and are shown in Figure 4.20.

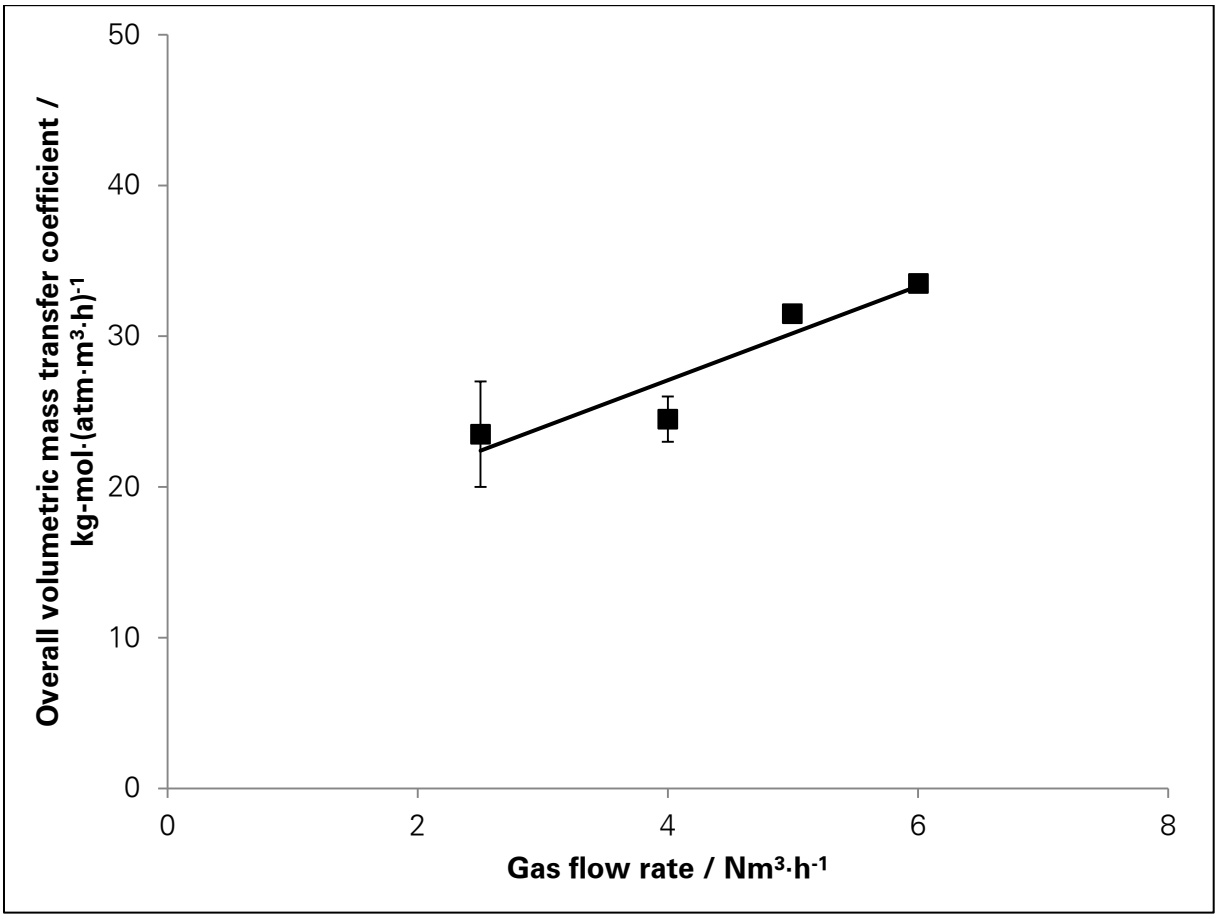

Figure 4.20 Overall mass transfer coefficients at various gas flow rates for a solvent flow rate of 100 kg·h^{-1} and a degree of separation of 0,98 mol CO_2·(mol CO_2)$^{-1}$

K_Ga increases with increasing gas flow rate due to the increase in contact between the gas and the solvent in the column. The source of uncertainty is the inaccurate determination of the driving force of CO_2 mass transfer at the column bottom, which is attributed to the inaccurate calculation of the CO_2 vapour pressure.

4.4.6 HEATING AND COOLING ENERGY

Hot utility is required in the preheater and reboiler, and cold utility is required in the cooler and condenser. Heating and cooling-energy consumption measured in the test rig for the case of 5 Nm^3·h^{-1} feed gas flow rate and 100 kg·h^{-1} solvent flow rate (liquid to gas ratio of 7,5 mol DGA·(mol CO_2)$^{-1}$, which is close to the optimal value) is shown in Table 4.5. In

addition, theoretically calculated or the minimum necessary values for these process conditions are presented.

Table 4.5 Experimentally measured and theoretically calculated heat and cold duties of heat-exchange apparatuses at the test rig

Parameter	Unit	Measured	Calculated
Cooler duty	kWh·(Nm^3 biomethane)$^{-1}$	0,73	0,74
Condenser duty	kWh·(Nm^3 biomethane)$^{-1}$	0,26	0,31
Preheater duty	kWh·(Nm^3 biomethane)$^{-1}$	0,33	0,00
Reboiler duty	kWh·(Nm^3 biomethane)$^{-1}$	1,71	1,03

The measured cooler and condenser duties are smaller than the calculated values because heat is lost by the solvent to the surroundings which cools the solvent. Consequently, the cooling energy actually consumed is smaller than the theoretical value. The measured preheater and reboiler duties are larger than the calculated values because heat lost to the surroundings must be compensated by adding more heat.

By conducting a heat balance across the whole test rig (Table 4.5), it was determined that 1,06 kWh·(Nm^3 biomethane)$^{-1}$ energy (heat) was lost to the surroundings. The primary source of this heat loss was the lean solvent that flowed from the stripper to the solvent-solvent heat exchanger. If the corresponding solvent pipes were to be comprehensively insulated (improved insulation), the total heat demand would reduce from 2,04 to 1,30 kWh·(Nm^3 biomethane)$^{-1}$ assuming a minimum approach temperature of 10 K in all four heat exchangers (Table 4.6). This is because the preheater would become superfluous as the solvent-solvent heat exchanger would heat the spent solvent to over 95 °C, and furthermore, less energy would be spent in heating the solvent in the stripper as the solvent would have a higher temperature at the stripper inlet.

The heat demand measured on the test rig is larger than that from the state-of-the-art plants because heat loss in the test rig (a small plant) is larger on account of its higher specific surface area, viz. m^2·(kg solvent)$^{-1}$ (Ohle, 2009). The heat demand in kWh·(Nm^3 biogas) of the test rig with improved insulation is within the range of state-of-the-art plants (Table 4.6). The exact value depends upon the gas flow rate, CO_2 content in biogas, the desired CO_2 content in biomethane, absorber and stripper pressure, and stripper temperature; therefore, a direct comparison between the test rig and a state-of-the-art plant is not possible.

Table 4.6 Heat duty measured on the test rig and expected on the test rig with improved insulation, and state-of-the-art values

Heat duty unit	Experiments on test rig	With improved insulation on test rig	State of the art	
			Value	Source
kWh·(Nm^3 biogas)$^{-1}$	1,2	0,8	0,5 to 0,8	Fachagentur für Nachwachsende Rohstoff e.V., 2012
kWh·(Nm^3 biomethane)$^{-1}$	2,0	1,3	1,1	RES Projects GmbH, 2013
MJ·(kg CO_2)$^{-1}$	5,8	3,7	3,6 to 3,8	Notz et al., 2012

4.4.7 NTU DIAGRAM

Column or packing height is the product of *NTU* and *HTU*. Since column height influences investment costs, process conditions must be chosen such that column height and *NTU* remain as small as possible. The dependence of *NTU* on the liquid to gas ratio and CO_2 content in the lean solvent X_{in} is illustrated using Figure 4.21, which is termed as the "NTU diagram". The NTU diagram is an optical cue to comprehend the relationships between the difficulty in mass transfer *NTU*, liquid to gas ratio and lean CO_2 loading.

NTU in the absorber was calculated according to Equation 3.26 for y_{bot} or y_{in} of 0,40 mol CO_2·(mol CO_2+N_2)$^{-1}$ and y_{top} or y_{out} of 0,02 mol CO_2·(mol CO_2+N_2)$^{-1}$ for various lean CO_2 loadings X_{in} or X_{top} and liquid to gas ratios. Figure 4.21 shows that for a constant liquid to gas ratio, with decreasing lean CO_2 loading, *NTU* decreases substantially at first and then negligibly. Consequently, decreasing lean CO_2 loading beyond a certain point "loading threshold" will not effectively decrease *NTU*. In addition, as lean CO_2 loading decreases, the minimum liquid to gas ratio necessary to achieve the desired degree of separation increases. For a lean CO_2 loading greater than 0,14 mol CO_2·(mol DGA+H_2O)$^{-1}$, it is not possible to achieve the desired degree of separation of 0,98 mol CO_2·(mol CO_2)$^{-1}$, even at liquid to gas ratios greater than 16 mol DGA·(mol CO_2)$^{-1}$ because the CO_2 vapour pressure of the solvent at the absorber top exceeds the partial pressure of CO_2 in the gas. Figure 4.21 also shows that for a constant lean CO_2 loading, *NTU* decreases with increasing liquid to gas ratio.

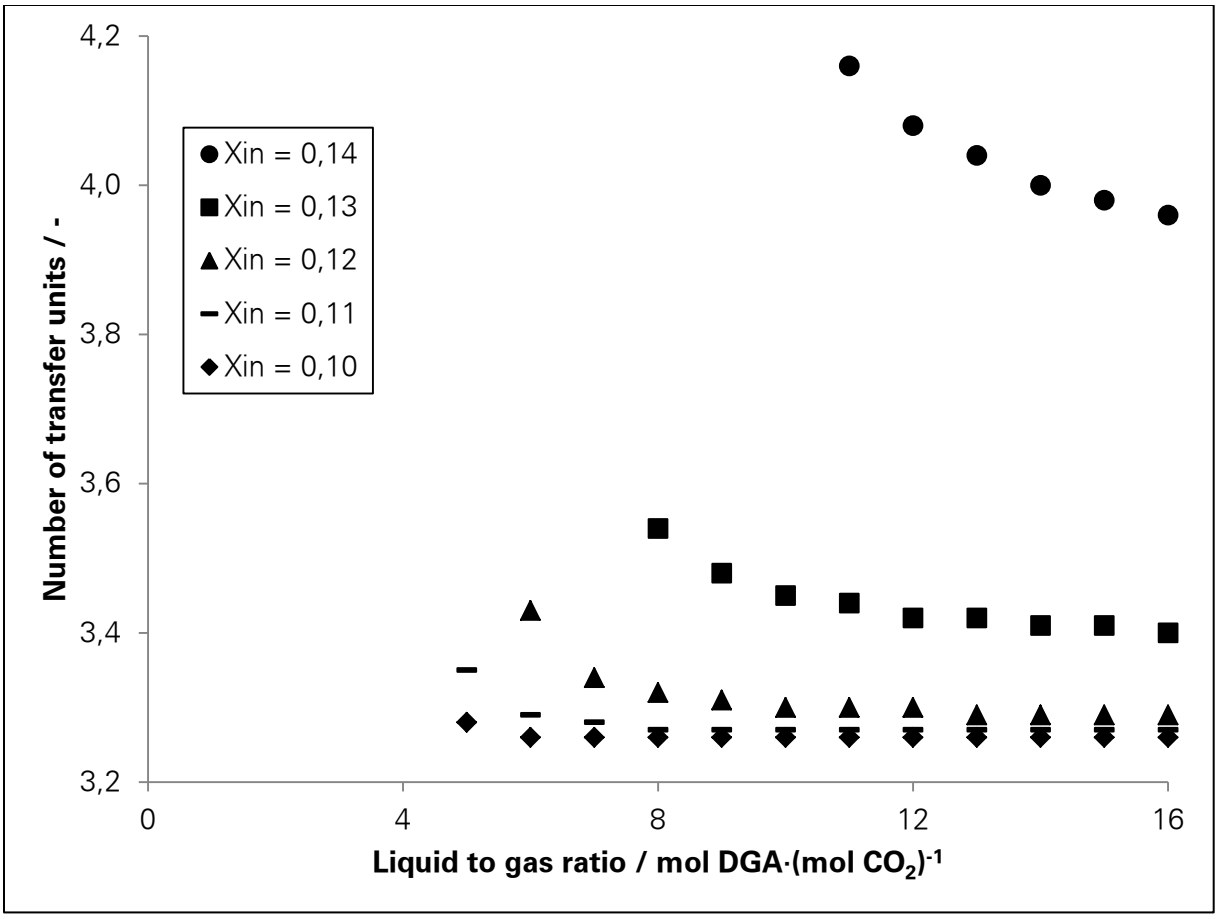

Figure 4.21 Number of transfer units necessary to achieve the degree of separation of 0,98 mol CO_2·(mol CO_2)$^{-1}$ at various lean CO_2 loadings and liquid to gas ratios

4.4.8 CO_2 AS A PRODUCT

The off gas (gas stream at the stripper top after the condenser) had a temperature of 21 °C and a relative humidity of 100 %: it was saturated with water vapour. CO_2 content in off gas after drying the gas was measured to be above 99,9 vol. %, which implies that once water is separated from off gas, relatively pure CO_2 is obtained. Nevertheless, before using this CO_2, it is recommended that the CO_2 gas stream pass through a so-called "police filter" that catches the smallest quantities of organic substances in the gas stream. The activated carbon filter made of Norit RST3 (manufactured by Norit Nederland bv.) is an example of a police filter. Thus, CO_2 is an additional product of the absorption process used to upgrade biogas to biomethane.

Conclusions

The absorption solvent of 70 wt. % DGA in solvent is suitable to separate CO_2 from biogas at atmospheric pressure and upgrade biogas to biomethane. Separating CO_2 from biogas

using chemical absorption solvents such as aqueous DGA produces two products: biomethane and CO_2.

For a given absorber (height and packing), an optimal degree of separation exists, with respect to specific regeneration-energy consumption, which depends upon the liquid to gas ratio. The optimum shifts towards a greater degree of separation with increasing liquid to gas ratio, but the specific regeneration-energy consumption at the optimum also increases. Furthermore, for a given degree of separation, an optimal liquid to gas ratio exists with respect to specific energy consumption.

The degree of separation is limited when the driving force for the CO_2 mass transfer in the absorber approaches zero which can happen in two cases. In the first case, the partial pressure of CO_2 (in the gas) is so low that it approaches the saturated vapour pressure of CO_2 (above the solvent) at the absorber top. In the second case, the saturated vapour pressure of CO_2 is so high that it approaches CO_2 partial pressure at the absorber bottom. In the first case, decreasing CO_2 loading in the lean solvent or increasing the absorber height or using more efficient packings will enable the increase in degree of separation. In the second case, decreasing CO_2 loading in the lean solvent or increasing the liquid to gas ratio will enable the increase in degree of separation.

The difficulty of CO_2 mass transfer in the absorber decreases with decreasing lean CO_2 loading. However, one must not be tempted to decrease the lean CO_2 loading to the lowest possible value because as the lean CO_2 loading approaches its equilibrium value, the energy required to desorb CO_2 increases significantly. Therefore, it is energy efficient to design an absorption process with a moderate liquid to gas ratio and moderate lean CO_2 loading than a process with low liquid to gas ratio and very low lean CO_2 loading. The lean CO_2 loading must be selected such that it is below the "loading threshold" as a further decrease in lean CO_2 loading will not substantially decrease *NTU*. The "loading threshold" can be read from an NTU diagram. For a given *HTU*, a small *NTU* will lead to a short column and less investment costs.

4.5 MODEL ABSORPTION PLANT

4.5.1 DESIGN PARAMETERS

To upgrade 1000 $Nm^3 \cdot h^{-1}$ biogas that contains 40 vol. % CO_2 to biomethane that contains 2 vol. % CO_2, 15589 $kg \cdot h^{-1}$ of absorption solvent (70 wt. % DGA and 30 wt. % water) is

recommended. Design parameters for the absorber and stripper are presented in Table 4.7 and Table 3.17.

Table 4.7 Mole fraction of CO_2 in the solvent *x* at the inlet and outlet of the absorber and stripper

Symbol	Unit	Design value	
		Absorber	Stripper
x_{in}	mol CO_2·(mol CO_2+DGA+H_2O)$^{-1}$	0,107	0,115
x_{out}	mol CO_2·(mol CO_2+DGA+H_2O)$^{-1}$	0,140	0,107

4.5.2 PACKING CHOICE

Flow parameter *FP* of the absorber and the stripper was calculated to be 0,5 and 0,7, respectively, and random packings were selected for both, the absorber and the stripper. The random packing IMTP made out of metal (stainless steel) and manufactured by Koch-Glitsch LP was selected as the random packing. This packing is similar to I-ring manufactured by Sulzer Chemtech AG, Novalox-M manufactured by the Vereinigte Füllkörper Fabriken GmbH & co. KG and the Rauschert metal saddle ring manufactured by RVT Process Equipment GmbH.

As a first guess, the size of the random packing for both columns was selected to be 25 mm or 1". If the ratio of column diameter to packing diameter was not within the range from 20:1 to 8:1, the packing size of 40 mm or 1,5" was selected.

4.5.3 COLUMN DIAMETER

Two methods were used to calculate the column diameter d_{col} of the absorber and the stripper: the GPDC method, involving the packing factor, as described in Section 2.5.3, and the method based on the Mackowiak model described in Section 3.5.4.

Table 4.8 Diameter of the absorber and the stripper for IMTP 25 and 40 mm calculated using GPDC method

Packing diameter	Absorber diameter	Stripper diameter
m	m	m
0,025	0,562	0,498
0,040	0,511	0,457

The packing factor *PF* of the random packing IMTP 25 mm is 41 ft^{-1} and of IMTP 40 mm is 24 ft^{-1} (Coker, 2007). Diameter of the absorber and the stripper was calculated using the

GPDC method, and the values are shown in Table 4.8. Random packing size of 40 mm is recommended as the ratio of column diameter to packing diameter is within 20:1 to 8:1.

For the random packing of IMTP 40 mm, d_{col} was calculated using the method developed by Mackowiak (2010). The calculated diameters are shown in Table 4.9 which are 10 to 20 % smaller than the values determined using the GPDC method.

Table 4.9 Diameter of the absorber and the stripper for IMTP 40 mm calculated using the Mackowiak model

Packing diameter	Absorber diameter	Stripper diameter
m	m	m
0,040	0,436	0,403

Unlike the numerical method developed by Mackowiak (2010), the GPDC method is an analogue method, and the discrepancy in diameters determined using the two methods is due to the difficulty in accurately extrapolating in the GPDC scatter-and-line chart.

The absorber diameter, as presented in Table 4.9, was calculated for the feed gas flow rate at the absorber bottom. As the solvent absorbs CO_2, gas flow rate decreases from 1000 $Nm^3 \cdot h^{-1}$ at the absorber bottom to almost 600 $Nm^3 \cdot h^{-1}$ at the absorber top. Consequently, the diameter at the absorber top is too big, namely two times the required diameter, to facilitate efficient contact between the solvent and the gas. Therefore, designing the absorber as a conical frustum instead of a cylinder will improve the mass-transfer efficiency and reduce column height. However, the manufacturing costs of a conical frustum may be greater than those of a cylinder and thus outweigh the reduction in investment costs due to decreased column height. Therefore, an investment appraisal of the two options will identify the more economical option.

4.5.4 COLUMN HEIGHT

Column height is the product of *NTU* and *HTU*.

If biogas is assumed to be a dilute gas, the necessary *NTU* is underestimated (Table 4.10). This will lead to an underestimation of the column height by 5 to 10 %, and the desired mass transfer will not be achieved in the column. Therefore while calculating *NTU*, no simplifications should be made to Equation 3.26, and biogas should not be assumed to a dilute gas.

Table 4.10 Influence of the interval size and the dilute-gas assumption on the calculated *NTU*

Interval of y mol CO_2·(mol CO_2+CH_4)$^{-1}$	**NTU (concentrated gas)** -	**NTU (dilute gas)** -
0,1	7,63	7,34
0,01	3,87	3,63
0,001	3,50	3,26
0,0001	3,50	3,26

While calculating *NTU* (solving Equation 3.26), the interval size or d*y* should be selected such that it does not influence the result. Table 4.10 shows that as d*y* decreases from 0,1 to 0,0001 mol CO_2·(mol CO_2+CH_4)$^{-1}$, *NTU* decreases and reaches a constant value. Therefore, a minimum interval size d*y* of 0,001 mol CO_2·(mol CO_2+CH_4)$^{-1}$ is recommended while calculating *NTU*; else, the column height will be overestimated.

Considering biogas to be a concentrated gas, and calculating *NTU* with an interval size of 0,001 mol CO_2·(mol CO_2+CH_4)$^{-1}$, *NTU* in the absorber was 3,5 and -1,4 in the stripper. Negative *NTU* indicates that CO_2 is transferred from the solvent into the gas.

HTU was estimated using Equation 3.27 to be 1,7 and 1,8 m in the absorber and stripper, respectively. This gave a packing height of 6,1 m for the absorber and 2,5 m for the stripper. It is expected that mass transfer coefficients in the scaled-up columns are larger than those measured in the test-rig columns; consequently, the column heights presented here are overestimated. Further research should investigate the estimation of *HTU* using theoretical methods such as those presented in Billet and Schultes (1999).

4.5.5 HEATING AND COOLING ENERGY

In the model absorption plant, groundwater at 12 °C can be used as the cooling fluid, and DOWTHERM A (Dow, 2001) at 115 °C can be used as the heating fluid. With a minimum approach temperature of 10 K for the cooler, condenser and reboiler, the cold and heat duties were calculated (Table 4.11).

Table 4.11 Cooler, condenser and reboiler duties in the model absorption plant

Parameter	**Duty / kW**
Cooler duty	583
Condenser duty	67
Reboiler duty	672

In the scaled-up (model) absorption plant, the heat demand would be lower than that in the test rig with improved insulation (Table 4.12 and Table 4.6). The absorber and stripper in the test rig suffer from solvent maldistribution, and if in the scaled-up plant, solvent maldistribution is avoided, the optimal liquid to gas ratio would reduce and the energy spent in heating the solvent and the specific energy consumption would also reduce. In addition, if the absorber is tall enough that the spent CO_2 loading approaches the equilibrium value, the specific energy consumption would decrease because the necessary lean CO_2 loading would be higher (Notz et al., 2012). Thus, heat demand in the absorption process that uses aqueous 70 wt. % DGA in solvent as the absorption solvent is expected to be smaller than that in the state-of-the-art absorption processes.

Table 4.12 Heat demand of the model absorption plant

Unit	Value
$kWh \cdot (Nm^3 \text{ biogas})^{-1}$	0,7
$kWh \cdot (Nm^3 \text{ biomethane})^{-1}$	1,1
$MJ \cdot (kg\ CO_2)^{-1}$	3,1

4.6 SOLVENT HAZARDS

Real hazards of seven absorption solvents are discussed in Section 4.6.1, and then, the disposition of the German population towards hazards is discussed in Section 4.6.2.

4.6.1 HAZARDS OF ABSORPTION SOLVENTS

All the six principal reactants MEA, DGA, DEA, MDEA, PZ and AMP are hazardous with PZ being the most hazardous and AMP being the least hazardous (Table F.1). A physical hazard is possessed only by PZ as PZ is flammable. Health hazards are possessed by all principal reactants. All six principal reactants are harmful to the skin and eyes, but only MEA, DGA, DEA and MDEA are acutely toxic. In addition, PZ is a skin and respiratory sensitizer, and it possesses reproductive toxicity. An environmental hazard is possessed only by PZ and AMP as they possess chronic aquatic toxicity.

Thirty-four by-products are hazardous, and seven by-products are not hazardous (Table F.1 and Table F.2). No data was found about the remaining fifteen by-products (Table F.3), and these substances must be analysed to determine their potential hazards.

Amongst the by-products, the most hazardous substance is N-(2-hydroxyethyl)ethylenediamine. Methylamine and NH_3 are flammable gases;

1,4-dimethylpiperazine, ethylenediamine, 2-(dimethylamino)ethanol, 2,6-lutidine, N,N-dimethylamine, formic acid, acetic acid, acetaldehyde and morpholine are flammable liquids, and triethylenediamine is a flammable solid. All thirty-four by-products possess a health hazard. Noteworthy are formaldehyde and acetaldehyde due to their carcinogenicity, and N-(2-hydroxyethyl)ethylenediamine and formamide due to their reproductive toxicity. Only three by-products possess an environmental hazard: NH_3 possesses an acute aquatic toxicity, and N-methyl-aminomethylpropanol and triethylenediamine possess chronic aquatic toxicity.

Table 4.13 shows hazards and the hazard category of seven absorptions solvents. All seven absorption solvents are hazardous. They all possess health hazards: they are harmful to skin and eyes. However, none are acutely toxic. 30 wt. % MEA, 30 wt. % DEA, 50 wt. % MDEA with 10 wt. % PZ, and 30 wt. % MEA with 30 wt. % AMP are skin and respiratory sensitizers, and they except 30 wt. % DEA possess reproductive toxicity. 60 wt. % AMP and 30 wt. % MEA with 30 wt. % AMP possess chronic aquatic toxicity. Amongst the seven solvents, 60 wt. % AMP is the least hazardous, whereas 30 wt. % MEA with 30 wt. % AMP is the most hazardous. 60 wt. % DGA is less hazardous than 30 wt. % MEA and 30 wt. % DEA. None of the solvents possess a physical hazard. If DGA content in the absorption solvent would be increased from 60 to 70 wt. %, it would still be less hazardous than the 30 wt. % MEA and 30 wt. % DEA.

By-products influence the toxicity of the solvents. Hazards of absorption solvents are not the same as the hazards of their principal reactants (Table F.1 and Table 4.13).

4.6.2 DISPOSITION TOWARDS HAZARDS FROM BIOGAS PLANTS

In all, 1012 complete responses were obtained in the public survey. The so-called response-rate-three was 0,152, which is the number of complete responses divided by the number of contacts, non-contacts and the number of cases with unknown eligibility that are eligible (The American Association of Public Opinion Research, 2011). The exact sample size (number of responses analysed), however, varied from question to question. If the target individual answered ‘no comment / not applicable’, the individual’s response was considered invalid and not considered for analysis. Furthermore, certain questions were asked only if the target individual responded with a particular answer to a prior question.

Table 4.13 Hazards of seven absorption solvents

Hazards	**Solvents**						
	30 wt. % MEA	**60 wt. % DGA**	**30 wt. % DEA**	**50 wt. % MDEA**	**50 wt. % MDEA with 10 wt. % PZ**	**60 wt. % AMP**	**30 wt. % MEA with 30 wt. % AMP**
Harmful to skin	1B	1B	2	1C	1B	2	1B
Harmful to eyes	1	1	1	1	1	2	1
Respiratory sensitizer	1		1		1		1
Skin sensitizer	1		1		1		1
Reproductive toxicity	1B				2		1B
Specific target organ toxicity, single exposure	3			3	3		3
Specific target organ toxicity, repeated exposure	2		2				2
Aquatic toxicity, chronic						3	3
Hazard points	**5,33**	**1,75**	**3,75**	**1,83**	**4,58**	**1,25**	**5,83**

The representativeness of the public survey was analysed by comparing the sample population and the German population using three criteria: percentage of males, average age, and percentage of individuals with education level of German *Abitur* or higher. A small discrepancy between the populations was observed for the first two criteria, but a large discrepancy was observed for the third criterion (Table F.4). It is common in surveys using telephone that target individuals with education level lower than the German *Abitur* frequently refuse to cooperate (Engels et al., 2013). Since the sample and the German populations were not identical, the statistics of the responses obtained from the survey were weighted in order to make the survey representative of the German population.

Of the German population, only 4 % reside in the immediate neighbourhood of a biogas plant, and 17 % reside within 3 km of a biogas plant. The majority of the German population reside away (> 3 km) from a biogas plant (Table F.5).

The majority (62 %) of the German population think that biogas plants are not hazardous, and only 29 % of the German population think that biogas plants are hazardous (Table F.6). However, 48 % of people residing directly next to a biogas plant think that biogas plants are hazardous (Table F.7). People residing in the immediate neighbourhood of a biogas plant have a different perception about biogas plants compared to those not residing in the immediate neighbourhood.

Out of those people who thought biogas plants are hazardous, 27 % did not know which hazards originate from a plant. The remaining people could associate one or more hazards with the biogas plant. Thus, not everybody who thinks that a biogas plant is hazardous knows which hazards originate from a biogas plant.

The most predominant hazard associated with a biogas plant was explosion with 30 % relative frequency, and the second-most predominant hazard was poisonous emissions with 17 % relative frequency. Other hazards had a relative frequency below 10 % (Table F.8). The assortment of hazards associated with a biogas plant is very large and included in addition to physical, health, and environmental hazards, other hazards such as ‘fraud’, ‘monoculture’ and ‘waste of land’. Therefore, people who think that a biogas plant is hazardous associate problems, so-called hazards, with biogas plants which do not directly originate from a biogas plant.

The German population considers physical, health and environmental hazards to be equally serious. They perceive a fire or an explosion to be as serious as polluted water endangering humans and equally serious is the environmental threat to plants and animals. The German

population on average considers physical, health and environmental hazards to be moderately serious (Table F.9).

Conclusions

The European Union regulation EC 1272 (2008) can be used to assess the severity of hazards of absorption solvents. The assessment can then be used in the hazard-analysis procedure developed in this study to quantitatively compare the hazards of absorption solvents and thus select the least hazardous absorption solvent. This procedure should be valid for substances other than the components of absorption solvents.

Information on the hazards of absorption solvents is provided by governmental and non-governmental organisations as well as by solvent manufacturers. However, limited information on the hazards of by-products from the reaction between absorption solvents and solutes, namely CO_2 and O_2, is available, and further experimental investigations are necessary to determine the hazards of reaction by-products.

For upgrading biogas to biomethane at atmospheric pressure, 70 wt. % DGA is a less hazardous alternative to the state-of-the-art absorption solvents such as 30 wt. % MEA and 30 wt. % DEA. As the chemical absorption solvents discussed in this study have been used in the past to treat natural gas and flue gas, the analyses presented here are relevant for the hydrocarbon and energy industry.

The German population will be equally disturbed when shoals of fish die due to a pollutant from a process or a human community is hit from an explosion in the plant. Therefore, equal importance should be given to avoid physical, health and environmental hazards to ensure public acceptance.

When developing public-engagement and public-outreach strategies, special attention must be paid to the community residing directly next to biogas plants.

4.7 LIFE CYCLE IMPACT ASSESSMENT AND INTERPRETATION

At first, the life cycle impact assessment and then, the last phase of the LCA study, which is the life cycle interpretation, are described (Muench et al., 2015).

4.7.1 LIFE CYCLE IMPACT ASSESSMENT

Table 4.14 Environmental impacts of biomethane and natural gas per functional unit

Impact category	Unit	Biomethane	Natural gas
ADP	kg Sb eq.	1,13E-07	3,66E-09
AP	kg SO_2 eq.	2,75E-04	5,84E-05
FAETP	kg 1,4-DCB eq.	8,11E-03	4,82E-04
MAETP	kg 1,4-DCB eq.	2,41E+01	1,07E+00
TETP	kg 1,4-DCB eq.	2,47E-04	1,95E-05
EP	kg PO_4^{3-} eq.	8,85E-05	5,33E-06
GWP	kg CO_2 eq.	-1,32E-02	1,58E-02
HTP	kg 1,4-DCB eq.	1,70E-02	8,13E-04
ODP	kg CFC-11 eq.	2,70E-09	1,12E-08
POCP	kg C_2H_4 eq.	1,29E-05	1,72E-05

The environmental impacts of biomethane and natural gas are shown in Table 4.14. Neither biomethane nor natural gas outperforms the other in all the impact categories. Biomethane has a lower global warming potential (GWP), ozone depletion potential (ODP) and photo oxidant creation potential (POCP) than natural gas, whereas natural gas has a lower abiotic resource depletion potential (ADP), acidification potential (AP), freshwater aquatic ecotoxicity potential (FAETP), marine aquatic ecotoxicity potential (MAETP), terrestrial ecotoxicity potential (TETP), eutrophication potential (EP) and human toxicity potential (HTP) than biomethane. Biomethane has a negative GWP, which shows that that biomethane is a CO_2 sink.

The sources of environmental impacts of biomethane are presented in Figure 4.22, which helps to identify the environmental hot spots in the biomethane-production process.

ADP: The principal contributor (89 %) to ADP is infrastructure, namely the material needed for constructing and decommissioning plants.

AP: The main contributor (68 %) to AP is biogas production, which necessitates biomass storage that results in NH_3 emissions. The second-largest contributor to AP (24 %) is desorption, which employs heat, and SO_2 emissions during heat production lead to acidification.

FAETP: The desorption process is the largest contributor (37 %) to FAETP due to the toxic emissions from the heat-production facility. Another noteworthy contributor to FAETP is infrastructure (28 %), namely the steel and copper needed for plant construction.

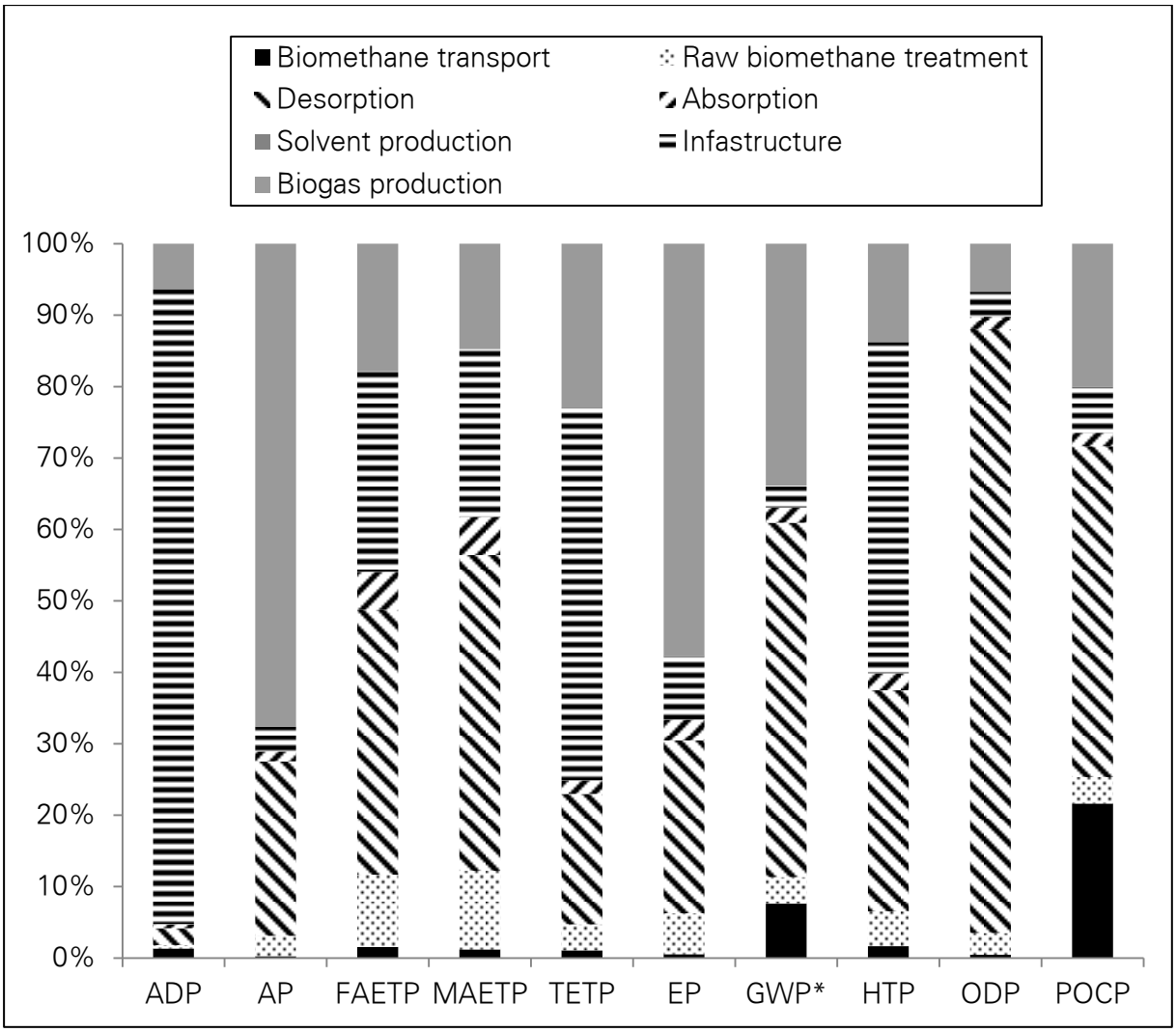

Figure 4.22 Sources of environmental impacts of biomethane
(*without biogenic CO_2)

MAETP: Desorption is the main source (44 %) of MAETP, and infrastructure is the second-largest source (24 %).

TETP: Infrastructure is the largest contributor (52 %) to TETP. Another noteworthy source (23 %) of TETP is biogas production, which causes toxic emissions.

EP: The largest contributor (58 %) to EP is biogas production, which necessitates biomass storage that causes NH_3 emissions. The desorption process contributes 24 % to the EP.

GWP: As biomethane is a greenhouse-gas sink, biogenic CO_2 is not considered in the following analysis. Desorption is the largest contributor (50 %) to GWP, which is explained by the process' heat demand. Another major contributor (34 %) is biogas production, which causes nitrous oxide emissions.

HTP: The major source (46 %) of HTP is infrastructure, namely the heavy metals used and inorganic emissions caused during plant construction and decommissioning. Desorption is the second-largest contributor (31 %) to HTP.

ODP: The principal contributor (85 %) to ODP is the desorption process, which needs heat, and emissions from the heat-production facilities damage the ozone layer.

POCP: Desorption is the largest contributor (46 %) to POCP. The second-largest contributor (22 %) is biomethane transport where leakages in the low-pressure natural-gas grid are to be blamed. The third-largest contributor (20 %) is biogas production, which causes NMVOC emissions.

Thus, the desorption process and the infrastructure requirements are the two biggest environmental hot spots in the biomethane-production process.

The environmental impacts (LCA results) of biomethane produced using the process involving DGA cannot be compared with biomethane produced using processes involving MEA and DEA (Starr et al., 2012; Starr et al., 2014) because their system boundaries are not identical. Moreover, LCA results cannot be always transferred between bioenergy systems (Muench, 2014).

4.7.2 LIFE CYCLE INTERPRETATION

Significance of uncertainty in input parameters

The input parameters of the LCA study had uncertainties. However, the uncertainty importance analysis showed that only one input parameter "CH_4 content in biogas", with a sensitivity of 18 %, contributed 81 % to the cumulative sensitivity. Of the remaining 19 %, input parameters related to infrastructure requirements of plants contributed 11 %, and 8 % came from all other parameters. The Monte Carlo simulation showed that in spite the uncertainties, all environmental impacts except photo oxidant creation (or POCP) of biomethane were significantly different (at a statistical significance level of 0,05) than those of natural gas. Photo oxidant creation was different at a statistical significance level of 0,10. Therefore, conclusions drawn from the comparison of environmental impacts of biomethane and natural gas in this study are robust.

Impact of CO_2 valorisation

In the investigated product system (Base Case), off gas from the desorption process was emitted into the atmosphere (Section 3.7.2). However, off gas has a composition of

97,5 vol. % CO_2, 2,3 vol. % H_2O and 0,2 vol. % CH_4 and can be treated to obtain CO_2 with a higher concentration which can be liquefied and sold as a product.

If CO_2 is valorised, the additional product of CO_2 can be dealt with in the LCA by expanding the product system such that it encompasses the off-gas treatment and CO_2 liquefaction (two additional processes). Biomethane as the principal product is allocated with the environmental impacts of additional processes and also credited with those environmental impacts, which are avoided due to the substitution of CO_2 obtained from other processes (e.g. CO_2 from wells). Such an approach is suitable only if the substituted CO_2 is the main product of the CO_2-production process such as CO_2 from wells. If the substituted CO_2 is a by-product (e.g. CO_2 obtained from natural-gas-sweetening or syngas-treating units), the environmental impacts are not mitigated, but are merely shifted to another product system. The production of natural gas or syngas will not be stopped if their CO_2 is not sold as a product.

System expansion is one option to deal with the multi-output challenge. A second option is to allocate the environmental impacts based on physical relationships such as mass or energy content, but this is inappropriate because different processes are required to produce biomethane and CO_2, and they cannot be thought of as two products of a single process. A third option is the allocation based on non-physical relationships such as price, but this is also not suitable here because biomethane (natural gas) price fluctuates and CO_2 price varies with purity, region and procurement volume (Aresta, 2010; Global CCS Institute and Parsons Brinckerhoff, 2011). This approach lacks generic validity.

A fourth option is to allocate using a consequential approach: environmental impacts of processes necessary to produce biomethane and make it a product are allocated to biomethane, and environmental impacts of additional processes necessary to produce CO_2 and make it a product are allocated to CO_2.

The changes in environmental impacts of biomethane from Base Case to the case of CO_2 valorisation are shown in Table 4.15. A negative change in the impact potential except GWP indicates a lower environmental impact. As GWP has a negative value in the Base Case scenario, a positive change in GWP indicates a larger greenhouse-gas sink or a better environmental impact. In case of CO_2 valorisation, the environmental impacts of biomethane are reduced irrespective of the allocation approach. In case of allocation based on system expansion, the credit of substituting existing CO_2-production processes is larger than the environmental impacts of additional processes, i.e. off-gas treatment and CO_2 liquefaction.

In case of allocation based on the consequential approach, POCP decreases as methane slip is allocated to CO_2 and not to biomethane.

Table 4.15 Changes in the environmental impacts of biomethane from Base Case to the case of CO_2 valorisation for two allocation methods

Impact category	Unit	System expansion	Consequential approach
ADP	kg Sb eq.	-78 %	0 %
AP	kg SO_2 eq.	-10 %	0 %
FAETP	kg 1,4-DCB eq.	-34 %	0 %
MAETP	kg 1,4-DCB eq.	-31 %	0 %
TETP	kg 1,4-DCB eq.	-61 %	0 %
EP	kg PO_4^{3-} eq.	-16 %	0 %
GWP	kg CO_2 eq.	297 %	188 %
HTP	kg 1,4-DCB eq.	-127 %	0 %
ODP	kg CFC-11 eq.	-40 %	0 %
POCP	kg C_2H_4 eq.	-33 %	-1 %

Conclusions

Biomethane is a greenhouse-gas sink, and substituting natural gas by biomethane will help to mitigate climate change. Although biomethane is a renewable energy carrier, it is not intrinsically a sustainable energy carrier. Biomethane is not more sustainable than natural gas in all the investigated impact categories. The differences between the environmental impacts of biomethane and natural gas are significant (at least at a statistical significance level of 0,10), and the results of this LCA study are robust. Biomethane production should be encouraged if the goal is to reduce global warming, ozone depletion, and photo oxidant creation. In addition, CO_2 obtained from biogas should be valorised if it substitutes another CO_2 process.

Adverse environmental impacts of the biomethane-production process can be reduced by improving the desorption process, as well as the processes of plant construction and decommissioning.

5 SUMMARY AND OUTLOOK

Biomethane is a renewable substitute of natural gas, and biomethane use is a step towards converting the energy system from fossil-fuel based to renewable-fuel based. Since 2006, when the first biomethane plant was built in Germany, biomethane production has been increasing, and in 2013, biomethane injection in the natural-gas pipelines of Germany was 106 x 1000 $m^3 \cdot h^{-1}$, which catered to approximately 1,1 % of the total natural-gas demand.

Biomethane is produced by treating biogas which includes the removal of solids, liquids (e.g. H_2O) and unwanted gas components (CO_2, H_2S, NH_3 etc.). Although certain biogas components are undesired in biomethane, their worth should not be underestimated. CO_2 is a valuable product, and H_2S can be converted into a valuable product (e.g. elemental sulphur). In order to keep the option of obtaining CO_2 as a product, other undesired gas components such as H_2S and NH_3 must be separated from biogas prior to CO_2 separation (Figure 1.2).

The concentration of H_2S in biogas varies between 100 and 30000 ppm, and the maximum permissible concentration of H_2S in biomethane is 5 ppm. To select a process that is suitable to remove H_2S from biogas, ten desulphurisation processes were theoretically analysed using five parameters, namely treatment range, desired H_2S separation, end form of sulphur, need of O_2 for operation and the possibility to regenerate the consumable (Table 2.3).

If chemical absorption is to be used for CO_2 separation, desulphurisation processes that do not require O_2 for operation must be selected because the unconsumed O_2 will react with the absorption solvent and degrade it. For biogas units handling more than 200 kg sulphur per day, the LO-CAT process combined with selective H_2S separation or the THIOPAQ process should be used for rough desulphurisation. In biogas units that deal with less than 200 kg sulphur per day, the THIOPAQ process is recommended for rough desulphurisation. If adsorption or physical absorption is to be used for CO_2 separation, biological desulphurisation should be used for rough desulphurisation. Activated carbon (solid scavenging) is recommended for fine desulphurisation. Activated carbon can be impregnated with an oxidizer (e.g. $KMnO_4$) if the presence of O_2 in biogas is undesired. If the desired H_2S concentration in the treated gas is less than 1 ppm, ZnO should be used as a solid scavenger (Section 2.2).

In the process of upgrading biogas to biomethane, CO_2 separation is the pivotal point because CO_2 is the largest entity volume wise to be separated from biogas. CO_2 content in

biogas varies between 25 and 55 volume (vol.) %, and CO_2 content in biomethane (H-Gas) must be below 4 vol. %. Biogas is available at atmospheric pressure, and biomethane should be preferably injected in the natural-gas distribution grid at near-atmospheric pressure (< 2 bar). In such a scenario, chemical absorption is the most suitable process to separate CO_2 from biogas on account of its advantages over other processes such as physical absorption, adsorption, permeation and cryogenic separation. With chemical absorption, CH_4 with high purity (above 99 vol. %) can be obtained, CH_4 slip is low, operational flexibility with respect to feed gas is high and electricity consumption is low.

The key component of the absorption process is the absorption solvent. Diglycolamine (DGA) or amino-diethylene glycol (ADEG) is a better absorption solvent than solvents such as monoethanolamine (MEA), diethanolamine (DEA) and N-methyldiethanolamine (MDEA)-with-piperazine (PZ), which are used in the state-of-the-art processes because DGA has lower volatility than MEA, larger CO_2 loading compared to DEA and a higher reaction rate than MDEA-with-PZ (Figure 2.1).

Aqueous DGA solvents with DGA content of 50, 60, 70, 80 and 90 mass (wt.) % were investigated to determine the optimal DGA content. Four crucial solvent properties, namely equilibrium CO_2 solubility, density, viscosity and surface tension, were experimentally determined as these properties are needed to design the absorption process (Section 3.2).

Equilibrium CO_2 solubility α_{CO2} in the solvents was determined at the absorption temperature of 30 °C and a CO_2 partial pressure p_{CO2} of 44 kPa using a bubble column. α_{CO2} at desorption temperatures of 90 and 105 °C was determined using a stirred-cell reactor. The absorption and desorption setups were validated by comparing experimentally determined values of α_{CO2} in 50 wt. % MDEA in solvent with values from literature. α_{CO2} of spent DGA solvents (solvents after CO_2 absorption at 30 °C) remained constant in the DGA mass fraction w_{DGA} range from 0,5 to 0,8 kg DGA·(kg DGA+H_2O)$^{-1}$ or from 50 to 80 wt. % DGA. However, at 90 wt. % DGA, α_{CO2} decreased. The tactic of increasing the DGA content in the solvent to increase CO_2 loading and thereby decrease energy demand becomes non-functional when the mole fraction of DGA exceeds the mole fraction of water in the solvent, viz. above 87 wt. % DGA in solvent, because then, not all of DGA can react with CO_2 which leads to a decrease in α_{CO2}.

For a given w_{DGA}, α_{CO2} decreases with increasing desorption temperature. However, desorption temperature is limited by the boiling point and the degradation temperature of the solvent. After desorption at 90 °C, α_{CO2} of lean solvents remained constant for w_{DGA} from 0,5 to 0,8 kg DGA·(kg DGA+H_2O)$^{-1}$. However after desorption at 105 °C, α_{CO2} increased with

increasing w_{DGA} which is ascribed to the increase in p_{CO2} with increasing w_{DGA} at the same temperature.

A high differential α_{CO2} is preferred because it reduces the solvent circulation rate, which in turn reduces the electricity consumption by the solvent pumps, cooling-energy consumption by the cooler and the condenser, and heat consumption by the preheater and the reboiler. Considering absorption at 30 °C and desorption at 105 °C, the maximum $\Delta\alpha_{CO2}$ was 0,35 mol CO_2·(mol DGA)$^{-1}$ at 70 wt. % DGA (Section 4.1.1).

Density ρ, viscosity μ and surface tension σ of solvents before absorption (raw form), after absorption (spent form) and after desorption (lean form) were experimentally determined. For raw DGA solvents, with increasing DGA mole fraction x_{DGA}, ρ increased, reached a maximum and then decreased. With increasing x_{DGA}, μ of the raw solvent always increased, whereas σ always decreased. Change in ρ, μ and σ was large at small x_{DGA} values, and the change decreased with increasing x_{DGA}. For a given w_{DGA}, with increasing CO_2 loading α_{CO2}, ρ linearly increased, μ exponentially increased and σ quadratically increased. Furthermore, with increasing w_{DGA}, the increase in ρ and μ became larger (Section 4.1.2).

Comparing the properties of DGA with those of MEA, also a single-chain primary alkanolamine, it can be said that ρ, μ and σ of single-chain primary alkanolamines are affected by the total number of atoms in the molecule and the presence of other functional groups (such as the ether group) in the molecule. The degree of self-association between DGA molecules is greater than the degree of self-association between MEA molecules. Moreover, intermolecular forces between DGA and water molecules are stronger than intermolecular forces between MEA and water molecules. However, the intermolecular forces prevalent within a CO_2-loaded DGA solvent are weaker than those within a CO_2-loaded MEA solvent. Therefore, the trends followed by the properties of raw aqueous alkanolamines are not necessarily valid for spent aqueous alkanolamines. It is recommended that properties of the solvent-of-interest be experimentally determined, and results not be transferred from one solvent to a similar solvent without verification.

To treat biogas at atmospheric pressure, the aqueous absorption solvent with 70 wt. % DGA is recommended due to its large differential CO_2 loading (0,35 mol CO_2·(mol DGA)$^{-1}$) and moderate viscosity (60 mPa·s). In a subsequent research study, α_{CO2} at other p_{CO2} values as well as solvent properties such as ρ, μ and σ at other temperatures should be experimentally determined to create a database that can be used while designing the absorption plant.

The vapour-liquid equilibrium of the CO_2-aqueous DGA system was modelled using Henry's law. Fugacity coefficients were calculated using the Peng-Robinson equation combined with the Twu generalized α-function and the generalized mixing rule. Activity coefficients were calculated using the electrolyte non-random two liquid (eNRTL) model. Henry's constant for the CO_2-H_2O system was used, and the Poynting correction factor was assumed to be one. All model parameters except the NRTL binary interaction parameters τ were obtained from literature. τ values were determined by regressing experimentally determined α_{CO2} values from this and other studies (Section 3.3).

The model was implemented using a commercial software. Using this software tool, it is possible to estimate α_{CO2} in aqueous DGA solvents with DGA content between 60 and 70 wt. % at absorption temperatures from 30 to 50 °C and in the germane p_{CO2} range with an uncertainty of less than ± 20 %. For α_{CO2} values calculated at desorption temperatures (90 to 105 °C) at p_{CO2} above 30 kPa, the uncertainty will be still lower, but will increase with decreasing p_{CO2} (Section 4.2).

The model should be used in a subsequent research study to simulate the absorption test rig and design the absorption plant. The simulation results are expected to have an uncertainty of ± 20 % or more. However, prior to that, the vapour-liquid equilibrium for the CH_4-aqueous DGA system must be simulated.

The absorption test rig was used to determine the optimal parameters of the process to separate CO_2 from biogas at atmospheric pressure. The absorber and stripper of the test rig have an inner diameter of 0,1 m and an active height of 3 m. The feed gas was 60 vol. % N_2 and 40 vol. % CO_2, and the absorption solvent was composed of 70 wt. % DGA and 30 wt. % water (Section 3.4.1). The test rig was revamped, and its capacity was increased from 4 to 10 $Nm^3 \cdot h^{-1}$ by installing a N_2-PSA (pressure swing adsorption) unit, a CO_2-cylinder battery and replacing the random packing Pall rings 15 and 30 mm in the absorber by Novalox-M 15 mm. The test-rig capacity can be further increased to 25 $Nm^3 \cdot h^{-1}$ by using feed-gas pipes with an inner diameter of 16 mm instead of 8 mm as this will reduce the pressure drop tenfold (Section 3.4.3).

It was experimentally determined that the columns in the test rig are thin columns, which suffer from solvent maldistribution: a noteworthy amount of solvent flows down the column walls. This solvent portion cannot interact with the gas as much as the solvent flowing through the central part of the column cross section (Section 4.3.2). Mass transfer coefficients and resistance coefficients determined using two phase flow in the test-rig

columns are underestimations. Before using this data to design or rate a column with a different diameter, the coefficients must be modified according to the column diameter.

The Mackowiak model (Section 3.5.1) was selected to predict the specific pressure drop $\Delta P/l$ in the test-rig columns because the model uses only three packing-specific constants, which are valid below and above the loading point. These constants were determined for the random packing Novalox-M 15 mm and the structured packing Mellapak 250.Y by regressing measured $\Delta P/l$ values. The Mackowiak model could predict $\Delta P/l$ in the test-rig columns under current operational conditions and is expected to function when the test-rig capacity is further increased.

The optimal liquid to gas ratio of the absorption process, with respect to specific energy consumption, was determined by conducting experiments on the test rig. Gas flow rate was changed for a constant solvent flow rate, and the regeneration power was selected such that the degree of separation of 0,98 mol CO_2·(mol CO_2)$^{-1}$ was obtained. The optimal liquid to gas ratio was determined to be 7 mol DGA·(mol CO_2)$^{-1}$, and with this parameter, the solvent flow rate must be calculated while designing the absorption process (Section 4.4.4).

The driving force of CO_2 mass transfer (reciprocal of number of transfer units or 1/*NTU*) in the absorber increases with decreasing CO_2 loading of the lean solvent. Lean CO_2 loading should be selected such that it is just below the "loading threshold" as a further decrease in lean CO_2 loading will not substantially decrease *NTU*, but significantly increase energy demand (as shown by the experiments). A lean CO_2 loading of 0,12 mol CO_2·(mol DGA+H_2O)$^{-1}$ is recommended based upon theoretical calculations, and the reboiler power should be selected such that this lean CO_2 loading is obtained at the desorption temperature of 105 °C (Section 4.4.7).

The average capacity of biomethane plants in Germany is 600 $Nm^3 \cdot h^{-1}$ biomethane, and a model absorption plant was designed to treat 1000 $Nm^3 \cdot h^{-1}$ biogas. The random packing IMTP 40 mm was selected for the columns. Column diameter was calculated using the Mackowiak model: absorber had a diameter of 0,44 m, and stripper had a diameter of 0,40 m. Active column height or packing height was calculated using the rate-based approach (the *HTU-NTU* method). *NTU* was calculated using the brute-force method with the interval size dy of 0,001 mol CO_2·(mol CO_2+CH_4)$^{-1}$. As biogas is a concentrated gas, the slope of the equilibrium curve and the gas flow rate change significantly across the column height. Packing height in the absorber and stripper was calculated to be 6,1 m and 2,5 m, respectively (Section 4.5).

The absorption process with 70 wt. % DGA and 30 wt. % water as the absorption solvent (the new process presented here) is suitable to upgrade biogas to biomethane at atmospheric pressure and is also suitable to treat other concentrated gases such as flue gas from oxy-fuel combustion power plants. The specific energy consumption of the new process is estimated to be 3,1 MJ·(kg CO_2)$^{-1}$, which is 16 % lower than the specific energy consumption of the state-of-the-art processes (3,6 to 3,8 MJ·(kg CO_2)$^{-1}$). Thus, the new process is more energy-efficient than the state-of-the-art processes.

CO_2 with high purity, i.e. > 99,9 vol. %, is obtained at the condenser outlet (at the stripper head) in the new absorption process (Section 4.4.8). CO_2 is an additional product that will make the new process more lucrative in the market.

A newly developed process can be successfully implemented only if it enjoys public acceptance. Gaining public acceptance can be facilitated by designing a safe process, and a less hazardous absorption solvent constitutes a safe absorption process.

The European Union regulation EC 1272 was used to assess the severity of hazards of six principal reactants in absorption solvents: MEA, DGA, DEA, MDEA, PZ and AMP (aminomethylpropanol). The hazards were compared using a quantitative method developed in this study. Information on the hazards was obtained from reports published by governmental and non-governmental organisations as well as by solvent manufacturers. However, only limited information was available on the hazards of by-products of reactions between absorption solvents and solutes CO_2 and O_2, and further experimental investigations should aim at determining the hazards of reaction by-products.

All the six principal reactants MEA, DGA, DEA, MDEA, PZ and AMP are hazardous with PZ being the most hazardous and AMP being the least hazardous. Of the 56 by-products, 34 are hazardous, 7 are not hazardous, whereas no data was found about the remaining 15 by-products. The aqueous absorption solvent containing 70 wt. % DGA is less hazardous than solvents that are used in the state-of-the-art absorption processes such as 30 wt. % MEA in solvent or 30 wt. % DEA in solvent. Therefore, the new process with aqueous DGA as the absorption solvent should be safer than the state-of-the-art absorption processes. As the absorption solvents discussed in this study have been used in the past to treat natural gas and flue gas, the analyses presented here are relevant to the hydrocarbon and energy industries.

It is essential that the information that a process is safe is conveyed to the public; only then will the public not tend to be apprehensive about the process. Dispelling imaginative fears is crucial to public acceptance.

A representative telephonic survey of the German population was conducted to determine if they think that biogas plants are hazardous; if yes, which hazards originate from biogas plants, and how serious physical, health and environmental hazards are considered relative to each other (Section 3.6.2). In the survey, 1012 complete responses were obtained. The responses were weighted using age, gender and education level in order to make the survey representative of the German population.

The majority (62 %) of the German population think that biogas plants are not hazardous. However, 48 % of the people residing directly next to a biogas plant think that biogas plants are hazardous compared to 27 % of the people that do not reside in the immediate neighbourhood. Out of those people who think biogas plants are hazardous, 27 % do not know which hazards originate from a biogas plant. Consequently, strategies that are tailor-made to the perception of the human communities should be used to improve public acceptance of biogas plants.

The representative survey also showed that the German population considers physical, health and environmental hazards to be equally serious. Therefore, equal importance must be given to avoid physical, health and environmental hazards.

A life cycle assessment (LCA) was used to determine the environmental impacts of the biomethane-production process, i.e. the process chain from biogas production to biomethane transport. The environmental impacts of biomethane production were compared with those of natural-gas production.

The quality of input parameters was quantitatively assessed using a pedigree matrix, which employs data quality indicators (DQIs) such as reliability, completeness, temporal correlation, geographical correlation and further technological correlation. Approximately 76 % of the input data parameters had good quality (additional standard deviation $\leq 0{,}1$), and 32 % had the best quality. The uncertainty in the LCA results was determined using a sensitivity analysis and a Monte Carlo simulation. The differences between the environmental impacts of biomethane and natural gas were significant (at least at a statistical significance level of 0,10), and the results were deemed robust.

The principal source of adverse environmental impacts of the biomethane-production process is solvent stripping. Therefore, subsequent research must concentrate on how the energy consumption of the solvent-stripping process can be reduced.

Biomethane is a renewable energy carrier, but it is not more sustainable than natural gas. The use of biomethane over natural gas should be supported if the goal is to reduce global warming, ozone depletion and photo oxidant creation. Natural gas should be preferred over biomethane if the goal is to reduce abiotic resource depletion, acidification, human toxicity and ecotoxicity.

If CO_2 obtained from biogas is valorised, the environmental impacts of biomethane are reduced. Moreover, if CO_2 obtained from biogas substitutes CO_2 from a process, whose principal product is CO_2 (e.g. CO_2 from wells), biomethane production becomes a CO_2 sink.

REFERENCES

Addington, L., & Ness, C. (2014). *An evaluation of general "Rules of Thumb" in amine sweetening unit design and operation.* Bryan Research and Engineering Inc.

Al-Juaied, M., & Rochelle, G. (2006a). Absorption of CO_2 in aqueous diglycolamine. *Industrial & Engineering Chemistry Research,* 45(8), 2473-2482.

Al-Juaied, M., & Rochelle, G. (2006b). Thermodynamic and equilibrium solubility of carbon dioxide in diglycolamine-morpholine-water. *Journal of Chemical and Engineering Data,* 51(2), 708-717.

Alper, E. (1990). Kinetics of reactions of carbon dioxide with diglycolamine and morpholine. *The Chemical Engineering Journal,* 44(2), 107-111.

Althaus, H., Chudacoff, M., Hischier, R., Jungbluth, N., Osses, M., & Primas, A. (2007). *Life cycle inventories of chemicals.* Ecoinvent report No. 8, Swiss Centre for Life Cycle Inventories, Dübendorf, Switzerland.

Appl, M., Wagner, U., Henrici, H., Kuessner, K., Volkamer, K., & Fuerst, E. (1982). *Removal of CO_2 and or H_2S and or COS from gases containing these constituents.* Patent. US 4336233. BASF AG.

Arbeitsgemeinschaft für sparsamen und umweltfreundlichen Energieverbrauch e.V. (2011). *Bio-Erdgas – Regenerative Energie mit Zukunft*.

Aresta, M. (2010). *Carbon dioxide as chemical feedstock.* John Wiley & Sons, Weinheim, Germany.

Aspentech. (2001). *Physical property methods and models.* Version 11.1. Aspen Technology Inc.

Asprion, N. (2005). Surface tension models for aqueous amine blends. *Industrial & Engineering Chemistry Research,* 44(18), 7270-7278.

Austgen, D. (1989). *A Model of vapor-liquid equilibria for acid gas-alkanolamine-water systems*. Ph.D. Thesis. University of Texas at Austin, USA.

Azapagic, A., & Perdan, S. (2000). Indicators of sustainable development for industry: a general framework. *Process Safety and Environmental Protection,* 78(4), 243-261.

BASF Intermediates. (2008). *Glyoxal – The substance solution for your business.* BASF SE, Ludwigshafen, Germany.

BASF Intermediates. (2013). *Glyoxal as a H_2S scavenger.* BASF SE, Ludwigshafen, Germany.

Billet, R., & Schultes, M. (1999). Prediction of mass transfer columns with dumped and arranged packings. *Chemical Engineering Research and Design,* 77, 498-504.

Biogaspartner. (2014). *Biogas Einspeisung in Deutschland – Übersicht.* URL: http://www.biogaspartner.de/index.php?id=10074&L=0&fs=/trackback (Date of access: 01.02.2014)

Blohm, C., & Riesenfeld, F. (1955). *Amino-ether gas treating process.* Patent. US 2712978. Fluor Corporation Ltd.

Bradley, A., Duan, H., Elion, W., van Soest-Vercammen, E., & Nagelvoort, R. (2009). Innovation in the LNG Industry – Shell's approach. *24th World Gas Conference,* Buenos Aires, Argentina.

Bromley, L. (1973). Thermodynamic properties of strong electrolytes in aqueous solutions. *AIChE Journal,* 19(2), 313-320.

Brooks, S. (2008). *Toxicity of selected primary amines and secondary products to aquatic organisms.* Norwegian Institute for Water Research. ISBN 978-82-577-5433-4.

Brundick, W. (2011). H_2S removal through fixed bed technologies. *9th Biogas Conference*, Montreal, Canada.

Bucklin, R. (1982). DGA – a workhorse for gas sweetening. *Oil & Gas Journal,* 80(45), 193-197.

C&CS – a division of GWP mbH. (2013). *Entschwefelung*. URL: http://www.candcs.de/produkte/herstellung-von-ammoniak-methanol-wasserstoff/entschwefelung/ (Date of access: 18.10.2013)

Cameron. (2010). *THIOPAQ bio-desulfurization process*. Datasheet TC9814-047.

Chen, C. (2006). Toward development of activity coefficient models for process and product design of complex chemical systems. *Fluid Phase Equilibria,* 241, 103-112.

Chen, C., & Evans, L. (1986). A local composition model for the excess Gibbs energy of aqueous electrolyte systems. *AIChE Journal,* 32(3), 444-454.

Chen, C., Britt, H., Boston, J., & Evans, L. (1982). Local composition model for excess Gibbs energy of electrolyte systems. Part I. Single solvent, single completely dissociated electrolyte systems. *AIChE Journal,* 28(4), 588-596.

Chen, X., Closmann, F., & Rochelle, G. (2011). Accurate screening of amines by the wetted wall column. *Energy Procedia,* 4, 101-108.

Chiu, L., & Li, M. (1999). Heat capacity of aqueous alkanolamine solutions. *Journal of Chemical and Engineering Data,* 44(6), 1396-1401.

Christensen, S., Christensen, J., & Izatt, R. (1986). Enthalpies of solution of CO_2 in aqueous DGA solutions. *Thermochimica Acta,* 106, 241-251.

Coker, A. (2007). *Ludwig's applied process design for chemical and petrochemical plants* (3rd ed.). Gulf Publishing Company, TX: Houston, USA.

Dardea, V., Thomsena, K., van Well, W., & Stenby, E. (2009). Chilled ammonia process for CO_2 capture. *Energy Procedia,* 1, 1035-1042.

De Dietrich Process Systems GmbH. (2014). *Personal communication* with Mr. Unterseher on 13th of October, 2014.

DENA. (2011). *Biogaseinspeisung in Deutschland und Europa – Markt, Technik und Akteure*. Deutsche Energie-Agentur. Article Number 5009.

DENA. (2014). *Biomethane: The energy system's all-rounder*. Deutsche Energie-Agentur. Article Number 5028.

Derks, P. (2006). *Carbon dioxide absorption in piperazine activated N-methyldiethanolamine.* Ph.D. Thesis. University of Twente, Netherlands.

Deshmukh, R., & Mather, A. (1981). A mathematical model for equilibrium solubility of hydrogen sulfide and carbon dioxide in aqueous alkanolamine solutions. *Chemical Engineering Science,* 36(2), 355-362.

Diez, R., Lampe, F., Rieger, R., & Riemann, C. (2010). Einsatz von Puratreat R+ zur Aufbereitung von Biogas. *gwf Gas|Erdgas*, 616-623.

Dingman, J., Jackson, J., Moore, T., & Branson, J. (1983). Equilibrium data for the H_2S-CO_2-DGA agent-water system. *62nd Annual Convention of Global Processors Association,* San Francisco, USA.

Dixit, O., & Mollekopf, N. (2013). Hazard analysis of a biomethane plant. *3rd International Conference on Energy Process Engineering,* Frankfurt am Main, Germany.

Dixit, O., & Mollekopf, N. (2014a). Designing absorption processes with aqueous diglycolamine. *Chemical Engineering & Technology,* 37(9), 1583-1592.

Dixit, O., & Mollekopf, N. (2014b). Biogasaufbereitung mittels Absorption zur Gewinnung von Biomethan. *Chemie Ingenieur Technik,* 86(9), 1394-1395.

Dixit, O., & Mollekopf, N. (2014c). Desulphurising biogas. *Sulphur - BCInsight,* 355, 32-34.

Dixit, O., Ohle, A., & Mollekopf, N. (2012). Absorption solvents for upgrading biogas to biomethane. *Gas for Energy,* 03, 54-61.

Dow. (2001). *DOWTHERM A.* Product information.

DVGW G 260 (2000). *Gasbeschaffenheit.* Deutsche Vereinigung des Gas- und Wasserfachs e.V.

EC 1272 (2008). *Regulation on classification, labelling and packaging of substances and mixtures.* European Parliament and Council.

Ecoinvent association. (2014). *The ecoinvent database.* URL: http://www.ecoinvent.org/database/ (Date of access: 01.04.2014)

Engels, A., Hüther, O., Schäfer, M., & Held, H. (2013). Public climate-change skepticism, energy preferences and political participation. *Global Environmental Change,* 23(5), 1018-1027.

Fachagentur für Nachwachsende Rohstoffe e.V. (2012). *Biomethan.* Order number 531.

Fachagentur Nachwachsende Rohstoffe e.V. (2010). *Leitfaden Biogas – Von der Gewinnung zur Nutzung*. ISBN 3-00-014333-5.

Flynn, R., Bellaby, P., & Ricci, M. (2006). Risk perception of an emergent technology: the case of hydrogen energy. *Forum Qualitative Sozialforschung / Forum: Qualitative Social Research,* 7(1).

Foral, A., & Al-Ubaidi, B. (1993). *Evaluation of H_2S scavenger technologies.* Gas Research Institute, USA. GRI report No. GRI-94/0197.

Fraunhofer UMSICHT. (2011). *BioSX – Biologische Entschwefelung von Biogas ohne Lufteintrag*.

Gahlert, C. (2013). *Gefahr- und Risikobetrachtung einer Biomethananlage.* Großer Beleg. TU Dresden, Germany.

Gal, E. (2010). *Ultra cleaning of combustion gas including the removal of CO_2.* Patent. US 7641717. Eig Inc.

Gasnetzzugangsverordnung. (2010). *Verordnung über den Zugang zu Gasversorgungsnetzen.* German Federal Ministry for Economic Affairs and Energy.

Global CCS Institute and Parsons Brinckerhoff. (2011). *Accelerating the uptake of CCS: industrial use of captured carbon dioxide.*

Goedkoop, M., Heijungs, R., Huijbregts, M., Schryver, A., Struijs, J., & van Zelm, R. (2013). *ReCiPe 2008. Characterisation.* Ruimte en Milieu, Netherland.

Graubard, D., Rouleau, W., & Bogner, J. (2008). *Cost-effective technologies for removing H_2S from landfill gas.* Merichem LLC, USA.

Grubb, M., Jamasb, T., & Pollitt, M. (2008) *Delivering a low carbon electricity system: technologies, economics and policy.* Cambridge University Press, UK.

Guinee, J. (2004). *Handbook on life cycle assessment.* Kluwer Academic Publishers, Netherlands.

Günther, L. (2007). Biomethanherstellung mit dem BCM Verfahren. *Schweizerischer Verein des Gas- und Wasserfaches Fachtagung "Biogas im Erdgasnetz",* Zürich, Switzerland.

Günther, L. (2011). *Verfahren und Vorrichtung zur Trennung von Methan und Kohlendioxid aus Biogas.* Patent. EP 2066796. MT-Biomethan GmbH.

Hakka, L., & Ouimet, M. (2006). *Method for recovery of CO_2 from gas streams.* Patent. US 7056482. Cansolv Technologies Inc.

Henley, E., Seader, J., & Roper, D. (2011). *Separation process principles* (3rd ed.). John Wiley & Sons Inc., Asia.

Henni, A., Tontiwachwuthikul, P., Chakma, A., & Mather, A. (2001). Volumetric properties and viscosities for aqueous diglycolamine solutions from 25 °C to 70 °C. *Journal of Chemical and Engineering Data,* 46(1), 56-62.

Herbert, W., Kohrt, H., Becker, R., Danulat, F., Danulat, H., Danulat, I., Danulat, H., & Danulat, D. (1958). *Process for the purification of gases.* Patent. US 2863527. Metallgesellschaft AG.

Hikita, H., Asai, S., Ishikawa, I., & Honda, M. (1977). The kinetics of reactions of carbon dioxide with monoisopropanolamine, diglycolamine, and ethylenediamine by a rapid mixing method. *The Chemical Engineering Journal,* 14(1), 27-30.

Hikita, H., Ishikawa, H., Murakami, T., & Ishi, T. (1981). Densities, viscosities and amine diffusivities of aqueous MIPA, DIPA, DGA and EDA solutions. *Journal of Chemical Engineering Japan,* 14(5), 411-413.

Hochgesand, G., Heidl, H., Unland, H., Doerges, A., & Bratzler, K. (1970). *Scrubbing process for removing carbon dioxide from low-sulphur fuel gases or synthesis gases.* Patent. US 3505784. Metallgesellschaft AG.

Holder, H. (1966). Diglycolamine – a promising new acid-gas remover. *Oil & Gas Journal,* 64(18), 83-86.

Hu, W., & Chakma, A. (1990). Modelling of equilibrium solubility of CO_2 and H_2S in aqueous diglycolamine solutions. *The Canadian Journal of Chemical Engineering,* 68(3), 523-525.

Huntsman Corporation. (2005). *Diglycolamine agent.*

Huttenhuis, P., Agrawal, N., Solbraa, E., & Versteeg, G. (2008). The solubility of carbon dioxide in aqueous N-methyldiethanolamine solutions. *Fluid Phase Equilibria,* 264(1-2), 99-112.

Huval, M., & van de Venne, H. (1981). DGA proves out as a low-pressure gas sweetener in Saudi Arabia. *Oil & Gas Journal,* 79(3), 91-103.

IRENA. (2013). *Statistical issues: bioenergy and distributed renewable energy.* International Renewable Energy Agency.

ISO 14040. (2006). *Life cycle assessment – principles and framework.* International Organization for Standardization.

Jäkel, A. (2014). *Biogasaufbereitung mittels einer Druckwasserwäsche.* Großer Beleg. TU Dresden, Germany.

Jayarathna, S., Weerasooriya, A., Dayarathna, S., Eimer, D., & Melaaen, M. (2013). Densities and surface tensions of CO_2 loaded aqueous monoethanolamine solutions with r = (0.2 to 0.7) at T = (303.15 to 333.15) K. *Journal of Chemical and Engineering Data,* 58(4), 986-992.

Jou, F., Carroll, J., Otto, F., & Mather, A. (1998). Solubility of methane in aqueous solutions of 2-(2-aminoethoxy)ethanol. *Industrial & Engineering Chemistry Research,* 37(8), 3519-3523.

Jungbluth, N., Chudacoff, M., Dauriat, A., Dinkel, F., Doka, G., Faist-Emmenegger, M., Gnansounou, E., Keller, M., Kljun, N., Schleiss, K., Spielmann, M., Stettler, C., & Sutter, J. (2007). *Life cycle inventories of bioenergy.* Ecoinvent report No. 17, Swiss Centre for Life Cycle Inventories, Dübendorf, Switzerland.

Jury, C., Benetto, E., Koster, D., Schmitt, B., & Welfring, J. (2010). Life cycle assessment of biogas production by monofermentation of energy crops and injection into the natural gas grid. *Biomass and Bioenergy,* 34(1), 54-66.

Kapadi, U., Hundiwale, D., Patil, N., & Lande, M. (2002). Viscosities, excess molar volume of binary mixtures of ethanolamine with water at 303.15, 308.15, 313.15 and 318.15 K. *Fluid Phase Equilibria,* 201, 335-341.

Karlsson, L. (2011). *Biogas upgrading.* Patent. WO 2011136733. Läckeby Water AB.

Katdare, S., Somalwar, P., Ramaswamy, V., & Srinivasan, S. (2012). *Process for the preparation of 2-(2-aminoethoxy)ethanol (2AEE) and morpholine with 2AEE:morpholine > 3.* Patent. US 0202995. Alkyl Amines Chemicals Ltd.

Kent, R., & Eisenberg, B. (1976). Better data for amine treating. *Hydrocarbon Processing,* 55(2), 87-90.

Kister, H. (1992). *Distillation design*. McGraw-Hill, USA.

Kister, H., Scherffius, J., Afshar, K., & Abkar, E. (2007). Realistically predict capacity and pressure drop for packed columns. *Chemical Engineering Progress,* 28-38.

Klinski, S. (2006). *Studie – Einspeisung von Biogas in das Erdgasnetz*. Fachagentur für Nachwachsende Rohstoffe e.V.

Knudsen, S., Karl, M., & Randall, S. (2009). *Amine emissions to air during carbon capture.* Norwegian Institute for Air Research. ISBN 978-82-425-2076-0.

Koch-Glitsch LP. (2010). *IMTP high performance packing.*

Kohl, A., & Miller, F. (1960). *Organic carbonate process for carbon dioxide.* Patent. US 2926751. Fluor Corporation Ltd.

Kohl, A., & Nielsen, R. (1997). *Gas purification* (5th ed.). Gulf Publishing Company, TX: Houston, USA.

KOMETEC Karl Oelkers e.K. (2003). *Fibel über Rauchgas*. URL: http://www.kometec.de/shop/pdf/fibelrauchgas.pdf (Date of access: 26.04.2012)

Kraut, A. (2014). *Experimentelle Untersuchung des Desorptionsverhaltens verschiedener Aminlösungen, bei hohen Temperaturen im Zuge der Aufbereitung von Biogas zu Biomethan.* Diplomarbeit. TU Dresden, Germany.

Kunesh, J. (1987). Practical tips on tower packing. *Chemical Engineering,* 94(18), 101-105.

Kutsher, G., & Smith, G. (1968). *Process for hydrogen sulphide removal from gas mixtures containing H_2S and CO_2.* Patent. US 3362133. Allied Chemical Corporation.

Lag, M., Andreassen, A., Instanes, C., & Lindeman, B. (2009). *Health effects of different amines relevant for CO_2 capture.* Norwegian Institute for Air Research. ISBN 978-82-425-2077-7.

Lutsch, S. (2013). *Untersuchung der Wirtschaftlichkeit der Vermarktung von CO_2 aus Biogas-Anlagen*. Diplomarbeit. TU Dresden, Germany.

Mackowiak, J. (2010). *Fluid dynamics of packed columns.* Springer, Germany.

Maddox, R., Bhairi, A., Diers, J., & Thomas, P. (1987). *Equilibrium solubility of carbon dioxide or hydrogen sulphide in aqueous solutions of MEA, DGA, DEA and MDEA.* Gas Processor's Association Research Report 104, Tusla, Oklahoma, USA.

Mangalapally, H., Notz, R., Hoch, S., Asprion, N., Sieder, G., Garcia, H., & Hasse, H. (2009). Pilot plant experimental studies of post combustion CO_2 capture by reactive absorption with MEA and other solvents. *Energy Procedia,* 1, 963-970.

Martin, J., Otto, F., & Mather, A. (1978). Solubility of hydrogen sulfide and carbon dioxide in a diglycolamine solution. *Journal of Chemical and Engineering Data,* 23(2), 163-164.

McCabe, W., Smith, J., & Harriott, P. (1993). *Unit operations of chemical engineering* (5th ed.). McGraw-Hill, Singapore.

Mcjannett, J. (2012). *Using physical solvent in multiple applications.* Digital Refining. URL: http://www.digitalrefining.com/article/1000359 (Date of access: 11.07.2012)

Meier, T. (2013). *Messung der Eigenschaften von Absorptionsmitteln: Diglykolamin und Methyldiethanolamine.* Großer Beleg. TU Dresden, Germany.

Merikoski, R. (2012). *Flue gas processing in amine-based carbon capture systems.* Master Thesis. Tampere University of Technology, Finland.

Mettler Toledo. (2009). *Karl Fischer Titration.* GTP brochure.

M-I SWACO. (2010). *Sulfatreat – setting the standard in H_2S removal*.

Mimura, T., Shimojo, S., Iijima, M., & Mitsuoka, S. (1998). *Method for removal of CO_2 and H_2S from a gas containing these gases.* Patent. EP 0827772. Kansai Electric Power Co. and Mitsubishi Jukogyo Kabushiki Kaisha.

Mimura, T., Shimojo, S., Suda, T., Iijima, M., & Mitsuoka, S. (1995). Research and development on energy saving technology for flue gas carbon dioxide recovery and steam system in power plant. *Energy Conversion and Management,* 36(6-9), 397-400.

Moore, T., Dingman, J., & Johnson, F. (1984). A review of current diglycolamine agent gas treating applications. *Environmental Progress,* 3(3), 207-212.

Muench, S. (2014). Greenhouse gas mitigation potential of electricity from biomass. *Journal of Cleaner Production,* in press. URL: dx.doi.org/10.1016/j.jclepro.2014.08.082

Muench, S., & Guenther, E. (2013). A systematic review of bioenergy life cycle assessments. *Applied Energy,* 112, 257-273.

Muench, S., Dixit, O., Guenther, E., & Mollekopf, N. (2015). Uncertainty in the life cycle assessment of biomethane production. *Biomass and Bioenergy,* under review.

Nagl, G. (2007). *Small capacity sulfur recovery units*. Merichem LLC, USA.

Norit Nederland bv. (2011). *H_2S removal with Norit RST*. Document No. TB 0164.

Notz, R., Mangalapally, H., & Hasse, H. (2012). Post combustion CO_2 capture by reactive absorption: pilot plant description and results of systematic studies with MEA. *International Journal of Greenhouse Gas Control,* 6, 84-112.

OECD. (1995). *Surface tension of aqueous solutions*. OECD guideline 115 for the testing of chemicals.

Ohle, A. (2009). *CO_2-Abtrennung aus Gasströmen durch Absorption in Polymethyldiglykolamin.* Ph.D. Thesis. TU Dresden, Germany.

Pacheco, M., Kaganoi, S., & Rochelle, G. (2000). CO_2 absorption into aqueous mixtures of diglycolamine and methyldiethanolamine. *Chemical Engineering Science,* 55(21), 5125-5140.

Papadopoulus, M., La, M., & Deal, C. (1967). *Method of separating acidic gases from gaseous mixtures.* Patent. US 3347621. Shell Oil Company.

Paques bv. (2013). *THIOPAQ*.
URL: http://de.paques.nl/produkte/featured/thiopaq (Date of access: 09.10.2013).

Peng, D., & Robinson, D. (1976). A new two-constant equation of state. *Industrial & Engineering Chemistry Fundamentals,* 15(1), 59-64.

Perry, D., Fedich, R., & Parks, L. (2010). Better acid gas enrichment. *Sulphur - BC Insight,* 326, 38-42.

Poling, B., Prausnitz, J., & O'Connell, J. (2001). *The properties of gases and liquids* (5th ed.). McGraw-Hill, USA.

Prausnitz, J., Lichtenthaler, R., & Gomes de Azevedo, E. (1999). *Molecular thermodynamics of fluid phase equilibria* (3rd ed.). Prentice Hall, NJ: Upper Saddle River, USA.

PURAC Puregas. (2012). *Biogas upgrading plants.*

Ragas, M., Etienne, R., Willemsen, F., & van de Meent, D. (1999). Assessing model uncertainty for environmental decision making: a case study of the coherence of independently derived environmental quality objectives for air and water. *Environmental Toxicology and Chemistry,* 18(8), 1856-1867.

Reddy, S., Scherffius, J., Freguia, S., & Roberts, C. (2003). Fluor's Econamine FG Plus technology – an enhanced amine-based CO_2 capture process. *2nd National Conference on Carbon Sequestration,* Alexandria, USA.

Reddy, S., Scherffius, J., Gilmartin, J., & Freguia, S. (2008). *Split flow process and apparatus.* Patent. US 7377967. Fluor Technologies Inc.

Redlich, O., & Kister, A. (1948). Algebraic representation of thermodynamic properties and the classification of solutions. *Industrial and Engineering Chemistry,* 40(2), 345-348.

Redlich, O., & Kwong, J. (1949). On the thermodynamics of solutions V. An equation of state. Fugacities of gaseous solutions. *Chemical Reviews,* 44(1), 233-244.

Reichelt, W. (1972). Zur Berechnung des Druckverlustes einphasig durchströmter Kugel- und Zylinderschüttungen. *Chemie Ingenieur Technik,* 44(18), 1068-1071.

Renon, H., & Prausnitz, J. (1968). Local compositions in thermodynamic excess functions for liquid mixtures. *AIChE Journal,* 14(1), 135-144.

RES Projects GmbH. (2013). *Biogasaufbereitungs- und -einspeiseanlage am Standort Unsleben inkl. Gasnetzrückspeisestation und Netzertüchtigung*.

Rho, S., Yoo, K., Lee, J., Nam, S., Son, J., & Min, B. (1997). Solubility of CO_2 in aqueous methyldiethanolamine solutions. *Journal of Chemical and Engineering Data,* 42(6), 1161-1164.

Ritchie, D. (2010). Invest in the future. *2nd Annual Gas Asia Summit,* Kuala Lampur, Malaysia.

Roscher, N. (2014). *Simulation einer Aminwäsche zur Biogasaufbereitung.* Diplomarbeit. TU Dresden, Germany.

Sartori, G., & Leder, F. (1978). *Process for removing carbon dioxide from gaseous mixtures using aqueous amine scrubbing solutions.* Patent. US 4112052. Exxon Research & Engineering Co.

Sartori, G., & Savage, D. (1980). *Process and composition for removing carbon dioxide containing acid gases from gaseous mixtures.* Patent. US 4217236. Exxon Research & Engineering Co.

Sattler, K. (1995). *Thermische Trennverfahren* (2nd ed.). VCH Verlagsgesellschaft, Weinheim, Germany.

Schreiner, B. (2008). Der Claus-Prozess. *Chemie in unserer Zeit,* 42(6), 378-392.

Schubert, C., Forte, P., & Dean, J. (2002). *Absorbent compositions for the removal of acid gas from gas streams.* Patent. US 6337059. Union Carbide Chemicals & Plastics Technology Corporation.

Shao, R., & Stangeland, A. (2009). *Amines used in CO_2 capture – health and environmental impacts.* Bellona Foundation.

Shaw, D. (2009). Cansolv CO_2 capture: the value of integration. *Energy Procedia,* 1, 237-246.

Shell. (2012). *Switching to ADIP-X or Sulfinol-X.*

Slovic, P. (1987). Perception of risk. *Science,* 236(4799), 280-285.

Smith, F., & Harvey, A. (2007). Avoid common pitfalls when using Henry's law. *Chemical Engineering Progress,* 33-39.

Soave, G. (1972). Equilibrium constants from a modified Redlich-Kwong equation of state. *Chemical Engineering Science,* 27(6), 1197-1203.

Soland, M., Steimer, N., & Walter, G. (2013). Local acceptance of existing biogas plants in Switzerland. *Energy Policy,* 61, 802-810.

Starr, K., Gabarrell, X., Villalba, G., Peiro, L., & Lombardi, L. (2014). Potential CO_2 savings through biomethane generation from municipal waste biogas. *Biomass and Bioenergy,* 62, 8-16.

Starr, K., Gabarrell, X., Villalba, G., Talens, L., & Lombardi, L. (2012). Life cycle assessment of biogas upgrading technologies. *Waste Management,* 32(5), 991-999.

Strigle, R. (1994). *Packed tower design and applications* (2nd ed.). Gulf Publishing Company, TX: Houston, USA.

TA Luft. (2002). *Technische Anleitung zur Reinhaltung der Luft.* German Federal Ministry for the Environment, Nature Conservation, Building and Nuclear Safety.

Taylor, C., van der Zwet, G., Claessen, M., Wijntje, R., Patil, P., & Schneider, A. (2009). Sulfinol-X – leveraging the advantages of well-proven and established and technologies in a single acid gas removal process. *Gas Processors Association's 88th Annual Convention*, Texas, USA.

Thakore, S., & Bhatt, B. (2007). *Introduction to process engineering and design*. Tata McGraw-Hill, New Delhi, India.

The American Association of Public Opinion Research. (2011). *Standard definitions.* Final dispositions of case codes and outcome rates for surveys.

Treybal, R. (1981). *Mass transfer operations* (3rd ed.). McGraw-Hill, Singapore.

Twu, C., Bluck, D., Cunningham, J., & Coon, J. (1991). A cubic equation of state with a new alpha function and a new mixing rule. *Fluid Phase Equilibria,* 69, 33-50.

Ueno, M., Takasawa, Y., Miyashige, H., Tabata, Y., & Meguro, K. (1981). Effects of alkyl chain length on surface and micellar properties of octaethyleneglycol-n-alkyl ethers. *Colloid and Polymer Science,* 259(7), 761-766.

UOP LLC. (2009). *Amine Guard FS technology for acid gas removal.*

Urban, W., Lohmann, H., & Girod, K. (2009). *Technologien und Kosten der Biogasaufbereitung und Einspeisung in das Erdgasnetz.* Final Report of the BMBF Project „Biogaseinspeisung" Volume 4.

US Department of Energy. (2012). *Syngas in Detail.* URL: http://www.netl.doe.gov/research/coal/energy-systems/gasification/gasifipedia/syngas-composition-igcc (Date of access: 31.05.2012)

Vazquez, G., Alvarez, E., Navaza, J., Rendo, R., Romero, E. (1997). Surface tension of binary mixtures of water + monoethanolamine and water + 2-amino-2-methyl-1-propanol and tertiary mixtures of these amines. *Journal of Chemical and Engineering Data,* 42(1), 57-59.

VFF. (2012). *Your expert for tower packings, catalyst support material and column equipment.* Vereinigte Füllkörper Fabriken GmbH & co. KG.

Wagner, R., Lichtfers, U., & Schuda, V. (2009). *Removal of carbon dioxide from combustion exhaust gases.* Patent. US 20090320682. BASF SE.

Wei, Y., & Sadus, R. (2000). Equations of state for the calculation of fluid-phase equilibria. *AIChE Journal,* 46(1), 169-196.

Weidema, B., & Wesnaes, M. (1996). Data quality management for life cycle inventories – an example of using data quality indicators. *Journal of Cleaner Production,* 4(3-4), 167-174.

Weidema, B., Bauer, C., Hischier, R., Mutel, C., Nemecek, T., Reinhard, J., Vadenbo, C., & Wernet, G. (2013). *Overview and methodology. Data quality guideline for the ecoinvent database version 3.* Ecoinvent report No. 1, Swiss Centre for Life Cycle Inventories, St. Gallen, Switzerland.

Weiland, R., Chakravarty, T., & Mather, A. (1993). Solubility of CO_2 and H_2S in aqueous alkanolamines. *Industrial & Engineering Chemistry Research,* 32(7), 1419-1430.

Weiland, R., Dingman, J., Cronin, D., & Browning, G. (1998). Density and viscosity of some partially carbonated aqueous alkanolamine solutions and their blends. *Journal of Chemical and Engineering Data,* 43(3), 378-382.

Wörsdörfer, A. (2010). *Katalytisches Reinigungsverfahren zur Deponie-, Klär- und Biogasaufbereitung*. Patent. DE 102009009376. Pro2 Anlagentechnik GmbH.

Wüstenhagen, R., Wolsink, M., & Bürer, M. (2007). Social acceptance of renewable energy innovation: an introduction to the concept. *Energy Policy,* 35(5), 2683-2691.

Xu, Q., & Rochelle, G. (2011). Total pressure and CO_2 solubility at high temperature in aqueous amines. *Energy Procedia,* 4, 117-124.

Zemaitis, J., Clark, D., Rafal, M., & Scrivner, N. (1986). *Handbook of aqueous electrolyte thermodynamics.* Wiley-Interscience, New York, USA.

Züblin Umwelttechnik GmbH. (2012). *CarbonEx – Aktivkohlefilter zur Feinentschwefelung*.

APPENDIX

A DESULPHURISATION PROCESSES

H_2S-removal processes are briefly described below (Dixit and Mollekopf, 2014c).

A.1 COMMERCIAL PROCESSES

Modified Claus process: In this process, H_2S is oxidized in the gas phase to elemental sulphur (Equation A.1) in the presence of a catalyst at a temperature between 170 and 350 °C (Schreiner, 2008). The application of the process has three prerequisites: H_2S content in the gas stream must be above 20 vol. %; ratio of CO_2 to H_2S must be below five, and amount of sulphur processed must be above 15 tpd (ton per day) (Nagl, 2007; Schreiner, 2008). The first two prerequisites can be fulfilled by selective H_2S absorption from biogas. However, the third prerequisite can be fulfilled only by very large biogas plants: a stream of 16000 $Nm^3 \cdot h^{-1}$ biogas with 3 vol. % H_2S contains about 15 tpd sulphur, whereas a typical biogas plant in Germany produces merely 1000 $Nm^3 \cdot h^{-1}$ biogas. Tail gas from the process must be treated to fulfil emission standards. However, tail-gas treatment exacts further resources, which makes the application of modified Claus process uneconomical in small-scale plants. The modified Claus process is not recommended for removing H_2S from biogas.

$$H_2S + \frac{1}{2}O_2 \rightarrow \frac{1}{x}S_x + H_2O \qquad \text{A.1}$$

LO-CAT process: At first, H_2S is separated from biogas using selective absorption. Then, the H_2S-concentrated gas stream is fed to the LO-CAT (liquid oxidation catalyst) unit. The process, which is licensed by Merichem LLC, employs an iron-based catalyst in an aqueous solution to absorb H_2S into the liquid phase and then oxidize it to elemental sulphur. Iron in its ferric state (Fe^{3+}) is held in the aqueous solution using the chelating agent EDTA (ethylenediaminetetraacetic acid). In the aqueous solution, H_2S reduces Fe^{3+} to Fe^{2+}, thereby producing sulphur. Subsequently, Fe^{2+} is oxidized back to Fe^{3+} by O_2. Thus, in the liquid phase, consecutive reduction and oxidation reactions take place: a redox process. Using the LO-CAT process, a concentration of less than 10 ppm H_2S in the gas stream can be achieved (Nagl, 2007; Graubard et al., 2008). This process is economical for a sulphur production of above 200 $kg \cdot day^{-1}$ that corresponds to at least 0,9 vol. % H_2S in 1000 $Nm^3 \cdot h^{-1}$ biogas or

2 vol. % H_2S in 500 $Nm^3 \cdot h^{-1}$ biogas. The LO-CAT process is suitable for rough desulphurisation of biogas.

Biological desulphurisation: Special bacteria such as chlorobium thiosulfatophilum oxidize H_2S to elemental sulphur in a liquid medium in the presence of O_2 and H_2O. This process can be implemented directly inside the biogas fermenter or in an external vessel to which air or O_2 is externally added (Fachagentur Nachwachsende Rohstoffe e.V., 2010). However, the unused O_2 can hamper the subsequent process step of CO_2 separation: O_2 reacts with the chemical absorption solvent (e.g. DGA) and degrades it. Biological desulphurisation is suitable for rough desulphurisation of biogas, but is not recommended if chemical absorption is used for subsequent CO_2 separation.

Liquid scavenging with aqueous glyoxal: BASF SE licenses a scrubbing liquid that uses aqueous glyoxal (40 wt. %) for scavenging H_2S (BASF Intermediates, 2013). The concentration of H_2S in treated gas depends upon reaction time, temperature and pH value. In a typical operation, an H_2S concentration of approximately 100 ppm in the output gas stream can be obtained (BASF Intermediates, 2008). Although this process is suitable for rough desulphurisation of biogas, it is not recommended because the sulphur-containing product must be separately disposed of.

Liquid scavenging with aqueous triazine: Merichem LLC licenses the process Eliminator wherein a mixture of triazine and H_2O is used as the scrubbing liquid (Nagl, 2007). However, Merichem has stopped supporting this process.

THIOPAQ process: An aqueous solution of sodium hydroxide (NaOH) is used to absorb H_2S, thereby converting H_2S into sodium bisulphite (NaHS) (Equation A.2). The absorption solvent is then regenerated by special bacteria in the presence of O_2 to produce sulphur and NaOH. A solvent pH value of approximately 9 must be maintained during absorption; else, CO_2 present in biogas will react with the solvent to produce sodium carbonate (Na_2CO_3) and sodium bicarbonate ($NaHCO_3$). These products cannot be regenerated by the bacteria, and they must be disposed of separately (Cameron, 2010; Paques bv., 2013). The process is recommended for rough desulphurisation of biogas.

$$NaOH + H_2S \rightarrow NaHS + H_2O \qquad \text{A.2}$$

SulfaCheck process: Nalco ELME licenses the SulfaCheck process that uses an aqueous solution of sodium nitrite ($NaNO_2$) and NaOH as the scrubbing liquid wherein H_2S is converted into sulphur and H_2O (Equation A.3). However, in the presence of CO_2, NaOH is converted to Na_2CO_3 and $NaHCO_3$ and the system foams (Foral and Al-Ubaidi, 1993; Kohl

and Nielsen, 1997). As CO_2 is present in biogas, the SulfaCheck process is not suitable for biogas desulphurisation.

$$NaNO_2 + 3H_2S \rightarrow NaOH + NH_3 + 3S + H_2O \quad \text{A.3}$$

Solid scavenging with zinc oxide (ZnO): ZnO reacts with H_2S at elevated temperatures (200 to 300 °C) to produce zinc sulphide (ZnS) (Equation A.4). However, ZnS is hazardous and must be separately disposed of. H_2S concentration in the gas stream after treatment is below 1 ppm, and the treated gas (biomethane) can be used in applications where sub-ppm level H_2S is desired (e.g. in fuel cells) (C&CS - a division of GWP mbH, 2013). ZnO is suitable for fine desulphurisation of biogas, but is over qualified if biomethane is injected into a natural-gas pipeline.

$$ZnO + H_2S \rightarrow ZnS + H_2O \quad \text{A.4}$$

Solid scavenging with iron sponge: Hydrated ferric oxide ($Fe_2O_3.H_2O$) coated on a supporting material (e.g. wooden chips) is called iron sponge, and it can be used as a solid scavenger. H_2S reacts with Fe_2O_3 to produce ferric sulphide (Fe_2S_3) (Equation A.5). Fe_2S_3 can be regenerated by exposing it to air, but then, freed H_2S must be separately disposed of. Dry Fe_2S_3 is a pyrophoric substance: on contact with air, dry Fe_2S_3 instantaneously catches fire (Kohl and Nielsen, 1997). Iron sponge is suitable for rough desulphurisation of biogas, but is not recommended due to the fire hazard.

$$Fe_2O_3 + 3H_2S \rightarrow Fe_2S_3 + 3H_2O \quad \text{A.5}$$

SulfaTreat process: SulfaTreat process uses a mixture of Fe_2O_3 and Fe_3O_4 ($FeO.Fe_2O_3$) as the adsorbent. It reacts with H_2S to produce iron sulphides such as FeS, FeS_2 and Fe_2S_3. These end products can be used for the production of sulphuric acid (H_2SO_4) (M-I SWACO, 2011) and bitumen asphalt. Contrary to iron sponge, SulfaTreat is non-pyrophoric (Brundick, 2011). It is conjectured that the base material of the iron oxides absorbs the heat produced by the oxidation of iron sulphides which prevents over-heating and spontaneous ignition. The SulfaTreat process is suitable for rough desulphurisation of biogas.

Solid scavenging with activated carbon: Activated carbon is an adsorbent that separates not only H_2S, but also volatile organic compounds (VOCs) from gas streams. Activated carbon can be regenerated by liquid water or steam, but then, freed H_2S must be separately disposed of. The functionality of activated carbon varies according to the raw material used during its manufacturing. An example: RST3 is an activated carbon manufactured by Norit Nederland bv. that also functions as a catalyst. Adsorbed H_2S is converted to sulphur or

H_2SO_4 in the presence of O_2 (Norit Nederland bv., 2011). Thus, activated carbon is suitable for fine desulphurisation of biogas, but is not recommended if chemical absorption is used for CO_2 separation (a subsequent process step in biomethane production).

Solid scavenging with impregnated activated carbon: If the activated carbon is impregnated with an oxidizer such as potassium permanganate ($KMnO_4$), the presence of gaseous O_2 is unnecessary (Fachagentur Nachwachsende Rohstoffe e.V., 2010). However, impregnated activated carbon cannot be regenerated and must be separately disposed of (Züblin Umwelttechnik GmbH, 2012). Impregnated activated carbon is suitable for fine desulphurisation of biogas and is recommended if chemical absorption is used for CO_2 separation.

There are several other processes that have been commercially used to remove H_2S by liquid-phase oxidation or solid/liquid scavenging, but they are primarily of historical importance. Interested readers may refer to Kohl and Nielsen (1997).

A.2 PROCESSES UNDER DEVELOPMENT

In addition to the aforementioned processes, two other processes are worth mentioning because they are being developed specifically for biogas desulphurisation.

Pro2 process: In the Pro2 process, biogas is heated to a temperature of approximately 300 °C and is pumped through a packed-bed reactor that consists of three layers of adsorbents. In the bottom-most layer (1st layer), siloxanes are catalytically oxidized to silicon dioxide (SiO_2) where the adsorbent is aluminium oxide (Al_2O_3). In the 2nd layer, H_2S is catalytically oxidized to sulphur dioxide (SO_2) where the adsorbent is a mixture of vanadium pentoxide (V_2O_5) and titanium oxide (TiO_2). In the 3rd layer, acid gases such as SO_2 are adsorbed on the Al_2O_3-based catalyst, which is impregnated with sodium (Na), and converted into sodium sulphate (Na_2SO_4) (Wörsdörfer, 2010). No further details are available about the Pro2 process.

BioSX process: The process consists of an absorption column and a subsequent liquid-conditioning unit. The absorption column is filled with small pipe-shaped objects on which H_2S-oxidizing bacteria grow. In the absorption column, diluted digestate (the solvent) flows down the column, whereas biogas flows up the column. H_2S is absorbed into the solvent and is converted by the bacteria into sulphur or sulphates. Subsequently, the solvent flows into the conditioning unit in which air is pumped to saturate the solvent with O_2. The solvent then returns to the absorption column. This cyclic operation continues until the solvent

attains a pH value of less than 6. The solvent is then discharged from the column and can be used as a fertilizer (Fraunhofer UMSICHT, 2011). The BioSX process is still in the research phase.

B SCREENING OF ABSORPTION SOLVENTS

B.1 SOLVENTS WITH HIGH SUITABILITY

The operating characteristics of absorption solvents with high suitability are shown in Table B.1, and reasons for not selecting a solvent to separate CO_2 from biogas at atmospheric pressure are mentioned below.

Table B.1 Operating characteristics of absorption solvents with high suitability

Solvent	Operating conditions in absorber		Operating conditions in desorber		Volatility	Corrosive-ness	Chemical and thermal stability
	P / bar	T / °C	P / bar	T / °C			
MEA	> 1	30 to 60	2 to 3	120	high	high	low
Econamine FG+	1 to 2	40 to 50	> 3	120	high	low	high
ADEG/DGA	> 1	35 to 40	~ 2	110 to 130	low	medium	medium
DEA	> 1	30 to 60	2 to 3	120	low	medium	medium
BCM-Sorb	> 1	10 to 50	2 to 30	120	low	low	medium
MDEA	> 1	30 to 70	1 to 2	120	low	low	high
aMDEA	> 1	40 to 60	~ 1	110 to 120	low	low	high
ADIP-X	> 1	20 to 60	unknown	120	low	low	high
Amine Guard FS	> 1	30 to 65	1 to 3	100 to 130	low	low	high
CApure	1 to 2	45 to 55	< 1	80 to 95	low	unknown	high
OASE Green	1 to 2	35 to 45	~ 1	110	low	low	high
Cansolv DC 101	> 1	25 to 60	1 to 3	100 to 120	low	low	high
Chilled ammonia	1 to 2	0 to 10	> 2	100 to 150	high	low	high
KS-1	> 1	30 to 70	1 to 4	110 to 120	high	low	high
Flexsorb SE	> 1	40 to 60	1 to 2	80 to 150	high	low	high

Monoethanolamine (MEA): Since several decades, aqueous MEA has been used for the separation of CO_2 and H_2S from natural gas. The solvent typically contains 15 to 20 mass (wt.) % MEA in solvent. Absorber and desorber can be operated at atmospheric pressure. However, MEA is volatile (it has high vapour pressure), and a water wash system in the absorber for amine recovery is recommended (Kohl and Nielsen, 1997). The solvent is not recommended for CO_2 separation from biogas at atmospheric pressure.

Econamine FG+: Fluor Daniel purchased the Dow Chemical GAS/SPEC FT-1 technology in 1981 and renamed it as Econamine FG. Econamine FG+ was developed for flue-gas treatment and employs 30 wt. % MEA in solvent as the absorption solvent (Reddy et al., 2003). A proprietary, copper-based chemical is added to the solvent to prevent solvent

degradation by O_2. The absorber can be operated at pressures up to 2 bar. In the stripper, steam at a pressure of at least 3 bar should be used to regenerate the solvent (Reddy et al., 2008). MEA has a high vapour pressure, and a water wash system must be installed in the absorber to prevent solvent loss. The solvent is not recommended for CO_2 separation from biogas at atmospheric pressure.

Amino-diethylene glycol (ADEG) or diglycolamine (DGA): ADEG is a solvent licensed by BASF, while DGA, which is the same solvent, is licensed by Huntsman Corporation. The solvent is used for separating CO_2 and H_2S from gas streams at near-atmospheric pressure. DGA has a lower vapour pressure than MEA and is also less corrosive compared to MEA. Aqueous DGA solvents with up to 70 wt. % DGA have been used in commercial plants (Huval and van de Venne, 1981; Bucklin, 1982; Dixit and Mollekopf, 2014a). The solvent is recommended for CO_2 separation from biogas at atmospheric pressure.

Diethanolamine (DEA): Aqueous DEA solvents with 25 to 30 wt. % DEA are used for gas treatment when besides CO_2 and H_2S, components such as carbonyl sulphide (COS) and carbon disulphide (CS_2) must be separated from the gas stream (Kohl and Nielsen, 1997). Compared to primary amines such as DGA and MEA, DEA, a secondary amine, has a smaller differential CO_2 loading at atmospheric pressure (Ohle, 2009). Therefore, the solvent is not recommended for CO_2 separation from biogas at atmospheric pressure.

BCM-Sorb: The process was developed by DGE GmbH and is used for biogas treatment. At first, NH_3 and H_2S are separated by H_2SO_4 and Na_2CO_3 scrubbing, respectively. Subsequently, CO_2 is separated using aqueous DEA (20 to 30 wt. %) at atmospheric pressure and 30 °C. The solvent is regenerated by steam stripping at 120 °C at a pressure between 2 and 30 bar (Günther, 2007; Günther, 2011). DEA has a smaller differential CO_2 loading at atmospheric pressure than DGA (Ohle, 2009). Therefore, the solvent is not recommended for CO_2 separation from biogas at atmospheric pressure.

N-methyldiethanolamine (MDEA): MDEA has been used for the separation of CO_2 and H_2S from gas mixtures since several years. Aqueous MDEA solvents typically contain 20 to 60 wt. % MDEA. The absorber and desorber can be operated at atmospheric pressure (Appl et al., 1982). However, the reaction rate of MDEA, a tertiary amine, with CO_2 is lower than the reaction rate of MEA, a primary amine, with CO_2 (Meier, 2013). Therefore, the solvent is not recommended for CO_2 separation from biogas at atmospheric pressure.

Activated MDEA (aMDEA): The solvent is licensed by BASF SE and contains MDEA up to 50 wt. %, piperazine up to 7 wt. % and water as rest. The solvent can be used to separate

CO_2, H_2S and COS from gas mixtures. The absorber and desorber can be operated at atmospheric pressure (Appl et al., 1982). The addition of piperazine to MDEA increases the viscosity and the vapour pressure of the solvent, but not adversely. The reaction rate of the piperazine-MDEA mixture with CO_2 is higher than that of MDEA alone (Derks, 2006; Meier, 2013). However, piperazine is a flammable substance and poses a physical hazard. Therefore, the solvent is not recommended for CO_2 separation from biogas at atmospheric pressure.

ADIP-X: The solvent is licensed by Shell Global Solutions and is used for deep removal (ppm level) of CO_2 when H_2S is present in low concentrations. ADIP-X is a mixture of MDEA, piperazine and water. MDEA (50 wt. %) is used as the main reactant, and piperazine is the accelerator. The recommended absorber pressure is from 15 to 60 bar, but the absorber can be operated at atmospheric pressure (Bradley et al., 2009; Ritchie, 2010; Shell, 2012). Piperazine is a flammable substance and poses a physical hazard; therefore, the solvent is not recommended for CO_2 separation from biogas at atmospheric pressure.

Amine Guard FS: The process is licensed by UOP LLC and uses a solvent from the UCARSOL AP 800 series. The solvent preferably consists of 30 to 50 wt. % MDEA, 10 wt. % piperazine, 10 to 40 wt. % of another physical or chemical solvent, and up to 5 wt. % of additives such as corrosion inhibitors and defoamers. The process is used for the separation of CO_2 and H_2S. The absorber and desorber can be operated at atmospheric pressure (Schubert et al., 2002; UOP LLC, 2009). Piperazine is a flammable substance and poses a physical hazard. The solvent is not recommended for CO_2 separation from biogas at atmospheric pressure. In addition, it is not possible to further assess the solvent because adequate information about solvent composition is not available.

CApure: The process was developed by PURAC Puregas for separation of CO_2 and H_2S from biogas. The solvent is an amine (e.g. MDEA), at 50 wt. % in solvent. The absorber can operate at atmospheric pressure, but CO_2 desorption is carried out under vacuum at around 0,3 bar (Karlsson, 2011; PURAC Puregas, 2012). The solvent is unsuitable to separate CO_2 from biogas at atmospheric pressure. In addition, it is not possible to further assess the solvent because adequate information about solvent composition is not available.

OASE Green (Puratreat R+): The process was developed by a cooperative undertaking of BASF SE, WINGAS, BIS E.M.S and Wintershall Holding. The solvent is an aqueous solution of a potassium amino acid salt (15 to 50 wt. %) and a primary alkanolamine (2 to 20 wt. %). The solvent can be used to separate CO_2, H_2S and NH_3 from biogas. The recommended absorber temperature is between 30 and 50 °C at atmospheric pressure (Wagner et al.,

2009; Diez et al., 2010). Although, the solvent is suitable to separate CO_2 from biogas at atmospheric pressure, it is impractical to conduct any further research with the solvent because adequate information about solvent composition is not available.

Cansolv DC 101: The process is licensed by Cansolv Technologies Inc., which is now a subsidiary of Shell. The solvent preferably consists of one tertiary alkanolamine (25 to 40 wt. %), one secondary amine (10 to 30 wt. %), one O_2 scavenger (0,1 to 10 wt. %) and inert salts (0 to 10 wt. %). The absorber can be operated at atmospheric pressure at a temperature between 25 and 60 °C (Hakka and Ouimet, 2006; Shaw, 2009). Although, the solvent is suitable to separate CO_2 from biogas at atmospheric pressure, it is impractical to conduct any further research with the solvent because adequate information about solvent composition is not available.

Chilled ammonia: The solvent is an aqueous solution of up to 28 wt. % NH_3; the solvent is licensed by Alstom. The recommended absorber temperature is from 0 to 10 °C (Dardea et al., 2009; Gal, 2010). At atmospheric pressure and ambient temperature, the solvent is volatile; therefore, the solvent is not recommended for CO_2 separation from biogas at atmospheric pressure.

KS-1: The solvent is an aqueous solution of a sterically hindered amine selected from the mono-(C1 to C4)-alkyl amino-(C1 to C4)-alkanol series with a concentration between 15 and 75 wt. %. The solvent is a proprietary product of Kansai Electric Power Co. Inc. and Mitsubishi Heavy Industries Ltd. The solvent can be used for the separation of CO_2 from gases at atmospheric pressure (Mimura et al., 1995; Mimura et al., 1998). However, the solvent is almost four times as expensive as MEA (Merikosi, 2012). Although, the solvent is suitable to separate CO_2 from biogas at atmospheric pressure, it is impractical to conduct any further research with the solvent because adequate information about solvent composition is not available.

Flexsorb SE: The solvent is licensed by Exxon Research & Engineering Co. and can be used for separating CO_2 and H_2S from gas mixtures. The solvent consists of an aqueous solution of a sterically hindered alkanolamine (40 to 60 wt. %) and a tertiary alkanolamine (5 to 15 wt. %). The absorber and desorber can be operated at atmospheric pressure (Sartori and Savage, 1980; Perry et al., 2010). Although, the solvent is suitable to separate CO_2 from biogas at atmospheric pressure, it is impractical to conduct any further research with the solvent because adequate information about solvent composition is not available.

B.2 SOLVENTS WITH LOW SUITABILITY

Reasons why certain solvents are deemed to have low suitability are presented below.

Fluor solvent: The solvent is a propylene carbonate solution and is licensed by Fluor Corporation. The solvent is recommended for CO_2 separation at an absorber pressure of above 12 bar (Kohl and Miller, 1960). The solvent is not suitable to separate CO_2 from biogas at atmospheric pressure.

Selexol or Genosorb 1753: The process is currently licensed by UOP Honeywell and is used to separate CO_2 from gas mixtures wherein the minimum recommended absorber pressure is 4 bar (Kutsher and Smith, 1968; Mcjannett, 2012). The solvent is a mixture of homologues of dimethylether of poly-(tri to hepta)-ethylene-glycol (at least 95 wt. %); the solvent is manufactured by Clariant Produkte GmbH. The solvent is not suitable to separate CO_2 from biogas at atmospheric pressure.

Water: Pressurized water has been used for separating CO_2 from biogas. Water has several advantages over chemical solvents: water is cheap, and it does not pollute the environment. However, the rate of CO_2 absorption in water is low, and a minimum absorber pressure of 8 bar is recommended. The solvent is not suitable to separate CO_2 from biogas at atmospheric pressure (Jäkel, 2014).

ADIP-D: Shell licenses the solvent ADIP-D wherein diisopropanolamine (DIPA) is the major reactant. The solvent is used for treating gases that contain COS in addition to CO_2 and H_2S. At atmospheric pressure, H_2S is selectively absorbed. However, ADIP-D is no longer offered and has been replaced by a solvent named as ADIP-X (Kohl and Nielsen, 1997; Ritchie, 2010).

Sepasolv MPE: The process is licensed by BASF AG and uses Genosorb 1753 (or Selexol) as the solvent. The process was primarily developed for selective separation of H_2S, but now it is no longer supported (Kohl and Nielsen, 1997).

Purisol: The solvent is licensed by Lurgi GmbH (currently Air Liquide) and is an aqueous solution of 97 to 99 wt. % N-methyl-2-pyrrolidone. It is used for the selective separation of H_2S and is suitable for CO_2 separation at high pressures (above 8 bar). The solvent has a high vapour pressure: it is volatile (Hochgesand et al., 1970). The solvent is not suitable to separate CO_2 from biogas at atmospheric pressure.

Rectisol: This process uses methanol as the solvent and is licensed by Linde AG. The process is suitable for separating cyanogen compounds, aromatics and organic sulphur compounds from gas mixtures. The preferred absorber temperature is from -30 to -75 °C, which makes the process highly energy consuming (Herbert et al., 1958). The solvent is not suitable to separate CO_2 from biogas at atmospheric pressure.

Amisol: It is a solvent licensed by Lurgi GmbH (currently Air Liquide), and the solvent is a mixture of an amine and methanol. The amine can either be an alkanolamine like MEA or DEA, or an alkylamine like diisopropylamine or diethylamine. The solvent is suitable for selective absorption of H_2S or for complete removal of CO_2, H_2S, COS and other sulphur compounds. The minimum absorber pressure is however 10 bar (Kohl and Nielsen, 1997). The solvent is not suitable to separate CO_2 from biogas at atmospheric pressure.

Sulfinol-D: The solvent is made up of DIPA, sulpholane and water. It is used when complete removal of H_2S and CO_2 is expected with deep removal of COS. It also removes mercaptans and alkyl sulphides to low levels. (Papadopoulus et al., 1967; Kohl and Nielsen, 1997). The solvent is not only overqualified, but also unsuitable to separate CO_2 from biogas at atmospheric pressure.

Sulfinol-M: It is licensed by Shell Global Solutions, and the solvent is made up of MDEA, sulpholane and water. It is used when selective removal of H_2S over CO_2 with partial removal of COS is expected (Kohl and Nielsen, 1997). The solvent is not suitable to separate CO_2 from biogas at atmospheric pressure.

Sulfinol-X: The solvent consists of MDEA as the main reactant, piperazine as the accelerator, and sulpholane as an enhancer. The solvent is used to remove organic sulphur compounds (e.g. COS, RSH) from gas streams at a minimum absorber pressure of 15 bar (Taylor et al., 2009; Ritchie, 2010). The solvent is not suitable to separate CO_2 from biogas at atmospheric pressure.

Hybrid Flexsorb SE: The process uses a solvent that is a mixture of a sterically hindered secondary amine and a physical solvent (e.g. sulpholane). The process is used for complete removal CO_2, H_2S, COS, SO_2, hydrogen cyanide (HCN), as well as O_2 and N_2 derivatives of lower hydrocarbons. The minimum absorber pressure is recommended to be 8 bar (Sartori and Leder, 1978). The solvent is not suitable to separate CO_2 from biogas at atmospheric pressure.

Alkacid M: The solvent is sodium alanine in water and is licensed by BASF AG. Although, the process is used for the absorption of CO_2 and H_2S at atmospheric pressure, salts (solids) precipitate out of the solution at high CO_2 loading. Compared to MEA, the solvent is more corrosive and degrades more rapidly in the presence of O_2 (Kohl and Nielsen, 1997). Therefore, the solvent is not recommended for separating CO_2 from biogas at atmospheric pressure.

Caustic wash: NaOH or KOH in water can be used as solvents to absorb CO_2 and/or H_2S, but the solvent cannot be regenerated (Kohl and Nielsen, 1997). Therefore, the solvent is suitable to treat gas streams with trace amounts of CO_2 or H_2S. As biogas has approximately 40 vol. % CO_2, caustic wash is not suitable to separate CO_2 from biogas at atmospheric pressure.

Alkali carbonate: Sodium or potassium carbonate (Na_2CO_3 or K_2CO_3) solutions can be used to separate CO_2 from gas mixtures at atmospheric pressure. However, the solvent has a lower reaction rate and higher energy demand for regeneration compared to chemical solvents (Kohl and Nielsen, 1997). The solvent is not recommended for separating CO_2 from biogas at atmospheric pressure.

Benfield process: It is licensed by UOP Honeywell, and the solvent is an aqueous solution of 20 to 30 wt. % K_2CO_3. The absorber and desorber operate at high temperatures (70 to 120 °C), and the operating pressure in the absorber is over 10 bar. If a promoter such as DEA is added to the solvent, the solvent can be used to separate CO_2 at an absorber pressure of around 8 bar (Kohl and Nielsen, 1997). The solvent is not suitable to separate CO_2 from biogas at atmospheric pressure.

C MODELLING EQUILIBRIUM CO_2 SOLUBILITY

Equilibrium CO_2 solubility in aqueous DGA can be calculated using the Henry's law (Equation 2.1), which is based upon the postulate that at vapour-liquid equilibrium, the fugacity of the vapour is equal to the fugacity of the liquid (Equation C.1). The fugacity coefficient $\emptyset$ of a component is the ratio of its gas-phase fugacity f_{vap} and its pressure P (Equation C.2a). The liquid fugacity f_{liq} of a component is equal to the product of its activity coefficient γ, its mole fraction in the liquid x and a constant f_0 that is arbitrarily chosen (Equation C.3a). Thus γ values depend on f_0 (Prausnitz et al., 1999; Smith and Harvey, 2007). To avoid problems due to missing information and to usher standardisation, Henry's constant k_H is generally used as f_0 (Equation C.3b). Equations C.1, C.2b and C.3c can be combined to obtain Equation 2.1, the vapour-liquid equilibrium equation of CO_2.

$$p_{CO2}\emptyset_{CO2} = x_{CO2}\gamma_{CO2}k_H \qquad 2.1$$

$$f_{vap} = f_{liq} \qquad C.1$$

$$f_{vap} = \emptyset P \qquad C.2a$$

$$f_{CO2,vap} = \emptyset_{CO2}p_{CO2} \qquad C.2b$$

$$f_{liq} = \gamma x f_0 \qquad C.3a$$

$$f_{liq} = \gamma x k_H \qquad C.3b$$

$$f_{CO2,liq} = \gamma_{CO2}x_{CO2}k_H \qquad C.3c$$

It should be noted that Equations C.3b and C.3c are applicable at atmospheric pressures only. At above-atmospheric pressures, the Poynting correction factor should be incorporated in the equation (Prausnitz et al., 1999). In this study, the Poynting correction factor was assumed to be 1 as the CO_2-aqueous DGA system was at atmospheric pressure.

In Equation C.3c, as x_{CO2} approaches 0, γ_{CO2} approaches 1, whereas as x_{DGA} and x_{H2O} approach 1, γ_{DGA} and γ_{H2O} approach 1. The tendency of γ of the solute and the solvent are opposite to each another, and this is denoted as the unsymmetrical normalisation of γ (Prausnitz et al., 1999).

C.1 CALCULATING THE FUGACITY COEFFICIENT USING THE PENG-ROBINSON EQUATION

Equation C.4a is the Peng-Robinson equation of state (Peng and Robinson, 1976), which can be used to calculate $\emptyset$ of a pure substance (a single-component system). However, the CO_2-aqueous DGA system is composed of several components: it is a component mixture. In order to calculate $\emptyset$ of a component in a mixture, a mixing rule must be employed in conjugation with the cubic equation of state. It was decided to use the generalized mixing rule because it is mathematically simple and is suitable for application at atmospheric pressure (Peng and Robinson, 1976; Prausnitz et al., 1999). Other mixing rules should be used for calculating $\emptyset$ at above-atmospheric pressures (Roscher, 2014).

$$\ln \emptyset = Z - 1 - \ln(Z - B) - \frac{A}{2\sqrt{2}B} \ln \frac{Z+2{,}414B}{Z-0{,}414B} \qquad \text{C.4a}$$

$$\ln \emptyset_k = \ln \frac{f_k}{p_k} = \frac{b_k}{b}(Z - 1) - \ln(Z - B) - \frac{A}{2\sqrt{2}B}\left(\frac{2\sum_i y_i a_{ik}}{a} - \frac{b_k}{b}\right) \ln \frac{Z+2{,}414B}{Z-0{,}414B} \qquad \text{C.4b}$$

$\emptyset$ of component *k* in a component mixture is given by Equation C.4b; *i* and *j* are other components in the mixture. *Z* is the compressibility factor of the component (Equation C.5), and *A* and *B* are constants defined by Equations C.6 and C.7. *a* is the component's attraction parameter; *b* is the van der Waal covolume of the component; *R* is the universal gas constant; V_{mo} is the component's molar volume; *p* is the component's partial pressure, and *T* is the component's temperature. Equations C.8, C.9 and C.10 show how *a* and *b* are calculated. P_c is the critical pressure; T_c is the critical temperature; α is the alpha term as defined in Equation C.10a (not to be confused with "loading" which has the same symbol); *y* is the mole fraction in the gas phase; ω is the acentric factor; T_r is the reduced temperature, and *L0, L1*, *M0, M1*, *N0* and *N1* are α-function parameters.

$$Z = \frac{PV_{mo}}{RT} \qquad \text{C.5}$$

$$A = \frac{aP}{R^2T^2} \qquad \text{C.6}$$

$$B = \frac{bP}{RT} \qquad \text{C.7}$$

$$a = a(T_c)\alpha \qquad \text{C.8a}$$

$$a(T_c) = \sum_i \sum_j y_i y_j a(T_c)_{ij} \qquad \text{C.8b}$$

$$a(T_c)_{ij} = \left(1 - \delta_{ij}\right)\sqrt{a(T_c)_i a(T_c)_j} \qquad \text{C.8c}$$

$$a(T_c)_i = \frac{0{,}45724 R^2 T_c^2}{P_c} \quad \text{C.8d}$$

$$b = \sum_i y_i b_i \quad \text{C.9a}$$

$$b_i = \frac{0{,}07780 R T_c}{P_c} \quad \text{C.9b}$$

$$\alpha = \alpha_0 + \omega(\alpha_1 - \alpha_0) \quad \text{C.10a}$$

$$\alpha_0 = T_r^{N0(M0-1)} exp[L0(1 - T_r^{N0M0})] \quad \text{C.10b}$$

$$\alpha_1 = T_r^{N1(M1-1)} exp[L1(1 - T_r^{N1M1})] \quad \text{C.10c}$$

$$T_r = \frac{T}{T_c} \quad \text{C.10d}$$

The Twu generalized α-function (Twu et al., 1991) was selected to calculate α because the function is valid for temperatures below and above critical. Critical properties (P_c, T_c and ω) as provided by Aspen Plus 25 are shown in Table C.1. The interaction coefficients δ_{ij} as provided by Aspen Plus 25 are shown in Table C.2. α-function parameters (*L0, L1*, *M0, M1*, *N0* and *N1*) are generic values provided by Aspen Plus 25 and are shown in Table C.3. Using a spreadsheet software such as Microsoft Excel, the Peng-Robinson equation can be used to calculate $\emptyset_{CO2}$.

Table C.1 Critical pressure P_c, critical temperature T_c and acentric factor ω of substances

Component	**P_c / bar**	**T_c / K**	**ω**
CO_2	73,80	304,16	0,226
N_2	33,94	126,20	0,040
H_2O	221,39	647,31	0,343
DGA	48,81	721,20	-0,584

Table C.2 Interaction coefficient δ_{ij}

Component i **Component j**	**CO_2** **H_2O**	**CO_2** **N_2**	**CO_2** **DGA**	**N_2** **DGA**	**N_2** **H_2O**	**H_2O** **DGA**
$\delta_{ij} = \delta_{ji}$	0,120	-0,017	0,000	0,000	0,000	0,000

Table C.3 α-function parameters below and above critical temperature T_c

Parameter	Below T_c	Above T_c
L0	0,272838	0,373949
M0	0,924779	4,730200
N0	1,197640	-0,200000
L1	0,625701	0,023904
M1	0,792014	1,246150
N1	2,460220	8,000000

C.2 CALCULATING THE ACTIVITY COEFFICIENT USING THE ENRTL MODEL

The electrolyte non-random two liquid (eNRTL) model was selected to calculate the activity coefficient γ of components in the CO_2-aqueous DGA system. The theory of the eNRTL model can be read in Chen et al. (1982) and Chen and Evans (1986). According to the eNRTL model, activity coefficient γ of a solute *k* in the solvent is given by Equation C.11. The first and second term on the right-hand side of the equation reckon with the long-range forces, whereas the third term reckons with the short-range forces.

$$ln\gamma_k = ln\gamma_k^{PDH} + ln\gamma_k^{Born} + ln\gamma_k^{NRTL} \quad \text{C.11}$$

Equation C.12 shows how the Pitzer-Debye-Hückel component of the activity coefficient γ_k^{PDH} can be calculated. M_{solv} is the molecular mass of the solvent. k_{DH} is the Debye-Hückel parameter for the solvent (Equation C.13) where N_A is the Avogadro number (6,023 x 10^{23}); ρ_{solv} is the density of the solvent; Q_e is the electron charge (1,602 x 10^{-19} J); k_B is the Boltzmann constant (1,381 x 10^{-23} J·K^{-1}); *T* is the temperature, and ε_W is the dielectric constant of water. *I* is the ionic strength of the solvent (Equation C.14) where *z* is the charge number of the component, and *x* is the mole fraction of the component in the liquid. Table C.4 shows the ion parameters (Aspentech, 2001).

$$ln\gamma_k^{PDH} = -\sqrt{\frac{1000}{M_{solv}}}k_{DH}\left\{\left[\left(\frac{2z_k^2}{14{,}9}\right)ln(1+14{,}9I^{0,5})\right] + \left[\frac{(z_k^2 I^{0,5} - 2I^{1,5})}{1+14{,}9I^{0,5}}\right]\right\} \quad \text{C.12}$$

$$k_{DH} = \frac{1}{3}\left(\frac{2\pi N_A \rho_{solv}}{1000}\right)^{\frac{1}{2}}\left(\frac{Q_e^2}{\epsilon_w k_B T}\right)^{\frac{3}{2}} \quad \text{C.13}$$

$$I = \frac{1}{2}\sum_i x_i z_i^2 \quad \text{C.14}$$

Table C.4 Ion parameters

Name	Symbol	Charge number	Born radius / 10^{-10} m
Hydronium	H_3O^+	1	3
Hydroxide	OH^-	-1	3
Bicarbonate	HCO_3^-	-1	3
Carbonate	CO_3^{2-}	-2	3
Alkyl ammonium	RNH_3^+	1	3
Carbamate	$RNHCO_2^-$	-1	3

The Born correction of the activity coefficient is depicted by γ_k^{Born} and can be calculated using Equation C.15. z_k is the charge number of the component. Q_e is the electron charge; k_B is the Boltzmann constant; T is the temperature; ε_{solv} is the dielectric constant of the solvent; ε_w is the dielectric constant of water, and r_k is the component's Born radius (Aspentech, 2001). The Born correction is necessary for mixed solvents such as aqueous DGA, which consist of water and DGA (Aspentech, 2001).

$$ln\gamma_k^{Born} = \frac{Q_e^2}{2k_BT}\left(\frac{1}{\varepsilon_{solv}} - \frac{1}{\varepsilon_w}\right)\frac{z_k^2}{r_k}10^{-2} \quad \text{C.15}$$

The solvent is a mixture, and the dielectric constant of the solvent ε_{solv} is the weighted sum of the ε of its components (Equation C.16). The weighting factor is the mass fraction w of the component in the mixture. ε of a substance is dependent upon the temperature T as shown in Equation 3.1 where A_{di}, B_{di} and C_{di} are substance-specific coefficients. In the CO_2-aqueous DGA system, the solvent is composed of DGA and water whose dielectric-constant coefficients are shown in Table C.5 (Aspentech, 2001).

$$\varepsilon_{solv} = \sum_i w_i\varepsilon_i \quad \text{C.16}$$

$$\varepsilon = A_{di} + B_{di}\left(\frac{1}{T} - \frac{1}{C_{di}}\right) \quad \text{3.1}$$

For molecules (and not ions), $z_k = 0$, which makes γ_k^{PDH} and γ_k^{Born} equal to 0. Therefore, for components that are molecules, the eNRTL model reduces to the NRTL model.

Table C.5 Coefficients of the dielectric-constant equation

Component	A_{di}	B_{di}	C_{di}
H_2O	78,54	31989,38	298,15
DGA	28,01	9277,00	273,15

The NRTL model describes the solvent as a mixture of binary systems. For a binary liquid mixture with component *i* and *j*, activity coefficients γ_i^{NRTL} and γ_j^{NRTL} can be calculated according to Equations C.17a and C.17b, respectively.

$$ln\gamma_i^{NRTL} = x_j^2\left[\tau_{ji}\left(\frac{G_{ji}}{x_i+x_jG_{ji}}\right)^2 + \left(\frac{\tau_{ij}G_{ij}}{(x_j+x_iG_{ij})^2}\right)\right] \quad \text{C.17a}$$

$$ln\gamma_j^{NRTL} = x_i^2\left[\tau_{ij}\left(\frac{G_{ij}}{x_j+x_iG_{ij}}\right)^2 + \left(\frac{\tau_{ji}G_{ji}}{(x_i+x_jG_{ji})^2}\right)\right] \quad \text{C.17b}$$

In Equations C.17a and C.17b, *x* is the mole fraction, *G* is a term defined as per Equations C.18a and C.18b, and τ is a NRTL interaction parameter that is dependent on temperature *T* (Equation 3.2) and on system-specific coefficients A_{ip} and B_{ip}. In addition, τ is also specific to the direction of the interaction in the system (τ_{ij} is not always equal to τ_{ji}). β is the nonrandomness factor (Renon and Prausnitz, 1968).

$$lnG_{ij} = -\beta_{ij}\tau_{ij} \quad \text{C.18a}$$

$$lnG_{ji} = -\beta_{ji}\tau_{ji} \quad \text{C.18b}$$

$$\tau = A_{ip} + \frac{B_{ip}}{T} \quad \text{3.2}$$

For a system with more than two components, Equation C.19 can be used to determine the activity coefficient of component *k* γ_k^{NRTL} in a mixture with components *i*, *j*, *k* and *l* (Renon and Prausnitz, 1968).

$$\gamma_k^{NRTL} = \frac{\sum_i \tau_{ik}G_{ik}x_i}{\sum_j G_{jk}x_j} + \sum_i \frac{x_iG_{ki}}{x_jG_{ji}}\left(\tau_{ki} - \frac{\sum_l \tau_{li}G_{li}x_l}{\sum_j G_{ji}x_j}\right) \quad \text{C.19}$$

For the CO_2-aqueous DGA system, the coefficients of the NRTL interaction-parameter equation A_{ip} and B_{ip} together with the nonrandomness factor β are shown in Table C.6 and Table C.7.

Table C.6 Coefficients of the NRTL-interaction-parameter equation together with the nonrandomness factor β for binary systems (Austgen (1989) and Section 3.3.2 of this study)

System	A_{ip}	B_{ip}	β
CO_2-DGA	-1,980	-1000,000	0,3
DGA-CO_2	-1,980	-1000,000	0,3
H_2O-DGA	1,992	-770,410	0,2
DGA-H_2O	1,992	-770,410	0,2
H_2O-CO_2	10,064	-3268,135	0,2
CO_2-H_2O	10,064	-3268,135	0,2

Table C.7 Coefficients of the NRTL-interaction-parameter equation together with the nonrandomness factor β for ternary systems (Aspen Plus 25)

System	A_{ip}	B_{ip}	β
H_2O - $DGA^+/DGACOO^-$	24,157	-5594,339	0,2
$DGA^+/DGACOO^-$ - H_2O	-11,293	2384,912	0,2
H_2O - DGA^+/HCO_3^-	8,000	0,000	0,2
DGA^+/HCO_3^- - H_2O	-11,753	2482,463	0,2
H_2O - H_3O^+/HCO_3^-	8,045	0,000	0,2
H_3O^+/HCO_3^- - H_2O	-4,072	0,000	0,2
H_2O - H_3O^+/OH^-	8,045	0,000	0,2
H_3O^+/OH^- - H_2O	-4,072	0,000	0,2
H_2O - H_3O^+/CO_3^{2-}	8,045	0,000	0,2
H_3O^+/CO_3^{2-} - H_2O	-4,072	0,000	0,2

D OPERATING PROCEDURES

The procedure to change the absorption solvent in the test rig is described at first. Then, the start-up and shutdown procedures of the absorption test rig and the N_2-PSA (pressure swing adsorption) unit are described. These procedures were developed to ensure safety of personnel and property and are meant for use by operators only (not meant for use by laymen).

D.1 ABSORPTION-SOLVENT CHANGING PROCEDURE

The following procedure describes how the absorption solvent was changed, and this procedure can be used in the future if a different solvent is to be used.

1. Approximately 80 l of solvent is present in the test rig. The solvent is drawn off by opening the drain valve of pumps P1 and P3. The solvent is collected in high-density polyethylene (HDPE) canisters having 10 l volume which help to store and manually transport the solvent. It should be noted that solvent accumulated in the preheater W6 (6 l volume) cannot be drawn off through the drain valve of the pumps. This solvent remains in the test rig.
2. Tap water is filled in the buffer vessel B1 through its head. Using pump P1, water is pumped at the flow rate F2 of 200 $kg \cdot h^{-1}$ through the test rig. When the level L1 in buffer vessel B1 decreases below 20 %, pump P1 is stopped. More water is poured in the buffer vessel, and the process is repeated till 60 l of water is present in the test rig.
3. Flow rate F2 of pump P1 is set to 200 $kg \cdot h^{-1}$ and level L3 of buffer vessel B3 is set at 20 %. Pump P1 and pump P3 are started, and the water is circulated through the test rig for 30 minutes.
4. The water mixes with the rests of the old solvent (especially from the preheater W6), and the mixture is then drawn off by opening the drain valve of pumps P1 and P3. The mixture is collected in HDPE canisters having 10 l volume and is disposed of as chemical waste.
5. Steps 2, 3 and 4 are repeated at least ten times.
6. The new solvent, in this case DGA and tap water in the desired ratio, is poured in the buffer vessel B1 such that the total volume of the liquid mixture (water and DGA) does not exceed 20 l. The buffer vessel B1 is used as a flask to mix the solvent components. The solvent is pumped through the test rig using pump P1 at the flow rate F2 of 200 $kg \cdot h^{-1}$. This procedure is repeated till approximately 60 l of new solvent is present in the test rig. Keeping in mind that approximately 6 l of water is already present in the test

rig (in the preheater W6), DGA should be further added so that the desired ratio of DGA to water is maintained.

7. Flow rate F2 of pump P1 is set to 200 $kg \cdot h^{-1}$ and level L3 of buffer vessel B3 is set at 40 %. Pump P1 and pump P3 are started, and the new solvent is circulated through the test rig for 120 minutes.
8. Solvent samples are drawn from the bottom of the absorber and analysed for water content using a volumetric Karl-Fischer titration with a one-component reagent (Mettler Toledo, 2009). Depending upon the result, either DGA or water is added to the buffer vessel B1 to obtain the desired ratio of DGA and water in the solvent.
9. Steps 7 and 8 are repeated till the desired DGA to water ratio in the solvent is obtained.

D.2 TEST-RIG START-UP PROCEDURE

The procedure includes several steps. At first, each step must be fully read, and then, it must be executed.

1. Manually switch on the power to the test rig by turning the main-switch knob on the switchboard 90° clockwise.
2. Manually switch on the power sequentially to the two pumps by turning the two knobs labelled "Pumpe P1" and "Pumpe P3" on the switchboard 90° clockwise.
3. Manually open the valve that connects the plastic feed-gas pipe to the humidifier K4. If the plastic feed-gas pipe contains water, disconnect the pipe at the sampling point and remove water from the plastic feed-gas pipe. Subsequently, reconnect the pipe at the same port where it was disconnected.
4. Boot the computer, and start the process-control software WinersRT.
5. Start-up the N_2-PSA (pressure swing adsorption) unit (Section D.4). Check the pressure of the N_2-storage vessel; the pressure should not exceed 7 bar.
6. Manually open the main valve of the CO_2-cylinder battery. Check the pressure of the CO_2 header at the inlet of the gas-regulator unit; the pressure should not exceed 7 bar.
7. Manually open the valve that connects the N_2 header to the gas-regulator unit by turning the valve handle 90° anticlockwise. The pressure before the N_2 flow regulator should not exceed 7 bar.
8. Inside the gas-regulator unit, manually turn the valve handles, two before the N_2 flow regulator and one before the CO_2 flow regulator, 90° anticlockwise.
9. Set the solvent flow rate F2 of pump P1 to 200 $kg \cdot h^{-1}$ and the level L3 of buffer vessel B3 to 40 % using the process-control software.

10. Start pumps P1 and P3 using the process-control software. Immediately thereafter, manually open the valve that connects buffer vessel B1 to pump P1.
11. After the solvent cycle is established, set the desired solvent flow rate F2 of pump P1 and the desired level L3 of buffer vessel B3.
12. Set preheater temperature T5 to 95 °C, and switch on the preheater W6 using the process-control software.
13. Set the desired power level of the reboiler W4.y and switch on the reboiler W4 using the process-control software.
14. Manually open the valve of the cooling-water header by turning the valve handle 90° anticlockwise. Manually start cooling-water supply to the cooler W1 and condenser W3 by sequentially rotating the knobs anticlockwise. Rotate till the desired cooling-water flow rates F6 and F8 are achieved.
15. Wait till the solvent has reached the desired temperature at the stripper inlet.
16. Sequentially set the N_2 and CO_2 flow rates F9 and F10 to their desired values using the process-control software.
17. Manually switch on the Infralyt. When the Infralyt begins to calibrate, connect the pipe between the Infralyt and the gas dryer.
18. Monitor process parameters using the process-control software, and monitor the test-rig operation visually.

D.3 TEST-RIG SHUTDOWN PROCEDURE

The procedure includes several steps. At first, each step must be fully read, and then, it must be executed.

1. Manually switch off the Infralyt, and disconnect the pipe between the Infralyt and the gas dryer at the gas-dryer end.
2. Manually close the main valve of the CO_2-cylinder battery, and shutdown the N_2-PSA unit (Section D.5).
3. Monitor the N_2 and CO_2 flow rates F9 and F10 using the process-control software, and wait till both flow rates F9 and F10 become less than 0,05 $Nm^3 \cdot h^{-1}$.
4. Manually close the valve that connects the N_2 header to the gas-regulator unit by turning the valve handle 90° clockwise.
5. Inside the gas-regulator unit, manually turn the valve handles, two before the N_2 flow regulator and one before the CO_2 flow regulator, 90° clockwise.
6. Set the N_2 and CO_2 flow regulators F9 and F10 to 0 $Nm^3 \cdot h^{-1}$ using the process-control software.

7. Manually close the valve that connects the plastic feed-gas pipe to the humidifier K4.
8. Switch off the preheater W6 and reboiler W4 using the process-control software.
9. Manually increase the cooling-water flow rates F6 and F8 to their respective maximum values.
10. Set the solvent flow rate F2 of pump P1 to 200 $kg \cdot h^{-1}$ and the level L3 of buffer vessel B3 to 40 % using the process-control software.
11. Manually open the bypass valves that connect the outlet of pump P3 to cooler W1, one at the pump end and the other at the cooler end. Manually half-close the valve that connects the pump P3 to heat exchanger W5.
12. Monitor the solvent temperatures T11 and T12 at the outlet of the heat exchanger W5 using the process-control software, and wait till the two temperature values are below 30 °C. Monitor the solvent temperature T5 at the stripper inlet and the temperature of the reboiler surface, and wait till both temperature values are below 40 °C.
13. Manually open the valve that connects the pump P3 to heat exchanger W5. Manually close the bypass valves that connect the outlet of pump P3 to cooler W1, one at the pump end and the other at the cooler end.
14. Monitor all the temperatures in the process unit using the process-control software, and wait till all the temperature values are below 40 °C.
15. Switch off the pumps P1 and P3 using the process-control software. Immediately thereafter, manually turn off the valve that connects buffer vessel B1 to pump P1.
16. End the process-control software, and shutdown the computer.
17. Manually stop the cooling-water supply to the cooler W1 and condenser W3 by sequentially rotating the knobs clockwise. Manually close the valve of the cooling-water header by turning the valve handle 90° clockwise.
18. Manually switch off the power sequentially to the two pumps by turning the two knobs labelled “Pumpe P1” and “Pumpe P3” on the switchboard 90° anticlockwise.
19. Manually switch off the power to the test rig by turning the main-switch knob on the switchboard 90° anticlockwise.

D.4 N_2-PSA UNIT START-UP PROCEDURE

The procedure includes several steps. At first, each step must be fully read, and then, it must be executed. All steps must be manually executed.

1. Check if valve V1 is open. If valve V1 is open, proceed to Step 2. If valve V1 is closed, contact the technician.
2. Sequentially open the valves V2 and V3.

3. Switch on the power to the PSA unit by turning the knob (*Hauptschalter*) on the front side of the switchboard 90° clockwise. Wait till two beeps are heard.
4. Switch on the gas-monitoring unit by turning the knob on the side of the gas-monitoring unit 90° clockwise. Wait till two beeps are heard.
5. Wait till the unit computer has booted.
6. Switch the operation-mode (*Betriebswahl*) knob on the switchboard to "A" by turning the knob 45° anticlockwise. Wait till the green and white light on the switchboard glow.
7. On the touch screen, start the adsorption operation by touching the "*Automatik*" icon.
8. Check the pressure of the N_2-storage vessel. If the pressure is below 6 bar, proceed with Step 9. If the pressure is above 6 bar, jump to Step 11.
9. Monitor the pressure of the N_2-storage vessel, and wait till two adsorption cycles are complete: on the touch screen, monitor the green filling of the two adsorbers, and wait till each adsorber has been two times completely filled with and emptied of the green filling.
10. Quarter-open the valve V4, and wait till the pressure of the N_2-storage-vessel exceeds 5 bar. Then half-open valve V4, and wait till the pressure of the N_2-storage-vessel exceeds 6 bar.
11. Slowly open valve V4 to its full extent.
12. Slowly open valve V5.

D.5 N_2-PSA UNIT SHUTDOWN PROCEDURE

The procedure includes several steps. At first, each step must be fully read, and then, it must be executed. All steps must be manually executed.

1. On the touch screen, touch the "Stop" icon to stop the adsorption operation.
2. Switch the operation-mode (*Betriebswahl*) knob on the switchboard to "0" by turning the knob 45° clockwise. Wait till the green and white lights on the switchboard stop glowing. Wait till the valve noise (squeaking) stops.
3. Wait till the pressure in the adsorbers has equalised: on the touch screen, monitor the green filling of the two adsorbers, and wait till both adsorbers are half green.
4. Switch off the gas-monitoring unit by turning the knob on the side of the gas-monitoring unit 90° anticlockwise.
5. Switch off the power to the PSA unit by turning the knob (*Hauptschalter*) on the front side of the switchboard 90° anticlockwise.
6. Sequentially close valves V5, V4, V3 and V2.
7. Let the valve V1 remain open.

E TEST-RIG SENSORS AND DATA

Table E.1 Process parameters recorded by computer (online)

Parameter	Code	Unit	Least count	Range
N_2 flow rate	F9	$Nm^3 \cdot h^{-1}$	0,01	0 to 16
CO_2 flow rate	F10	$Nm^3 \cdot h^{-1}$	0,01	0,0 to 9,1
CO_2 content in feed gas	yE	vol. %	0,01	0 to 50
CO_2 content in treated gas	yR	vol. %	0,01	0 to 50
Pressure difference in absorber K1	PD1	mbar	0,1	0 to 20
Pressure difference in stripper K3	PD3	mbar	0,1	0 to 20
Solvent flow rate from pump P1	F2	$kg \cdot h^{-1}$	0,1	0 to 1029
Load of pump P1	F.P1	%	0,1	0 to 100
Load of pump P3	F.P3	%	0,1	0 to 100
Cooling-water flow rate through cooler W1	F6	$l \cdot min^{-1}$	0,1	0 to 25
Cooling-water flow rate through condenser W3	F8	$l \cdot min^{-1}$	0,1	0 to 14
Solvent temperature at absorber K1 inlet and at cooler W1 outlet	T3	°C	0,1	0 to 100
Solvent temperature at stripper K3 inlet and at preheater W6 outlet	T5	°C	0,1	2,5 to 97,5
Solvent temperature at heat exchanger W5 inlet and at pump P1 outlet	T14	°C	0,1	5,3 to 105,2
Solvent temperature at heat exchanger W5 inlet and at pump P3 outlet	T15	°C	0,1	0 to 100
Solvent temperature at heat exchanger W5 outlet and at cooler W1 inlet	T11	°C	0,1	0 to 100
Solvent temperature at heat exchanger W5 outlet and at preheater W6 inlet	T12	°C	0,1	0 to 100
Gas temperature at absorber K1 inlet	T1	°C	0,1	0 to 100
Gas temperature at stripper K3 top	T6	°C	0,1	5,3 to 105,2

Table E.2 Process parameters recorded by hand

Parameter	Code	Unit	Least count	Range
Reboiler W4 surface temperature	T_{reb}	°C	0,1	0 to 120
Reboiler W4 power	W4.y	%	1	0 to 100
Energy consumption by reboiler W4	W4.e	kWh	0,01	0 to 999
Energy consumption by preheater W6	W6.e	kWh	0,01	0 to 999

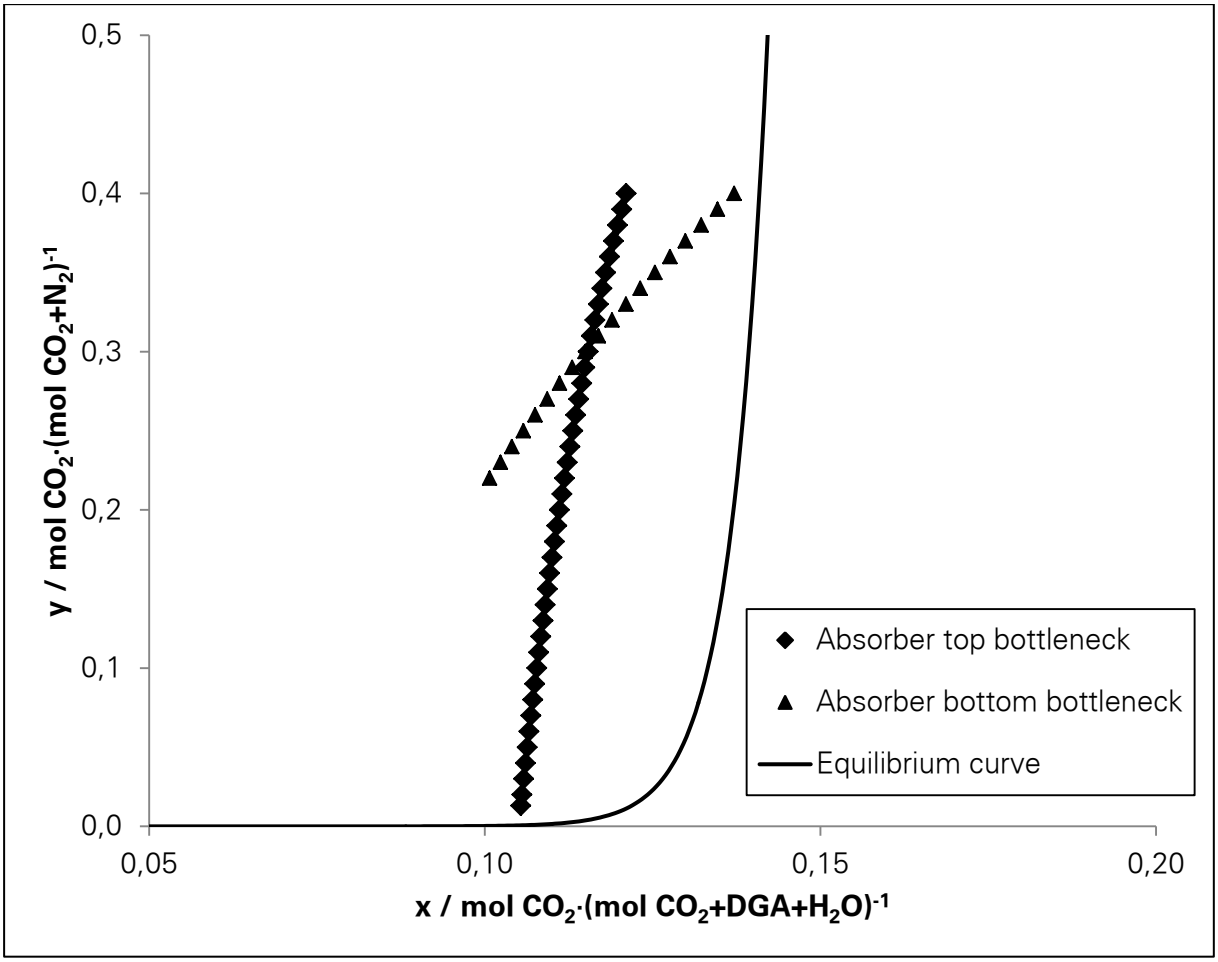

Figure E.1 Operating lines for the liquid to gas ratios of 14,9 and 3,8 mol DGA·(mol CO_2)$^{-1}$ and the equilibrium curve at 30 °C

F HAZARDS

F.1 REAL HAZARDS

Table F.1 Hazard points *HP* allocated to substances according to the severity of their hazards.

The hazard number corresponds to the serial number allocated in Table 3.18.

Sr. No.	Substance	CAS No.	Hazard number																HP
			1	2	3	4	5	6	7	8	9	10	11	12	13	14	15	16	17	
1	monoethanolamine (MEA)	141-43-5					4	4	4	1B	1					3	2			3,33
2	diglycolamine (DGA)	929-06-6						4		1B	1									2,00
3	diethanolamine (DEA)	111-42-2					4			2	1						2			2,00
4	N-methyldiethanolamine (MDEA)	105-59-9					4	4		1C	1					3				2,33
5	piperazine (PZ)	110-85-0			1					1B	1	1	1		2				3	5,75
6	aminomethylpropanol (AMP)	124-68-5								2	2								3	1,25
7	water	7732-18-5																		0,00
8	N-(2-hydroxyethyl)piperazine	103-76-4								2	2					3				1,08
9	1,4-dimethylpiperazine	106-58-1		2						1B										1,42
10	ethylenediamine	107-15-3		3			4	4		1B		1	1							3,58
11	ethyleneglycol	107-21-1					4													0,25
12	2-(dimethylamino)ethanol	108-01-0		3			4	4	4	1B										1,83
13	2,6-lutidine	108-48-5		3			4			2	2					3				1,66
14	2-methylaminoethanol	109-83-1					4	4		1B										1,25
15	diisopropanolamine	110-97-4									2									0,50
16	N-(2-hydroxyethyl)-ethylenediamine	111-41-1								1B	1	1	1		1B					4,50
17	diethylenglycol	111-46-6					4													0,25

Sr. No.	Substance	CAS No.	Hazard number																HP
			1	2	3	4	5	6	7	8	9	10	11	12	13	14	15	16	17	
18	N-2-(hydroxyethyl)acetamide	142-26-7								2	1					3				1,58
19	oxalic acid	144-62-7					4	4			1									1,50
20	1-(2-hydroxyethyl)imidazole	1615-14-1								2	2					3				1,08
21	N,N-bis(2-hydroxyethyl)formamide	25209-66-9								2	2					3				1,08
22	N-methyl-aminomethylpropanol	27646-80-6								2	2								3	1,25
23	triethylenediamine	280-57-9			1		4			2	2					3			3	2,83
24	1-(2-hydroxyethyl)-2-imidazolidinone	3699-54-5								2	2					3				1,08
25	N,N′-bis(2-hydroxyethyl)ethylenediamine	4439-20-7								1B										0,75
26	oxamide	471-46-5					4			2	2									1,00
27	2-oxazolidone	497-25-6					4				2		1							1,75
28	formaldehyde	50-00-0					3	3	2	1B			1	2						3,83
29	1-(2-hydroxyethyl)-4-methylpiperazine	5464-12-0								2	2					3				1,08
30	N-glycylglycine	556-50-3									2									0,50
31	N,N-dimethylethylamine	598-56-1		2			4		4	1B										1,92
32	formic acid	64-18-6		3						1A										1,33
33	acetic acid	64-19-7		3						1A										1,33
34	N-2-hydroxyethylformamide	693-06-1									2									0,50
35	methylamine	74-89-5	1						4	2	1					3				2,83
36	acetaldehyde	75-07-0		1			4				2		1	2		3				3,41
37	formamide	75-12-7													1B					0,75
38	ammonia	7664-41-7	2						3	1B								1		2,75
39	glycolic acid	79-14-1					4			1B										1,00
40	1-formylpiperidine	2591-86-8					4	3	4	2	2	1								2,75
41	morpholine	110-91-8		3			4	4	4	1B										1,83

Table F.2 Non-hazardous substances and their Chemical Abstracts Service (CAS) numbers

Sr. No.	Substance	CAS No.
1	glycolaldehyde	141-46-8
2	glycine	56-40-6
3	triethanolamine	102-71-6
4	1,4-bis(2-hydroxyethyl)piperazine	122-96-3
5	N,N-bis(2–hydroxyethyl)-glycine	150-25-4
6	3-(hydroxyethyl)-2-oxazolidone	3356-88-5
7	4,4-dimethyloxazolidone	26654-39-7

Table F.3 Substances for which no information on their hazards is known and their Chemical Abstracts Service (CAS) numbers

Sr. No.	Substance	CAS No.
1	3-hydroxyethylamino-N-hydroxy-ethylpropanamide	144236-39-5
2	1,3-bis(2-hydroxyethyl) urea	15438-70-7
3	1-(2-hydroxyethyl) diethylentriamine	1965-29-3
4	4-(2-gydroxyethyl)-2-piperazinone	23936-04-1
5	2,6-dimethyl-4-pyridinamine	3512-80-9
6	1-hydroxyethyl-2-piperazinone	59702-23-7
7	aminoacetaldehyde	6542-88-7
8	1,3-bis(2-hydroxyethyl)-2-imidazolidinone	71298-49-2
9	N,N,N-tris(hydroxyethyl) ethylenediamine	60487-26-5
10	hydroxymethylpropyloxazolidone	3375-84-6
11	N,N'-bis(2-hydroxyethxyethyl) urea	-
12	oxazolidone	504-76-7
13	N-(2-hydroxyethyl)-N-methyl formamide	1590-50-7
14	methyl-N,N,N-tris(hydroxyethyl) ethylenediamine	187731-33-5
15	methyl-4,4-dimethyloxazalodione	15833-17-7

F.2 PERCEIVED HAZARDS

The part of the questionnaire in the public survey that is relevant to this study is presented verbatim in German here.

Frage 15: „Jetzt eine Frage zu Biogasanlagen. Sie werden ja dazu genutzt, Strom und Wärme zu erzeugen. Denken Sie eigentlich, dass von Biogasanlagen Gefahren ausgehen oder denken Sie das nicht?“ Antwortoptionen sind ‚Ja‘, ‚Nein‘, und ‚Ich weiß nicht / kann nicht beurteilen‘.

Frage 16 nur für Befragte, die bei Frage 15 ‚Ja‘ angegeben haben: „Und welche Gefahren von Biogasanlagen sind Ihnen bekannt?“ Mehrfachantworten möglich.

Frage 17: „Ich lese Ihnen nun eine Reihe von allgemeinen Gefahren vor. Bitte sagen Sie mir immer auf einer Skala von 1 bis 10 für wie schwerwiegend Sie die jeweilige Gefahr halten. Eine ‚1' bedeutet dabei ‚nicht schwerwiegend' und ‚10' ‚höchst schwerwiegend'. Mit den Werten dazwischen können Sie Ihre Meinung abstufen.

- Brand- und Explosionsgefahr
- Gefährdung von Menschen durch Verunreinigung von Luft oder Wasser
- Umweltgefahren für Tiere und Pflanzen"

Antwortmöglichkeiten sind ganzen Zahlen von 1 bis 10 und ‚Ich weiß nicht / kann nicht beurteilen'.

Frage 18: „Wohnen Sie selbst in unmittelbarer Nähe oder im Umkreis von 3 Kilometern zu einer Biogasanlage?" Antwortmöglichkeiten sind ‚in unmittelbarer Nähe', ‚Umkreis von 3 km', ‚nichts davon', und ‚Ich weiß nicht / kann nicht beurteilen'.

Table F.4 Characteristics of the sample and the German population

Characteristic	**Unit**	**Sample population**	**German population**
Gender	% male	44	49
Average age	years	50	44
Education level	% German *Abitur* or higher	51	28

Table F.5 Relative frequency of answers to question 18 (sample size of 1012)

Answer	**Relative frequency / %**
In immediate neighbourhood	4
Within 3 km	17
None of these	76
Do not know / cannot assess	3

Table F.6 Relative frequency of answers to question 15 (sample size of 1012)

Answer	Relative frequency / %
Yes	29
No	62
Do not know / cannot assess	9

Table F.7 Correlation between the answer to question 15 and the location of a biogas plant relative to the residential location

Answer	Relative frequency / % Location of a biogas plant			
	In immediate neighbourhood	Within 3 km	None of these	Do not know / cannot assess
Yes	48	25	29	32
No	52	67	61	59
Do not know / cannot assess	0	8	10	9

Table F.8 Relative frequency of answers to question 16 (sample size of 294)

Answer	Relative frequency / %
Explosion	30
Poisonous emissions	17
Respiratory hazard	7
Leakage of lethal substances	5
Aquatic hazard	5
Fire	3
Depletion of ozone layer	3
Mutation or genetic defects	3
Eye hazard	2
Reproductive toxicity	2
Corrosion	2
Irritation and sensitization	0
Cancer	0
Others	24
Do not know / cannot assess	27

Table F.9 Relative frequency of answers to question 17

Answer	Relative frequency / %		
	Fire and explosion hazard	Threat to human beings due to polluted air and water	Environmental threat to plant and animals
	Sample size of 1004	Sample size of 1006	Sample size of 1007
1 (not serious)	6	4	7
2	8	6	6
3	13	9	11
4	9	8	8
5	15	15	20
6	6	9	9
7	11	12	12
8	12	16	13
9	4	5	3
10 (very serious)	14	15	10
Do not know / cannot assess	2	1	1
Average answer	**5,7**	**6,2**	**5,7**

G LIFE CYCLE ASSESSMENT INPUT PARAMETERS

Table G.1 Reliability (DQI_1), completeness (DQI_2), temporal correlation (DQI_3), geographical correlation (DQI_4), further technological correlation (DQI_5) and additional standard deviation of input parameters of the LCA

Parameter / Unit	Data quality indicators					Additional Standard deviation
	DQI_1	DQI_2	DQI_3	DQI_4	DQI_5	
Electricity consumed by the biogas compressor / MJ	1	1	1	1	1	0,00
Distance between solvent and biomethane plant / km	1	1	1	1	1	0,00
Electricity consumed by the biomethane compressor / MJ	1	1	1	1	1	0,00
Electricity consumed by the biomethane dryer / MJ	1	1	1	1	1	0,00
Electricity consumed by the spent-solvent pump / MJ	1	1	1	1	1	0,00
Electricity consumed by the lean-solvent pump / MJ	1	1	1	1	1	0,00
Cooling water needed in the condenser / kg	1	1	1	1	1	0,00
Cooling water needed in the cooler / kg	1	1	1	1	1	0,00
Heat demand of the desorption process / MJ·(kg CO_2)$^{-1}$	1	1	1	1	1	0,00
Temperature difference between spent and lean solvent / K	1	1	1	1	1	0,00
Solvent heat capacity / kJ·(kg·K)$^{-1}$	1	1	1	1	1	0,00
Electricity consumed during purifying and liquefying CO_2 / MJ	2	3	3	3	2	0,06
Diethylene glycol requirement / kg	3	5	1	1	1	0,10
Ammonia requirement / kg	3	5	1	1	1	0,10
Electricity consumed during DGA production / MJ	3	5	4	3	4	0,24
Chemical plants needed for producing 1 kg DGA / pcs	3	5	4	3	4	0,24
DGA yield / kg	3	5	1	1	1	0,10
Morpholine yield / kg	3	5	1	1	1	0,10
Water yield / kg	3	5	1	1	1	0,10
DGA transport by lorry / 1000 km	3	3	4	3	4	0,23

Parameter / Unit	Data quality indicators					Additional Standard deviation
	DQI_1	DQI_2	DQI_3	DQI_4	DQI_5	
DGA transport by rail / 1000 km	3	3	4	3	4	0,23
Heat demand of the DGA-production process / MJ·(kg DGA)$^{-1}$	3	5	1	1	1	0,10
Ethane emissions per MJ biomethane transported / kg	3	1	4	2	1	0,10
Propane emissions per MJ biomethane transported / kg	3	1	4	2	1	0,10
Butane emissions per MJ biomethane transported / kg	3	1	4	2	1	0,10
Methane emissions per MJ biomethane transported / kg	3	1	4	2	1	0,10
CO_2 emissions per MJ biomethane transported / kg	3	1	4	2	1	0,10
NMVOC emissions per MJ biomethane transported / kg	3	1	4	2	1	0,10
Heat lost from natural gas per MJ biomethane transported / MJ	1	1	4	2	1	0,09
Pipeline needed to transport 1 Nm^3 biomethane / m	2	1	1	3	1	0,03
CH_4 content in biogas / vol. %	2	2	1	3	4	0,20
CO_2 content in biomethane / vol. %	1	1	1	1	1	0,00
DGA life / a	4	1	1	1	1	0,09
CH_4 slip / vol. %	1	1	1	1	4	0,20
Chemical plants needed for treating 1,5 Nm^3 biogas / pcs	4	5	4	3	5	0,38
Operating hours of the plant / h·a^{-1}	3	1	1	2	4	0,21
Plant life / a	3	1	1	2	4	0,21
Natural-gas injection for 1 MJ natural gas at consumer / MJ	2	1	4	4	1	0,10

H SOLVENT PROPERTIES

Table H.1 Figure-table correlation

w_{DGA} is DGA mass fraction; w_{MEA} is MEA mass fraction; x_{DGA} is DGA mole fraction; α_{CO2} is equilibrium CO_2 solubility and CO_2 loading; m_{CO2} is CO_2 molality; Δm_{CO2} is differential CO_2 molality; p_{CO2} is CO_2 partial pressure; T is temperature; ρ is density; μ is viscosity; σ is surface tension, and E symbolizes excess property.

Figure	X-axis	Y-axis	Variable	Source table
4.1	w_{DGA}	α_{CO2}	T	H.2
4.2	w_{DGA}	m_{CO2}	T	H.2
4.3	p_{CO2}	α_{CO2}	T, w_{DGA}	H.3
4.4	w_{DGA}	Δm_{CO2}	T	H.4
4.5	α_{CO2}	ρ	w_{DGA}	H.5
4.6	α_{CO2}	μ	w_{DGA}	H.7
4.7	α_{CO2}	σ	w_{DGA}	H.9
H.1	x_{DGA}	ρ	T	H.5, H.6
H.2	x_{DGA}	μ	T	H.7, H.8
H.3	x_{DGA}	σ	T	H.9, H.10
H.4	x_{DGA}	ρ^E	-	H.11
H.5	x_{DGA}	μ^E, σ^E	-	H.11
H.6	α_{CO2}	ρ	w_{DGA}, w_{MEA}	H.5, H.12
H.7	α_{CO2}	μ	w_{DGA}, w_{MEA}	H.7, H.13
H.8	α_{CO2}	σ	w_{DGA}, w_{MEA}	H.9, H.14

Table H.2 Equilibrium CO_2 solubility α_{CO2} and CO_2 molality m_{CO2} in raw, spent and lean DGA solvents determined at temperature T and CO_2 partial pressure p_{CO2} at various DGA mass fractions w_{DGA}

w_{DGA}	p_{CO2}	T	α_{CO2}	m_{CO2}
kg DGA·(kg DGA+H_2O)$^{-1}$	kPa	°C	mol CO_2·(mol DGA)$^{-1}$	mol CO_2·(kg DGA+H_2O)$^{-1}$
Spent solvent after absorption at T ≈ 30 °C				
0,5	43,55 ± 0,14	30,25 ± 0,46	0,69 ± 0,02	3,29 ± 0,10
0,6	47,60 ± 0,32	29,98 ± 0,13	0,70 ± 0,02	4,02 ± 0,10
0,7	44,42 ± 0,14	29,89 ± 0,39	0,72 ± 0,02	4,80 ± 0,10
0,8	47,41 ± 0,14	29,59 ± 0,14	0,71 ± 0,01	5,44 ± 0,10
0,9	44,52 ± 0,14	29,94 ± 0,16	0,59 ± 0,01	5,08 ± 0,08
Lean solvent after desorption at T ≈ 90 °C				
0,5	43,15 ± 0,14 *	89,00 ± 0,07	0,51 ± 0,01	2,44 ± 0,07
0,6	48,82 ± 0,14 *	91,15 ± 0,11	0,48 ± 0,01	2,73 ± 0,07
0,7	57,26 ± 0,14 *	90,00 ± 0,07	0,47 ± 0,01	3,13 ± 0,07
0,8	69,53 ± 0,14 *	91,15 ± 0,07	0,50 ± 0,01	3,78 ± 0,07
0,9	84,72 ± 0,14 *	90,20 ± 0,07	0,48 ± 0,01	4,08 ± 0,07
Lean solvent after desorption at T ≈ 105 °C				
0,7	32,94 ± 0,14 *	105,85 ± 0,07	0,37 ± 0,01	2,49 ± 0,05
0,8	51,56 ± 0,14 *	105,75 ± 0,11	0,40 ± 0,01	3,03 ± 0,06
0,9	75,91 ± 0,14 *	105,15 ± 0,07	0,46 ± 0,01	3,92 ± 0,06

** calculated values*

Table H.3 Equilibrium CO_2 solubility α_{CO2} at temperature T and CO_2 partial pressure p_{CO2} at various DGA mass fractions w_{DGA} from literature and from this study

w_{DGA} kg DGA·(kg DGA+H_2O)$^{-1}$	p_{CO2} kPa	T °C	α_{CO2} mol CO_2·(mol DGA)$^{-1}$	Source
0,60	48	30	0,70	This study
0,40	7	40	0,52	Maddox et al., 1987
	16		0,54	
	91		0,62	
0,65	7	38	0,49	Dingman et al., 1983
	21		0,52	
	69		0,55	
0,60	49	90	0,48	This study
0,51	50	80	0,45	Chen et al., 2011
	18	110	0,31	
0,60	14,6	100	0,27	Martin et al., 1978
	28,4		0,33	
	51,5		0,38	

Table H.4 Differential CO_2 molality Δm_{CO2} at various DGA mass fractions w_{DGA}

w_{DGA} kg DGA·(kg DGA+H_2O)$^{-1}$	Δm_{CO2} mol CO_2·(kg DGA+H_2O)$^{-1}$	
	30 °C | 90 °C	30 °C | 105 °C
0,5	0,85 ± 0,04	-
0,6	1,29 ± 0,03	-
0,7	1,67 ± 0,04	2,31 ± 0,07
0,8	1,66 ± 0,03	2,41 ± 0,06
0,9	1,00 ± 0,02	1,16 ± 0,03

Table H.5 Density ρ of raw, spent and lean DGA solvents at various DGA mass fractions w_{DGA} and mole fractions x_{DGA} at 30,00 °C ± 0,02 K

w_{DGA}	x_{DGA}	ρ
kg DGA·(kg DGA+H_2O)$^{-1}$	**mol DGA·(mol DGA+H_2O)$^{-1}$**	**kg·m^{-3}**
Raw solvent		
0,0	0,00	0,995 ± 0,001
0,5	0,15	1,043 ± 0,001
0,6	0,20	1,050 ± 0,001
0,7	0,29	1,055 ± 0,001
0,8	0,41	1,056 ± 0,001
0,9	0,61	1,053 ± 0,001
1,0	1,00	1,046 ± 0,001
Spent solvent after absorption at T ≈ 30 °C		
0,5	0,15	1,142 ± 0,001
0,6	0,20	1,165 ± 0,001
0,7	0,29	1,184 ± 0,001
0,8	0,41	1,199 ± 0,001
0,9	0,61	1,201 ± 0,001
Lean solvent after desorption at T ≈ 90 °C		
0,5	0,15	1,125 ± 0,001
0,6	0,20	1,142 ± 0,001
0,7	0,29	1,165 ± 0,001
0,8	0,41	1,179 ± 0,001
0,9	0,61	1,196 ± 0,001
Lean solvent after desorption at T ≈ 105 °C		
0,7	0,29	1,136 ± 0,001
0,8	0,41	1,152 ± 0,001
0,9	0,61	1,176 ± 0,001

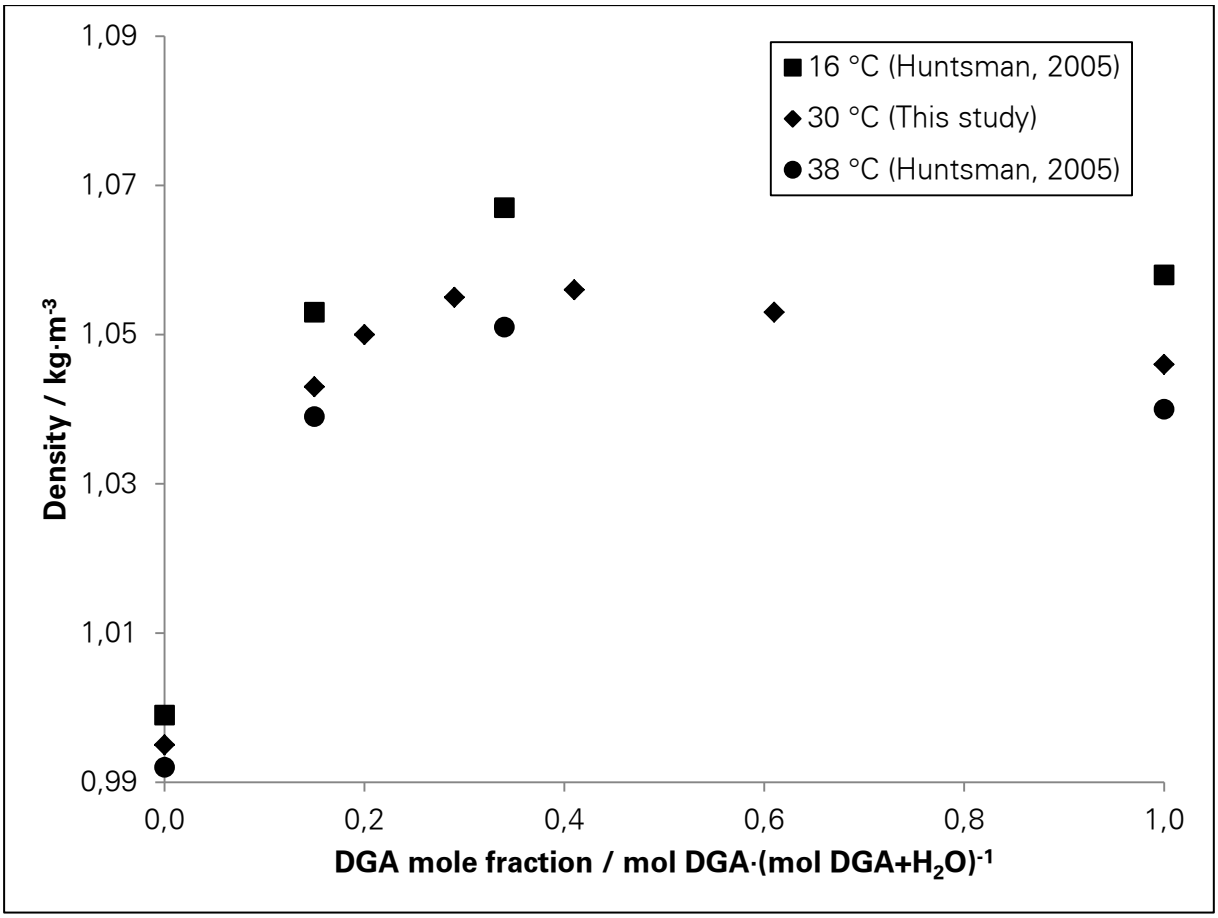

Figure H.1 Density ρ of raw DGA solvents at various DGA mole fractions and temperatures

Table H.6 Density ρ of raw DGA solvents at various DGA mole fractions x_{DGA} at temperature T (Huntsman, 2005)

x_{DGA}	T	ρ	T	ρ
mol DGA·(mol DGA+H_2O)$^{-1}$	°C	kg·m^{-3}	°C	kg·m^{-3}
0,00	16	0,999	38	0,992
0,15	16	1,053	38	1,039
0,34	16	1,067	38	1,051
1,00	16	1,058	38	1,040

Table H.7 Viscosity μ of raw, spent and lean DGA solvents at various DGA mass fractions w_{DGA} and mole fractions x_{DGA} at temperature T

w_{DGA}	x_{DGA}	T	μ
kg DGA·(kg DGA+H_2O)$^{-1}$	**mol DGA·(mol DGA+H_2O)$^{-1}$**	**°C**	**mPa·s**
Raw solvent			
0,0	0,00	303,35 ± 0,20	1,01 ± 0,01
0,5	0,15	303,35 ± 0,20	4,84 ± 0,02
0,6	0,20	303,35 ± 0,20	7,29 ± 0,06
0,7	0,29	303,35 ± 0,20	10,71 ± 0,14
0,8	0,41	303,35 ± 0,20	14,63 ± 0,10
0,9	0,61	303,35 ± 0,20	17,66 ± 0,10
1,0	1,00	303,35 ± 0,20	18,02 ± 0,07
Spent solvent after absorption at T ≈ 30 °C			
0,5	0,15	303,35 ± 0,20	10,68 ± 0,05
0,6	0,20	303,35 ± 0,20	24,43 ± 0,12
0,7	0,29	303,35 ± 0,20	66,75 ± 0,63
0,8	0,41	303,35 ± 0,20	244,90 ± 1,57
0,9	0,61	303,35 ± 0,20	874,10 ± 5,24
Lean solvent after desorption at T ≈ 90 °C			
0,5	0,15	303,15 ± 0,50	10,71 ± 0,05
0,6	0,20	303,15 ± 0,50	21,56 ± 0,08
0,7	0,29	303,15 ± 0,50	62,10 ± 0,56
0,8	0,41	303,15 ± 0,50	181,59 ± 1,63
0,9	0,61	303,15 ± 0,50	823,56 ± 4,94
Lean solvent after desorption at T ≈ 105 °C			
0,7	0,29	303,15 ± 0,50	44,58 ± 0,34
0,8	0,41	303,15 ± 0,50	112,27 ± 0,79
0,9	0,61	303,15 ± 0,50	479,39 ± 3,93

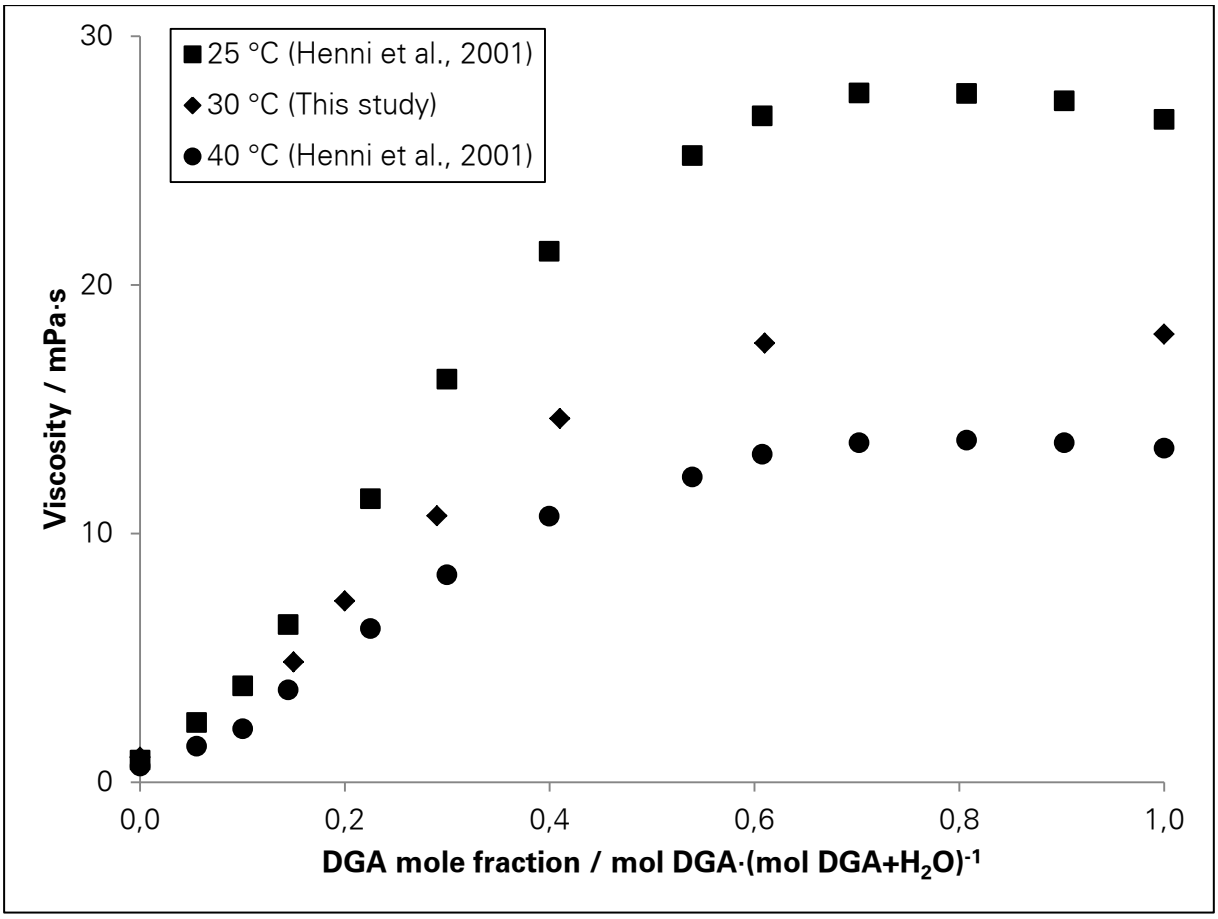

Figure H.2 Viscosity μ of raw DGA solvents at various DGA mole fractions and temperatures

Table H.8 Viscosity μ of raw DGA solvents at various DGA mole fractions x_{DGA} at temperature T (Henni et al., 2001)

x_{DGA}	T	μ	T	μ
mol DGA·(mol DGA+H_2O)$^{-1}$	°C	mPa·s	°C	mPa·s
0,00	25	0,89	40	0,65
0,06	25	2,40	40	1,45
0,10	25	3,87	40	2,15
0,14	25	6,34	40	3,72
0,22	25	11,40	40	6,18
0,30	25	16,21	40	8,34
0,40	25	21,35	40	10,70
0,54	25	25,20	40	12,28
0,61	25	26,80	40	13,19
0,70	25	27,72	40	13,65
0,81	25	27,70	40	13,76
0,90	25	27,40	40	13,65
1,00	25	26,66	40	13,43

Table H.9 Surface tension σ of raw, spent and lean DGA solvents at various DGA mass fractions w_{DGA} and mole fractions x_{DGA} at temperature T

w_{DGA}	x_{DGA}	T	σ
kg DGA·(kg DGA+H_2O)$^{-1}$	**mol DGA·(mol DGA+H_2O)$^{-1}$**	**°C**	**mN·m^{-1}**
Raw solvent			
0,0	0,00	303,72 ± 2,21	70,67 ± 0,13
0,5	0,15	301,98 ± 1,15	54,93 ± 0,10
0,6	0,20	302,48 ± 1,53	52,87 ± 0,18
0,7	0,29	301,65 ± 1,20	50,84 ± 0,09
0,8	0,41	303,82 ± 1,26	48,37 ± 0,21
0,9	0,61	302,88 ± 1,96	46,30 ± 0,11
1,0	1,00	302,98 ± 1,26	44,02 ± 0,20
Spent solvent after absorption at T ≈ 30 °C			
0,5	0,15	301,33 ± 1,07	59,89 ± 0,18
0,6	0,20	302,48 ± 0,70	57,71 ± 0,13
0,7	0,29	301,77 ± 1,05	55,90 ± 0,17
0,8	0,41	303,74 ± 0,64	54,01 ± 0,26
0,9	0,61	302,32 ± 0,53	52,58 ± 0,29
Lean solvent after desorption at T ≈ 90 °C			
0,5	0,15	303,95 ± 0,18	59,12 ± 0,23
0,6	0,20	303,60 ± 0,34	57,21 ± 0,37
0,7	0,29	303,45 ± 0,25	55,93 ± 0,12
0,8	0,41	303,60 ± 0,11	53,68 ± 0,08
0,9	0,61	303,45 ± 0,32	52,53 ± 0,09
Lean solvent after desorption at T ≈ 105 °C			
0,7	0,29	303,25 ± 0,32	53,33 ± 0,25
0,8	0,41	303,30 ± 0,11	52,41 ± 0,11
0,9	0,61	303,60 ± 0,32	51,54 ± 0,08

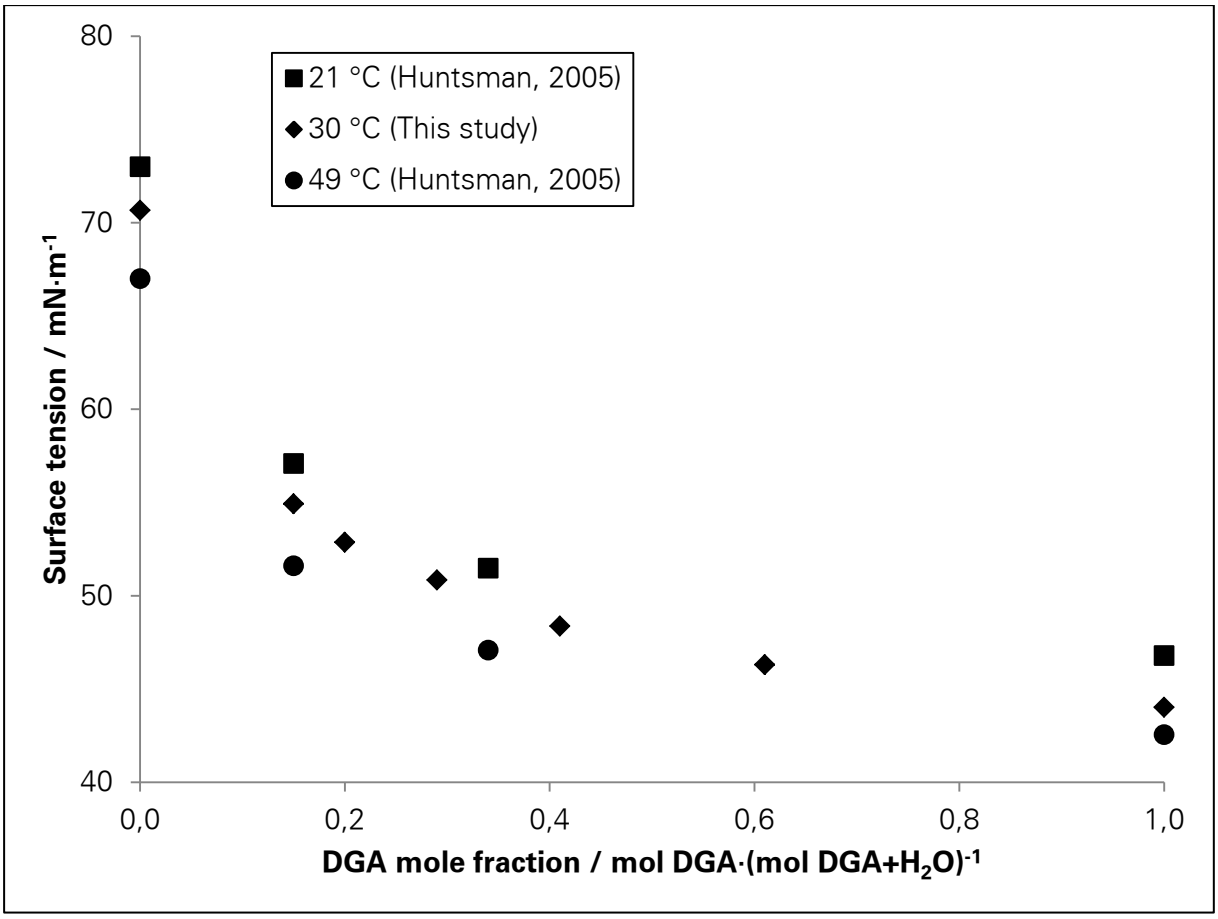

Figure H.3 Surface tension σ of raw DGA solvents at various DGA mole fractions and temperatures

Table H.10 Surface tension σ of raw DGA solvents at various DGA mole fractions x_{DGA} at temperature T (Huntsman, 2005)

x_{DGA}	T	σ	T	σ
mol DGA·(mol DGA+H_2O)$^{-1}$	°C	mN·m^{-1}	°C	mN·m^{-1}
0,00	21	73,00	49	67,00
0,15	21	57,09	49	51,61
0,34	21	51,47	49	47,08
1,00	21	46,79	49	42,55

Table H.11 Excess density ρ^E, viscosity μ^E and surface tension σ^E of raw solvents at various DGA mole fractions x_{DGA} at 30 °C

x_{DGA} **mol DGA·(mol DGA+H_2O)$^{-1}$**	ρ^E **kg·m^{-3}**	μ^E **mPa·s**	σ^E **mN·m^{-1}**
0,00	0,000 ± 0,000	0,00 ± 0,00	0,00 ± 0,00
0,15	0,040 ± 0,000	1,28 ± 0,02	-11,74 ± 0,06
0,20	0,044 ± 0,000	2,88 ± 0,04	-12,47 ± 0,07
0,29	0,045 ± 0,000	4,77 ± 0,08	-12,10 ± 0,06
0,41	0,040 ± 0,000	6,65 ± 0,09	-11,37 ± 0,07
0,61	0,027 ± 0,000	6,27 ± 0,08	-8,11 ± 0,04
1,00	0,000 ± 0,000	0,00 ± 0,00	0,00 ± 0,00

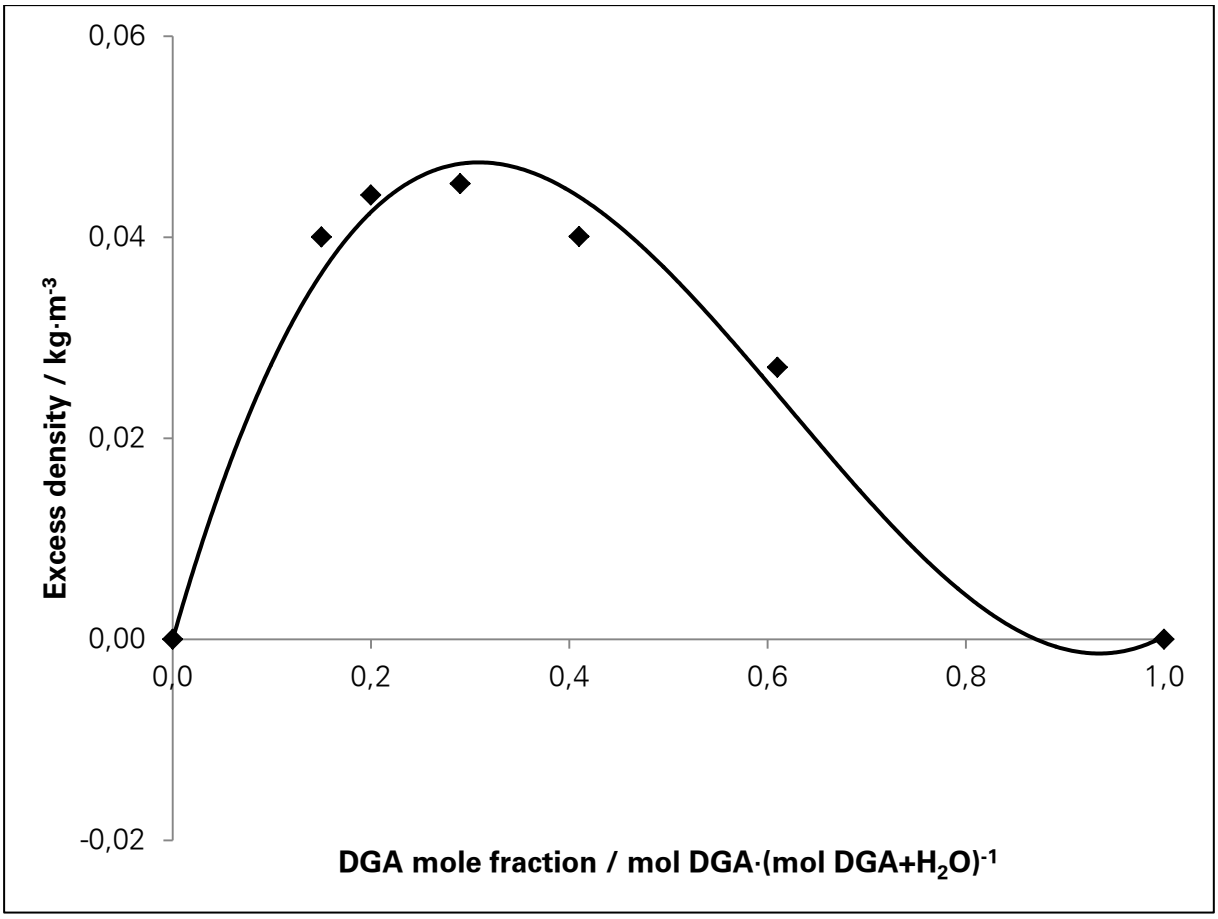

Figure H.4 Excess density of raw DGA solvents at 30 °C at various DGA mole fractions

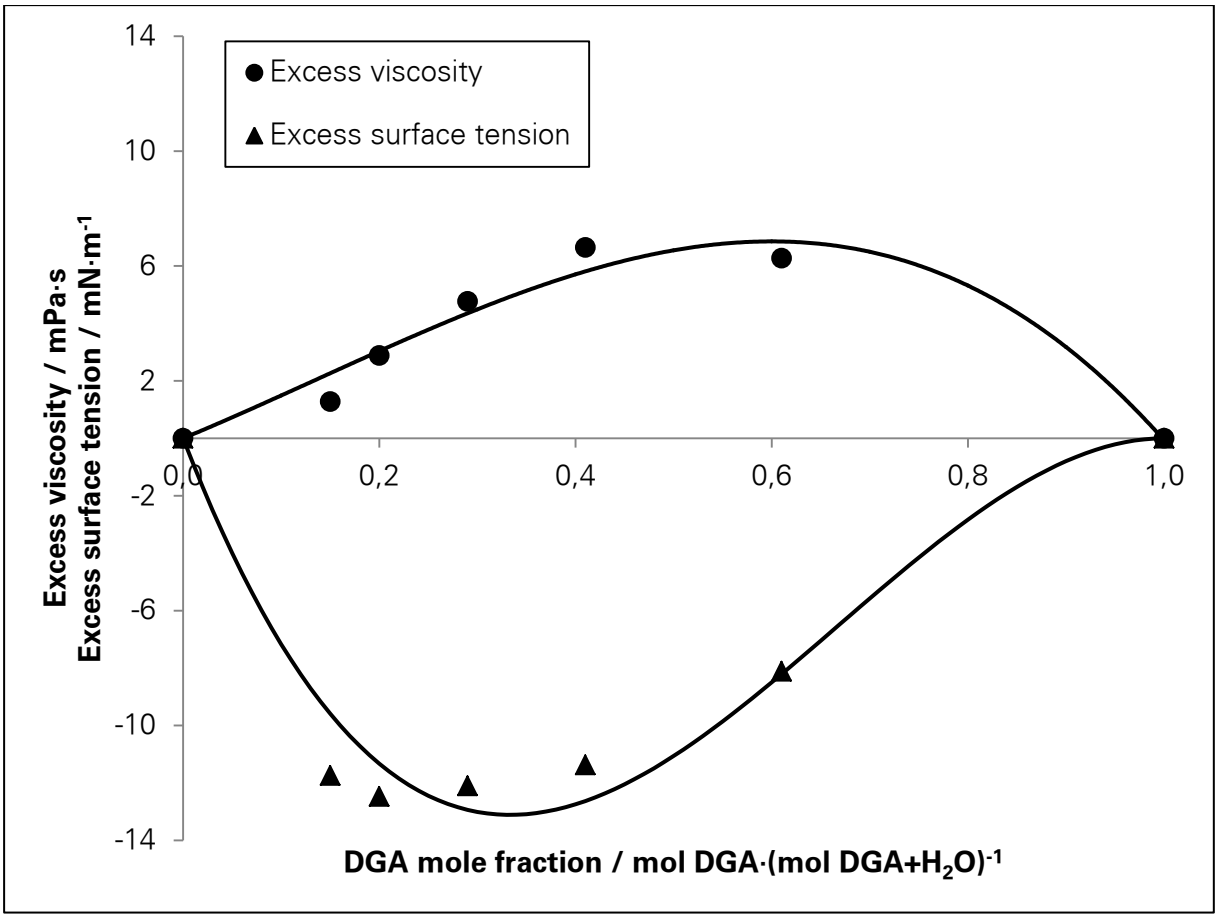

Figure H.5 Excess viscosity and surface tension of raw DGA solvents at 30 °C at various DGA mole fractions

Table H.12 Density ρ of MEA solvents at various CO_2 loadings α_{CO2} at 25 °C (Weiland et al., 1998)

α_{CO2} mol CO_2· (mol MEA)$^{-1}$	ρ kg·m^{-3}	
	30 wt. % MEA	40 wt. % MEA
0,0	1,013	1,017
0,1	1,033	1,043
0,2	1,054	1,070
0,3	1,073	1,096
0,4	1,095	1,126
0,5	1,117	1,147

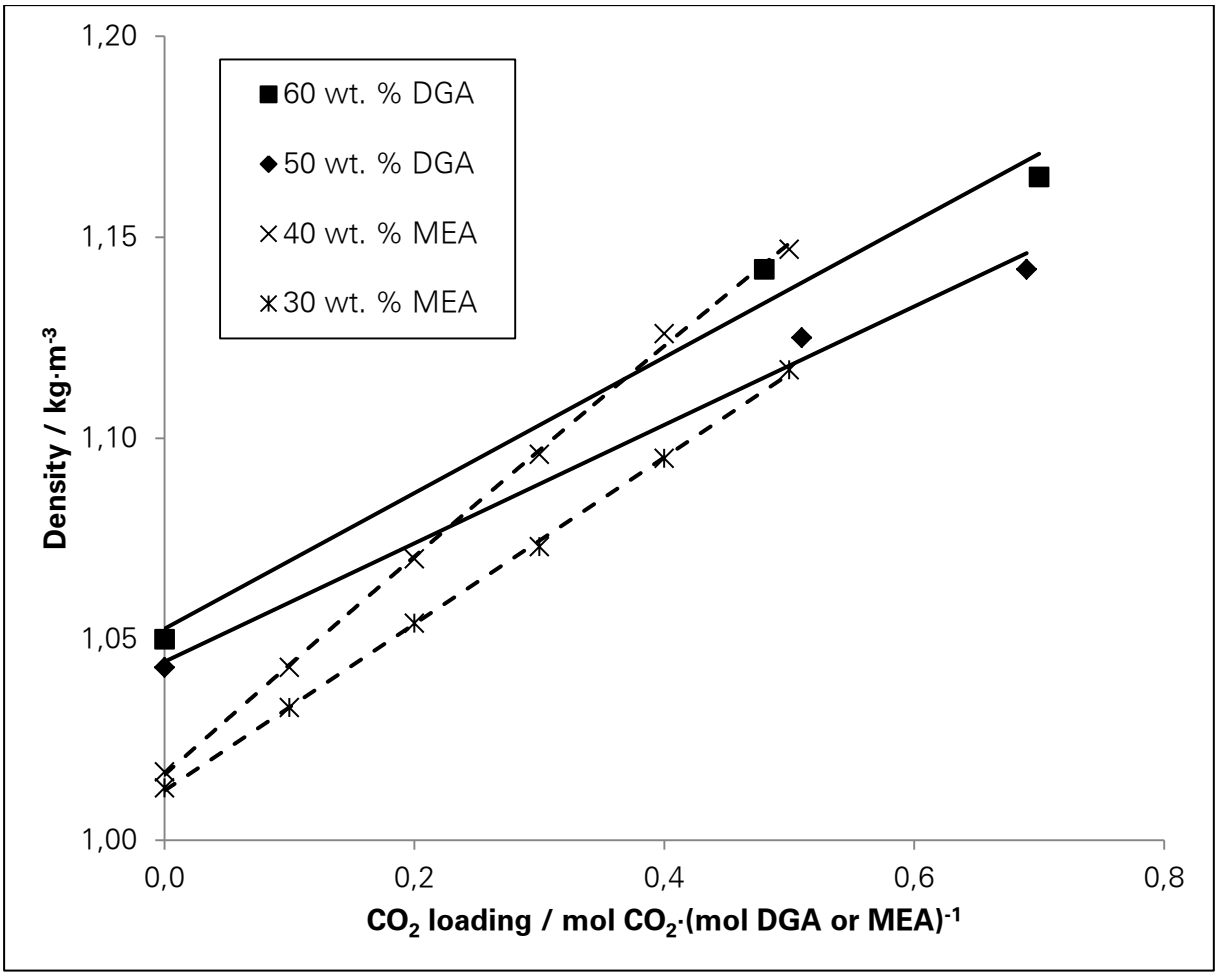

Figure H.6 Density of DGA and MEA solvents at various CO_2 loadings
(DGA data is from this study, and MEA data is from Weiland et al. (1998))

Table H.13 Viscosity μ of MEA solvents at various CO_2 loadings α_{CO2} at 25 °C
(Weiland et al., 1998)

α_{CO2}	μ	
mol CO_2· (mol MEA)$^{-1}$	**mPa·s**	
	30 wt. % MEA	**40 wt. % MEA**
0,0	2,52	3,41
0,1	2,72	3,76
0,2	2,92	4,30
0,3	3,21	4,97
0,4	3,51	5,90
0,5	3,82	6,73

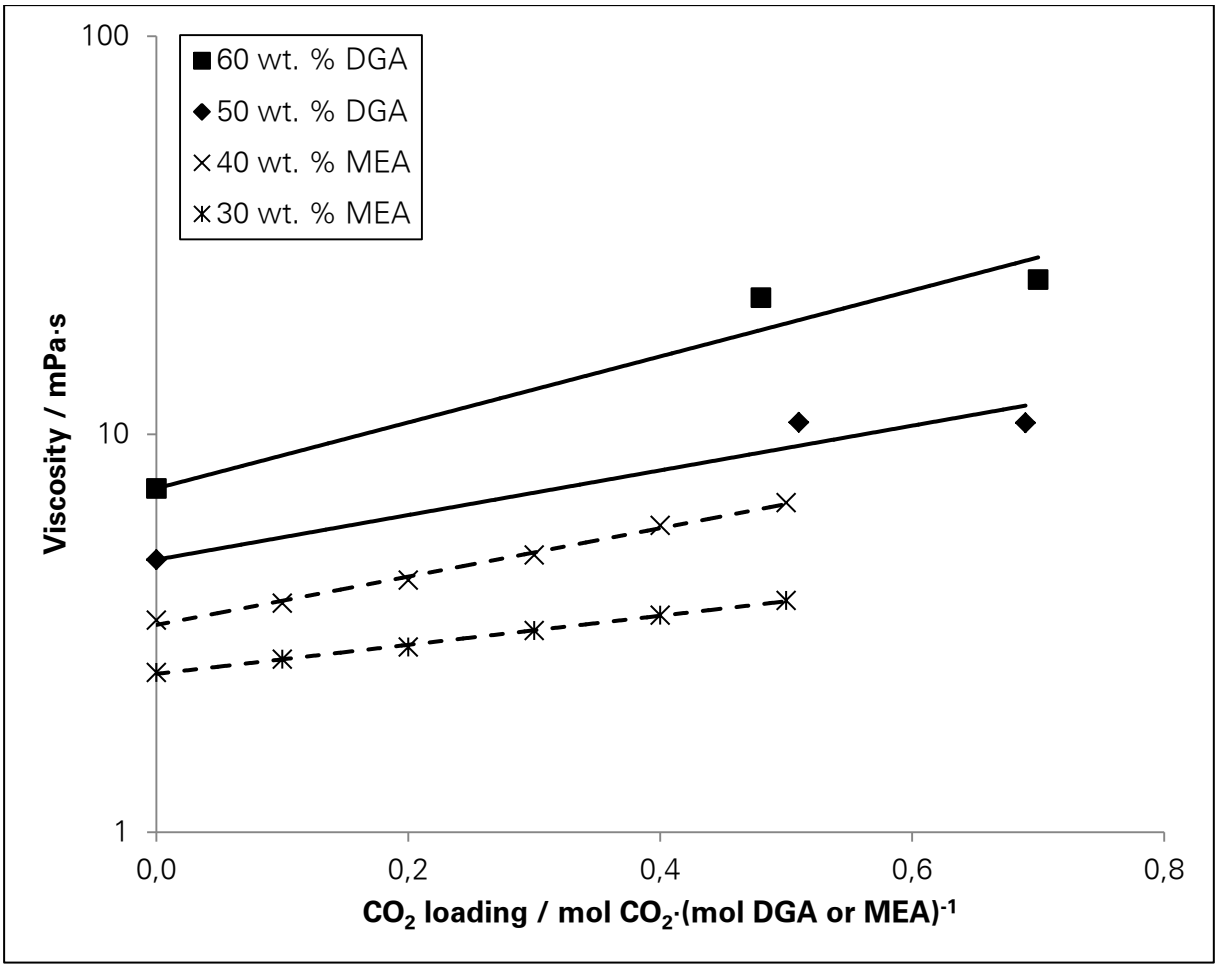

Figure H.7 Viscosity of DGA and MEA solvents at various CO_2 loadings (DGA data is from this study, and MEA data is from Weiland et al. (1998).)

Table H.14 Surface tension σ of MEA solvents at various CO_2 loadings α_{CO2} at 30 °C (Jayarathna et al., 2013)

α_{CO2} mol CO_2·(mol MEA)$^{-1}$	σ mN·m^{-1}		
	30 wt. % MEA	50 wt. % MEA	70 wt. % MEA
0,0	63,7	59,6	54,5
0,1	65,0	60,9	57,0
0,2	66,4	62,7	59,0
0,3	67,8	64,4	61,2
0,4	69,8	67,1	65,5
0,5	72,8	70,5	69,2

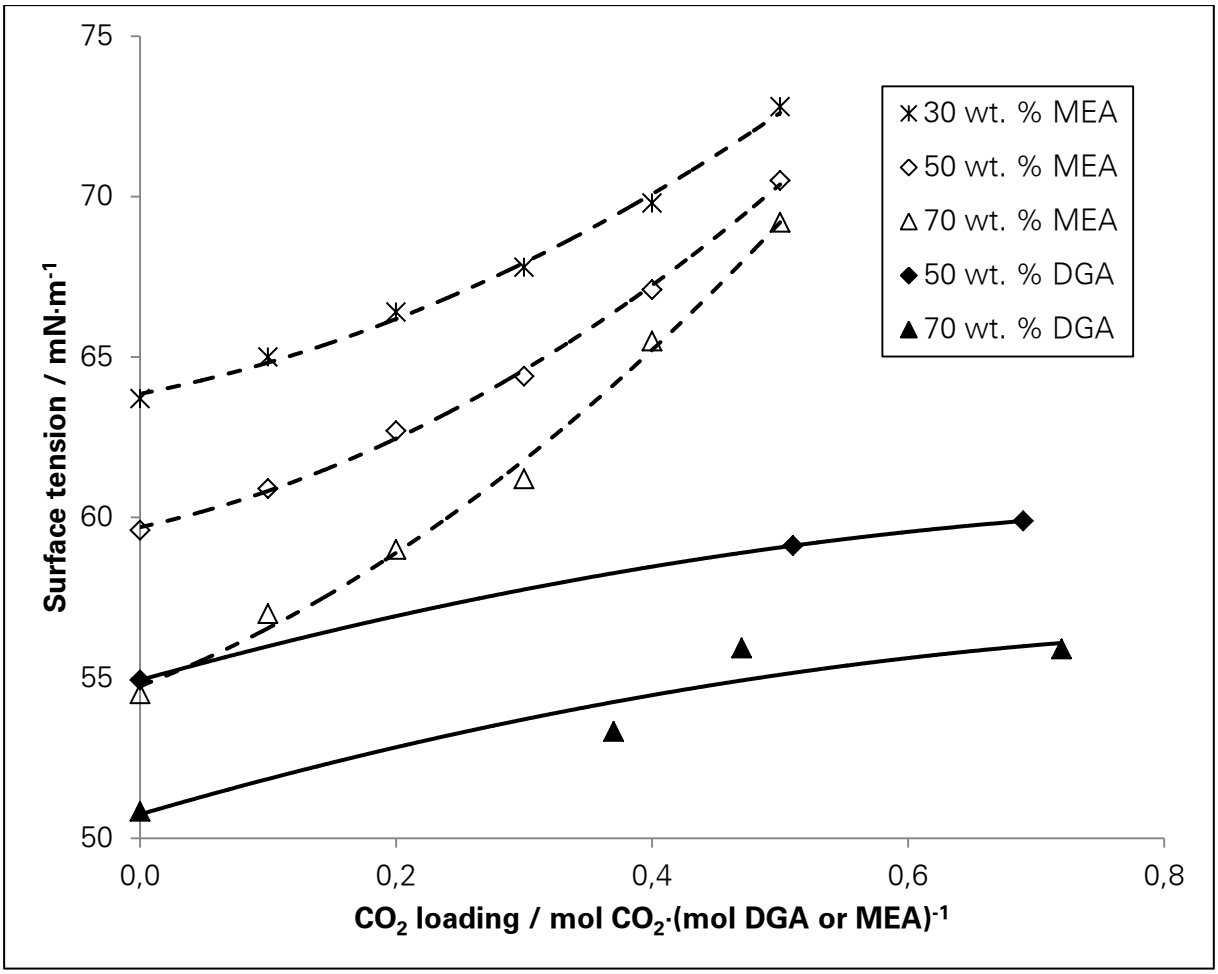

Figure H.8 Surface tension of DGA and MEA solvents at various CO_2 loadings (DGA data is from this study, and MEA data is from Jayarathna et al. (2013).)

I SIMULATED EQUILIBRIUM CO_2 SOLUBILITY

Table I.1 Equilibrium CO_2 solubility α_{CO2} of 60 wt. % DGA in solvent determined by experiments in Martin et al. (1978) and by simulations in this study for various CO_2 partial pressures p_{CO2} at temperature T

Experiments		Simulations	
p_{CO2} kPa	α_{CO2} mol CO_2·(mol DGA)$^{-1}$	p_{CO2} kPa	α_{CO2} mol CO_2·(mol DGA)$^{-1}$
	At T = 50 °C		
1,6	0,40	2,5	0,41
2,3	0,43	5,0	0,43
3,2	0,44	10,0	0,45
12,4	0,48	15,0	0,46
69,1	0,51	70,0	0,50
	At T = 100 °C		
2,5	0,13	2,5	0,29
3,8	0,15	5,0	0,30
6,4	0,20	10,0	0,32
9,6	0,23	15,0	0,34
14,6	0,27	20,0	0,35
28,4	0,33	25,0	0,35
51,5	0,38	30,0	0,36
-	-	40,0	0,37
-	-	50,0	0,38

Table I.2 Equilibrium CO_2 solubility α_{CO2} determined by experiments (exp) and by simulations (sim) in this study at a CO_2 partial pressure of 44 kPa at temperature T for solvents with various DGA mass fractions w_{DGA}

w_{DGA}	α_{CO2}		$\alpha_{CO2,\,sim}$ / $\alpha_{CO2,\,exp}$
kg DGA·(kg DGA+H_2O)$^{-1}$	mol CO_2·(mol DGA)$^{-1}$		-
	Experiments	Simulations	
	At T ≈ 30 °C		
0,5	0,69	0,65	0,94
0,6	0,71	0,62	0,87
0,7	0,72	0,59	0,82
0,8	0,72	0,57	0,78
0,9	0,60	0,54	0,90
	At T ≈ 90 °C		
0,5	0,51	0,37	0,73
0,6	0,48	0,39	0,81
0,7	0,47	0,42	0,88
0,8	0,49	0,45	0,91
0,9	0,47	0,47	1,00
	At T ≈ 105 °C		
0,7	0,37	0,38	1,04
0,8	0,40	0,43	1,08
0,9	0,46	0,47	1,02

Table I.3 Simulated equilibrium CO_2 solubility α_{CO2} of 70 wt. % DGA in solvent at temperature T for various CO_2 partial pressures p_{CO2}

p_{CO2}	α_{CO2}	
kPa	mol CO_2·(mol DGA)$^{-1}$	
	T ≈ 30 °C	T ≈ 105 °C
0,5	0,47	-
1,0	0,48	-
2,0	0,49	-
10,0	0,53	0,33
20,0	0,55	0,36
30,0	0,57	0,37
40,0	0,58	0,39